QC
1
.456
v.64C
no.3

THE UNIVERSITY
OF MICHIGAN
AUG 26 1960
LIBRARY

Volume 64C

Number 3

July–Sept. 1960

Journal of Research

of the

NATIONAL BUREAU OF STANDARDS

C. ENGINEERING AND INSTRUMENTATION

Journal of Research

of the

National Bureau of Standards

C. Engineering and Instrumentation

JULY–SEPT. • 1960

VOLUME • 64C

NUMBER • 3

Editor: W. A. Wildhack

Associate Editors: G. F. Montgomery, R. B. Jacobs

Publication dates:
Feb. 15, May 15, Aug. 15, Nov. 15, 1960

JOURNAL OF RESEARCH

The National Bureau of Standards Journal of Research reports research and development in the fields of activity shown at right. Also included from time to time are survey articles on topics closely related to the Bureau's scientific and technical program.

The Journal is published in four separate sections as follows:

A. Physics and Chemistry

Contains papers of interest primarily to scientists working in these fields. Issued six times a year. Annual subscription: domestic, $4.00; foreign, $4.75.

B. Mathematics and Mathematical Physics

Presents studies and compilations designed mainly for the mathematician and the theoretical physicist. Issued quarterly. Annual subscription: domestic, $2.25; foreign, $2.75.

C. Engineering and Instrumentation

Reports research and development results of interest chiefly to the engineer and the applied scientist. Issued quarterly. Annual subscription: domestic, $2.25; foreign, $2.75.

D. Radio Propagation

Reports work in radio propagation physics and upper atmospheric research. Issued six times a year. Annual subscription: domestic, $4.00; foreign, $4.75.

U.S. DEPARTMENT OF COMMERCE
Frederick H. Mueller, Secretary

NATIONAL BUREAU OF STANDARDS
A. V. Astin, Director

Functions and Activities

The functions of the National Bureau of Standards are set forth in the Act of Congress, March 3, 1901, as amended. These include the development and maintenance of the national standards of measurement and the provision of means and methods for making measurements consistent with these standards; the determination of physical constants and properties of materials; the development of methods and instruments for testing materials, devices, and structures; advisory services to government agencies on scientific and technical problems; invention and development of devices to serve special needs of the Government; and the development of standard practices, codes, and specifications. The work includes basic and applied research, development, engineering, instrumentation, testing, evaluation, calibration services, and various consultation and information services. The Bureau also serves as the Federal technical research center in a number of specialized fields. The scope of activities of the National Bureau of Standards is suggested in the following listing of the divisions and sections engaged in technical work.

Washington, D.C.

Electricity and Electronics. Resistance and Reactance. Electron Devices. Electrical Instruments. Magnetic Measurements. Dielectrics. Engineering Electronics. Electronic Instrumentation. Electrochemistry.

Optics and Metrology. Photometry and Colorimetry. Optical Instruments. Photographic Technology. Length. Engineering Metrology.

Heat. Temperature Physics. Thermodynamics. Cryogenic Physics. Rheology. Engine Fuels. Free Radicals Research.

Atomic Physics. Spectroscopy. Radiometry. Mass Spectrometry. Solid State Physics. Electron Physics. Atomic Physics.

Radiation Physics. Neutron Physics. Radiation Theory. Radioactivity. X-ray. High Energy Radiation. Nucleonic Instrumentation. Radiological Equipment.

Chemistry. Organic Coatings. Surface Chemistry. Organic Chemistry. Analytical Chemistry. Inorganic Chemistry. Electrodeposition. Molecular Structure and Properties of Gases. Physical Chemistry. Thermochemistry. Spectrochemistry. Pure Substances.

Mechanics. Sound. Mechanical Instruments. Fluid Mechanics. Engineering Mechanics. Mass and Scale. Capacity, Density, and Fluid Meters. Combustion Controls.

Organic and Fibrous Materials. Rubber. Textiles. Paper. Leather. Testing and Specifications. Polymer Structure. Plastics. Dental Research.

Metallurgy. Thermal Metallurgy. Chemical Metallurgy. Mechanical Metallurgy. Corrosion. Metal Physics.

Mineral Products. Engineering Ceramics. Glass. Refractories. Enameled Metals. Concreting Materials. Constitution and Microstructure.

Building Technology. Structural Engineering. Fire Protection. Air Conditioning, Heating, and Refrigeration. Floor, Roof, and Wall Coverings. Codes and Safety Standards. Heat Transfer.

Applied Mathematics. Numerical Analysis. Computation. Statistical Engineering. Mathematical Physics.

Data Processing Systems. SEAC Engineering Group. Components and Techniques. Digital Circuitry. Digital Systems. Analog Systems. Applications Engineering.

• Office of Basic Instrumentation. • Office of Weights and Measures

Boulder, Colorado

Cryogenic Engineering. Cryogenic Equipment. Cryogenic Processes. Properties of Materials. Gas Liquefaction.

Radio Propagation Physics. Upper Atmosphere Research. Ionosphere Research. Regular Prediction Services. Sun-Earth Relationships. VHF Research. Radio Warning Services. Airglow and Aurora. Radio Astronomy and Arctic Propagation.

Radio Propagation Engineering. Data Reduction Instrumentation. Radio Noise. Tropospheric Measurements. Tropospheric Analysis. Propagation-Terrain Effects. Radio-Meteorology. Lower Atmosphere Physics.

Radio Standards. High-Frequency Electrical Standards. Radio Broadcast Service. Radio and Microwave Materials. Atomic Frequency and Time Standards. Electronic Calibration Center. Microwave Circuit Standards.

Radio Communication and Systems. Low Frequency and Very Low Frequency Research. High Frequency and Very High Frequency Research. Modulation Systems. Antenna Research. Navigation Systems. Systems Analysis. Field Operations.

Order all publications from the Superintendent of Documents
U.S. Government Printing Office, Washington 25, D.C.

Use of funds for printing this publication approved by the Director of the Bureau of the Budget (June 24, 1958).

DEPOSITED BY THE
UNITED STATES OF AMERICA

JOURNAL OF RESEARCH of the National Bureau of Standards—C. Engineering and Instrumentation
Vol. 64C, No. 3, July–September 1960

A New Method of Measuring Gage Blocks

James B. Saunders

(April 4, 1960)

Since the publication of a description of the parallel testing interferometer it has been discovered that this instrument, without modification, is quite applicable to the comparison of lengths of gage blocks. This note describes the testing of gage blocks of all lengths, up to several meters, without having to contact them to optical flats.

Since publishing a description of the parallel testing interferometer [1] this author has realized the applicability of this instrument, without modification, to the comparison of long gage blocks. Accordingly, this note may be considered a supplement to *Parallel Testing Interferometer*.[1]

Figure 1, which is a modification of figure 2 in footnote 1, together with footnote 1, shows the optical arrangement and details of the instrument. The two gage blocks, G and S in figure 1 are placed so that the images of the two ends, facing one prism, are superimposed so that fringes of interference are obtained from the two beams that are reflected from them. The order of interference at the center (usually chosen as the reference point) is a measure of the relative axial position of the two faces. Similarly, the order observed from the other ends of the two blocks is a measure of the relative axial position of these faces. The difference in these two orders of interference, when proper choice of sign is considered, is a measure of the difference in length of the two blocks. Thus, the length of gage blocks can be compared without the necessity of wringing or optically contacting them to optical planes.

If the order of interference observed on one pair of faces is adjusted to zero the difference in length is given by the order of interference observed on the second pair of faces. The length of the unknown block need not approximate the length of the standard. If the difference is large, however, the orders of interference will also be large and monochromatic light of high purity will have to be used to produce fringes of adequate visibility.

This method of measurement permits the attainment of less gravitational distortion of very long blocks than when optical planes are contacted to them. It also permits faster testing because the blocks can be handled without coming into contact with the operator's hands—practically unavoidable in wringing operations—thus eliminating a serious source of thermal disturbance.

The above description of measuring length applies equally well to the testing of short blocks with the "Short-Block Interferometer," also described in footnote 1.

[1] J. B. Saunders, Parallel testing interferometer, J. Research NBS, **61**, 491 (1958) RP2917.

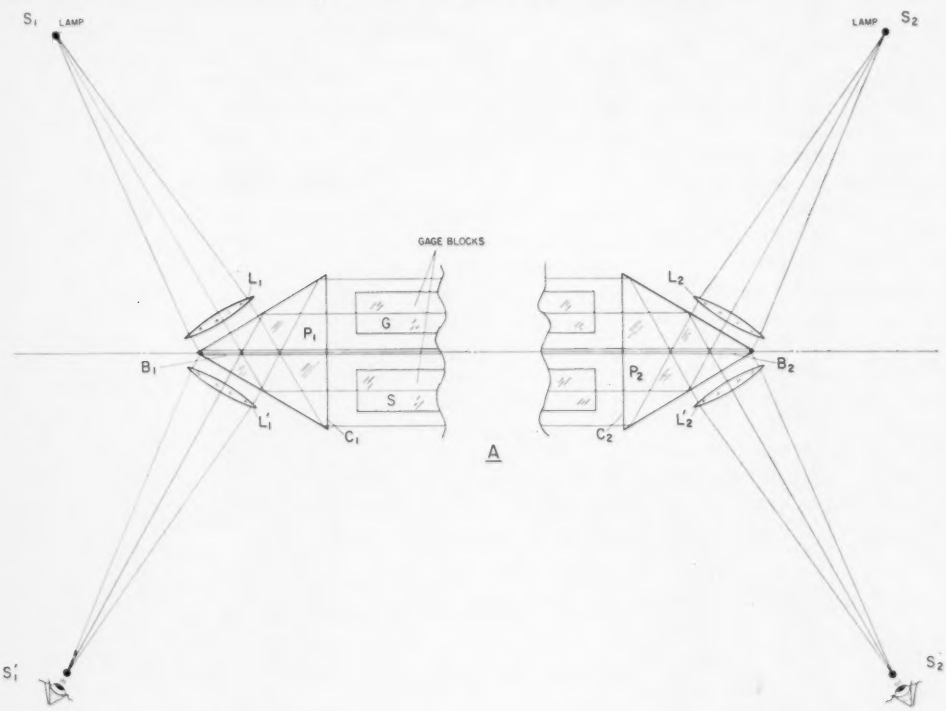

FIGURE 1. *Optics of interferometer for comparison of long gage blocks.*

(Paper 64C3–37)

JOURNAL OF RESEARCH of the National Bureau of Standards—C. Engineering and Instrumentation
Vol. 64C, No. 3, July–September 1960

Gage Blocks of Superior Stability: Initial Developments in Materials and Measurement

M. R. Meyerson, T. R. Young, and W. R. Ney

(April 1, 1960)

Increased demands on modern technology have established a requirement for gage blocks with higher accuracy of length calibration than is currently available. The desired improvement is tenfold and involves an increase in reliability from 2×10^{-6} in./in. to 1 or 2×10^{-7} in./in. The problem of achieving gage blocks dimensionally stable to this degree is fundamental and has two aspects; (1) the development of a suitable material and treatment to produce a gage block with the desired dimensional stability, surface quality, and several other physical properties, (2) the development of instrumentation and techniques for the precise measurement of temporal changes of length, so that stability of test samples may be determined to the required precision.

To date the program has been successful in developing three sets of gage blocks from two materials that have met the requirements and have shown a dimensional stability of 2×10^{-7} in./in./yr over an observed period of one year. A technique for measurement based on the use of a mechanical-electronic comparator and a rigorous application of statistical control have supplied data precise to within $\pm2\times10^{-7}$ in. The processes, technical aspects, and techniques involved in these developments are fully explained, and plans for further investigation and improvement are indicated.

1. Introduction

Gage blocks are precise representatives of the national standard of length maintained at the National Bureau of Standards. As such they are in general use throughout industry and government for direct measurements or as standards for the calibration of measuring tools and other devices. Their sizes not only should be known and measurable to a high degree of precision, but once established, the sizes should remain within a desired constancy with the passage of time. Many instances are reported [1,2,3][1] where hardened steel gage blocks have changed dimensions upon aging. This dimensional instability has been reported as a shrinkage, a growth, or even as a change from one to the other at different times of measurement.

Gage blocks purchased for governmental use are obtained in accordance with Federal Specification GGG–G–15, June 7, 1956. The standards of quality specified therein are also in general use throughout industry. The best steel gage blocks currently available are made to standards designated as AA, Laboratory Grade, Class 1, which provide for tolerances on lengths of $\pm2\times10^{-6}$ in./in. on blocks longer than 1 in. and $\pm2\times10^{-6}$ in. on blocks 1 in. or shorter. A minimum hardness of 65 Rockwell C (65 R_c) or equivalent on or adjacent to the wringing surface is required. The specification also contains allowable tolerances on flatness, parallelism, and finish of the wringing surfaces, but there are no quantitative requirements for dimensional stability; only the statement, ". . . suitably treated to assure dimensional stability of the finished gages."

Gage blocks are not used to measure to the extreme limits of the indicated tolerances; a factor of ten is usually allowed to compensate in part for inaccuracies established by dimensional instability, wear, and the summation of errors formed in combining two or more blocks. With that criterion, current commercial blocks are used to measure no closer than $\pm2\times10^{-5}$ in./in. With the advent of the space and atomic era, the need for measuring to ±1 or 2×10^{-6} in./in. is anticipated by industry and recognized by the Congress of the United States. Such a degree of precision would necessitate gage blocks with a tolerance of ±1 or 2×10^{-7} in./in. The development of gage blocks to meet this specification presents a dual problem of materials and measurement. Accordingly, the investigation was designed to study both facets of this problem and the cooperative efforts of personnel from two divisions of the National Bureau of Standards (Metallurgy, and Optics and Metrology) were applied. The Metallurgy Division was given the responsibility for the selection, development, treatment and evaluation of materials, and the Optics and Metrology Division for the development and improvement of measuring techniques and the determination of stability of experimental gage blocks. Several companies [2] interested in the manufacture or application of gage blocks, are actively cooperating in the program and have supplied invaluable advisory service, the bulk of the blank materials used, all of the facilities and personnel for lapping, and a portion of the operating funds.

[1] Figures in brackets indicate the literature references at the end of this paper.

[2] Brown & Sharpe Co.
Dearborn Gage Co.
DoAll Co.
E. I. du Pont de Nemours & Co., Inc.
Fonda Gage Co.
General Electric Co.
Greenfield Tap & Die Corp.
Hughes Aircraft Co.
International Business Machines Corp.
Link Aviation, Inc.
New Departure Division of General Motors Corp.
Pratt & Whitney Co., Inc.
Taft-Peirce Mfg. Co.
The Sheffield Corp.
The Timken Roller Bearing Co.
The Van Keuren Co.

It was apparent from the onset that the program was to be a lengthy one which would require years to complete. Once suitable techniques for measuring blocks to one or two parts in ten million were developed, it would still require about eighteen months to manufacture a gage block to the required specifications, and obtain sufficient stability data to indicate a trend. Thus, gage blocks made in 1957 or 1958 and under observation since 1958 have just begun to produce significant data. As a result of these observations, additional gage blocks are being designed for improved performance, but these will not show results until the end of 1960. In fact, any ideas developed in the program require about eighteen months to verify or disprove, and even then such a verification can be considered only as tentative pending observation over longer periods of time.

The purpose of this paper is to acquaint the reader with the scope of the entire program, to describe the materials and procedures being used to produce experimental gage blocks and the technical aspects involved, to describe the instrumentation and techniques developed to measure the gage blocks, and to present results on two of the selected materials which have been observed for stability sufficiently long to have produced significant trends.

2. Previous Investigations

The dimensional instability of hardened steel for gage blocks was described by Rolt [1] in 1929 and was recognized by Johansson and others prior to that time. In this country many excellent investigations have been concerned with the mechanism of instability of hardened steels and methods of alleviating the condition, notably the work of Scott [4], Cohen and his associates [5, 6, 7, 8, 9, 10] and Gippert and Butler [11]. As a result, hardened steel gage blocks undoubtedly can be made more stable today than they could many years ago, but more stringent requirements make further improvement necessary.

A set of gage blocks, said to be of uniform chemical composition and processed alike, was purchased in 1929 by the National Bureau of Standards from C. E. Johansson. These blocks were personally selected by Johansson for excellence of planeness, parallelism, surface finish and dimensional stability. The stabilizing treatment consisted of several cycles of annealing, hardening, tempering and a refrigeration treatment at 32° F, although the exact mechanisms involved were not fully understood. Several gage blocks had also been purchased from the same source two years earlier, in 1927, and at that time were presumed to have a similar composition and to have been given the same heat treatment. These two lots of blocks have been observed for length changes since their procurement, and the results have been varied [2]. Some have a history of constant and large growth (up to 2×10^{-5} in./in.), others have not varied more than 2×10^{-6} in./in., and the rest have remained stable or have shrunk slightly for a period of one to seven years and then have proceeded to grow. Two of the more stable and two of the less stable blocks were independently analyzed for retained austenite at the Timken Roller Bearing Co. [12] and the National Bureau of Standards; the results of the two laboratories agreed closely. The two more stable blocks contained about 11 percent of retained austenite. The least stable of the four had 20 percent, and the other unstable block had 15 percent. These tests not only indicate the large variation in stability that may be obtained with what must be presumed to be very small variations of composition and/or treatment, but also the inadequacy of judging dimensional stability on the basis of short-time observations. These blocks also supply evidence that the presence of some retained austenite need not necessarily promote dimensional instability, and may in fact contribute to stability. Observations based on measurements of one year or less and which indicate a desirable degree of stability, while a favorable sign, cannot be interpreted as final. Conversely, an indication of instability during the first year may portend further instability during future years, although the degree may change and exceptions have been noted.

Other observations of interest have also been reported. In individual blocks, rates of change in length have varied in different portions of the blocks so as to introduce uneveness to previously flat surfaces [13]. Several instances have been noted at the National Bureau of Standards and elsewhere, where the disturbance of a nongaging side surface by relapping or even by etching produced an immediate change in length. Such observations indicate the presence in hardened steel gage blocks, of a delicate balance of residual stresses that produces dimensional changes when disturbed.

The concern for the dimensional stability of hardened steel gage blocks has led to the pursuit of other methods of obtaining suitable materials. Rolt mentioned development work in England in the 1920's on unhardened gage blocks, coated with Stellite or electroplated iron or chromium. In more recent times development has been directed towards the use of stable carbides, such as tungsten or chromium, but these are considered to have an unfavorable coefficient of thermal expansion. Quartz single crystals have been considered frequently, but both the coefficient of thermal expansion and the thermal conductivity of quartz are too low to permit convenient use with most metals.

3. Materials

3.1. Requirements

a. Dimensional Stability and the Structural Relationship

Dimensional stability is a prime requirement for gage blocks, and stability is affected by structure and stresses within materials. All steels have a metastable structure when hardened to the 65 R_c specified for gage blocks. As such there is a tendency for the structure (mostly martensite) to reject carbon in the form of carbides and for the distorted

tetragonal lattice to become cubic. These processes, one of the stages of tempering, occur with relative ease at elevated temperatures and with great difficulty and slowness at room temperature, but the forces promoting the decomposition of martensite are present and can be expected to cause a reduction in volume of the gage block whenever a degree of decomposition occurs, no matter how slight. Hardened steel frequently contains various quantities of a second structural phase, austenite, which had failed to transform to martensite during the quenching and subsequent tempering operations. This phase is also metastable and can transform to martensite or bainite upon aging at room temperature. Such a transformation contributes to an increase in volume, a growth of the gage block. Superimposed upon the possible structural changes are the dimensional changes caused by the relief of residual stresses. Residual stresses are present in hardened steel gage blocks as the result of at least three processes; those put into the block by the thermal gradients formed on heating and cooling, those formed as the result of structural changes, and those resulting from surfaces plastically strained in the fabricating processes. The relief of residual stresses can occur slowly at room temperature and can produce either a growth or shrinkage depending on the sign and orientation of the stresses. The ideal solution to the stabilization of a hardened steel block would be to treat it so that the shrinkage caused by the decomposition of martensite would be counteracted by the growth contributed by the transformation of austenite; and the balance of these changes compensated for in full by changes in the residual stress pattern. Such a solution is not belived entirely feasible with hardened steels, but with careful selection of suitable heat treatment and processing, it is hoped to reduce dimensional changes resulting from these factors to the desirable limits of 2×10^{-7} in./in./yr.[3]

It was believed that the metastable structure alone was a severe deterrent to obtaining the degree of dimensional stability desired, and for that reason materials other than hardened steels were included in the program. Nevertheless, the wide usage and popularity enjoyed by hardened steel gage blocks precluded the omission of these materials, and efforts were directed towards improving their performance characteristics.

A fully annealed steel is at or near its equilibrium condition. Provided all residual stresses are absent, it should be dimensionally as well as structurally stable. It was reasoned that a thin nitrided case applied to such a structure would produce an overall stable block with high surface hardness and wear resistance, even if the thin case should show some instability. The modulus of elasticity of steel is about the same whether the steel is annealed or hardened, and the support given by a steel to its nitrided case is the same whether that steel is annealed or hardened, provided the elastic limit of the annealed steel is not exceeded. For the extremely mild service for which these ultra stable gage blocks are intended, an annealed core should be ample. The same reasoning was applied to types of hard surfacing treatment other than nitriding, and several have been considered including flame plating with tungsten carbide or aluminum oxide, chromium plating, and thermal spraying with nickel-chromium boron alloy.

b. Other Required Characteristics and Properties

Several other characteristics and properties are necessary or desirable in addition to dimensional stability. A high degree of surface finish, flatness of surfaces, and parallelism of opposite faces are required for precise measurements. These characteristics are related to the hardness and structure of the surfaces and their degree of development also depends on the skill of the final lappers. Ideally, the coefficient of thermal expansion, thermal conductivity, and other thermal properties should be approximately equal to those of high carbon steel. The necessity of this value of the coefficient of expansion is often misunderstood, and frequently materials with zero or very low coefficients have been recommended. In actual application, a laboratory grade of gage block is most frequently used to calibrate other high carbon steel gage blocks or tools by a comparison technique. Precise temperature control is essential and both the gage block and the measured piece must be allowed to come to the same temperature. If there are very slight fluctuations in temperature or its measurement, similar coefficients may produce a compensation of the error. Otherwise the exact fluctuation and temperature as well as the exact coefficients involved must be known and appropriate mathematical computations made. With high carbon steel, a temperature discrepancy of only 0.03° F is sufficient to change length by 2×10^{-7} in./in., which is equivalent to the desired maximum tolerance being sought in this investigation. Other thermal properties are not generally considered important factors, but in the development of the measuring techniques, they were found to have considerable significance (see discussion in section 5). Surface hardness and wear resistance are related conditions, although the relationship may not be as direct as is customarily believed. However, it is easier to obtain a good lapped surface on a hard material than on a soft one, and a block that wears excessively will not maintain its size after repeated wringings. The ability to wring well is a necessary requirement. This characteristic is a function of the quality of the surface and it may be related to the material. Resistance to atmospheric and fingerprint corrosion is desirable not only from the standpoint of appearance, but because the build-up of oxide films on gaging faces may cause a change in length and will produce a deterioration in wringing ability.

[3] The addition of a time factor to the tolerance is not normally done in gage block usage, since a tolerance is the maximum permissible variation from a given size. However, in a discussion of stability, where absolute stability may be unattainable, it is necessary to affix a time parameter. The time increment selected, one year, also implies that the gage block need not be calibrated at more frequent intervals than 1 year.

3.2. Selection and Application

The chemical compositions of the materials selected for investigation are given in table 1; the hardness values and available pertinent physical properties are summarized in table 2. The materials can be divided conveniently into three groups as follows:

1. Steels hardenable throughout by heat treatment—52100 modified, W4, D2, and T15 modified.

2. Steels readily amenable to surface hardening treatments—1010, 8620, 304, 410, 420, 17–4 PH and Nitralloy 135.

3. Materials other than steel—aluminum oxide and three forms of titanium carbide.

Some of the steels of group 2 are also hardenable, but without additional surface conditioning the final hardness obtained is too low for a gaging surface.

Several treatments have been applied to most of the materials. Thus, a total of 41 major combinations of materials and treatments are being investigated (table 3). For example, 8620 steel has been both pack and liquid carburized and has been carbonitrided to give three combinations. In addition there are some secondary variations in processing which are not reflected in the table, but are discussed later in the text or in an appropriate appendix. These consist of such items as differences in case thickness, grinding procedures, and in tempering or stress-relieving treatments.

Experimental blocks of only two steels, 52100 and 410 stainless, have been under observation for stability sufficiently long to have produced significant results. Data for these blocks were obtained from five major combinations on the 52100 steel and four on the 410 stainless. The 52100 steel was processed to produce five additional heat-treating variations, and one variation in grinding. Both directly quenched and martempered blocks were tempered to obtain a hardness of 65 R_c and also 62 and 60 R_c, and one group was martempered in oil instead of $NaNO_3$—$NaNO_2$. One major combination on the 410 was also given a variation in processing. In those blocks receiving single stage gas nitriding, the cases on the nongaging faces of some were completely removed by grinding, whereas on others only the white layer was removed. All of the other materials are under observation or are in various stages of processing. Therefore, all further discussion will be limited to these two steels.

TABLE 1. *Designation and chemical composition of the materials selected for investigation*

Materials	NBS designation	Chemical composition, percent by weight																
		C	Mn	P	S	Si	Cu	Ni	Cr	V	Mo	Co	W	Ti	Al	Al_2O_3	Cb	Fe
1010	L	0.083	0.42	0.002	0.023	0.029	0.13	0.075	0.088	0.005	0.01			0.006	0.057			bal
W4 tool steel	W	1.00	.44	.006	.011	.19	.074	.18	.31	.01	.045			.01	.01			bal
52100 mod	T	1.04	.68	.015	.013	.25	.23	.15	1.44	.01	.27							bal
8620	E	0.20	.80	.008	.012	.28	.12	.50	.51	.007	.19			.01	.047			bal
304 stainless	A	0.034	.4	.022	.014	.40	.16	9.3	18.9	.07	.10			.01	.01			bal
410 stainless	F	0.15	.36	.025	.008	.34	.13	.58	11.2	.02	.13			.01	.04			bal
420 stainless	C	0.37	.34	.010	.013	.30	.05	.13	12.2	.06	.1			.01	.01			bal
D2 tool steel	D	1.51	.28	.024	.005	.35	.08	.18	13.5	.7	.54			.01	.04			bal
Nitralloy 135 mod	N	0.40	.60	.014	.011	.26	.14	.21	1.4	.014	.34			.009	.89			bal
17–4 PH stainless	P	0.031	.34	.025	.005	.38	3.6	4.3	16.4									bal
Titanium carbide A [a]	KA	11.2						25.0			5.0			52.0			4.5	bal
Titanium carbide B [a]	KB	9.2						40.0	3.0		4.0			36.0	3.0		4.5	
Titanium carbide, steel binder	S	6.8							1.78					29.12				62.2
T15 mod, tool steel	V	1.55	.17		.006	.32	.08		4.5	6.0	.5	4.8	14.4					bal
Aluminum oxide [a]	Q															100		

[a] Nominal composition supplied by the producer; all others were analyzed at NBS.

TABLE 2. *Hardness and pertinent physical properties of the selected materials*

Materials	NBS designations	Hardness, annealed or as received	Density	Modulus of elasticity	Coefficient of thermal expansion	Thermal conductivity
			lb/in.^{3}	*psi*	*in./in./°F*	*Btu/ft*^{2}*/in./sec/°F*
1010	L	56 R_B	*0.284* [a]	*30×10*^{6}	*6.5×10*$^{-6}$ (68 to 212°)	*0.1112* (212°)
W4 tool steel	W	81 R_B	*.283*	*30*	*6.0* (68 to 212°)	*.0894* (212°)
52100	T	81 R_B	*.283*	*30*	6.3 annealed (85°)	
					6.4 65 R_c (85°)	
					6.4 62 R_c (85°)	
					6.2 60 R_c (85°)	
8620	E	87 R_B	*.283*	*30*	6.6 carbonitrided (85°)	
304 stainless	A	70 R_B	*.29*	*29*	9.0 (85°)	*.0313* (212°)
410 stainless	F	83 R_B	*.280*	*29*	5.4 annealed (85°)	*.0480* (212°)
420 stainless	C	93 R_B	*.278*	*32*	5.7 hardened (85°)	*.0443* (390°)
D2 tool steel	D	95 R_B	*.277*		5.7 hardened (85°)	*.0482* (390°)
Nitralloy 135 mod	N	94 R_B			6.5 nitrided (85°)	
17–4 PH stainless	P	29 R_c	*.280*	*28*	*6.0* annealed (70 to 200°)	*.0344* (300°)
Titanium carbide A	KA	68 R_c	*.228*	*50*	*6.0*	*.0770* (212°) est.
Titanium carbide B	KB	72 R_c	*.217*	*57*	*5.3*	*.0770* (212°) est.
Titanium carbide, steel binder	S	*57* R_c			*6.85* (70 to 1300°)	
T15 tool steel	V	98 R_B	*.305*	*52*	5.4 (85°)	*.0497* (32 to 1020°)
Aluminum oxide	Q	*>70* R_c			3.0 (85°)	

[a] Italics indicate values obtained from published data, or private communication with manufacturer. All others were obtained at NBS.

TABLE 3. *Summary of treatments used for the selected materials*

Materials	NBS designations	Treatments												
		Harden		Carburize			Nitride			Hard coat				As manufactured
		Direct quench, stabilize	Martemper, stabilize	Pack or gas, harden, stabilize	Liquid, harden, stabilize	Carbonitride, harden, stabilize	Gas, one stage	Gas, two stage	Liquid	Thermal-sprayed Ni-Cr-B	Flame-plated tungsten carbide	Flame-plated Al_2O_3	Electro-plated Cr	
1010	L			X	X	X				X			X	
W4 tool steel	W	X	X							X	X	X		
52100	T	X	X							X	X	X	X	
8620	E			X	X	X								
304 stainless	A						X		X					
410 stainless	F						X	X		X	X	X	X	
420 stainless	C	X					X							
D2 tool steel	D	X					X				X	X	X	
Nitralloy 135	N						X		X					
17–4 PH stainless	P						X							
Titanium carbide A&B	KA&KB													X
Titanium carbide, steel binder	S	X												
T15 tool steel	V	X												
Aluminum oxide	Q													X

Type 52100 steel is being used in this program principally, but not in every instance, as a through-hardened steel (group 1). It was selected for a prominent place in the program because it is widely used as a gage block material and for many kinds of tools and precision devices. Preliminary hardenability tests with a standard composition indicated failure to harden completely through with an oil quench in the size section required for this investigation. To obtain improved hardenability, a 52100 steel modified by the addition of 0.3 percent molybdenum was specified. A few blocks of 52100 were also employed in the annealed condition in an attempt to obtain improved stability and a coefficient of thermal expansion more favorable than that obtainable with the 410 stainless. A variety of hard coatings was applied to produce a suitable wear resistant surface.

Stainless steel, type 410, is a martensitic type of stainless with relatively low hardness after hardening, but it possesses several properties of interest for gage block application. In the annealed condition it has essentially a single phased structure (except for spheroidal carbides) with its elements in solid solution. Its surface can be hardened by nitriding and it has good resistance to atmospheric corrosion, either when annealed or hardened. Its major apparent deficiency is a coefficient of thermal expansion reasonably close to but slightly lower than high carbon steel. Nitriding was the principal process used to harden the surfaces of the 410, but the other treatments indicated in table 3 were also applied.

4. Procedures for Processing and Fabrication

4.1. As Received Steels

Each type of steel was obtained from a single heat and was commercially made in accordance with the accepted practices for that type, so that it would represent typical steels available on the market. With the exception of the T15 and 17–4 PH steels, each was hot rolled by the manufacturer into rectangular bars 1½ in. × ½ in. After hot rolling and straightening, all bars were fully annealed by the manufacturer and precautionary measures taken to hold decarburization to a minimum. The gage blocks made from these bars were rectangular parallelepipeds with a gaging length of 2 in. and other dimensions of 1⅜ in. × ⅜ in.

The typical microstructures of the 52100 as annealed and after hardening and the 410 as annealed are shown in figure 1.

4.2. Heat Treating of 52100 Steel

With hardened steels, the difficulty of completely balancing the dimensional changes occurring from structural transformations against residual stresses can be minimized by keeping these factors at low levels. As a starting point, it was decided to eliminate almost all of the retained austenite, which would reduce the possibility of growth and provide data on the stability characteristics of an austenite-free steel, and would possibly give a higher hardness and allow a higher tempering temperature or longer time at temperature to obtain a final hardness of 65 R_c. The higher tempering temperature was considered beneficial in the reduction of residual stresses. The standard procedure used for hardening by direct quench was to austenitize at 1550° F for 15 min and quench to room temperature in a quenching oil having an accelerated cooling rate.

The residual stresses resulting from thermal gradients on cooling from the hardening temperature are often reduced by martempering. The martempering treatment adopted consisted of austenitizing in a chloride bath at 1550° F for 15 min, quenching in a sodium nitrate-nitrite bath at 300° F for 30 sec, and then quenching to room temperature in oil.

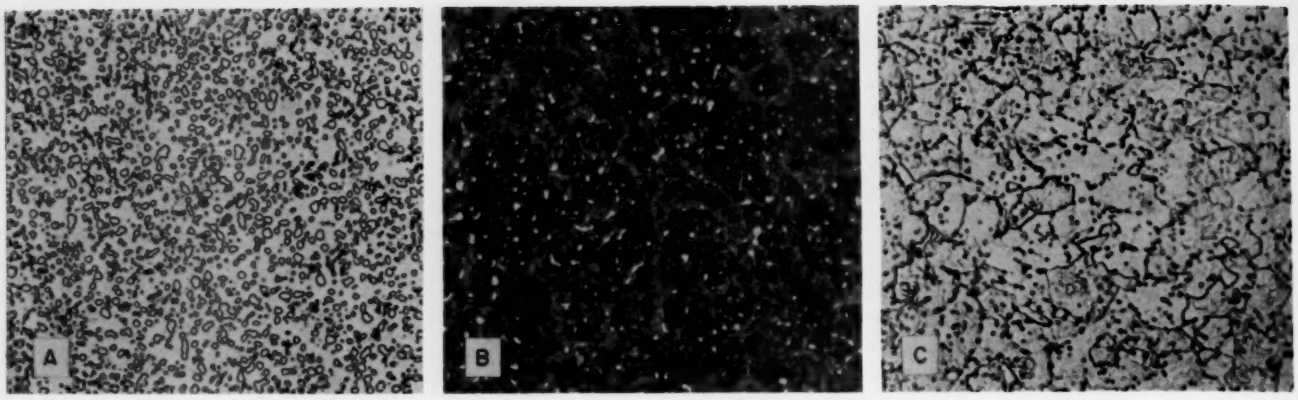

FIGURE 1. *Microstructure of 52100 and 410 stainless steel.* ×750

A. 52100, annealed, etched with 1% Nital.
B. 52100, hardened, etched with 1% Nital.
C. 410 stainless, annealed, etched with hydrochloric + picric acids in ethanol

Both of the above hardening treatments were followed by a stabilization treatment designed to remove retained austenite, temper the martensite, and reduce residual stresses. This treatment for blocks hardened to 65 R_c consisted of an immediate refrigeration at −140° F for an overnight period (18 to 22 hr), followed by a tempering treatment at 250° F for 1 hr, a second refrigeration treatment at −140° F for an overnight period, and a final temper at 250° F for 9 hr. The interval between steps was kept as short as possible. Details of the investigation performed to establish this stabilization treatment as an optimum for the 52100 steel are given in appendix A.

The temperature of the final temper was raised in some instances where a hardness of less than 65 R_c was desired. The prescribed hardness of 65 R_c is believed to have been an arbitrary selection to obtain good wear resistance, and it was thought that a block with slightly lower hardness such as 62 or 60 R_c might be satisfactory from a wear standpoint and possess greater stability. Details of the heat and stress relieving treatments given individual blocks, and the final hardness of each, are shown in table 4. A stress relieving treatment was applied to all gage blocks after finish machining and prior to final lapping.

4.3. Nitriding of 410 Stainless Steel

The 410 stainless was the first of the group 2 materials (steels readily amenable to surface hardening treatments) studied. The 410 steel was to be used in the annealed condition only, with the surface nitrided or otherwise hardened. The details of nitriding and stress relieving of each block are given in table 4.

Tests were run to establish suitable procedures for nitriding this steel. No unusual techniques were required for effective nitriding. The surfaces of the blocks were prepared by grinding and thereafter were scrubbed in an aqueous detergent just prior to nitriding. A nitriding time of 40 to 44 hr at 1010 to

TABLE 4. *The heat treatment and hardness of gage blocks* [a]

Gage block no.	Method of hardening	Final temper, 9 hr, ° F	Stress relief, 3 hr, ° F [b]	Date of final stress relief	Hardness R_c [c]
T-301	Flame plate, tungsten carbide.	Not applicable	975	May 1957	72
T-302	Flame plate, tungsten carbide.	Not applicable	975	May 1957	72
T-309	Thermal spray, Ni-Cr-B.	Not applicable	975	July 1957	62
T-312	Thermal spray, Ni-Cr-B.	Not applicable	975	July 1957	62
T-314	Electroplate, Cr	Not applicable	400 (5 hr)	Jan. 1958	68
T-318	Electroplate, Cr	Not applicable	400 (5 hr)	Jan. 1958	68
T-337	Martemper	250 [e]	240	Jan. 1958	65
T-341	Martemper	250 [e]	240	Jan. 1958	65
T-343	Direct quench	250	240	Jan. 1958	65
T-344	Direct quench	250	240	Jan. 1958	65
T-348	Direct quench	250	240	Jan. 1958	65
T-351	Martemper	350	340	Jan. 1958	62
T-356	Martemper	350	340	Jan. 1958	62
T-357	Martemper	450	440	Feb. 1958	60
T-359	Martemper	450	440	Feb. 1958	60
T-369	Martemper (oil)	250	240	Feb. 1958	65
T-377	Direct quench	350	340 (4 hr)	May 1958	62
T-378	Direct quench	350	340 (4 hr)	May 1958	61
T-384	Direct quench	475 (23 hr)	465 (4 hr)	May 1958	59
T-386	Direct quench	475 (23 hr)	465 (4 hr)	May 1958	59
F-302	Nitride	Not applicable [d]	975	Mar. 1957	67
F-305	Nitride		975	Mar. 1957	70
F-316	Flame Plate, tungsten carbide.		975	May 1957	72
F-317	Flame plate, tungsten carbide.		975	May 1957	72
F-322	Nitride, 2 stage		975	Mar. 1957	67
F-323	Nitride, 2 stage		975	Mar. 1957	67
F-325	Nitride, 2 stage		975	Mar. 1957	65
F-327	Nitride, 2 stage		975	Mar. 1957	67
F-330	Nitride		975	Apr. 1957	65
F-333	Nitride		975	Apr. 1957	69
F-340	Nitride		975	Apr. 1957	67
F-349	Nitride		975	July 1957	72
F-352	Electroplate, Cr		400 (5 hr)	Jan. 1958	68
F-358	Electroplate, Cr		400 (5 hr)	Jan. 1958	68
F-360	Nitride		975	July 1957	67
F-361	Nitride		975	July 1957	69
F-363	Nitride		975	July 1957	69

[a] All gage blocks were nominally 2 in.×1⅜ in.×⅜ in.
[b] Stress relief was applied to all gage blocks after finish machining and prior to final lapping.
[c] This value represents hardness of the case or coating where applicable. Where appropriate, hardness was measured with a micro tester such as the Vickers and converted to R_c.
[d] This applies from F-302 through F-363.
[e] The length of time held at final temper is uncertain.

1030° F produced a case about 0.009 in. thick. Dissociation of the ammonia was maintained at 20 to 25 percent. As the result of nitriding, the blocks grew different amounts in each of the three directions; on the order of 0.0025 in. in the 2 in. dimension, 0.0020 in. in the 1⅜ dimension, and 0.0015 in. in the ⅜ in. dimension.

The two stage Floe process was also employed in an attempt to reduce or eliminate the white layer formed with conventional single stage nitriding. In this process, the first step consisted of nitriding for 20 to 24 hr at 1000° F with a dissociation of 20 to 25 percent. Thereafter, the temperature of the retort was raised to 1050° F and cracked ammonia blended with the uncracked ammonia to give a dissociation of 75 to 80 percent. The second stage was maintained for about 24 hr.

The microstructures of a nitrided case produced by the single stage method are shown in figure 2. The hardness of the case nitrided by the single stage process exceeded 1260 KHN (Knoop Hardness Number, 200 g load) over its entirety. The hardness of the case produced with the two stage process was somewhat less than the case formed with single stage nitriding. Immediately adjacent to the surface the hardness was 880 KHN, the greater portion of the case had a hardness of 1020 KHN, and next to the core, hardness fell to 930 KHN (500 g loads). All of these values are appreciably greater than the minimum of 65 R_c specified for gaging surfaces.

In the grinding and lapping operations applied to the gaging surfaces after nitriding, approximately 0.0025 in. was removed, which left from 0.006 in. to 0.007 in. of the case. The finish produced on the nitrided 410 blocks by commercial lapping is worthy of note. It was superior to finishes produced on hardened 52100 steel, but took about one third more time for the removal of equivalent amounts of stock. The final microfinish, as measured with a tracertype surface roughness instrument, closely approached zero. Wringing characteristics were excellent. An interferogram of the surface of one of these blocks and a photograph of the surface of another is shown in figure 3. There was a sharp interface and an intermediate zone of nitrogen diffusion between the case and the core (fig. 2), which was unlike the gradual blending associated with the nitrided case of Nitralloy. This type of interface is generally believed to be a plane of weakness in the steel and a region where spalling can occur easily. After removal of the white layer, several blocks were subjected to rough handling, including severe grinding and impact deformation of lapped surfaces, and no spalling occurred. The mild mechanical service to which this type of gage block should be subjected further reduces the possibility of trouble from spalling.

The corrosion resistance of the case is different from that of the original steel. As can be seen from the microstructure in figure 2, dilute nitric acid and Vilella's reagent attack the nitrided layers more readily than the ferritic matrix. On the other hand, the nitrided surfaces are less subject to coating by tinted surface films in such processes as stress relieving in a cracked ammonia atmosphere. Nitrided and lapped surfaces with no protective wrapping, oil or wax film, or other corrosion preventive treatments have been exposed for two years under normal indoor conditions of humidity and temperature in the atmosphere of Washington, D.C., and have shown no tendency to become dull or to rust.

The single stage nitriding treatment was applied to two series of blocks that were fabricated differently after nitriding. In one series the nitrided layer was completely removed from the four nongaging faces by grinding parallel to the 2 in. dimension. In the other series, only about 0.002 in. was ground from each nongaging surface so as to produce a bright nitrided finish. The first series, as a result, was finished with nitrided cases on the two gaging faces only, while the second series had nitrided cases all over.

In a third series, the blocks were nitrided by the two stage process, and the four nongaging surfaces were not ground or otherwise disturbed after nitriding.

4.4. Hard Coatings

Both the 52100 and the 410 stainless were coated with hard-facing materials in four different ways: 1, Thermal spraying with a nickel-chromium-boron alloy; 2, flame plating with tungsten carbide; 3, flame plating with aluminum oxide; 4, electroplating with chromium. In each instance the base material was in the annealed condition. The stability of the 410 stainless thermally sprayed with nickel-chromium-boron is not reported in this paper because the blocks required additional shortening and the final lapping has not been completed. No report is made on these two steels flame plated with aluminum oxide because of the difficulties of obtaining a good interferometric fringe pattern on this surface. The same difficulties were not experienced on blocks of solid aluminum oxide incorporated into the measuring program at a later date. Details of each coating and the methods of application are given in appendix B. Subsequent stress relief treatments and the final hardness of each coating are given in table 4.

4.5. Fabrication

The hardening and stabilization of the 52100 steel, the nitriding of the 410 stainless, and the chromium electroplating were carried out in laboratories of the National Bureau of Standards. Thermal spraying of nickel-chromium-boron alloy and flame plating with tungsten carbide were applied by commercial firms. All machining operations except lapping were performed in the Bureau's machine shop. Lapping was done by several commercial firms [4] in accordance with the best commercial practices. The procedures for grinding and other details of fabrication are given in appendix C. Considerable care was exercised in fabricating these blocks and recording the details thereof, because of the potential significance attributed to residual stress patterns induced by these processes.

[4] Brown & Sharpe Co., Dearborn Gage Co., DoAll Co., and Pratt and Whitney Co., Inc.

549993—60——2

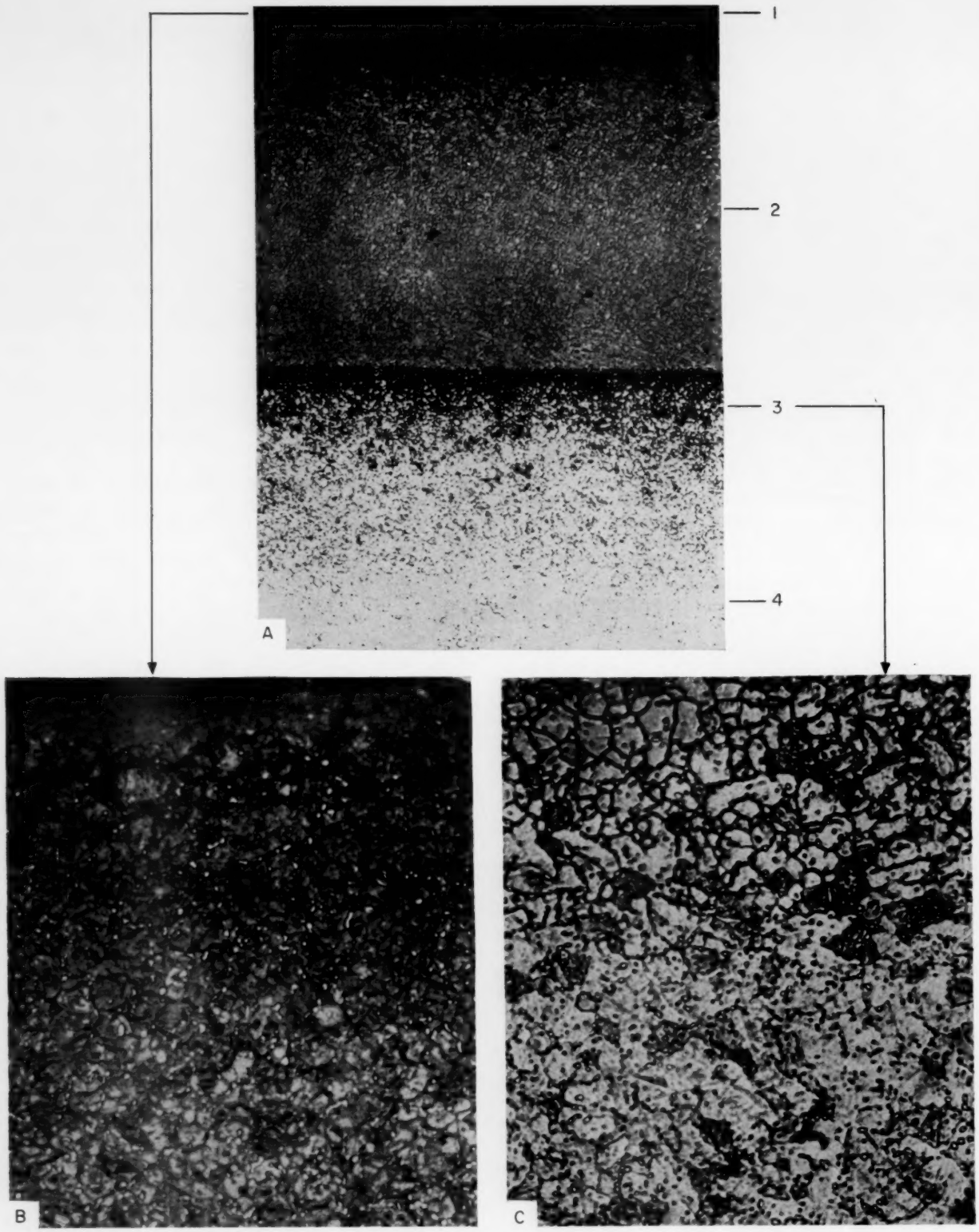

FIGURE 2. *Microstructure of nitrided 410 stainless steel.*

Dual etch: 1% Nital followed by Vilella's Reagent.
A. 1. White layer; 2. Nitrided case; 3. Intermediate zone; 4. Core; ×250.
B. Case. White layer is at the top and appears gray with etchants used. ×1000.
C. Intermediate zone and core. ×1000.

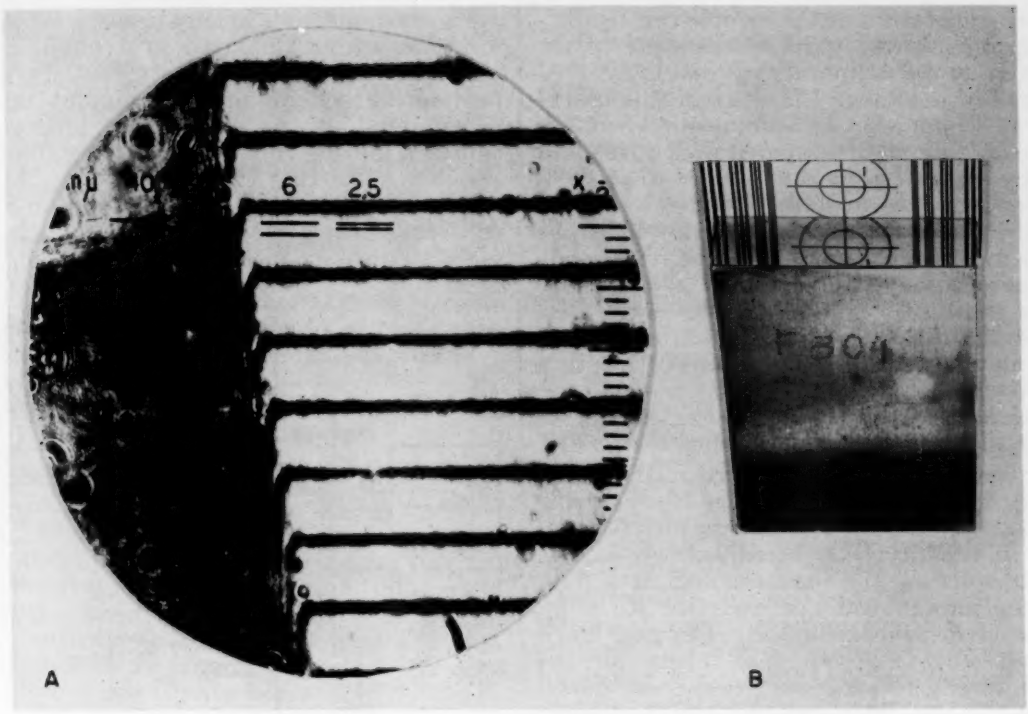

FIGURE 3. *Nitrided surfaces on initially annealed 410 stainless steel.*

A. Interferogram (courtesy the DoAll Co.). The interference fringe interval is about 250 mμ.
B. Reflection from mirror-like surface. The form of chart has no significance other than to provide an image for reflection.

5. Metrology

5.1. Development of the Measuring Technique

The measurement phase of the stability program required a testing technique that would provide frequent measurements of a large number of test samples and precision of length measurement on the order of 2 parts in 10 million.

The degree of precision would determine the time interval required to acquire significant data indicating change of length of the test samples. Frequent measurements would provide information on the nature of the change. As the test samples are 2 in. in length, a practical limitation to the error of measurement of 0.4μ in. was established as a goal (0.2μ in./in.).

To establish the change in length of the test samples it was necessary to define a length scale whose stability characteristics were known. An ideal procedure would be to compare the sample with a length scale formed by the interference of light of known wavelength. It is generally believed that a wavelength of light, λ, is constant in time and may be expressed by

$$\lambda = \frac{c}{\mu\nu}$$

where c is the velocity of light in vacuum,
μ is the index of refraction of the material through which the light is transmitted,
ν is the frequency of light radiation.

Procedures and instrumentation are available that provide such absolute measurements of the test samples [14]. Although the Bureau is now engaged in the development of procedures and instrumentation to achieve precision in such absolute measurements to 1 or 2 parts in 10 million, the best that could be done when the stability program was initiated was 1 part in 1 million.

The precision of such measurements is limited by the differing effects of temperature on the sample and the interference scale formed in the air surrounding the sample. The index of refraction of air is dependent upon temperature, so from the equation it is observed that the wavelength of light is dependent upon temperature. For visible light in an approximate standard atmosphere (760 mm Hg, 68° F), the wavelength scale might be considered as having a coefficient of expansion approximately 1/10 that of steel, which was the material used for most of the stability samples. In addition, problems are encountered if the temperature of the measurement area is not stable. Because of thermal lag, the temperature of the air in which the wavelength scale is formed will, in general, be different than the temperature of the sample. For example, Evans [15] reports the thermal lag time of a polished iron cylinder of 2 cm diam immersed in air to be 2,000 sec., causing the axial temperature of the rod to differ from air by 1.0° F when the temperature of the air is increasing 1.8° F per hour. Thus the relationship between the sample and the wavelength scale is critically dependent upon temperature, and

the effective temperature of the sample can be difficult to determine as the axial temperature of the sample is likely to differ from its surroundings.

One method of avoiding difficulties of this nature is to resort to comparison measurements where the length of the test sample is compared with a standard length having thermal properties similar to those of the sample. A specially designed optical interference comparator [16] of a type originally developed by Kösters [17] was available that could be relied upon to provide precision to approximately 1 part in 10 million. As most of the test samples were steel blocks 1⅜ in.×⅜ in.×2 in. long, it was considered highly desirable to select as a standard of length a steel gage block with the same cross sectional size and nominal length and having a long history of absolute length measurements to indicate stability.

Absolute measurements made at irregular periods since January 1954 on a 2 in. steel gage block serving as a length standard for the NBS Engineering Metrology Section indicated it to be exceedingly stable. The curve best fitting the measurement data indicated that its growth had not exceeded 0.2 μ in. since the measurement series began. This gage block was chosen as the basic reference length for the stability measurement program. Since the initiation of the program this block has been subjected to more frequent absolute length measurements. These recent measurements continue to justify its choice as a stable standard.

The difficulty encountered in using the interference comparator as the measuring instrument was an insufficient testing capacity to measure all the test samples as frequently as desired. For test samples of 2 in. length, a minimum time of 4 hr is considered necessary between the operation of wringing the test specimen to the platen and the comparison of this specimen with the master gage block. This interval is believed necessary to allow the test specimen to attain thermal equilibrium with the master block and to allow the wringing film to attain its minimum thickness in case more wringing lubricant is used than is necessary. During this time interval, it is necessary to maintain the platen in the location occupied during the measurement. Thus, the need for this time interval limited the test capacity of the interferometer.

During the initial months of investigation of any specimen, it was desired that its length be determined weekly. Thus it was foreseen that a test program having a capacity of 50 measurements a week was required. The classical methods of precise length comparison rely upon the comparison of static lengths and are time consuming because they require thermal equilibrium. The most apparent solution to the problem of increasing test capacity was to abandon the concept of static length comparisons and replace it with the concept of dynamic length comparisons. In general, such comparisons had not been refined to a degree giving the precision that was required. It was questionable whether the instrumentation usually employed in such comparisons would provide the necessary repeatability.

Figure 4 indicates schematically a typical mechanical comparator employed in dynamic length comparisons. The measuring styluses are mounted in reed spring systems to avoid binding that could be encountered in piston-cylinder arrangements. A core of a moving core transducer is mounted on each stylus. A moving core transducer consists of a primary coil and two oppositely wound secondary coils. The relative potential induced in each secondary is dependent upon the position of the core.

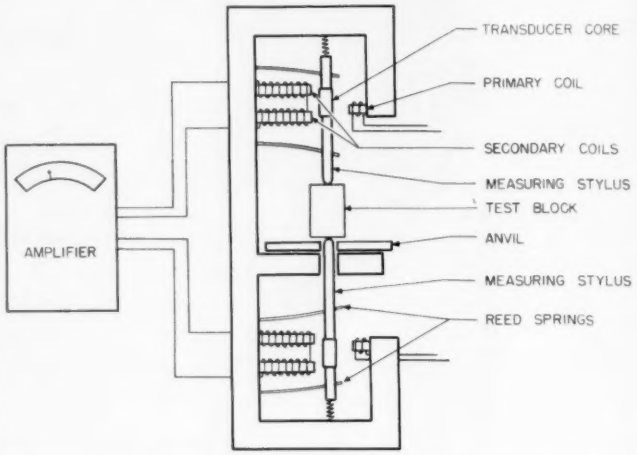

FIGURE 4. *Elements of a mechanical comparator of length.*

Thus, the position of the stylus is indicated. Amplification of the signal is provided so that deflection of the milliammeter needle magnifies movement of the stylus by approximately 2×10^5. In this instrument the top and bottom transducers provide opposing signals of equal magnitude so that effects of translation of the test piece in the direction of its critical length are cancelled in the combined signal. This reduces the need for extremely critical seating of the test piece on the anvil. Comparison of length is accomplished by noting the difference in readings of the calibrated scale as the test pieces are successively positioned between the measuring styluses. This type of comparison is referred to in this paper as a dynamic comparison because of the handling and transportation of the test piece just prior to the measurement, which in general, will cause growth or shrinkage due to change of thermal conditions. Attempts are usually made to control these thermal changes within practical limits.

In determining whether or not this type of length comparison would provide the precision necessary for the stability measurements, it was necessary to distinguish errors in comparison caused by lack of control of the dynamic effects from those due to the inherent randomness of the measuring instrument. The former could possibly be reduced to within acceptable limits, whereas the latter would establish the limit of precision that could be obtained with available instrumentation.

An indication of what might be expected in inherent randomness of the mechanical comparator was obtained in an acceptance test conducted when the

instrument was purchased. This test measured the relationship between the meter reading and the pressure exerted by the measuring stylus, and avoided the effect from dynamic changes mentioned as it is independent of length. The results indicated that the inherent randomness of the instrument might possibly be limited to 0.5 μ in. in comparisons of length. If this magnitude was a true indication of the instrument's potential performance in length comparisons, it was considered possible to achieve the desired precision provided thermal effects could be controlled to effectively eliminate or nullify the dynamic changes in length of the test specimens.

5.2. Concepts Applied in the Measurement of Dynamic Length

To effectively eliminate the dynamic changes, the comparison of test specimens would be required under temperature conditions that restricted temperature variation of the specimens to less than 0.02° F. This seemed impractical. An approach to the problem was selected that attempts to nullify the dynamic changes in the comparison. It was reasoned that if test specimens to be compared could be treated identically during the comparison and if the specimens responded to thermal variation in an equal manner, dynamic changes of length could be nullified. Therefore the test specimens were divided into groups, all blocks in a group having similar thermal properties. One block of each group was selected as a secondary master. As the secondary masters would in general have different thermal characteristics than the primary master block, it was planned to compare the secondary masters with the primary master by using the interference comparator The secondary masters would then be used in dynamic comparisons with test specimens of their respective groups using the mechanical comparator.

Traditionally the secondary master would be compared with each test specimen in its group. This technique, however, gives special emphasis to the test specimen that was designated as a secondary master and thus violates the requirement of equal handling of all test specimens to nullify dynamic changes occurring during the comparisons. A more appropriate comparison system is one that has been used at NBS for the comparison of line standards of length with the national standard of length [18]. In this system, the master is handled as one of the test specimens of a group. All possible comparisons of specimens within the group are made to form one intercomparison test. If the group consists of n specimens, $n(n-1)$ comparisons are made of $n(n-1)/2$ pairs. For example table 5 indicates the comparisons to be made of a group containing four specimens, the secondary master A and test specimens B, C, and D.

A possible method of reducing the data is to sum the columns and divide by the number of specimens in the group; e.g., $(\Sigma/4)$.[5] This provides an average length of the specimen represented by the column relative to an average length of specimens within the group. The final results are obtained by forming all differences of column footings; i.e., the length of any specimen within the group relative to the length of any other specimen within the group is determined. Thus the lengths of B, C, and D can be determined relative to the length of the secondary master A and equal handling of all blocks of the group can be maintained. Each final result (difference in column footings) is then subtracted from the appropriate direct measurement; e.g., the column footing of B minus the column footing of A is subtracted from the actual measured comparison $B-A$. This provides a residual. A group of n test specimens provides $n(n-1)$ residuals that may be used to evaluate the precision of the results of an intercomparison test which consists of $n(n-1)$ comparisons.

Conventionally, the sum of the squares of the residuals is determined and the probable error or the standard deviation computed. A multiple of this value is considered to represent a limit to be assigned to the test result. A prediction is made that a certain percentage of repeated tests of the same speci-

[5] The usual statistical approach is to immediately reduce the measurement data by a least squares method which involves averaging the data obtained in the two measurements involving a given pair. Then the value appearing below the diagonal is the mirror image of the value of the reverse comparison appearing above the diagonal. This provides greater precision in the result as it employs all measurement data involving a given specimen in evaluating its result. However, this procedure can mask the presence of bias such as drift. In the initial development of the measurement technique, precision of results was of secondary importance to the information concerning systematic errors that could be derived by analysis of the spread of the actual comparisons. By initially employing the method of data reduction shown in table 5, the characteristics of the drift error were more apparent and a decision could be made as to whether particular measurement sequences, which are sometimes inconvenient, were required. In section 5.3. and appendix D, an evolution from this simple program to the employment of least squares solution and the type of measurement sequence finally utilized is described.

TABLE 5. *Comparisons performed in an intercomparison test on a group containing four specimens*

	A	B	C	D
A	•	$B-A$	$C-A$	$D-A$
B	$A-B$	•	$C-B$	$D-B$
C	$A-C$	$B-C$	•	$D-C$
D	$A-D$	$B-D$	$C-D$	•
Σ	$4A-(A+B+C+D)$	$4B-(A+B+C+D)$	$4C-(A+B+C+D)$	$4D-(A+B+C+D)$
$\Sigma/4$	$A-\frac{(A+B+C+D)}{4}$	$B-\frac{(A+B+C+D)}{4}$	$C-\frac{(A+B+C+D)}{4}$	$D-\frac{(A+B+C+D)}{4}$

mens, using the same measuring technique and equipment, will provide a similar test result within plus or minus this limit. For instance, it is usually accepted that three times the standard deviation will provide a limit within which 99.7 percent of the test results of a given specimen will be similar. This, in general, is a fallacy as such a condition depends upon the residuals being centered on zero and having a normal or Gaussian distribution.

Therefore, to obtain a better insight of the probable precision of the results of an intercomparison test and to possibly diagnose the type of measurement error occurring during an intercomparison test, it was decided to plot frequency distributions of the residuals, i.e., the magnitude of each residual plotted against the number of occurrences. It soon became evident that these distributions could serve as a powerful tool in the development of a satisfactory measuring technique. First, they allowed for a better estimate of the meaning of calculated probable error or standard deviation in regard to the precision of the results of an intercomparison test. Second, they indicated the success achieved in eliminating bias from the comparison procedures and indicated whether this success was temporary or was consistent in repeated intercomparison tests. Third, they served as a basis for hypothesizing the source of error and then served to indicate the effects of test refinements introduced in attempts to eliminate or nullify these sources.

The general procedure used in refining the comparison techniques was first to hypothesize from the residual distribution the nature of the systematic and random error. Then, when possible, the sequence of the comparisons was changed in an attempt to nullify the systematic error in the final results. When successful, a truer picture of the nature of the systematic error was obtained from the frequency distribution of the residuals. Attempts were then made to eliminate the systematic error from the comparisons until a random distribution of residuals was indicated. Even if systematic errors are nullified in the final results there is an advantage in eliminating the systematic errors from the individual comparisons. This can be accomplished by modification of the test procedure or fixtures in such a way as to eliminate the hypothesized systematic errors, or in some cases can be accomplished by variation in the treatment of the data; e.g., employing a least squares solution in the data reduction. When more random distributions are obtained as a result of such action, it not only verifies the hypothesis of the systematic error but provides frequency distributions of residuals that can more adequately indicate the origination of new systematic error in succeeding intercomparison tests. An example of this type of approach in the refinement of the testing technique is treated in appendix D.

First, with ten specimens and then with eleven in an intercomparison group, the comparison sequences were changed and, where indicated by frequency distributions, modifications were made in handling of the test specimens and in the test fixtures. Section 5.3. contains some specific examples of such refinement and includes some examples of frequency distributions obtained during the development of the testing technique. Figure 5 indicates typical frequency distributions obtained during the initial (fig. 5A) and more advanced (fig. 5B) phases of the development of a satisfactory measuring method for the stability project.

5.3. Statistical Control

One of the important features in the development of the measurement method was the use of the results of statistical analyses of the data to guide the evolution of a measuring technique. The measuring technique and the least squares method of data reduction finally employed actually evolved from a series of modifications in procedure and equipment made on the basis of information obtained from the statistical analyses. This statistical approach was then further utilized as a control in monitoring the measuring technique to insure continuing uniformity.

A number of examples illustrate such utilization of these statistical analyses in the stability measurement program. The first of these involves a modification of the comparison schedule (order in which the 110 comparisons which make up an intercomparison test are performed) based on information obtained in the statistical analyses of the data. Utilizing the method of computation illustrated in table 5, the frequency distributions of the residuals in some of

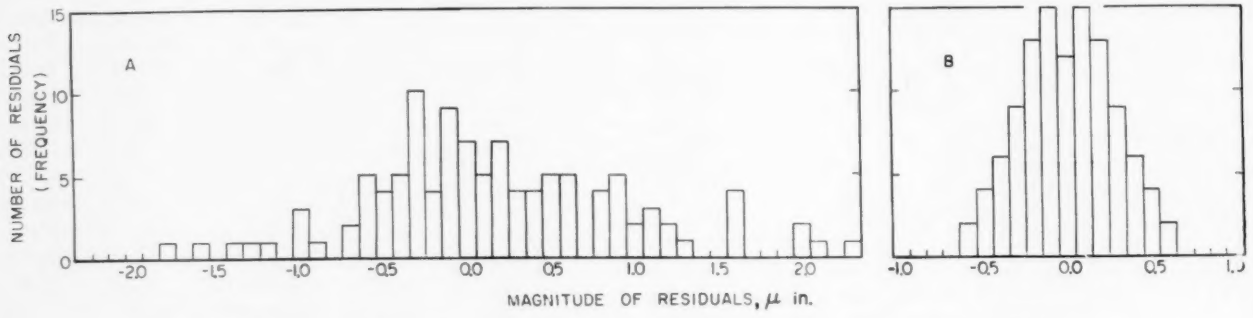

FIGURE 5. *Example of frequency distributions of residuals obtained in two intercomparison tests.*

A. Typical distribution obtained from an intercomparison test conducted during the initial development phase of the measuring technique.
B. Typical distribution obtained from an intercomparison test conducted during a more advanced development phase of the measuring technique.

of the early intercomparison tests in the program showed that the medians of these distributions were located at some point other than zero. This indicated a systematic error or drift which caused the system to quite consistently give either a larger or a smaller reading on each successive insertion of a sample into the comparator.[6] An example of a distribution evidencing such a condition is shown in figure 6 where the median of the distribution is indicated by the arrow. This particular distribution obtained in one of the early intercomparison tests indicates a drift of three 10-millionths of an inch.

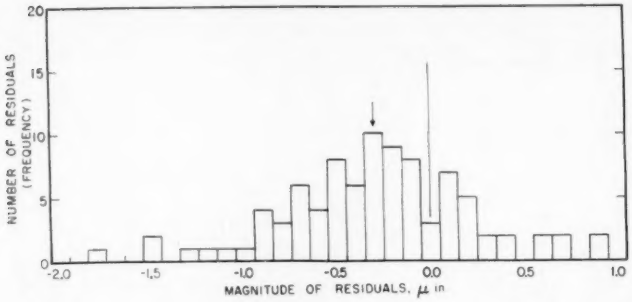

FIGURE 6. *Frequency distribution of residuals obtained from an intercomparison test showing the presence of a drift effect.*
Arrow indicates median of distribution.

To understand why the detection of this drift effect through statistical analysis of the data led to a change in the comparison schedule, it should be noted that there are two possible comparisons between any two sample blocks. Thus if the two blocks are block A and block B, the two comparisons would be block B against block A and block A against block B. The B against A comparison is made by placing block A in the comparator, obtaining a scale reading, and then placing block B in the instrument and again noting the scale reading. Subtracting the reading on block A from that on block B gives the result of the first comparison, block B minus block A. Similarly, the second comparison results in block A minus block B. Now, however, if the drift effect causes the system to give a larger or smaller reading on each subsequent block, it is quite evident that the first comparison results not in block B minus block A, but in block B minus block A plus a drift factor which is either positive or negative. Similarly, the second comparison gives block A minus block B plus a drift factor. The first effort to overcome this drift was an effort to insulate the final results of the intercomparison test from the drift effect. If the drift was constant in time, it would, in fact, be a constant error and would be nullified automatically and not affect the final results. (See footnote 13, appendix D.) Its effect on each measurement which would appear in the residuals could also be eliminated by employing a least squares solution in reducing the measurement data. This involves the following averaging procedure applied to the measurement data before the columns are summed. Consider again blocks A and B and let them have actual lengths a and b respectively. Let the drift effect contribute a variation in the length determinations of an amount $\alpha\Delta t$. Then the first comparison gives as a result $(b-a+\alpha\Delta t)$ and the second comparison gives $(a-b+\alpha\Delta t)$. Now if the result of the second comparison is subtracted from that of the first, and this quantity then divided by two, the drift effect is eliminated and for the first comparison the adjusted observed result, $(b-a)$, can be substituted. Similarly the negative of this, $(a-b)$, is obtained as an adjusted observed result for the second comparison.

On detection of this drift effect, such a least squares solution was quickly introduced into the data processing. However, at the time this drift was detected, the comparison schedule then employed called for a considerable lapse of time between the first and second comparisons on each pair of blocks. It was then thought quite possible that the drift would in general be a nonlinear function with respect to time, and in this case, of course, the least squares procedure would be ineffective in eliminating the influence of the drift effect upon the residuals. In addition it was believed that a more appropriate schedule of comparisons could be used to effectively eliminate such a nonlinear drift from the results of the intercomparison tests. For this reason, the comparison schedule was modified in such a way as to follow the form shown in appendix D, table 10. This schedule was in turn modified to follow the form shown in appendix D, table 11 when it was recognized that successive comparisons of a pair of blocks could cause inhomogeneous comparison data. Thus the detection of the drift effect through statistical analysis led directly to a modification in the measurement program.

The statistical analyses of the data resulted in a number of other modifications of the measuring technique which are not here included, but an example of how a modification in the actual handling of the sample blocks resulted from information obtained in the statistical analyses might be illustrative. As was indicated above, the measurement of dynamic length depends to a very great extent on a symmetry of handling of the samples being measured. The symmetry of handling employed in the stability measurements evolved largely from consideration of the statistical controls. At an early stage in the development of the measuring technique here employed, it had been determined that in making the two comparisons between any pair of blocks it was necessary to physically handle the two blocks together as a pair rather than individually. Thus, in making the comparisons the two blocks involved in any two comparisons would be picked up together with the gloved hand and placed in the comparator.[7]

[6] Employing the method of least squares solution in the reduction of the data would force the medians of the frequency distributions of residuals to zero and could reduce and possibly distort the indication of drift shown by the residuals.

[7] When it was realized that blocks were to be handled in pairs, it was decided to employ, if possible, the operator's hand as a tool to convey the blocks through the comparison procedures. Other tools, such as tongs, introduced too great a possibility that mechanical shock, because of accidental dropping, would be introduced as an uncontrolled factor affecting stability. To minimize thermal effect, cotton flannel gloves were used.

The first and then the second comparison would be made and the blocks then returned as a pair to the storage area. Such a handling procedure, it was believed at the time, resulted in the two blocks in any comparison receiving equal, symmetrical handling. Examination of the residual frequency distributions obtained at this time, however, indicated that the manner in which the blocks were held in the gloved hand had a significant effect on the residuals of the intercomparison tests. At the time this effect was noticed, the blocks were being held as illustrated in the upper portion of figure 7 with one block of the pair exposed to the palm of the glove insulated hand. The residual distribution obtained in an intercomparison test in which this handling technique was employed is shown in figure 8. It should be noted that the total distribution is plotted at the bottom of the figure, and this distribution is then broken down into the two distributions shown in the upper portion of the figure. The distribution of residuals resulting from first comparisons between each pair of blocks is shown in the central plot, while that obtained from second comparisons is plotted at the top of the figure. It can be seen that the medians of the first and second comparison distributions, shown by the arrows, are not alined, but are separated by seven 10-millionths of an inch.

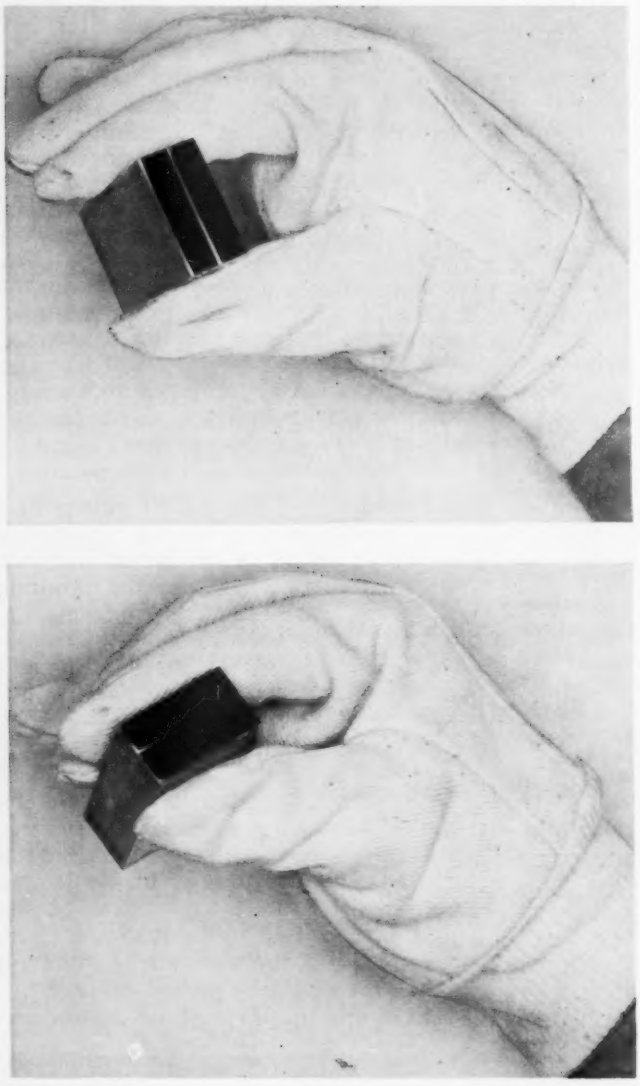

FIGURE 7. *Manner of handling two gage blocks for comparison measurement.*

Top—Handling that produced asymmetrical thermal effect.
Bottom—Modification employed to correct asymmetrical condition.

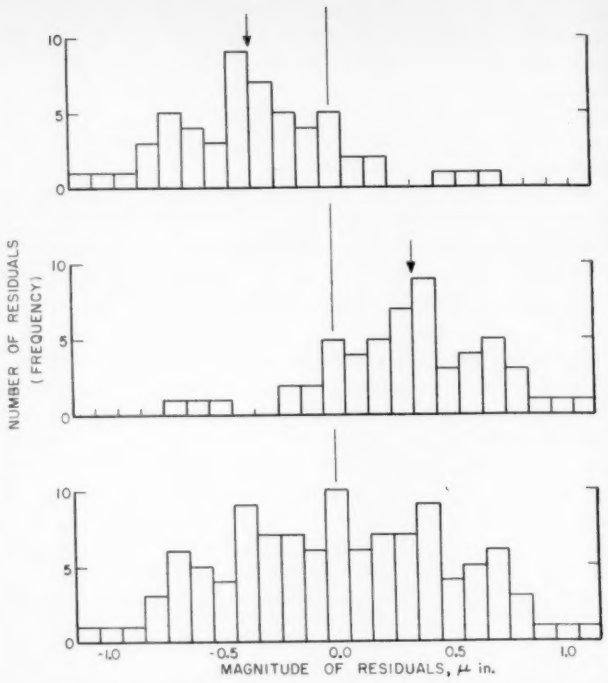

FIGURE 8. *Frequency distribution of residuals obtained in an intercomparison test.*

Handling introduced asymmetrical thermal effects as shown by separation of medians.
Top—Distribution obtained from second comparisons of pairs of gage blocks.
Center—Distribution obtained from first comparisons of pairs of gage blocks.
Bottom—Total distribution of residuals.

The asymmetry suspected as the cause of the split between the medians of the first and second comparison distributions shown in figure 8 was in the handling of the blocks; one block was exposed to the palm of the gloved hand while the other block was not so exposed. This can be seen in the illustration of the handling technique at that time employed, as shown in the upper portion of figure 7. This suspicion led to changing the manner in which the blocks were held to that shown in the lower view of figure 7. When this handling technique was employed the residual distribution shown in figure 9 was obtained. Here, the medians of the first and second comparison distributions are separated by only one 10-millionth of an inch indicating that the asymmetry has been sharply reduced. This shows how the use of the statistical controls led to a modification of the actual handling techniques employed.

One further example of the application of statistical control to the intercomparison tests will illustrate how statistical analyses can be effectively used to monitor the measuring technique and detect break-

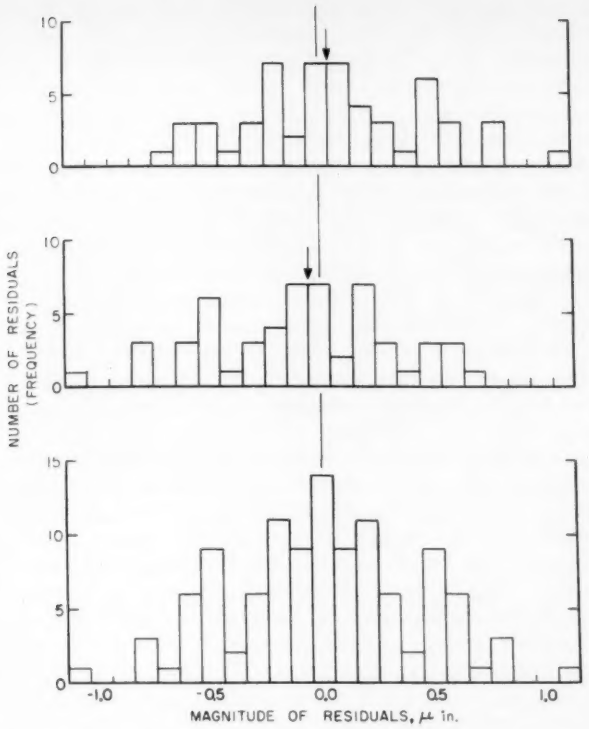

FIGURE 9. *Frequency distribution obtained from an intercomparison test when handling was modified to correct asymmetrical condition.*

Close alinement of the medians shows absence of asymmetrical condition.
Top—Distribution obtained from second comparisons of pairs of gage blocks.
Center—Distribution obtained from first comparisons of pairs of gage blocks.
Botton—Total distribution of residuals.

downs in the technique which might not otherwise be evident.

After a series of modifications in technique finally resulted in the development of a satisfactory intercomparison procedure, this procedure was employed on all the intercomparison tests and regularly gave residual distributions comparable to that shown in figure 9. Then, after a considerable number of intercomparison tests had been run using this procedure, the residual distribution shown in figure 10 was obtained. This again indicates, by the split between the medians of the first and second comparison distributions, that an asymmetry was present during this particular intercomparison test. A similar asymmetry was evidenced in the residual distributions of succeeding intercomparison tests indicating that some breakdown in the system had occurred. Careful examination revealed that actually there had been an asymmetry in the comparison procedure all along but that its effects had been eliminated from the earlier intercomparison tests by other precautions, and that these precautions had now broken down causing the asymmetry to be revealed. As indicated above, the gage blocks during comparison were always handled in pairs and gloves were employed for this handling to insulate the blocks, to a certain extent, from the hand. To get the two blocks of a pair together, since the blocks were

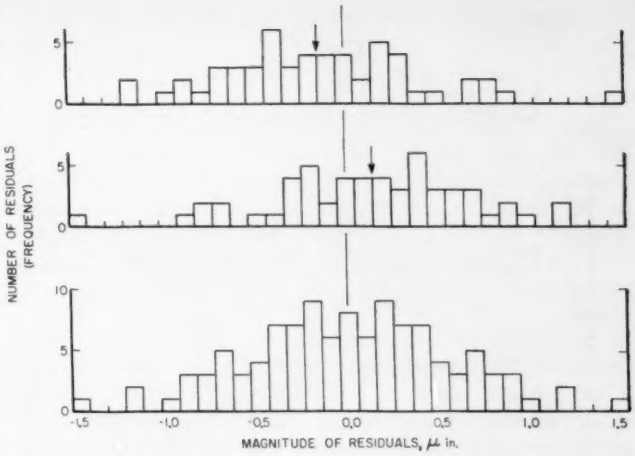

FIGURE 10. *Frequency distribution of residuals obtained in an intercomparison test when a breakdown of test fixtures activated a dormant asymmetry in technique.*

Separation of distribution medians shows the presence of an asymmetrical condition.
Top—Distribution obtained from second comparisons of pairs of gage blocks.
Center—Distribution obtained from first comparisons of pairs of gage blocks.
Bottom—Total distribution of residuals.

spread out on a storage area, it was necessary to pick up first one block and then the other. Thus, the first block picked up was given more time to be affected by the handling before its measurement than was the second block and this is an asymmetrical condition. The gloves had been used from the start to minimize the effects of handling, but at the time this asymmetry was detected, it was noticed that the gloves employed had become worn and impregnated with foreign material. It was suspected that in this condition the effectiveness of the gloves in shielding the comparisons from the asymmetry involved in picking up the blocks one at a time was reduced.

To determine whether this was indeed the case, the handling technique was modified in the following way. In previous tests, the gage blocks had been picked up one at a time from the storage area and placed on a loading stage so that the pair could then be picked up together for the comparisons. This procedure was modified by using a pair of tongs to pick up the blocks one at a time from the storage area and place them on the loading stage. The tongs were then put aside and the pair of blocks were picked up together from the loading stage as before, with the gloved hand. The comparisons were then made just as before.

This modification of the handling technique removed the gloved hand from the asymmetrical initial portion of the handling procedure and hence if the sudden appearance of the asymmetrical condition was due to the failure of the gloves, the asymmetry should have been eliminated with this modification. That this occurred is illustrated by figure 11 which shows the residual distribution obtained when the tongs replaced the gloved hand in the initial asymmetrical portion of the handling procedure. This modified technique was then

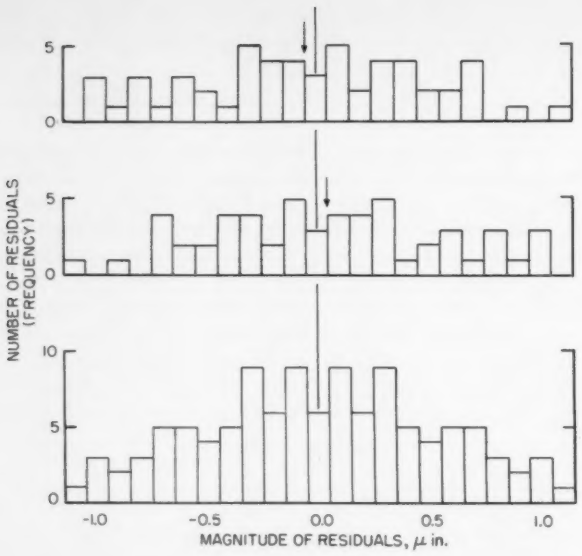

FIGURE 11. *Frequency distribution of residuals obtained in an intercomparison test when modification in test fixtures was introduced to correct an asymmetrical condition.*

Close alinement of the medians shows absence of asymmetrical condition.
Top—Distribution obtained from second comparisons of pairs of gage blocks.
Center—Distribution obtained from first comparisons of pairs of gage blocks.
Bottom—Total distribution of residuals.

adopted for all subsequent intercomparison tests, but this example illustrates how statistical control was employed to detect a breakdown in the technique and indicates the value of continuing to employ such control as a monitor of the measurement method.

This type of statistical control is, however, ineffective as a monitor in detecting certain types of nonuniformity in the measuring method. In particular, it will not detect variation in measurement technique which results in a change in the relationships between lengths of the blocks of an intercomparison group when these changed relationships continue throughout the time interval of one complete intercomparison test. An example of this type of variation in procedure occurred during the testing of one intercomparison group of gage blocks. Intercomparison tests had been run on this particular group for a period of several months. The regularly employed procedure was used in each intercomparison test, but on the date of one test an interferometric measurement of one block in the group was planned for the same date on which an intercomparison test was to be run. The normal procedure for an intercomparison test called for the eleven blocks in the group to be placed on the storage area of the intercomparison test equipment the night before the intercomparison test was to be run and left there overnight until the test was begun in the morning. The normal procedure for the interferometric measurement called for the placing of the block to be measured in the interferometer the night before the measurement was to be made. However, since the interferometric measurement of the one block in this set would only take a few minutes in the morning before the intercomparison test, it was decided to proceed with the interferometric measurement and the intercomparison test both on the same day. Thus the block to be measured interferometrically, the F302 block, was placed in the interferometer the night before the date of the two tests and left there overnight, while the other 10 blocks in the group were placed on the storage area of the intercomparison test equipment and left there overnight just as the normal procedure required. In the morning, the F302 block was measured interferometrically and was taken from the interferometer and placed on the storage area with the other 10 blocks, a horizontal movement of approximately 6 ft within the constant temperature room. An hour later the intercomparison test was begun following the normal procedure and this test took perhaps 4 hr. Calculation of the data and plotting of the residual distribution gave the distribution shown in figure 12, which shows an excellent distribution. However, when the relationships between the F302 block and the other blocks in the group were examined, the results of this intercomparison test appeared anomalous. This is illustrated in figure 13, where the differences in length are plotted for the following blocks: F323 minus F302, F327 minus F302, and F330 minus F302. These data were determined in successive intercomparison tests on the group containing these blocks. The plotted points

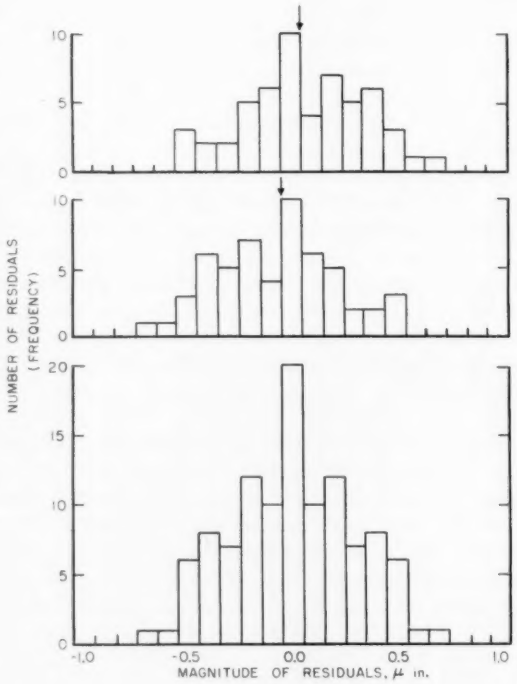

FIGURE 12. *Frequency distribution of residuals obtained in an intercomparison test which produced anomalous results.*

Notice that the distributions do not indicate the effect which produced the anomaly.
Top—Distribution obtained from second comparisons of pairs of gage blocks.
Center—Distribution obtained from first comparisons of pairs of gage blocks.
Bottom—Total distribution of residuals.

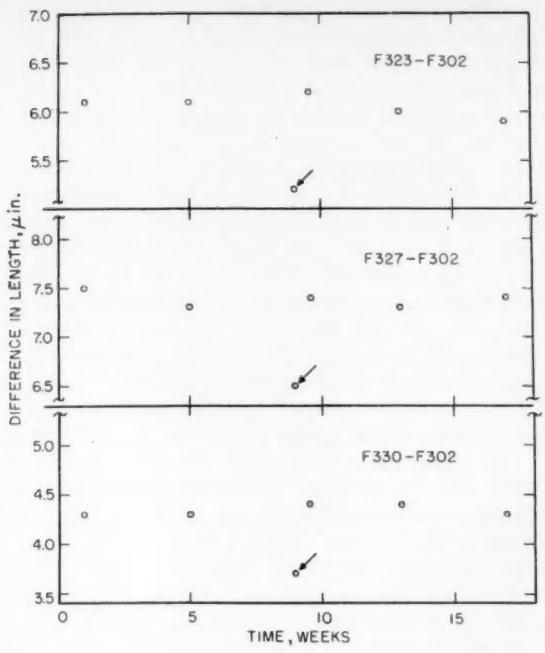

FIGURE 13. *Illustration of anomalous results obtained in one intercomparison test in which the F302 gage block received a different handling prior to the test.*

indicate the values obtained for these differences in each particular intercomparison test. The values obtained in the test here in question are marked on each graph by the small arrows. It can be seen that the values obtained in the intercomparison tests preceding this one show a certain consistency. The test in question, however, in each case gave a value several ten-millionths of an inch lower than the previously consistent values. Yet the only variation in testing procedure noticed was the different treatment afforded the F302 block prior to the intercomparison test, occasioned by the procedure involved in its interferometric measurement. To determine whether this variation was indeed the significant factor, another intercomparison test was run on this same group of blocks four days later, with care being taken that the normal procedure was followed throughout the handling and the test. The values obtained in this and subsequent intercomparison tests are shown in figure 13 to the right of those marked with the small arrows. These values are again consistent with those obtained prior to the intercomparison test in which the variation occurred. Thus it appears that the anomalous results are indeed due to the variation in procedure which caused the F302 block to receive different treatment from that received by the other ten blocks in the group. Further, it should be noted that this variation went undetected by the residual distributions employed as statistical controls (figure 12). This indicates that while these controls are of considerable value in maintaining uniformity of technique, they are, nevertheless, ineffective with certain types of variation.

6. Results of Stability Measurements

6.1. Method of Presenting Data

The data obtained from the observation of stability are presented in figures 14, 15, 16, and 17. In these figures, time elapsed since final heat treatment is plotted against change in length. Each plotted point has an upper and lower limit which is the estimated precision of the determination. This estimate was based upon the statistical information derived from the test itself. When the frequency distribution of all the measurement residuals of an intercomparison test indicated a near normal distribution and when the residuals were limited to a range within 3 times the calculated standard deviation of a single reading, the evaluated precision of the intercomparison test was estimated to be 3 times the computed standard deviation of the final result. When the range of the frequency distribution exceeded that to be expected from the calculated standard deviation, a factor of 4 times the standard deviation was applied as an estimate of precision.

Large backloads at the grinding shop and time spent accumulating sufficient blocks for an efficient lap load, in some cases, caused considerable delay in the interval between final heat treatment (stress relief) and final lapping. In addition, procedures for measuring the blocks were being developed simultaneously and were not ready until after some of the blocks had been completed for some time. Plotting the time elapsed since final heat treatment compensated for the delays and put each block on a more comparable basis.

6.2. Commercial Gage Blocks

As a basis of comparison, a total of seven 2 in. steel gage blocks, two from each of three manufacturers and one[8] from a fourth, were purchased on the open market and incorporated into the measuring program. The blocks were ordered as "AA" grade, the best quality available. The results obtained from observing the stability of these blocks are shown in figure 14. The abscissa for this figure is the number of months elapsed since purchase. While it would have been more desirable to have plotted the months elapsed since final heat treatment, such data were not available. All of the commercial blocks have become shorter, although block *A* of manufacturer 2 and blocks *A* and *B* of manufacturer 3 initially indicated a tendency towards growth. There is also a considerable degree of similarity between the stability characteristics of paired blocks from each manufacturer. The apparent overall stability of these blocks, extrapolated to a period of one year, ranges from a minimum of -0.7×10^{-6} in./in. to a maximum of -1.9×10^{-6} in./in. The average change in length for the seven blocks is -1.1×10^{-6} in./in./yr, which is adequate to maintain size within the current Federal specification for only 2 yr. It is

[8] Two blocks were purchased, but one was unsuitable for measurement.

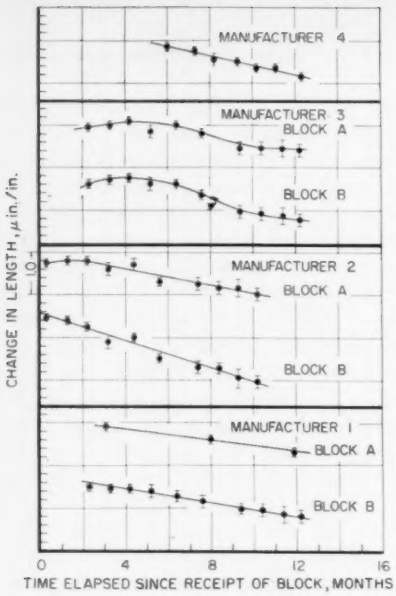

FIGURE 14. *The stability of commercial gage blocks of "AA" grade obtained directly from four manufacturers.*

a standard procedure of some manufacturers to finish their blocks on the positive side of the tolerance to allow for what is claimed to be wear. This procedure could extend the time within tolerance for the average of these blocks to 4 yr, assuming a uniform continuance of the contraction.

6.3. 52100, Hardened

The results of stability measurements on hardened 52100 steel gage blocks are shown in figure 15, and include blocks hardened either by martempering or by direct quenching. The six curves plotted in section A represent stability characteristics of blocks given the lowest final temper and stress relief so as to obtain a hardness of 65 R_c. Each block that was measured during the first 5 months became shorter, and became nearly stable for the remaining period of observation; block T–337 showed a slight tendency to decrease in length with increase in time over the entire period of its observation. The initial contraction was more pronounced in those blocks measured soon after final stress relief, and very small or absent in blocks whose initial measurements were made 5 months after heat treatment. All six curves have similar characteristics, regardless of whether the blocks they represent were martempered or quenched. The overall change in length computed on the basis of one year ranges from -0.2×10^{-6} to -0.7×10^{-6} in./in. The average change for the six blocks is -0.4×10^{-6} in./in., a value indicating approximately three times more stability than the commercial blocks. A more realistic approach is to compute the length changes after the sixth month, since the blocks appear essentially stable once the initial rate of contraction has subsided. On this basis the minimum change, extrapolated to 1 yr, is 0.0 and the maximum -0.3×10^{-6} in./in./yr. The average is a very low -0.1×10^{-6} in./in./yr, indicating about 10 times greater stability than the commercial average, and well within the goals of $\pm0.2\times10^{-6}$ in./in./yr set for this investigation.

The four curves in section B and the four in section C of figure 15 represent the stability of blocks that were given final tempers and stress relief treatments at temperatures in excess of 250° F to reduce nominal hardness to 62 R_c, and 60 R_c respectively. These stability results were not anticipated, for it was initially reasoned that the higher tempering and stress relief temperatures would produce a more stable structure and stress pattern. Instead, the eight blocks represented by the curves in B and C appear less stable than those in A. The directly quenched blocks in B and C (T–377, T–378, T–384, T–386) have not been observed sufficiently long to ascertain the exact shape of their stability curves. Although the curves for the four blocks have been drawn linearly, they all exhibit what could be a tendency to flatten during the last four measurements. Nevertheless, the shapes of the curves are undoubtedly different from the curves of the matching martempered blocks in sections B and C (T–351, T–356, T–357, T–359). The four directly quenched blocks were the only blocks whose nongaging surfaces were ground perpendicular to the 2 in. dimension; all others were ground parallel.

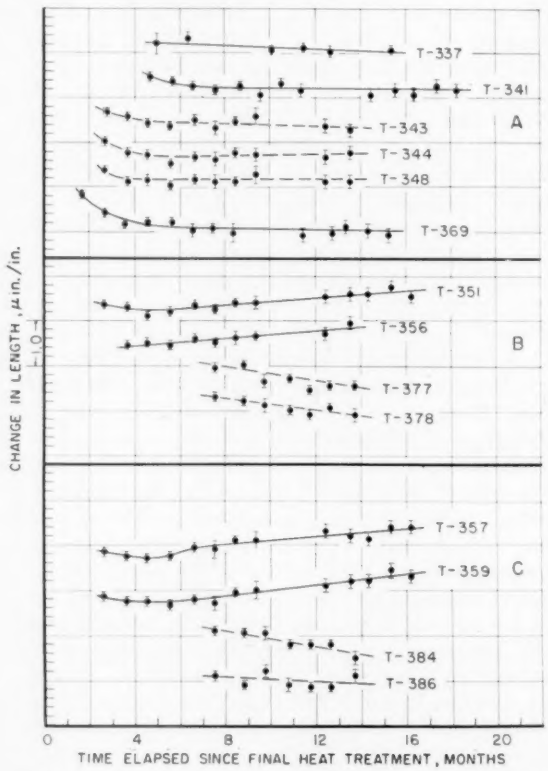

FIGURE 15. *The stability of hardened and stabilized 52100 experimental gage blocks.*

Solid lines represent martempered blocks, dashed lines represent directly quenched blocks.

A, 65 R_c; B, 62 R_c; C, 60 R_c.

The large surfaces adjacent to the gaging surfaces of two hardened 52100 gage blocks were analyzed for residual stresses by W. E. Littman and A. L. Christenson, The Timken Roller Bearing Co., in accordance with the X-ray techniques of Christenson and Rowland [19]. One of these blocks had been heat treated for maximum hardness (65 R_c) and ground in a manner identical to blocks T–343, T–344, and T–348 (section A, fig. 15). The other was prepared with a hardness of 60 R_c in a manner identical to that used for blocks T–384 and T–386. The block tempered at 250° F to a hardness of 65 R_c had a residual compressive surface stress of 14,400 psi parallel to the grinding direction and 60,200 psi perpendicular to the grinding direction. The block tempered at 465° F (60 R_c) had residual compressive stresses of 20,100 psi parallel and 70,500 psi perpendicular to the grinding direction. Thus, the data indicate that the compressive stresses in the surfaces of the blocks actually increase with an increase in the tempering temperature from 250° to 465° F. Therefore, it is postulated that the process of tempering at temperatures in excess of 250° F caused a structural change within the block which was accompanied by a contraction. The surface stresses, however, were not relieved at a rate sufficiently high to counterbalance the internal contractions, with the overall result that the compressive stresses in the surface were increased by the increase in tempering temperature. The net result seems to have been an unbalance between the subsequent structural and lattice changes and the distribution and size of residual stresses, which in turn has contributed to a growth of four blocks (T–351, T–356, T–357, T–359) in sections B and C, figure 15. On the other hand, grinding the other four blocks at a 90 degrees direction has shifted the maximum observed compressive stress by 90 degrees. It is suggested that the observed shrinkage in these blocks is caused by the change in the orientation of the stress patterns. These comments concerning the influence of grinding stresses are considered tentative and several experiments have been designed and are in progress which are expected to lead to a clarification of the problem.

6.4. 410 Stainless, Annealed and Nitrided

The results of stability measurements on annealed and nitrided 410 stainless gage blocks are shown in figure 16. The four curves plotted in section A represent the stability characteristics of blocks nitrided by the two stage process and whose nongaging surfaces were not ground or otherwise machined after nitriding. The entire group (A) exhibits similar stability characteristics; the slope of each curve is almost the same. There was practically no deviation from linearity during the entire 13 month period of observation, although a tendency towards additional flattening may be indicated in the last four measurements. It is unfortunate that no measurements could be made prior to the twelfth month after heat treatment, so that the behavior of these blocks during the first year could have been observed. The

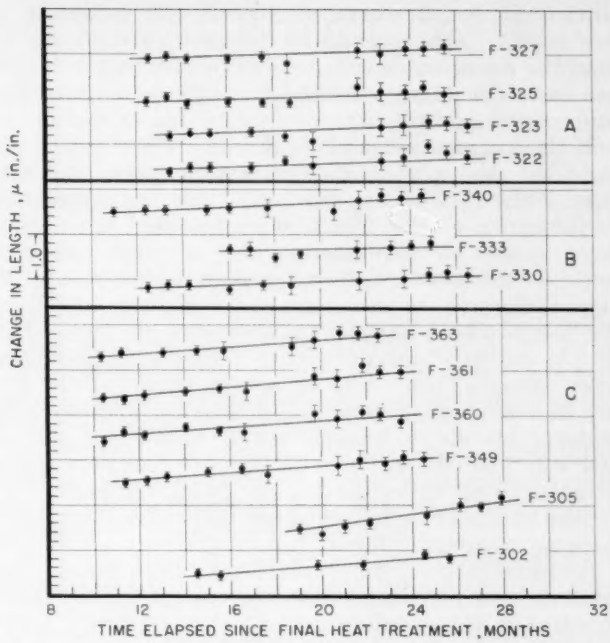

FIGURE 16. *The stability of nitrided, initially annealed 410 stainless steel gage blocks.*

A. Nitrided by two stage process, nongaging surfaces left as nitrided.
B. Nitrided by single stage process, white layer removed from nongaging surfaces.
C. Nitrided by single stage process, nitrided case completely removed from nongaging surfaces.

overall change in length computed on the basis of 1 year is a consistent $+0.2\times10^{-6}$ in./in./yr. This value just meets the degree of tolerance sought in this investigation. Based on a 1 year interval, any one of these blocks is about 3 times more stable than the best of the commercial blocks tested, 5 times more stable than the average, and 9 times more stable than the least stable.

The curves in section B of figure 16 represent data from three blocks which were nitrided by the conventional single stage process. The preparation of these blocks also differs from that in section A in that the white layer on the nongaging surfaces was ground off, so as to leave a hard, bright, nitrided case. The stability of these blocks is almost the same as for those in section A. The range is $+0.1\times10^{-6}$ to $+0.3\times10^{-6}$ in./in./yr with an average of $+0.2\times10^{-6}$. The curve for F–333 has an extremely low slope, but this block has been observed for only 9 months and the trend of the last four points is towards greater slope. The average of this group is equivalent to that of group A, but there is slightly more scatter.

The blocks represented by the curves in section C of figure 16 were nitrided by the single stage process and differ from those in B in that all of the nitrided cases were removed from the four nongaging faces by grinding. These blocks exhibit the same trend towards uniform linear growth, but the rate is higher. The range is $+0.4\times10^{-6}$ to $+0.9\times10^{-6}$ in./in./yr with an average of $+0.6\times10^{-6}$. Except for block F–305 each curve has a similar slope, and again the nonconforming curve was drawn through fewer points of observations. The last two or three points

plotted for each curve, except F–305, indicate a downtrend. The average of this group is more stable than the most stable commercial block observed, and has twice the degree of stability as the average of the commercial group.

If the assumption is made that the 410 stainless, as annealed, has a normal tendency to grow, and the data support this assumption, then the improved performance of the blocks with nitrided nongaging faces could be explained. The nitrided surfaces could serve as a restraining jacket, which would be more effective with increasing thickness. Thus, the blocks whose nongaging faces were not ground at all (A, fig. 16) had the thickest case and grew the least, those whose white layer was removed (B, fig. 16) had a thinner case and indicated slightly less uniform stability characteristics, and those whose case was removed entirely (C, fig. 16) had maximum growth. The investigation is being extended to further evaluate the effect of the thickness of nitrided cases on nongaging faces.

Residual stress determinations were made by Littman and Christenson on the nongaging surfaces of nitrided 410 stainless steel blocks. A block processed similarly to those in section A of figure 16 had residual tensile stresses of 3,000 psi parallel to the 2 in. gaging length and 2,800 psi perpendicular to the gaging length (these blocks not ground after nitriding). A block processed like those in section B had a residual tensile stress of 31,100 psi in the direction parallel to grinding (stresses perpendicular to grinding not determined), while a block representative of those in C had compressive stresses of 1,300 psi parallel to grinding and only 900 psi perpendicular to grinding. Except for the fact that the relief of residual compressive stresses would be expected to cause growth, no apparent relationship can be seen between the reported residual stresses and the rate of growth of the different blocks. In actuality, the values of residual stress reported for blocks in A and in C are very low and should not have contributed materially to length changes.

As with the hardened 52100 blocks, several additional experimental treatments have been designed which should contribute additionally to the understanding of the role of surface stresses.

6.5. Blocks With Hard Coatings

The results of stability measurements on both annealed 52100 and annealed 410 gage blocks with hard coatings are given in figure 17. The stability characteristics of 52100 steel coated only on the gaging surfaces with thermal sprayed nickel-chromium-boron alloy is represented in section A. The steel was heated after coating to fuse the particles and some degree of hardening occurred as a result. The hardness of the steel after the fusion treatment was 43 R_c. Both blocks have similar characteristics, both grew slowly at a linear rate. T–309 grew

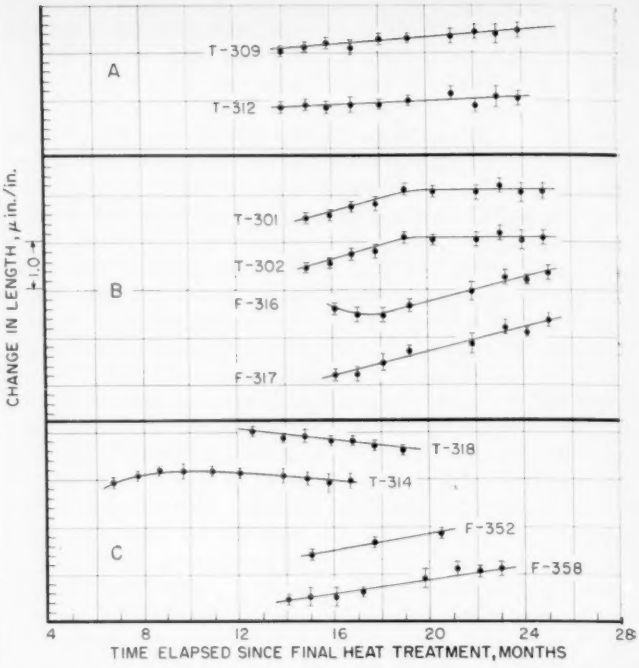

FIGURE 17. *The stability of initially annealed 52100 (T blocks) and 410 stainless steel gage blocks (F blocks) with hard coatings.*

A. Gaging surfaces coated with thermal sprayed nickel-chromium-boron alloy
B. Gaging surfaces coated with flame plated tungsten carbide.
C. Surfaces electroplated with chromium, T blocks on all surfaces, F blocks on gaging surfaces only.

0.5×10^{-6} in./in., extrapolated to 1 yr, and T–312 grew 0.3×10^{-6} in./in./yr.

The blocks represented in section B, figure 17, have been flame plated with tungsten carbide on gaging surfaces only. Both of the 52100 blocks (T–301 and T–302) have similar stability characteristics. Initially they expanded at a rate similar to 410 stainless block F–317 in section B, but they have exhibited more stable characteristics during the last 6 months of observation. The 410 blocks have grown rapidly, much more so than the nitrided blocks in section C of figure 16. This particular comparison is made because the blocks in figure 16C were ground on the nongaging faces and stress relieved at 975° F in the same manner as the blocks illustrated in section B of figure 17. Therefore, the core material in each group has essentially the same structure and residual surface stress pattern and the difference in behavior can be attributed to the cases.

The blocks whose stability characteristics are shown in section C figure 17 were chromium electroplated. T–314 and T–318 were plated on all six surfaces and the plating on the nongaging faces was ground sufficiently to obtain desired dimensions. Blocks F–352 and F–358 were plated on the ends only. The 52100 blocks are reacting similarly to one another and the two 410 stainless blocks also have curves similar to each other. The former are contracting although there was an initial increase in T–314. The chromium plated 410 stainless blocks are increasing in size at a fairly rapid rate.

6.6. Overall Observations

a. On Stability of Gage Blocks

The comparative changes in length for all of the blocks, arranged in order of increasing change, are summarized in table 6. A time increment of 1 yr has been used, which necessitated extrapolation in some cases. The most stable groups of blocks for the period observed were the nitrided 410 stainless with all or portions of the nitrided cases left on all surfaces. These blocks had stability characteristics that met the goal set for this investigation, namely, a maximum dimensional change of 2×10^{-7} in./in./yr. These blocks proved to be resistant to normal atmospheric corrosion and accepted the best lapped finish of any block tested. The reproducibility of performance in these blocks, as evidenced by the uniformity of slope and low spread of individual values in each group, was also excellent. There was no apparent deviation from linearity in the dimensional changes of any of the nitrided 410 stainless blocks, but all, including the coated and plated blocks, showed some tendencies towards growth. Disadvantageously, the coefficients of thermal expansion and conductivity are somewhat lower than desirable.

TABLE 6. *The stability of gage blocks over a one year period, in order of merit*

Steel and treatment	Avg change in length
	μ *in./in./yr*
1. 410 stainless, nitrided, two stage, nongaging faces as nitrided	+0.2
2. 410 stainless, nitrided, single stage, white layer removed	+0.2
3. 52100, hardened and tempered to 65 R_c	−0.4
(after 6th month)	(−0.1)
4. 52100, thermal sprayed with Ni-Cr-B	+0.4
5. 52100, hardened and tempered to 60 R_c, ground parallel to 2 in. axis	+0.4
6. 52100, chromium plated on all faces	−0.4
7. 52100, hardened and tempered to 62 R_c, ground parallel to 2 in. axis	+0.5
8. 410 stainless, nitrided, 1 stage, nongaging cases removed	+0.6
9. 52100, flame plated with tungsten carbide	+0.7
10. 52100, hardened and tempered to 60 R_c, ground perpendicular to 2 in. axis	−0.7
11. 52100, hardened and tempered to 62 R_c, ground perpendicular to 2 in. axis	−0.9
12. 410 stainless, chromium plated on ends	+1.0
13. Commercial "AA" grade	−1.1
14. 410 stainless, flame plated with tungsten carbide	+1.3

The best of the blocks made from 52100 were those hardened and stabilized at the high hardness of 65 R_c. The repetition obtained within this group was excellent, and included both directly quenched and martempered blocks. If the first 6 months after final heat treatment are disregarded, these blocks exhibited even greater stability than the best of the 410 stainless. All of the hardened 52100 blocks on which observations were made during the first 6 months contracted initially and then stopped contracting, or expanded according to the tempering or grinding treatment given them.

Several of the blocks with hard coatings were more stable than the commercial blocks tested. Both the sprayed Ni-Cr-B and the plated tungsten carbide apparently caused an overall growth, but on the 52100 blocks the growth was small or had subsided. The principal undesirable feature noted with the Ni-Cr-B and tungsten carbide coatings was the high porosity of surface obtained on lapping, which was readily apparent to the unaided eye.

b. On Precision of Length Measurements

Three types of measurement were employed in determining the length of the stability samples:

1. Absolute interferometric measurement in which the length of the primary master was determined with the wavelength of light.
2. Interferometric comparison measurement in which the lengths of the secondary masters were compared with the length of the primary master using the wavelength of light as a length scale.
3. Mechanical comparisons of the 10 stability samples of a group with the secondary master belonging to that group.

Of the various types of measurement, the absolute measurement was the most difficult and the least precise for reasons mentioned in section 5.1. Because absolute measurements of the primary master were initiated in 1954 and since many measurements have been made at irregular intervals from that time on, it was believed that its stability could be determined to a much greater precision than individual absolute measurements indicated. For instance, the largest deviation of a single measurement from the average of all 33 measurements made since 1954 was 1.2 μin. The standard deviation of a single reading was 0.55 μin. However, in fitting a curve to these data, it became obvious that a cyclic function with a yearly period best fitted the measurements. Using January 1, 1954 as a zero time reference, a curve calculated by the least squares method to fit the measurement data is expressed by the equation:

$$L=A\sin\left(\frac{2\pi t}{B}+\phi\right)+Ct+D$$

where L=length deviation from nominal size (2 in.)
A=+0.75 μin.
B=12 mo
t=time of measurement in months (January 1, 1954=0)
ϕ=1.19 π
C=+0.0035 μin./mo
D=+4.59 μin.

The standard deviation of all measurements from this curve was 0.28 μin. with the largest deviation for a single measurement being 0.5 μin. It was assumed that the instability of this gage block is expressed by the function $\Delta L=C\Delta t$ whereas the sinusoidal variation is an effect due to error in determination of the effective temperature of the gage block. All absolute measurements on this gage block were made using one interferometer occupying one location in a constant temperature room. The temperature of the

gage block was determined with one junction of a thermocouple held at the surface of the gage block with a spring clip. The other junction of the thermocouple was imbedded in a copper block surrounded by an insulated aluminum-sheathed box. The temperature of the copper block was determined with a platinum resistance thermometer. The temperature of the copper block related to that of the air in the room showed a seasonal variation, and was generally colder than the air in the winter and warmer in the summer. If the effective temperature of the gage block relative to the temperature measured by the thermocouple junction at its surface is analogous to the relationship of the copper block temperature to that of the air, and if the difference in temperature approaches a maximum of 0.05° F, the cyclic effect can be rationalized.

Based on the assumption that the instability of the primary standard can be expressed as $C\Delta t$, the primary standard, according to measurement, is growing at the rate of 0.04 μin./yr. It is believed that this value is accurate to within 100 percent. An error of such small magnitude in the determination of the instability of the primary master block would have no significant effect on the stability results of the samples reported.

Interferometric comparison of the primary master with the secondary master blocks (the stability samples serving as references for the groups of stability samples compared mechanically) were made with the interference comparator mentioned in section 5.1. This interferometer has been subjected to much investigation in regard to the precision of its measurements, [16] the uniformity of the wringing films, and the wear resulting from repeated wringings [20]. As a result of these investigations a precision of ± 0.2 μin. has generally been applied to individual comparisons. Stability samples block A, manufacturer 1, figure 14; T–337, figure 15; F–302, figure 16; and F–352, figure 17 are examples of these secondary master blocks.

From the metrological viewpoint, the results obtained with the mechanical comparator employing transducers in tandem were most interesting. Employing the concept of comparison of dynamic lengths and using statistical analysis of the measurement data to evolve the measurement program, it was possible to obtain residual measurement errors having very small spread and nearly normal distribution. Employing intercomparison tests involving 110 separate comparisons of the gage block samples of a group, it was found possible to limit the residual errors to a spread of ±0.6 μin. The standard deviation (σ) of the result of such an intercomparison test was found to be approximately 0.08 μin. As the residual errors formed a nearly Gaussian distribution, a 99.7 percent confidence limit of random error (3σ) of ±0.24 μin. was indicated for the results of such an intercomparison test.

As the tests were repeated at periodic intervals, it was possible to test the reliability of the above statistical evaluation of precision. Most measurements of the stability samples reported extended over a period approximating 1 yr. Three different operators were employed and the temperature of the rooms in which tests were conducted varied from a few tenths of a degree to approximately 2° F. A small advantage in the control of residual error spread seemed to be achieved in using the best temperature-controlled room. One operator's residual error distributions, in general, had more scatter in the tails of the distributions than did the other two operators. No seasonal variations, as appeared in the absolute interferometric measurement of the primary master block, were noticed. It was found that when care was taken to expose the blocks of a group to the same conditions for at least 18 hr prior to an intercomparison test, the consistency of the periodic results were within the limits of the precision calculated from the statistical evaluation, i.e., approximately 0.2 μin. Figure 13 illustrates the consistency obtained in monthly measurements and also illustrates, by the exception, the effects of treating the gage blocks differently prior to the intercomparison test.

Another indication that precision of the above magnitude is being obtained in mechanical comparison was derived from the results of mechanical comparison tests conducted to determine the thermal coefficient of linear expansion of the gage block samples. In this procedure, intercomparison tests on a group of samples are conducted at two temperatures. From the results of the two tests the magnitude of the changes in the length relationships of the blocks of the group can be determined. Knowing the difference in temperature of the two tests, the coefficients of all the blocks relative to that of the secondary master block of the group can be determined. The coefficient of the secondary master is then measured by interferometric methods (change of length with temperature determined in terms of wavelength of light) and thus the coefficients of all blocks of the group can be calculated. As a cross check on the precision of the mechanical measurement and as a check on the consistency of the calibration of the mechanical comparator, the coefficients of some blocks determined by mechanical comparison techniques were compared with coefficients determined by interferometric methods. In general, the agreement of results of such tests indicated that the length changes resulting from temperature variation as measured by the mechanical comparator were accurate to better than 0.2 μin.

A result obtained from the investigation of thermal coefficient of expansion is worthy of note. It is reported in the literature that 52100 steel has an approximately 2 percent smaller thermal coefficient of linear expansion in the annealed state than when hardened to 65 R_c. It was found in this investigation that this steel hardened to 60 R_c had a thermal coefficient of expansion about 3 percent lower than that hardened to 65 R_c (table 2). This was verified by both mechanical comparison and interferometric methods of measurement.

From the history of past interferometric measurements on the primary master; from the conclusions

of Dexter's work [20] on wear occurring using the interference comparator; and from the fact that interference measurements were made on a relatively infrequent basis, it was concluded that if wear did occur from interferometric measurements, it was negligible. However, no information was available on the wear effects to be expected in the mechanical comparisons. To allow an evaluation of this effect, the frequency of test was changed from weekly to monthly tests. It was reasoned that if wear did have an effect on the measured stability trends of the blocks, a change in the frequency of test would have an effect upon the trends of length changes exhibited by the blocks. Such effects did not occur.

7. Summary and Conclusions

1. A program has been described for the development of steel gage blocks with a maximum dimensional change of 2×10^{-7} in./in./yr, a degree heretofore unobtainable with consistency. The problem had a dual nature in that procedures for the selection and processing of materials and suitable techniques for measurement to the desired precision were developed simultaneously.

2. The data presented are the result of observations on two steels given a total of 14 treatments, but which represent only a small proportion of the blocks under development or observation. From this total, two treatments applied to 410 stainless steel produced gage blocks with an average and uniform dimensional change of 2×10^{-7} in./in./yr. One treatment applied to the 52100 steel produced gage blocks with an extremely high degree of stability (1×10^{-7} in./in./yr) after an initial less stable period of 6 months. Although the results indicate that the goal of the investigation may have been met, periods of observation greater than 1 yr are needed to establish the stability characteristics more firmly. Further improvements in the development of materials and measuring techniques seem possible and will be sought. The failure of other treatments of the 410 and 52100 steels to produce equally stable gage blocks in those cases where the treatments were similar except for small modifications, such as direction of grinding or thickness of nitrided case, has suggested other courses of investigation which are being pursued. Other more subtle influences on stability are being studied also, such as influence of residual magnetism (induced by magnetic grinding chuck) and environmental temperature changes.

3. The method of reporting length in inch per inch is a matter of convention and convenience and should not be construed as being directly convertible to any size of gage block, particularly those of less than 1 in. Size effects can influence both the metallurgical and metrological factors and consideration is being given to the investigation of these effects.

4. Mechanical comparators can be used for measurements with a precision approaching 2×10^{-7} in. The procedures involved are also applicable to the rapid measurement of a large number of parts of the same nominal size and thermal properties, and therefore can be adapted to industrial applications. Statistical analysis, used in conjunction with the comparator techniques, has application in determining the most suitable procedures and providing continued uniformity in the application of the technique.

The authors have received guidance, advice, encouragement, and technical support from many sources, both at the National Bureau of Standards and from industry. While a complete listing cannot be attempted, we are very grateful to: Irvine C. Gardner, Chief of the Optics and Metrology Division (Retired), who was responsible for the early planning of the program, general guidance in the metrological phases, and extensive coordination between industry and government; James I. Hoffman, Chief of the Metallurgy Division, who provided broad leadership and guidance in the metallurgical phases; Thomas G. Digges and Samuel J. Rosenberg of the Metallurgy Division, whose suggestions and ideas were always beneficial and contributed substantially to the metallurgical development; E. S. Rowland of The Timken Roller Bearing Co., who served as spokesman for the industrial group, contributed many ideas of his own, and was instrumental in obtaining the experimental materials; A. M. Dexter of the Pratt and Whitney Co., Inc., who as a resident guest worker provided invaluable assistance in the initial phases of the measurement program and who subsequently arranged for the lapping of many gage blocks; Norman Silver of the DoAll Co., who contributed much background information of commercial gage block manufacture and was also instrumental in providing lapping facilities; Arthur Strang of the Optics and Metrology Division, for his absolute interferometric length measurements of the primary master block; John Beers and Grace Chaconas of the Optics and Metrology Division, who analyzed specimens for length, parallelism, and flatness; Richard Kirby of the Optics and Metrology Division, for his interferometric determinations of coefficient of thermal expansion; Charles I. Ward, Jr., of the Instrument Shop, who performed nearly all of the grinding and fabrication on some very difficult surfaces; John T. Lynch of the Metallurgy Division, who performed much of the detailed heat treating and nitriding; and Gertrude Davis who typed the manuscript.

8. Appendix A: Establishment of Optimum Heat Treating Conditions for 52100 Steel

Specimens of the steel were heat treated by direct quenching or by martempering followed by various stabilizing treatments. All specimens used for these heat-treating experiments were ½ in. cubes. The retained austenite content was determined by X-ray diffraction on cross sections of the specimens. The method used employed cobalt Kα radiation with iron filtration, a geiger tube detector, and a step-scanning technique. Originally, both the (220) and (311)

ines of austenite and the (211) line of martensite were used in the computations, but the use of only the (220) line of austenite and the (211) line of martensite produced comparable results and thus eliminated a great deal of laborious step scanning, and in later determinations only these were used. Guided by the results of the X-ray analysis, the treatments were continuously revised until the austenite could no longer be detected. A summary of the treatments and the retained austenite measured as the result of each is shown in table 7.

Several pertinent observations can be made from these data. The maximum amount of retained austenite measured was about 15 percent and no values were obtained between 8 and 11 percent; the minimum amount obtained ranged from none detected to about 3 percent. There were no values between 3 and 4 percent and the intermediate quantities varied from greater than 4 percent to about 8 percent. These separations facilitate a convenient grouping into specimens with high austenite, 15 to 11 percent; intermediate austenite, 8 to 4 percent; and low austenite, 3 percent to none detected.

TABLE 7. *The effect of heat treatment and stabilization on the quantity of retained austenite in small specimens of 52100 steel*

Specimen No.	Method of hardening	Chronological order of procedures after hardening	Stabilizing treatment			Retained austenite after stabilization	Remarks
			Refrigeration time	Temper			
				Temperature	Time	Volume	
			hr	° F	hr	%	
T-216	Martemper	1st		250	1		Tempered prior to refrigeration.
		2d	Overnight				
		3d		250	1		
		4th	Overnight				
		5th		250	8	15.3	
T-219	Direct quench	Single step		250	1½	13.2	Tempered, no refrigeration.
T-208	Martemper	Single step		230	1	12.6	Tempered, no refrigeration.
T-220	Direct quench	1st		250	1		Tempered prior to refrigeration.
		2d	Overnight				
		3d		250	1		
		4th	Overnight				
		5th		250	8	11.5	
T-215	Martemper	1st	Overnight				
		2d		275	2		
		3d	Overnight				
		4th		275	2	7.7	
T-213	Martemper	1st	2				
		2d		230	1½		
		3d	2				
		4th		230	1½	7.5	
T-209	Martemper	1st	2				
		2d		230	1½	6.7	
T-214	Martemper	1st	3				
		2d		275	2		
		3d	Overnight				
		4th		275	2	6.5	
T-211	Martemper	1st	2				
		2d		275	1½	6.1	
T-212	Martemper	1st	2				
		2d		325	1	5.9	
T-222	Direct quench	1st	1¼				Steps 1 & 2 repeated 10 additional times.
		2d		275	1	4.9	
T-210	Martemper	1st	6				
		2d		230	1	4.4	
T-218	Martemper	1st	Overnight				
		2d		275	1		
		3d	Overnight				
		4th		250	9	2.8	
T-223	Martemper	1st	Overnight				Chilled in iced brine prior to 1st refrigeration.
		2d		250	1		
		3d	Overnight				
		4th		250	9	2.6	
T-217	Martemper	1st	Overnight				
		2d		250	1		
		3d	Overnight				
		4th		250	9	1.4	
T-221	Direct quench	1st	Overnight				
		2d		250	1		
		3d	Overnight				
		4th		250	9	None detected	
T-226	Martemper	1st	Overnight				Refrigeration temperature was −110° F.
		2d		250	2⅓		
		3d	Overnight				
		4th		250	9	None detected	

NOTES TO TABLE:

1. All specimens were ½ in. cubes austenitized at 1550° F for 15 min in a neutral salt. Martempered specimens were quenched to 300° F for 30 sec in a mixture of $NaNO_3$ and $NaNO_2$.
2. Both the directly quenched and martempered specimens were quenched to room temperature in an accelerated quenching oil.
3. Unless otherwise stated, all refrigeration treatments were at −140° F. An overnight refrigeration treatment may vary from 18 to 22 hr.

The four specimens in the high austenite group consist of two which were directly quenched and two which were martempered. The treatments given them had one feature in common; they were tempered immediately after hardening. No other specimen received this treatment and there is no doubt that it was responsible for stabilizing the retained austenite against substantial further transformation.

The specimens in the intermediate group received a variety of stabilization treatments; however, all were refrigerated at −140° F as a first step after hardening. The length of time of refrigeration was varied from overnight (18 to 22 hr) to 1¼ hr. The number of tempers and the temperatures used varied as did the number of refrigeration treatments. However, it is significant to note that most received individual refrigeration treatments of short duration (exception T–215) and tempers totaling 4 hr or less (exception T–222). None, including the two excepted specimens, received long time refrigeration treatments, combined with tempering treatments of more than 9 hr at the temperatures shown.

The specimens in the low austenite category, 3 percent or less, have several common treatments. All were refrigerated for 18 to 22 hr immediately after hardening, all were tempered initially at 250 to 275° F, all were refrigerated a second time for 18 to 22 hr, and all were given a final temper of 250° F for 9 hr. The slight variations in treatment given to each are shown in table 7 and seem relatively unimportant. The important features are a refrigeration of −110 to −140° F for 18 to 22 hr immediately after hardening, a short temper of 1 to 2 hr at 250° F, a second refrigeration for 18 to 22 hr, and a final temper of 9 hr. The total prescribed tempering time of 10 hr was selected to conform with the conclusions advanced by Lement, Averbach, and Cohen [9] for ball bearing steel.

On the basis of these data, the treatment given specimen T–221 was adopted for use with directly quenched gage blocks and that given T–217 for martempered blocks. The stabilizing treatment used with T–217 was adopted over that used with T–226 because of its similarity to that of T–221 and the convenience inherent in such an arrangement.

Another series of heat and stabilization treatments was devised for 2 in. × 1⅜ in. × ⅜ in. gage blocks to test the validity of the adopted treatments on full sized gage blocks, and to evaluate other variables. The treatments and the result of measurements of retained austenite are summarized in table 8. The readiness with which some austenite becomes stabilized with delay in treatment is shown in a number of cases. For example, block T–323 was treated similarly to small specimen T–217 and in almost the same manner as block T–333, except for a 48 hr. lapse between the final refrigeration and final temper of T–323. T–323 had a considerably greater amount of retained austenite. Shorter delays also appear injurious, as for example, in the comparison of specimens T–223 and T–217 (table 7). T–223 was held in iced brine for 2 min immediately after quenching to room temperature in oil, and then it was placed in liquid CH_3OH (methyl alcohol) at −140° F. On the other hand, T–217 went into the CH_3OH directly without the opportunity to age at a higher temperature and it contains less austenite. The same trend is indicated between blocks T–328 and T–331 (table 8). Blocks T–329 and T–332 contained somewhat more austenite than small specimen T–221 which was treated in the same way, and this may have been caused by the difference in cooling rate between the larger blocks and smaller specimen.

The greater austenite content may also have been caused by the differences in stress distribution in the differently sized and shaped specimens. To avoid difficulties from delays, a cold mixture (CH_3OH+ liquid N_2 at equilibrium, −144° F) was brought to the quenching tank and the blocks placed therein immediately after quenching. The cold container with the blocks was then transferred to the refrigeration unit where the temperature was maintained at −140° F for the required time. This is the two step refrigeration treatment listed in table 8.

It was pointed out in the discussion of table 7 that no specimen with intermediate austenite had received a combination of long time refrigeration treatments and tempering treatments exceeding 9 hr. To further check the necessity of long refrigerating time, while tempering time was held at 10 hr, block T–335 was given comparatively short time refrigeration treatments at −140° F and T–336 was given short time treatments at −110° F. Both had negligible amounts of retained austenite.

It was concluded from these tests on the 52100 treated for minimum retained austenite and a hardness of about 65 R_c that:

1. Refrigeration is a necessary first step immediately after hardening.
2. Stabilizing treatments should be accomplished with the least possible delay between steps.
3. Refrigeration temperatures in the range −110° to −140° F are equally satisfactory, and two treatments in this range are ample.
4. The time of holding at refrigeration temperature can be as short as 2 hr for the initial treatment and 3 hr for the second treatment.
5. A first temper of 1 hr at 250° F appears adequate, an extension of this temper beyond 2 hr, or above 250° F, may induce some stabilization of austenite.
6. A final temper of 9 hr at 250° F or slightly higher is adequate.

9. Appendix B: Hard Coatings, Description, and Application

9.1. Thermal Spray

The thermal spraying process consists of melting or softening a wire or powder in a suitable gun and directing the spray of liquid or softened particles onto the surface to be coated. The alloy used was a

TABLE 8. *The effect of heat treatment and stabilization on the amount of retained austenite in gage blocks of 52100 steel*

Gage block no.	Method of hardening	Chronological order of procedures after hardening	Stabilizing treatment			Retained austenite after stabilization	Remarks
			Refrigeration time	Temper			
				Temperature	Time	Volume	
			hr	*°F*	*hr*	%	
T-323	Martemper	1st	Overnight				48 hr lapse between steps 3 and 4.
		2d		250	1		
		3d	Overnight				
		4th		250	9	5.3	
T-328	Martemper	1st	Overnight				Quenched in water instead of oil. Given a brief iced brine quench between steps 2 and 3.
		2d		250	1		
		3d	Overnight				
		4th		250	9	1.8	
T-331	Martemper	1st	Overnight				Quenched in water instead of oil. Two step refrigeration (see text).
		2d		250	1		
		3d	Overnight				
		4th		250	9	1.4	
T-333	Martemper	1st	Overnight				Quenched in oil, two step refrigeration.
		2d		250	1		
		3d	Overnight				
		4th		250	9	None detected	
T-334	Martemper	1st	Overnight				Refrigeration temperature was −110° F. Long first temper.
		2d		250	2½		
		3d	Overnight				
		4th		250	9	3.8	
T-335	Martemper	1st	2				Refrigeration time reduced.
		2d		250	1		
		3d	4				
		4th		250	9	None detected	
T-336	Martemper	1st	2				Refrigeration time reduced. Temperature increased to −110° F.
		2d		250	1		
		3d	3				
		4th		250	9	1.0	
T-329	Direct quench	1st	Overnight				Brief iced brine quench between steps 2 and 3.
		2d		250	1		
		3d	Overnight				
		4th		250	9	2.4	
T-332	Direct quench	1st	Overnight				Two step refrigeration (see text).
		2d		250	1		
		3d	Overnight				
		4th		250	9	2.5	

NOTES TO TABLE:

1. All gage blocks were nominally 2 in. × 1⅜ in. × ⅜ in. in size, austenitized at 1550° F for 15 min in a neutral salt. Martempered specimens were quenched to 330° F for 30 sec in a mixture of $NaNO_3$ and $NaNO_2$.
2. Both the directly quenched and martempered blocks were quenched to room temperature in an accelerated quenching oil except where water is noted in the remarks column.
3. Unless otherwise stated, all refrigeration treatments were at −140° F. An overnight refrigeration treatment may vary from 18 to 22 hr.

self-fluxing alloy of nickel, chromium, and boron sold commercially as Thermospray [9] powder 16C. It was applied by a commercial firm to a thickness of about 0.015 in. on each gaging face. After lapping, the final thickness was 0.006 in. The coating required a fusing treatment after application and this was done by the firm, but the exact temperature to which the blocks were heated could not be ascertained. The hardness of the coating was measured as 62 R_c (converted from Vickers, 10 kg). After grinding and lapping, the surface of the coating appeared more porous than a wrought metal. A photomicrograph of the coating is shown in figure 18A.

9.2. Flame Plate

The flame plating process is somewhat similar to the thermal spray process, but its use is generally limited to the application of refractory alloys or ceramics, and with these materials a fusing treatment is not used. The coating is applied at supersonic velocities and is propelled by a controlled detonation within the barrel of the gun. The manufacturer claims that the surface of the piece being coated rarely exceeds 400° F. All flame plating was done by the originator of the process.[10] Both the tungsten carbide and the aluminum oxide coatings were applied to each gaging surface to a thickness of about 0.004 in. The thickness of the coating on each, after lapping, was on the order of 0.0025 in. After lapping, considerable porosity could be observed in each of these coatings with the unaided eye. The tungsten carbide coating contains about 8 percent of cobalt, whereas the Al_2O_3 is 99+% Al_2O_3. Hardness of both coatings is far in excess of 65 R_c. The coefficients of thermal expansion of both of these coatings are considerably lower than steel, and are given by the manufacturer as 2.89×10^{-6}/° F (70° to

[9] Trademark of the Metallizing Equipment Co., Inc.

[10] Linde Air Products Co.

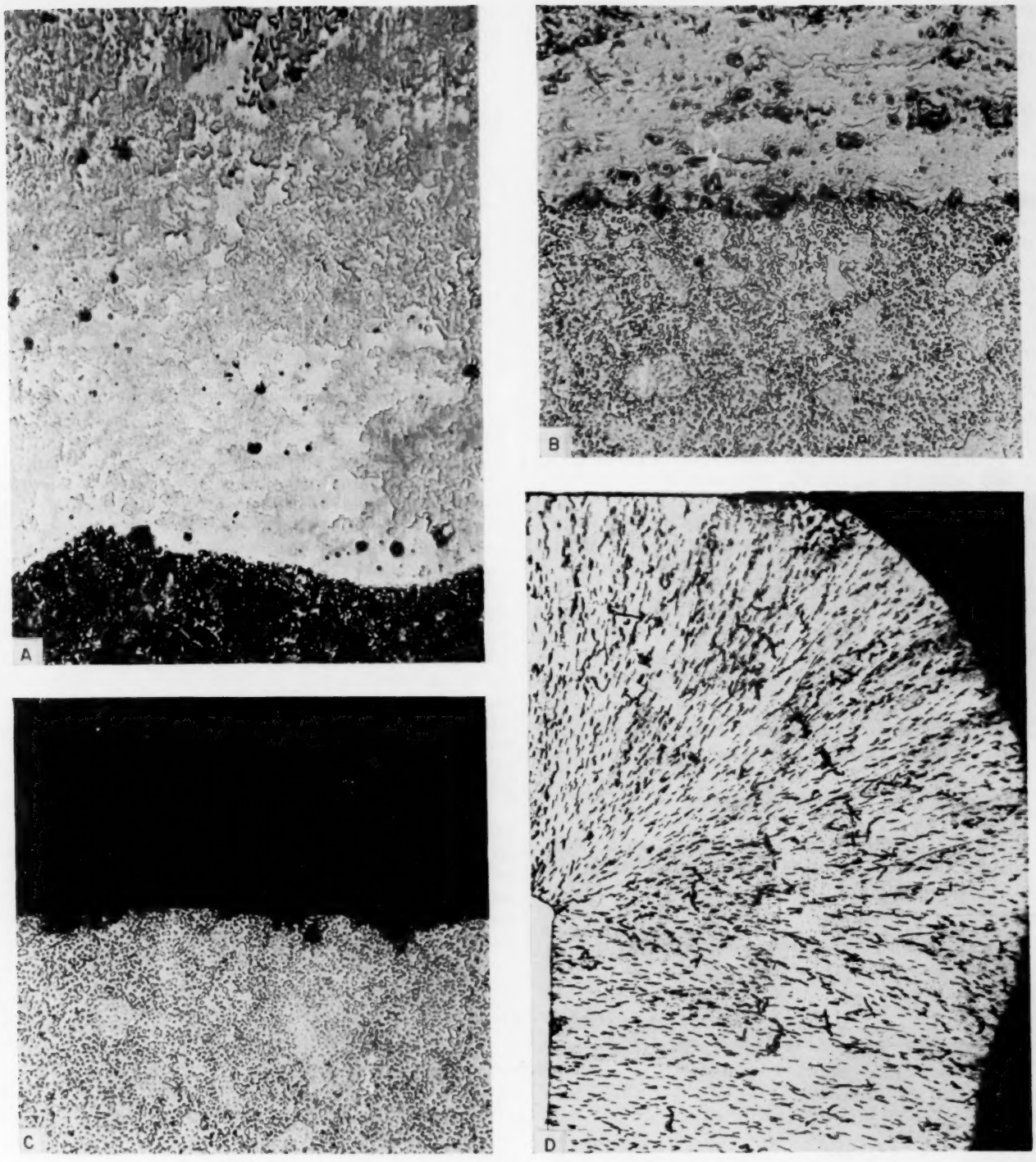

FIGURE 18. *Microstructures of hard coatings.*

All except the chromium have been ground and lapped to final thickness. The chromium is shown as plated and stress relieved.
A. Thermal sprayed Ni-Cr-B on 52100 steel. Etched with 1% Nital. ×500
B. Flame plated tungsten carbide on 52100 steel. Etched with 1% Nital. ×500
C. Flame plated aluminum oxide on 52100 steel. Etched with 1% Nital. ×500
D. Chromium plate on D-2 tool steel. Etched with HCl. ×200. White area at lower left is a corner of the steel block.

150° F) for tungsten carbide and 4.0×10^{-6}/° F (100 to 2,000° F) [11] for aluminum oxide. Photomicrographs of these two coatings are shown in figures 18B and C.

9.3. Chromium Plate

Chromium was applied directly over the steels by conventional electroplating techniques. The bath consisted of 0.53 oz (avdp) of sulfuric acid and 53 oz (avdp) of chromic acid per gallon of water. Current density was 180 to 190 amp/ft² and bath temperature was 120° F. The 52100 steel was plated on all surfaces and the 410 stainless was plated on the gaging surfaces only. The minimum thickness of the plating as applied was about 0.010 in. The finished thickness on the gaging faces and on the nongaging faces, when applied, was 0.005 in. Tests were run to ascertain the temperatures to which the plating could be subjected for the removal of hydrogen and for stress relief. As plated, the hardness was 68 R_c (converted from Knoop, 500 g) which did not fall below 65 R_c until a temperature in excess of 820° F was used. However, at this high temperature hairline cracks appeared in the plating, which were attributed to stresses caused by the differential thermal expansion of the block and the plating. A stress relieving temperature of 400° F for 5 hr was adopted to prevent cracking. A photomicrograph of the plated chromium after stress relieving at 820° F is shown in figure 18D. In appearance, it does not differ from the as-deposited coating.

10. Appendix C: Grinding Procedures and Other Details of Fabrication

10.1. 52100, Hardened

All of the 52100 blanks were ground to 2.04 in. $\times$1.39 in.$\times$0.39 in. prior to hardening and stabilization. After completion of the heat treatment, all but four of the blocks were ground to size on the four largest faces in a direction parallel to the 2 in. direction. The four excepted blocks (T–377, T–378, T–384, T–386) were ground on the four largest faces in a direction perpendicular to this dimension. The grinding wheel used and the operational settings of the surface grinder are given in table 9.

After final grinding the blocks were stress relieved for 3 hr at the temperatures shown in table 4, and sent to a commercial firm for lapping. The surfaces of the lapped blocks were surveyed for parallelism and flatness, some blocks were used for thermal expansion or other measurements, and the best of each lot as to parallelism and flatness were incorporated in the measuring program.

10.2. 410 Stainless, Nitrided

All 410 stainless blanks were ground to a length of 2.0050 in., but the width and thickness were varied so as to permit finishing to 1.375 in.$\times$0.375 in., since some of the surfaces received no grinding after nitriding and others received different amounts. Blanks intended for two stage nitriding, and on which the nongaging faces were to be left as nitrided, were ground to 1.374 in.$\times$0.374 in.; blanks on which only the frosty coating was to be removed were ground to 1.375 in.$\times$0.375 in.; and blanks on which the cases on nongaging faces were to be completely removed were made about 1.430 in.$\times$0.430 in. (earlier blocks were slightly smaller). Details of the nitriding treatments given individual blocks are shown in table 4. After nitriding, all three series of 410 blocks were ground to 2.0030 in. and two series were ground on the 4 nongaging surfaces to a width of 1.375 in. and a thickness of 0.375 in. Additional grinding details are given in table 9.

All of the nitrided 410 blocks were stress relieved at 975° F for 3 hr after grinding and before sending to commercial firms for lapping. The final hardness of the cases and the dates of the final stress reliefs are included in table 4. The blocks were then lapped commercially and the most suitable of each lot placed in the measuring program.

[11] The lower value for the coefficient of thermal expansion reported in table 2 was measured on solid Al_2O_3 blocks supplied by another manufacturer.

TABLE 9. *Details for grinding the hardened and coated gage blocks*

Type of surface	Grinding wheel		Crossfeed		Downfeed		Table speed	
	Rough	Finish	Rough	Finish	Rough	Finish [a]	Rough	Finish
			in.	*in.*	*in.*	*in.*	*ft/min*	*ft/min*
Hardened 52100	2A361G8V72K	2A361G8V72K	0.050	0.030	0.0015	0.0005	65	65
Nitrided 410 stainless	37C60J8V	37C100J8V or 37C100I7V	.010	.008	.0008	.0003	20	15
Thermal spray, Ni-Cr-B	37C46J8V	37C100I7V	.020	.015	.003	.0008	50	30
Flame plate, tungsten carbide	37C46J8V	37C100I8V or 37C100I8V	.025	.020	.0005	.0003	30	25
Chromium plate	8A461J12V22 or 38A8018BE	8A461J12V22	.030	.020	.001	.0005	65	20

[a] These values are for gaging surfaces and should be increased by about 50 percent on nongaging surfaces.

Notes to Table:

1. The nongaging faces of all blocks except four (T-377, T-378, T-384, T-386) were ground parallel to the 2 in. dimension. The four excepted blocks were ground perpendicular to the 2 in. direction.
2. The grinding wheel speed was 2300 RPM. All wheels were 10 in. in diam when new and were discarded when worn to about 6 in. All wheels were ¾ in. to 1 in. thick.
3. All grinding was done wet with White-Bagely WB-1500 solution diluted with water to approximately 150 parts of water per 1 part solution.
4. Downfeed was changed from rough to finish when 0.0005 in. of stock remained to be removed from each gaging surface and 0.002 in. to 0.005 in. remained on each nongaging surface.

10.3. Blocks With Hard Coatings

a. Thermal Spray

The 52100 steel blanks were ground to 1.987 in. $\times$1.375 in.$\times$0.375 in., and the nickel-chromium-boron coating applied on the gaging faces only to a thickness of about 0.015 in. The blocks were then ground in the same directions as described for the hardened 52100 blocks. The four nongaging surfaces were ground just sufficiently to remove the black scale formed during the fusing treatment. The gaging surfaces were ground to reduce overall length to 2.0030 in., leaving equal thickness of coating on each face. Further grinding details are given in table 9. After grinding, the blocks were stress relieved as shown in table 4, and sent to a commercial firm for lapping.

b. Flame Plate

The 52100 and the 410 stainless blanks were ground to 1.995 in.$\times$1.375 in.$\times$0.375 in. prior to coating the gaging surfaces to a thickness of about 0.004 in. The nongaging surfaces were not coated. The surfaces were ground to reduce overall length to 2.0030 in., leaving equal thickness of coating on each face. Additional grinding details are given in table 9. The nongaging faces were not ground after plating. The blocks were stress relieved as shown in table 4 prior to lapping.

c. Chromium Plate

It is a characteristic trait of the chromium plating process that thicker deposits of metal build up at sharp outside corners. Such a build up is shown in the photomicrograph in figure 18D. This condition makes necessary the careful alinement of the block in the grinding chuck to prevent the plating from being ground nonparallel to the underlying surface with a resultant nonuniform thickness of plating. This in turn can cause opposite gaging faces which are parallel at one temperature to become nonparallel at another temperature, particularly if the nongaging faces of the gage block are plated and ground nonuniformly. The need for extremely close control to avoid this condition can be eliminated by plating the gaging surfaces only. The 52100 blanks were ground to 1.990 in.$\times$1.365 in.$\times$0.365 in. prior to plating on all surfaces and the 410 stainless blanks were ground to 1.990 in.$\times$1.380 in.$\times$0.380 in. for plating on the gaging faces only. The blanks were stress relieved at 975° F for 3 hr in a cracked ammonia atmosphere prior to plating. After plating, each block was ground to 2.0030 in.$\times$1.375 in.$\times$0.375 in. in accordance with the details given in table 9. After grinding the blocks were stress relieved at 400° F for 5 hr in a cracked ammonia atmosphere and sent to a lapping firm for the final step in processing.

11. Appendix D: Nullification of Effects of Inhomogeneous, Nonlinear Measurement Error

One method that may be used in refining the intercomparison testing technique is to arrange the sequence of comparisons to annul the effects of measurement error. This can be illustrated by the following example. Consider the four test specimens, gage blocks A, B, C, D in table 10 to have lengths a, b, c, and d respectively. Consider the systematic error in the comparator reading to be a function of time with slope α_t, as shown in figure 19,[12] and for the present ignore random errors. If the time interval of one comparison of a pair of gage blocks is Δt, the systematic error in a comparison occurring at time t is $\alpha_t \Delta t$. However, the curve shown in figure 19 may be approximated by $(n-1)$

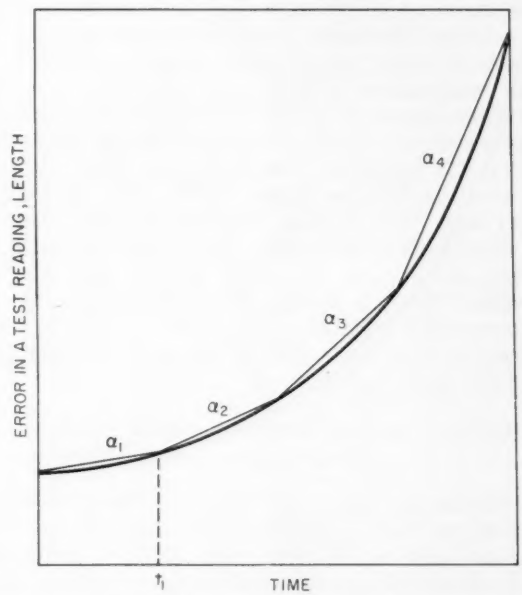

FIGURE 19. *A hypothetical nonlinear error function and its approximation by a number of linear segments.*

linear segments having slopes $\alpha_1, \alpha_2, \alpha_3, \ldots \alpha_{(n-1)}$ where n is the number of gage blocks in the group being intercompared, four in this example. The subscripts refer to periods of time in which n comparisons are made. If the interval of each comparison is again Δt, the errors occurring during the comparisons can be approximated by $\alpha_1 \Delta t$, $\alpha_2 \Delta t$, $\alpha_3 \Delta t$, . . . $\alpha_{(n-1)} \Delta t$. By arranging the sequence of comparisons these systematic errors may be distributed so that they are approximately nullified in the results obtained by means of the type of calculation illustrated in table 5. That is, if the sequence of comparisons is so arranged that each column contains equal increments of the systematic errors, then the column footings will contain equal amounts of

[12] This function need be continuous only during the time of each individual comparison.

such error and in that event computation by means of the method illustrated by table 5 will provide results in which these errors are nullified. Table 10 illustrates comparison data obtained when such a sequence of comparisons is utilized.[13] The circled numbers in table 10 indicate the sequence in which the comparisons were made. The residuals obtained with this sequence of comparison and utilizing the type of computation illustrated in table 5, would be grouped equally at $\alpha_1\Delta t$, $\alpha_2\Delta t$, and $\alpha_3\Delta t$. It will be noticed that with this sequence (table 10) these systemmatic errors may also be eliminated from the residuals as well as from the results by applying the least squares type of solution. This is because the comparisons symmetrical to the diagonal (table 10) are made in the same time period (while α remains constant), in fact one immediately following the other.

This latter requirement may introduce the necessity of further modification. With two comparisons of the same gage blocks being performed in a short time interval, thermal effects of handling in the first comparison may modify the error function in the second comparison so that two error functions exist; i.e., inhomogeneous comparison data are obtained. It was reasoned that if the second comparison always followed the first by a constant time interval, and if the handling of the gage blocks during the two comparisons was always consistent, then the two error functions would differ by a fixed amount. If α_{11}, α_{21}, α_{31}, . . . $\alpha_{(n-1)1}$ refer to the slopes of the first error function in the time periods 1, 2, 3, . . . $(n\text{-}1)$ respectively, and α_{12}, α_{22}, α_{32}, . . . $\alpha_{(n-1)2}$ refer to slopes of the second error function during these same time periods, then:

$$(\alpha_{11}-\alpha_{12})\Delta t=(\alpha_{21}-\alpha_{22})\Delta t=(\alpha_{31}-\alpha_{32})\Delta t =. \; . \; .(\alpha_{(n-1)1}-\alpha_{(n-1)2})\Delta t=k\Delta t \quad (1)$$

To eliminate this type of error from the final results of an intercomparison test there should exist, as was said above, an equal magnitude of error effect in each column of the calculation chart. For a group of n specimens there will be $n(n\text{-}1)$ comparisons in the intercomparison test; $n(n\text{-}1)/2$ comparisons of the first type, and an equal number of comparisons of the second type. If there is to be an equal number of comparisons of each type in a column, $(n\text{-}1)/2$ comparisons of a type should appear in a column. As this number must be an integer, n must be odd.

Table 11 indicates an intercomparison test schedule that would approximately nullify two nonlinear error functions in the final results, an additional gage block has been added to the group to fulfill the requirement that n be odd. Spaces containing two approximately equal values represent comparisons made at times when the error function could be indicated by either of two slopes; e.g., at time t_1 in figure 19.

Using eq (1) relating the error functions, the values indicated in table 12 are obtained from those shown in table 11. It will be noted that in the summations of each column of table 12 the amounts of systematic error are equal. This also holds true if a least squares type of solution is applied to the data in table 12. This is shown in table 13 where this method of computation is employed. Here the systematic error is cancelled within each column so that the column footings equally contain no systematic error. Thus employing either method of computation with this sequence of comparisons, appropriate comparison of the column footings provides the true relationships of the gage blocks even though inhomogeneous, nonlinear error functions are present in the observed measurements. The precision of the results obtained by the least squares method is, of course, greater than that obtained with the method of computation illustrated in table 5. Further, an examination of the residuals obtained with the two different methods of computation will indicate another reason for utilizing the least squares method. The residuals obtained from table 12 using the method of calculation illustrated in table 5 are given in table 14. It can be seen that residuals of various magnitude are obtained, the magnitude depending on the value of the two error functions (assuming Δt is constant). On the other hand, when the least squares method of computation is employed (table 13) the residuals shown in table 15 are obtained. It is obvious here that the magnitude of the residuals is dependent only upon the difference between the two error functions (again assuming Δt

[13] If α is constant, that is if $\alpha_1=\alpha_2=\alpha_3=$ . . . $\alpha_{(n-1)}$ then the systematic errors are nullified regardless of the sequence in which the comparisons are made since the equal increments of error always appear in each column.

TABLE 10. *Sequence of comparisons arranged to nullify effects of a nonlinear error function in an intercomparison test*

Blocks	*A*	*B*	*C*	*D*
A	*	① $b-a+\alpha_1\Delta t$	⑨ $c-a+\alpha_3\Delta t$	⑦ $d-a+\alpha_2\Delta t$
B	② $a-b+\alpha_1\Delta t$	*	⑤ $c-b+\alpha_2\Delta t$	⑪ $d-b+\alpha_3\Delta t$
C	⑩ $a-c+\alpha_3\Delta t$	⑥ $b-c+\alpha_2\Delta t$	*	③ $d-c+\alpha_1\Delta t$
D	⑧ $a-d+\alpha_2\Delta t$	⑫ $b-d+\alpha_3\Delta t$	④ $c-d+\alpha_1\Delta t$	*
Σ	$3a-b-c-d+\sum_{n=1}^{3}\alpha_n\Delta t$	$3b-a-c-d+\sum_{n=1}^{3}\alpha_n\Delta t$	$3c-a-b-d+\sum_{n=1}^{3}\alpha_n\Delta t$	$3d-a-b-c+\sum_{n=1}^{3}\alpha_n\Delta t$
Σ/4	$1/4(3a-b-c-d+\sum_{n=1}^{3}\alpha_n\Delta t)$	$1/4(3b-a-c-d+\sum_{n=1}^{3}\alpha_n\Delta t)$	$1/4(3c-a-b-d+\sum_{n=1}^{3}\alpha_n\Delta t)$	$1/4(3d-a-b-c+\sum_{n=1}^{3}\alpha_n\Delta t)$

TABLE 11. *Intercomparison test schedule nullifying the effects of two nonlinear error functions*

Blocks	*A*	*B*	*C*	*D*	*E*
A	•	② $b-a+\alpha_{12}\Delta t$	⑫ $c-a+\alpha_{32}\Delta t$	⑱ $d-a+\alpha_{31}\Delta t$	⑤ $e-a+\alpha_{11}\Delta t$
B	① $a-b+\alpha_{11}\Delta t$	•	⑧ $c-b+\alpha_{22}\Delta t$	㉑ $d-b+\alpha_{42}\Delta t$	⑮ $e-b+\alpha_{31}\Delta t$
C	$a-c+\alpha_{21}\Delta t$ ⑪ $\approx a-c+\alpha_{31}\Delta t$	⑦ $b-c+\alpha_{21}\Delta t$	•	④ $d-c+\alpha_{12}\Delta t$	⑱ $e-c+\alpha_{42}\Delta t$
D	$a-d+\alpha_{32}\Delta t$ ⑯ $\approx a-d+\alpha_{12}\Delta t$	⑲ $b-d+\alpha_{41}\Delta t$	③ $c-d+\alpha_{11}\Delta t$	•	⑩ $e-d+\alpha_{22}\Delta t$
E	$a-e+\alpha_{12}\Delta t$ ⑥ $\approx a-e+\alpha_{22}\Delta t$	⑭ $b-e+\alpha_{32}\Delta t$	⑰ $c-e+\alpha_{41}\Delta t$	⑨ $d-e+\alpha_{21}\Delta t$	•

TABLE 12. *Result of application of equation (1) to values in table 11, indicating equalization of error in column footings*

Blocks	*A*	*B*	*C*	*D*	*E*
A	•	$b-a+(\alpha_{11}-k)\Delta t$	$c-a+(\alpha_{21}-k)\Delta t$	$d-a+\alpha_{31}\Delta t$	$e-a+\alpha_{11}\Delta t$
B	$a-b+\alpha_{11}\Delta t$	•	$c-b+(\alpha_{21}-k)\Delta t$	$d-b+(\alpha_{41}-k)\Delta t$	$e-b+\alpha_{31}\Delta t$
C	$a-c+\alpha_{31}\Delta t$	$b-c+\alpha_{21}\Delta t$	•	$d-c+(\alpha_{11}-k)\Delta t$	$e-c+(\alpha_{41}-k)\Delta t$
D	$a-d+(\alpha_{41}-k)\Delta t$	$b-d+\alpha_{41}\Delta t$	$c-d+\alpha_{11}\Delta t$	•	$e-d+(\alpha_{21}-k)\Delta t$
E	$a-e+(\alpha_{21}-k)\Delta t$	$b-e+(\alpha_{31}-k)\Delta t$	$c-e+\alpha_{41}\Delta t$	$d-e+\alpha_{21}\Delta t$	•
Σ	$4a-b-c-d-e$ $+\left(\sum_{n=1}^{4}\alpha_{n1}-2k\right)\Delta t$	$4b-a-c-d-e$ $+\left(\sum_{n=1}^{4}\alpha_{n1}-2k\right)\Delta t$	$4c-a-b-d-e$ $+\left(\sum_{n=1}^{4}\alpha_{n1}-2k\right)\Delta t$	$4d-a-b-c-e$ $+\left(\sum_{n=1}^{4}\alpha_{n1}-2k\right)\Delta t$	$4e-a-b-c-d$ $+\left(\sum_{n=1}^{4}\alpha_{n1}-2k\right)\Delta t$
$\Sigma/5$	$1/5\left[4a-b-c-d-e+\left(\sum_{n=1}^{4}\alpha_{n1}-2k\right)\Delta t\right]$	$1/5\left[4b-a-c-d-e+\left(\sum_{n=1}^{4}\alpha_{n1}-2k\right)\Delta t\right]$	$1/5\left[4c-a-b-d-e+\left(\sum_{n=1}^{4}\alpha_{n1}-2k\right)\Delta t\right]$	$1/5\left[4d-a-b-c-e+\left(\sum_{n=1}^{4}\alpha_{n1}-2k\right)\Delta t\right]$	$1/5\left[4e-a-b-c-d+\left(\sum_{n=1}^{4}\alpha_{n1}-2k\right)\Delta t\right]$

TABLE 13. *Result of applying least squares type of solution to data in table 12*

Blocks	*A*	*B*	*C*	*D*	*E*
A	•	$b-a-\frac{k\Delta t}{2}$	$c-a-\frac{k\Delta t}{2}$	$d-a+\frac{k\Delta t}{2}$	$e-a+\frac{k\Delta t}{2}$
B	$a-b+\frac{k\Delta t}{2}$	•	$c-b-\frac{k\Delta t}{2}$	$d-b-\frac{k\Delta t}{2}$	$e-b+\frac{k\Delta t}{2}$
C	$a-c+\frac{k\Delta t}{2}$	$b-c+\frac{k\Delta t}{2}$	•	$d-c-\frac{k\Delta t}{2}$	$e-c-\frac{k\Delta t}{2}$
D	$a-d-\frac{k\Delta t}{2}$	$b-d+\frac{k\Delta t}{2}$	$c-d+\frac{k\Delta t}{2}$	•	$e-d-\frac{k\Delta t}{2}$
E	$a-e-\frac{k\Delta t}{2}$	$b-e-\frac{k\Delta t}{2}$	$c-e+\frac{k\Delta t}{2}$	$d-e+\frac{k\Delta t}{2}$	•
Σ	$4a-b-c-d-e$	$4b-a-c-d-e$	$4c-a-b-d-e$	$4d-a-b-c-e$	$4e-a-b-c-d$
$\Sigma/5$	$1/5(4a-b-c-d-e)$	$1/5(4b-a-c-d-e)$	$1/5(4c-a-b-d-e)$	$1/5(4d-a-b-c-e)$	$1/5(4e-a-b-c-d)$

is constant). This means that the residual distributions obtained when the least squares method of computation is employed will provide a more easily understood indication of inhomogeneity in the data. The fact that the two error functions differ by an amount k can be more readily determined from the residual distribution obtained when the least squares method is employed than when the method of computation illustrated in table 5 is used. Thus the method of least squares was adopted for the computation of all test results.

The above discussion assumed the absence of random errors and in that event indicated that if the method of least squares is employed when there are two error functions differing by an amount k present, residuals of $+(k\Delta t/2)$ and $-(k\Delta t/2)$ will

TABLE 14. *Residuals obtained by applying to the data in table 12 the method of computation illustrated in table 5*

Blocks	A	B	C	D	E
A	*	$(\alpha_{11}-k)\Delta t$	$(\alpha_{31}-k)\Delta t$	$\alpha_{31}\Delta t$	$\alpha_{11}\Delta t$
B	$\alpha_{11}\Delta t$	*	$(\alpha_{21}-k)\Delta t$	$(\alpha_{11}-k)\Delta t$	$\alpha_{31}\Delta t$
C	$\alpha_{31}\Delta t$	$\alpha_{21}\Delta t$	*	$(\alpha_{11}-k)\Delta t$	$(\alpha_{11}-k)\Delta t$
D	$(\alpha_{11}-k)\Delta t$	$\alpha_{11}\Delta t$	$\alpha_{11}\Delta t$	*	$(\alpha_{21}-k)\Delta t$
E	$(\alpha_{21}-k)\Delta t$	$(\alpha_{31}-k)\Delta t$	$\alpha_{11}\Delta t$	$\alpha_{21}\Delta t$	*

TABLE 15. *Residuals obtained by applying to the data in table 12 a least squares method of solution*

Blocks	A	B	C	D	E
A	*	$-\frac{k\Delta t}{2}$	$-\frac{k\Delta t}{2}$	$+\frac{k\Delta t}{2}$	$+\frac{k\Delta t}{2}$
B	$+\frac{k\Delta t}{2}$	*	$-\frac{k\Delta t}{2}$	$-\frac{k\Delta t}{2}$	$+\frac{k\Delta t}{2}$
C	$+\frac{k\Delta t}{2}$	$+\frac{k\Delta t}{2}$	*	$-\frac{k\Delta t}{2}$	$-\frac{k\Delta t}{2}$
D	$-\frac{k\Delta t}{2}$	$+\frac{k\Delta t}{2}$	$+\frac{k\Delta t}{2}$	*	$-\frac{k\Delta t}{2}$
E	$-\frac{k\Delta t}{2}$	$-\frac{k\Delta t}{2}$	$+\frac{k\Delta t}{2}$	$+\frac{k\Delta t}{2}$	*

be obtained. If random errors are present, the residuals will tend to distribute randomly about $+(k\Delta t/2)$ and $-(k\Delta t/2)$ providing a bimodal distribution.

If such a bimodal residual distribution is broken down into two distributions, one obtained from first comparisons and the other from the second comparisons in an intercomparison test, the medians of these two distributions will fall at $+(k\Delta t/2)$ and $-(k\Delta t/2)$ respectively. That such a separation between the medians of the residual distributions of the first and second comparisons evidences an inhomegeneity in the data brought about by an asymmetry in the actual handling of the blocks in each pair can be seen from the following example. Consider three blocks A, B, and C of actual lengths, a, b, and c respectively. Let these blocks be compared according to the following intercomparison schedule:

1. B minus A.
2. A minus B.
3. A minus C.
4. C minus A.
5. C minus B.
6. B minus C.

Assume that there is some variation or asymmetry in the handling of the gage blocks which causes each pair to have its correct length difference in the first comparison of each pair, but to appear to have a length difference departing from this correct value by an amount $\alpha\Delta t$ in the second comparison of each pair. Then the observed values obtained from the comparisons should be those shown in table 16, where the number of each comparison is also given by the circled figures on the chart.

TABLE 16. *Observed values which would be obtained in an intercomparison test affected by consistent asymmetrical handling of the gage blocks*

Blocks	A	B	C
A	*	① $b-a$	④ $c-a+\alpha\Delta t$
B	② $a-b+\alpha\Delta t$	*	⑤ $c-b$
C	③ $a-c$	⑥ $b-c+\alpha\Delta t$	*

Applying the first step in the least squares method of solution, that is dividing by two the alegebraic difference of comparisons symmetrical to the diagonal, gives what might be called adjusted observed values for each comparison. Thus for comparison 1, an adjusted observed value would be obtained by subtracting the observed value for comparison 2 (the comparison which is diagonally symmetrical to comparison 1) from the observed value for comparison 1; e.g., $(b-a)-(a-b+\alpha\Delta t)$ and then dividing this by two,

$$\frac{(b-a)-(a-b+\alpha\Delta t)}{2}=\frac{2b-2a-\alpha\Delta t}{2}$$

This value for comparison 1 and the adjusted observed values for the other five comparisons are given in table 17 which also illustrates the next step in the calculations. The columns are summed as indicated and these summations are divided by the number of gage blocks to give column footings. Next, a calculated result for each comparison is computed by subtracting the column footings one from another. Thus, the calculated result for comparison 1, the B minus A comparison, is obtained by subtracting the column footing of column A from that of column B; e.g.,

$$\left(\frac{2b-a-c}{3}\right)-\left(\frac{2a-b-c}{3}\right)=b-a.$$

TABLE 17. *Adjusted observed values calculated from data in table 16*

Blocks	A	B	C
A	*	① $\frac{2b-2a-\alpha\Delta t}{2}$	④ $\frac{2c-2a+\alpha\Delta t}{2}$
B	② $\frac{2a-2b+\alpha\Delta t}{2}$	*	⑤ $\frac{2c-2b-\alpha\Delta t}{2}$
C	③ $\frac{2a-2c-\alpha\Delta t}{2}$	⑥ $\frac{2b-2c+\alpha\Delta t}{2}$	*
Σ	$2a-b-c$	$2b-a-c$	$2c-a-b$
$\Sigma/3$	$\frac{2a-b-c}{3}$	$\frac{2b-a-c}{3}$	$\frac{2c-a-b}{3}$

These calculated results are shown in table 18. The residuals are then obtained by subtracting the calculated result for any comparison (table 18) from the adjusted observed value for that comparison

TABLE 18. *Calculated results obtained from data in table 17*

Blocks	A	B	C
A	*	①$b-a$	④$c-a$
B	③$a-b$	*	⑤$c-b$
C	②$a-c$	⑥$b-c$	*

TABLE 19. *Residuals obtained from data in tables 17 and 18*

Blocks	A	B	C
A	*	① $-\frac{\alpha\Delta t}{2}$	④ $+\frac{\alpha\Delta t}{2}$
B	② $+\frac{\alpha\Delta t}{2}$	*	⑤ $-\frac{\alpha\Delta t}{2}$
C	③ $-\frac{\alpha\Delta t}{2}$	⑥ $+\frac{\alpha\Delta t}{2}$	*

(table 17). Thus the residual for comparison 1 would be given in this case by:

$$\left(\frac{2b-2a-\alpha\Delta t}{2}\right)-(b-a)=-\frac{\alpha\Delta t}{2}.$$

The residuals for these comparisons are given in table 19 together with the number of the comparison.

It should be noted from the comparison schedule that comparisons 1, 3, and 5 are first comparisons on each pair of blocks involved while comparisons 2, 4, and 6 are, in each case, second comparisons. From the residuals obtained, it can be seen that each first comparison gives a residual of $-(\alpha\Delta t/2)$, while each second comparison gives a residual of $+(\alpha\Delta t/2)$.

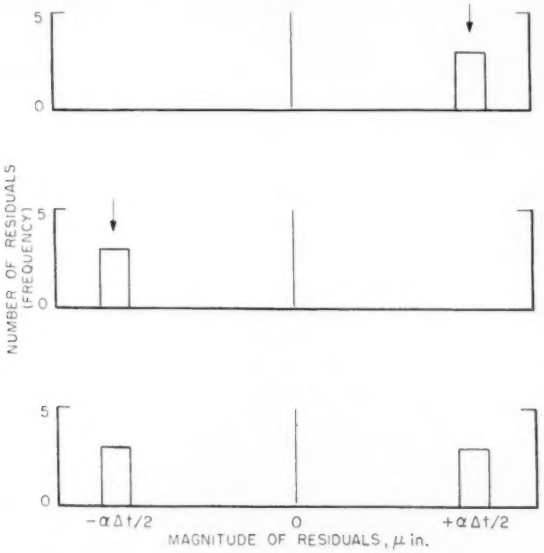

FIGURE 20. *Frequency distribution of residuals which would be obtained in an intercomparison test if the comparisons of lengths are affected only by a consistent asymmetrical handling of the gage blocks.*

The residual distributions when plotted appear as in figure 20 where the total distribution is plotted at the bottom, the residuals from the first comparisons in the center distribution, and the residuals from the second comparisons in the distribution at the top of the figure. The split between the medians of the first and second comparison distributions which are indicated by the arrows is very apparent and is evidence of an asymmetry in the handling of the gage blocks.

12. References

[1] F. H. Rolt, Gages and fine measurements, Vol. 1, (Macmillan & Co. Ltd., London, England, 1929).

[2] W. B. Emerson, Secular length changes of gage blocks during twenty-five years, metrology of gage blocks, NBS Circ. **581,** 71, (1957).

[3] F. C. Victory, Dimensional instability in gage blocks, metrology of gage blocks, NBS Circ. **581,** 81 (1957).

[4] H. Scott, Dimensional changes accompanying the phenomena of tempering and aging tool steels, Trans. Am. Soc. Steel Treating, **9,** 277 (1926).

[5] S. G. Fletcher, and M. Cohen, The dimensional stability of steel, Pt. I—Subatmospheric transformation of retained austenite, Trans. Am. Soc. Metals, **34,** 216 (1945).

[6] S. G. Fletcher, B. L. Averbach, and M. Cohen, The dimensional stability of steel, Pt. II—Further experiments on subatmospheric transformation, Trans. Am. Soc. Metals, **40,** 703 (1948).

[7] B. L. Averbach, M. Cohen, and S. C. Fletcher, The dimensional stability of steel, Pt. III—Decomposition of martensite and austenite at room temperature, Trans. Am. Soc. Metals, **40,** 728 (1948).

[8] B. L. Averbach, and M. Cohen, The isothermal decomposition of martensite and retained austenite, Trans. Am. Soc. Metals, **41,** 1024 (1949).

[9] B. S. Lement, B. L. Averbach, and M. Cohen, The dimensional stability of steel, Pt. IV—Tool steels, Trans. Am. Soc. Metals, **41,** 1061 (1949).

[10] W. J. Harris, and M. Cohen, Stabilization of the austenite-martensite transformation, Trans. AIME, **180,** 447 (1949).

[11] L. E. Gippert, and G. M. Butler, Changes in size and toughness of high carbon—high chromium steels due to subzero treatments, Trans. Am. Soc. Metals, **39,** 540 (1947).

[12] A. L. Christenson, Retained austenite and residual stress measurements on certain gage blocks, metrology of gage blocks, NBS Circ. **581,** 75 (1957).

[13] National Physical Laboratory, Report on the metrology department for the year 1927, Lab. Rept. 151, (1927).

[14] C. Candler, Modern interferometers, (Hilger and Watts Ltd., London, England, 1951).

[15] J. C. Evans, The determination of thermal lagging times, Proc. Phys. Soc., **59,** 242 (1947).

[16] T. R. Young, Achromatic interferometer for gage block comparison, NBS Circ. **581,** 43 (April 1957) and Gage block comparator, NBS Tech. News Bull. **40,** 176 (December 1956).

[17] W. Kösters, Der gegenwärtige Stand der Meter-Definition, des Meteranschlusses und seine internationale Bedeutung für Wissenschaft und Technik, Werkstattstichnik in Werksleiter **32,** 527 (1938).

[18] B. Page, Calibration of meter line standards of length at the National Bureau of Standards, J. Research NBS **54,** 1 (1955).

[19] A. L. Christenson, and E. S. Rowland, X-ray measurement of residual stress in hardened high carbon steel, Trans. Am. Soc. Metals, **45,** 638 (1953).

[20] A. M. Dexter, Zero point one, ASTE, **59,** Book 1, paper 195 (1959).

(Paper 64C3–38)

JOURNAL OF RESEARCH of the National Bureau of Standards—Engineering and Instrumentation
Vol. 64C, No. 3, July–September 1960

Variation of Resolving Power and Type of Test Pattern

Francis E. Washer and William P. Tayman

(April 7, 1960)

The plane of best average definition is located for a number of lenses of a type used in airplane mapping cameras. Three different types of test pattern are used for each lens. These patterns are the long-line, short-line, and annulus. Results of measurement that show the variation of resolving power throughout the region of usable imagery are given for each type of test pattern with two types of photographic emulsion. It is found that the plane of best average definition can be located equally well with each type of pattern. There are, however, pronounced differences in the numerical magnitudes of the values of resolving power determined with the various types of test pattern. In general, the highest values are attained with the long-line patterns. Values of the various rating indices $\sqrt{R_\beta T_\beta}$, AWAR, and ADWAR are given together with a comparison of the different order of merit assigned by these indices.

1. Introduction

The quality of definition throughout the image plane of lenses used in airplane mapping cameras is of prime importance in ensuring satisfactory photography upon which to base the compilation of reliable maps. In forming an estimate of the probable quality of definition for a given lens, it is customary to use the measured values of resolving power for specified areas of the image plane as the principal criterion upon which to base the estimate.

The measured values of the resolving power have in general proved satisfactory for locating the plane of best average definition and for determining the suitability of a given lens for use in an aerial camera. Consequently, most specifications dealing with aerial cameras contain requirements prescribing the minimum acceptable values of the resolving power. Unfortunately, there is marked variance in the type of test chart used in various laboratories and in the conditions of use. This variance is a source of difficulty in any attempt to formulate an international specification dealing with the calibration of photogrammetric cameras as was done at the Washington meeting of the International Society of Photogrammetry in 1952 [1].[1] To obviate the difficulty, a specification was adopted for trial and discussion that permitted the use of several different types of resolving power target. It was noted that it was not possible at the time to standardize on a single type of resolving power target.

Three types of test chart were included in this tentative specification which were the three-line target used by the U.S. Air Force [2], the Cobb two-line chart used in Great Britain [3], and the annulus chart used in Canada [4]. All of these charts were of low contrast except the three-line chart of the Air Force which included both high- and low-contrast versions. The three-line chart used by the National Bureau of Standards was not included, as it had been in existence for only a few months prior to the conference, and its properties were not widely known.

Each of the charts covered by the specification included a series of patterns whose sizes were in a geometric progression with the $\sqrt[6]{2}$ preferred for the common ratio between adjacent pattern sizes. The NBS chart of 1952 not only differed from the others in length of line but also in the ratio between successive pattern sizes which is $\sqrt[4]{2}$.

In the seven years that have passed since the adoption of this specification, agreement on a single type of chart has not yet developed. A few publications have appeared [5, 6] that permit an estimate of the differences in resolving power likely to be found for line charts compared with annulus charts.

Because of some of the differences that exist between the procedures recommended for the calibration of photogrammetric cameras and those used at the National Bureau of Standards, it is worthwhile to describe the methods used at the Bureau and to compare the results derived therefrom with those that would be obtained by the methods approved in the international standard. In the present paper measured values of resolving power obtained with the NBS chart of 1952 [7] are compared with those obtained with the three-line chart used by the U.S. Air Force and with an annulus chart which differs from that prescribed in the international specification in that it is a high-contrast instead of a low-contrast target. In addition, the size ratio for successive patterns in each type of target is $\sqrt[4]{2}$ instead of $\sqrt[6]{2}$.

Results are presented for six lenses using two types of emulsion. Values of the several indices that might be used as rating factors such as $\sqrt{R_\beta T_\beta}$, AWAR, and ADWAR are compared. It is found that the plane of best average definition may be located equally well with any of the three types. Values of resolving power obtained with the NBS chart are usually higher than those obtained with the other charts.

[1] Figures in brackets indicate the literature references at the end of this paper.

2. Method of Measurement

2.1. Test Camera

The National Bureau of Standards precision lens testing camera [8] was used in making the negatives from which the values of resolving power are determined. This device is well adapted for use in locating the plane of best average definition of a lens. Its construction and mode of operation simplifies the process of evaluating the resolving power of a lens in a series of focal planes spaced at definite intervals along the optical axis. Moreover, by using one type of chart in the odd-numbered collimators and another type in the even-numbered collimators, it is possible to register the imagery in the same identical series of focal planes for each type of chart for the same series of angular separations β from the axis on the same plate.

2.2. Test Charts

Three distinct types of test charts are used in the present investigation. All three are high-contrast charts, i.e., the difference in optical density between line and background exceeds 2.0. Each chart consists of a suitable range of sizes of the test object with the size proceeding in a geometric progression with $\sqrt[4]{2}$ (or 1.1892) as the common ratio. The various types of test chart are described in the following sections.

a. NBS Resolution Test Chart of 1952

This chart was introduced in 1952 and is described in detail in NBS Circular 533. The test chart, shown in figure 1, is a composite chart prepared by superimposing one test chart upon a four-times enlargement of the same chart. In this chart, all patterns have the same line count, namely three to each group. Two series of test patterns are included

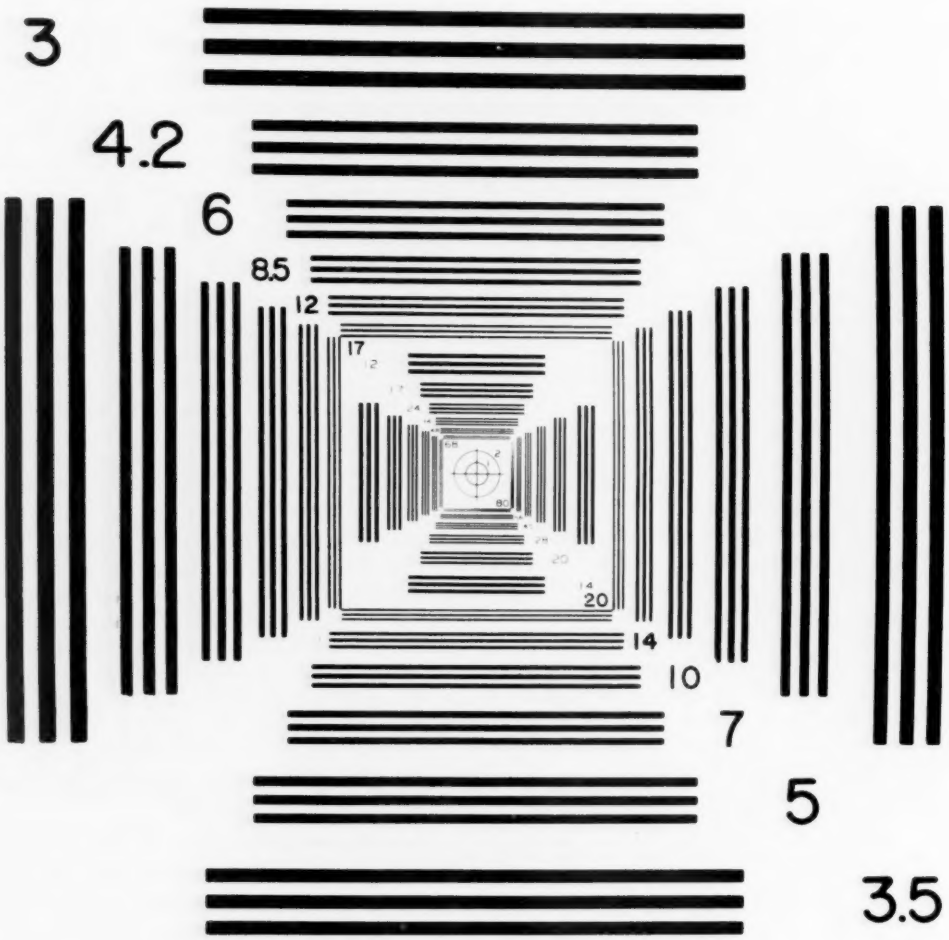

FIGURE 1. *NBS long-line resolution chart with extended range.*

This chart is a composite formed by superposing the NBS standard test chart upon a 4× enlarged copy of the master chart. The ratio of line spacings in adjacent groups of the master chart is equal to $\sqrt{2}$; however, the ratio of the line spacings of corresponding opposite patterns is $\sqrt[4]{2}$. Consequently, for this extended range chart, the values of resolving power that can be measured for a lens of 6-in. focal length range from 6.3 to 168 lines/mm, in a geometric series proceeding by $\sqrt[4]{2}$.

such that the spacings in the line pattern of a given group differ from those in the adjacent group in the ratio of $\sqrt[3]{2}$. However, the spacing in the initial pattern of one series differs from the initial pattern of the other series by $\sqrt[4]{2}$. Consequently, considered as a whole, the range of values provided by this chart proceeds by the $\sqrt[4]{2}$. The size of the chart used as a reticle in the collimators of the lens testing camera for this study was such that the range of values in the image plane of the lenses investigated extends from 6.3 to 168 lines/mm. The most striking feature of this chart is the relatively great length of the lines forming the patterns. The ratio of length to width of line is sufficiently great that the visual resolving power as read will not be subject to variations arising from end effects, and the images will continue to look like lines down to the limit of resolution. The ratio is also sufficiently great that the variation of resolving power with ratio of length to width of line can be neglected [5]. In addition, both the original test pattern and the images on a negative formed by a lens can be readily scanned with a recording microdensitometer. This property permits the user to make accurate measurements of the contrast between line and space for both object and image for studies involving degradation of contrast for a particular lens-emulsion combination.

The same size test chart is used in the various collimators so that it is necessary to apply the "cosine" and "cosine-squared" corrections to images formed off-axis.

b. Short Three-Line Charts

These charts, shown in figure 2, were adapted from that used in the camera calibrator [9]. The basic line pattern of this chart is the same as that prescribed in the specification prepared by Commission I of the International Society of Photogrammetry in 1952 [1] which is listed under paragraph 1.3.3 of the specification as the "three line high contrast target." The three-line patterns reduce in size in a geometric progression, the ratio being $\sqrt[4]{2}$. The sizes of the patterns in the off-axis targets have been modified to compensate for the "cosine" and "cosine-squared" factors affecting the resolving power values for radial and tangential lines. For lenses having a focal length of 6 in., the range of values of resolving power in the image plane of the lens under test extends from 5.9 to 264 lines/mm.

c. Annulus Test Chart

At the time the chart containing the series of short three-line patterns was made, a series of annulus patterns was included as may be seen in figure 2. The range of sizes is the same as for the short three-line patterns. The shape of the off-axis patterns was also distorted so that at specified angles they register on the test negative as circles. This pattern differs from that described in the international specification in paragraph 1.3.5 [1] in that it is high-contrast and consists of a dark circle on a light background.

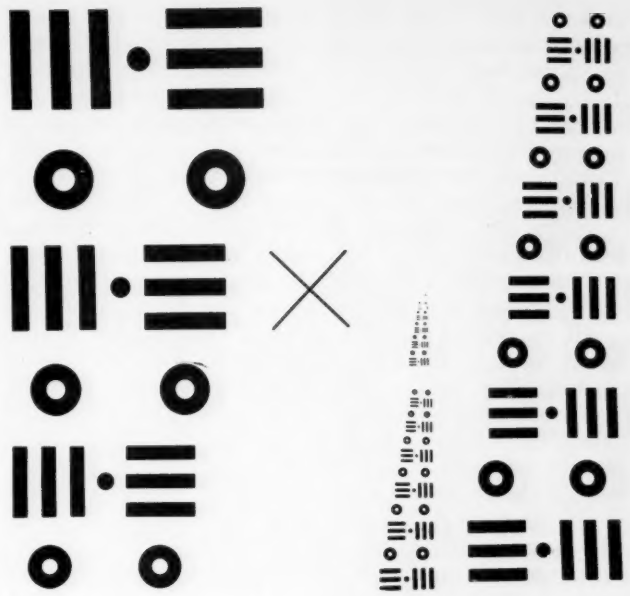

FIGURE 2. *Short three-line and annulus chart.*

The three-line chart consists of patterns of parallel lines in two orientations with spaces varying in a geometric progression by $\sqrt[4]{2}$. The circle or annulus charts change in size in a geometric progression by $\sqrt[4]{2}$. For a lens having a focal length of 6 in., the range of values in the image plane extends from 5.9 to 264 lines/mm.

2.3. Test Negative

In making the test negative, the lens under test is initially so alined that its optical axis is parallel to and approximately coincident with the axis of the collimated beam emergent from the first collimator. The lens is adjusted along the bench to a location such that the collimated beam at 40° from the axis fills the front aperture of the lens under test as viewed through the lens at an inclination of 40° from the axis. The plate holder is adjusted to a position such that the front surface of the emulsion is in the plane of best visual axial focus for the central row of images to be registered on the plate. The plate holder is then moved to a position 1.05 mm nearer to the lens, and an exposure is made by illuminating the reticles in odd-numbered collimators, which thus registers the imagery on the plate at 10° intervals for the range of angles from $\beta=0$ to $\beta=40°$. This process is repeated with the plate being moved 0.15 mm farther from the lens until 15 exposures have been made with the last for the plane 1.05 mm farther from the lens than the position of best visual axial focus. Between each exposure, the plate holder is also moved downward by an amount sufficient to avoid superposition of successive rows of images. The foregoing operation registers the imagery for the long-line patterns on the plate. The plate holder is then returned to its initial position for which the emulsion surface is 1.05 mm nearer to the lens than the plane of best visual axial focus; the plate is displaced sidewise in its holder approximately 12 mm; and the entire bench on which the camera is mounted is rotated on its pivot by 5° so

that the axis of the lens is now parallel to and nearly coincident with the axis of the collimated beam emergent from the second collimator. The foregoing procedure is then repeated with the exception that exposures are made by illuminating the reticles in the even-numbered collimators, which again register imagery on the plate at 10° intervals for the range of angles from $\beta=0°$ to $\beta=40°$. This process registers the imagery for the short three-line and annulus patterns on the plate. The exposed plate is then processed to form the finished negative from which values of resolving power are determined.

All exposures are made with the reticles illuminated by light from tungsten lamps with K–3 filters between the light source and test charts. Neutral filters are used to adjust the intensity of the illumination of the plate so that the final resulting optical density of each image on the negative is approximately the same for all values of β. The two types of photographic plates used in this work were Eastman Spectroscopic VF, which has a fine-grained panchromatic emulsion, and Eastman Super Panchro Press, Type C.

2.4. Reading the Negative

The negative images were examined with a microscope using powers ranging from 30× to 50×. The criteria for declaring a particular line pattern to be the finest resolved were that all coarser patterns were clearly resolved and that the number of lines in a given pattern was the same as that of the corresponding pattern in the object. For the annulus pattern, the prime criterion that all coarser patterns were resolved was used.

It was readily apparent that there were marked differences in the ease of reading the three types of patterns. The long-line pattern was the easiest of the three, and the feeling of confidence in the values recorded was accordingly the greatest. The short-line pattern was the next easiest, but there was an appreciably higher level of uncertainty in the reliability of the higher values of resolving power. The annulus pattern was the most difficult when attempting to determine the limit of resolution. It is noteworthy that the single circular black spot, which appears on the test chart in each cell of the target and which is identical in size with the white inner circular area of the annulus pattern, was easier to read than the annulus. It was usually possible to distinguish this single spot on the negative down to smaller sizes than the annulus; it could usually be detected down to one or two steps smaller in size. The presence of this spot was frequently used as an aid in determining the limiting resolution for the annulus.

3. Results of Measurements

The results of measurement on six wide-angle lenses are reported and analyzed in this study. Three lenses, designated Nos. 1, 2, and 5, are essentially distortion free; the other three, designated 3, 4, and 6, have moderate amounts of distortion. Measurements of resolving power were made at 10° intervals from 0° to 40°.

Negatives were made with both VF and SP emulsions for each of the six lenses. For a given lens, the plane of best visual axial focus is the same for each emulsion. The measured equivalent focal length for the plane of best visual axial focus for a given lens was the same for each emulsion and type of target pattern. The maximum range of change in measured equivalent focal length for the various conditions of test did not exceed ± 0.02 mm for a given lens.

In the presentation and analysis of the results of measurement in an investigation of this sort, it is necessary to keep in mind the primary aims of the study. First, the intercomparison of the magnitudes of the measured values of resolving power for each type of pattern and emulsion is important. Second, it is important to determine whether or not any shift of the plane of best definition occurs with type of target pattern. In addition, the manner in which the values of resolving power for the various patterns wax and wane as the image plane approaches and passes through the plane of best visual axial focus is of interest.

In an earlier paper [10], the measured values of resolving power for tangential lines (T_β) and radial lines (R_β) obtained with the short three-line chart using VF and SP emulsions for values of β ranging from 0° to 40° at 10° intervals are presented in tabular form for lens No. 1. In addition, the values of the geometric means values $\sqrt{R_\beta T_\beta}$ are also given. In this paper, a discussion of the various indices used in locating the plane of best average definition is given. These indices are as follows:

(*a*) *Root Mean Square Mean* (*RMSM*). This is defined as

$$\text{RMSM}=\sqrt{\frac{\sum R_\beta T_\beta}{n}}=\sqrt{\overline{R_\beta T_\beta}}.$$

In the above expression, R_β and T_β are measured values of resolving power for radial and tangential lines for discrete values of β ranging from 0° to 40° in 10° steps. The number of steps, n, in this instance is five.

(*b*) *Area Weighted Average Resolution* (*AWAR*). This is defined as

$$\text{AWAR}=\sum \frac{a_\beta}{A}\sqrt{R_\beta T_\beta},$$

where a_β is the area of a particular annular zone, R_β is the average resolving power for radial lines, and T_β is the average resolving power for tangential lines for that zone. The value of $\sum a_\beta$ is the entire area A of the picture formed.

(*c*) *Area and Depth-of-Focus Weighted Average Resolution* (*ADWAR*). This is defined as

$$\text{ADWAR}=\sum \frac{a_\beta r_\beta}{A}\sqrt{R_\beta T_\beta},$$

where

$$r_\beta^2 = \frac{d_0 d_0}{d_{T\beta} d_{R\beta}},$$

where $d_{T\beta}$ is the depth of focus for tangential lines, $d_{R\beta}$ is the depth of focus for radial lines, and d_0 is the depth of focus on axis for a given value of resolving power.

Because some of the results for one type of pattern used in this paper have already been presented in tabular form, it was decided to present the results of measurement and some of the quantities derived from the measurements in graphical form.

The results of measurement are presented in figures 3 through 9. Values of the resolving power for tangential lines (T) and radial lines (R) are shown for the two emulsions and three patterns for lenses 1 and 3 only. These results on these two lenses are given in the left and central columns of graphs in figures 3, 4, 5, and 6. The nature of the test pattern is indicated by the symbols, L for long-line, S for short-line, and A for annulus. The values obtained for the annular patterns are shown on both sets of graphs for ready comparison with the T and R values for L and S. It is readily apparent from these graphs that the higher values found for resolution of long lines are more evident for the regions inside focus (negative values of Δf) than for the regions outside focus (positive values of Δf). This is in keeping with a similar finding reported by Selwyn and Tearle [11]. This effect is present for both VF and SP emulsions for axial resloving power; it is usually more noticeable for the VF emulsion. The values found for the annulus pattern are generally substantially lower than the values for either tangential or radial lines throughout the region of usable imagery as might be inferred from similar comparisons previously reported [5, 6].

The values of $\sqrt{R_\beta T_\beta}$, the geometric mean value of resolving power for tangential and radial lines, are given for each value of β for each of the six lenses for both emulsions. For lenses No. 1 and 3, values of $\sqrt{R_\beta T_\beta}$ are shown in the right-hand column of figures 3, 4, 5, and 6. The values of $\sqrt{R_\beta T_\beta}$ for lenses No. 2, 5, 4, and 6 are presented in the five upper sets of graphs in figures 8 and 9. These curves permit a ready comparison of the average values of resolving power for the three types of patterns for the five values of β. It also seems more appropriate to use values of $\sqrt{R_\beta T_\beta}$ in a comparison of values obtained by line targets with that obtained by the annulus target. For the annulus, the value of $\sqrt{R_\beta T_\beta}$ is simply the observed value of the resolving power.

For lenses No. 1 and 3, values of the three indices $\sqrt{R_\beta T_\beta}$, AWAR, and ADWAR for the three types of line patterns and two emulsions are given in figure 7. For lenses 2, 5, 4, and 6, values of $\sqrt{R_\beta T_\beta}$ are shown in the lower row of graphs in figures 8 and 9. Values of AWAR and ADWAR were determined for these four lenses but are not shown.

3.1. Location of the Plane of Best Average Definition

The plane of best average definition was located for each lens both by graphical analysis and by location of the maximum value of the various indices for each type of pattern and each emulsion.

a. Graphical Analysis

The plane of best average definition for each lens for each set of conditions was located by the graphical method reported in a previous paper [10]. The separations, Δf, along the optical axis of the lens of the focal planes of best average definition for short-line and annular patterns selected by graphical analysis from the focal planes of best average definition for long-line patterns selected in the same manner, are shown in table 1. It is clear from this table that there is no significant variation in the location of the focal plane of best average definition for these three types of test pattern. Such variation, as appears is usually random and within the limits of experimental error. Table 2 shows the variation in location of the plane of best average definition for the three types of patterns using SP emulsion compared with that for long-line patterns and VF emulsion. In this instance, the optimum image plane for SP emulsion appears on the average to be slightly nearer the lens than the corresponding plane for VF emulsion.

TABLE 1. *Separations, Δf, of the focal plane of best average definition for long lines selected by graphical analysis from focal planes of best average definition for short-line and annulus patterns selected by graphical analyses*

Results are given for six lenses and two emulsions.

Lens No.	Values of Δf			
	VF emulsion		SP emulsion	
	Short line	Annulus	Short line	Annulus
	mm	*mm*	*mm*	*mm*
1	0.00	0.15	0.00	0.00
2	.00	.15	.00	−.15
3	.30	.00	.00	.00
4	.00	.15	.00	.00
5	.00	.00	.00	.00
6	.00	.00	.00	.00

TABLE 2. *Separations, Δf, of the focal plane of best average definition for long lines with VF emulsion selected by graphical analysis from the focal planes of best average definition for long line, short line, and annulus patterns obtained with SP emulsion by graphical analyses*

Lens No.	Values of Δf		
	Long line	Short line	Annulus
	mm	*mm*	*mm*
1	0.15	−0.15	−0.15
2	−.15	−.15	−.30
3	.00	.00	.00
4	.00	.00	.00
5	.00	.00	.00
6	−.15	−.15	−.15

549993—60——4

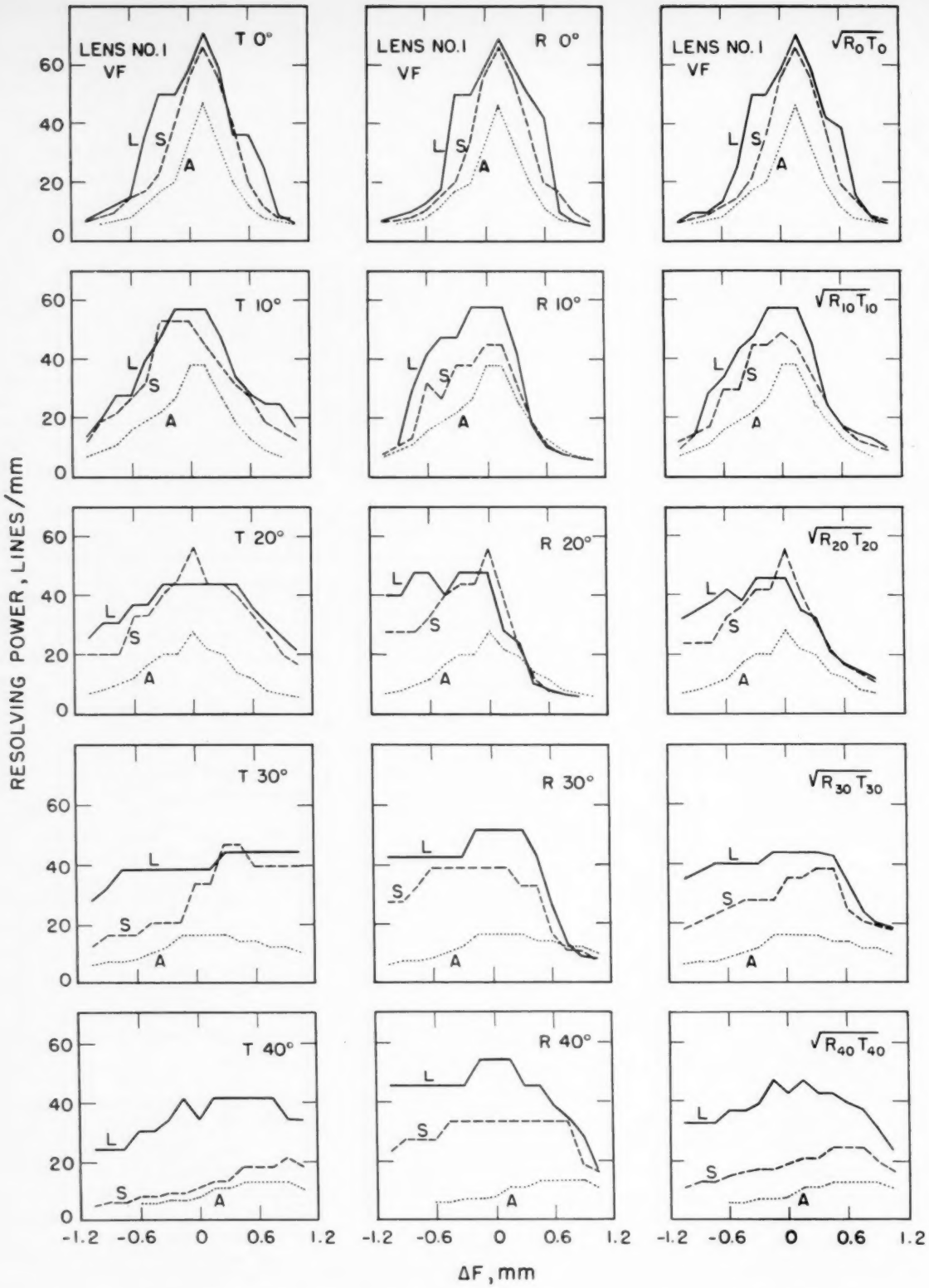

FIGURE 3. *Resolving power versus position of the image plane for lens No. 1 with VF emulsion.*

The resolving power throughout the region of usable imagery is shown for tangential (T) and radial (R) lines and for the average $\sqrt{R_\beta T_\beta}$ at 10° intervals from 0° to 40°. Values are given for long-line (L) and short-line (S) test patterns. Values for the annular (A) pattern are shown with the corresponding T, R, and $\sqrt{R_\beta T_\beta}$ values for ready comparison. The zero of abscissas (Δf) marks the position of best visual axial focus, and positive values of abscissas indicate positions farther from the lens.

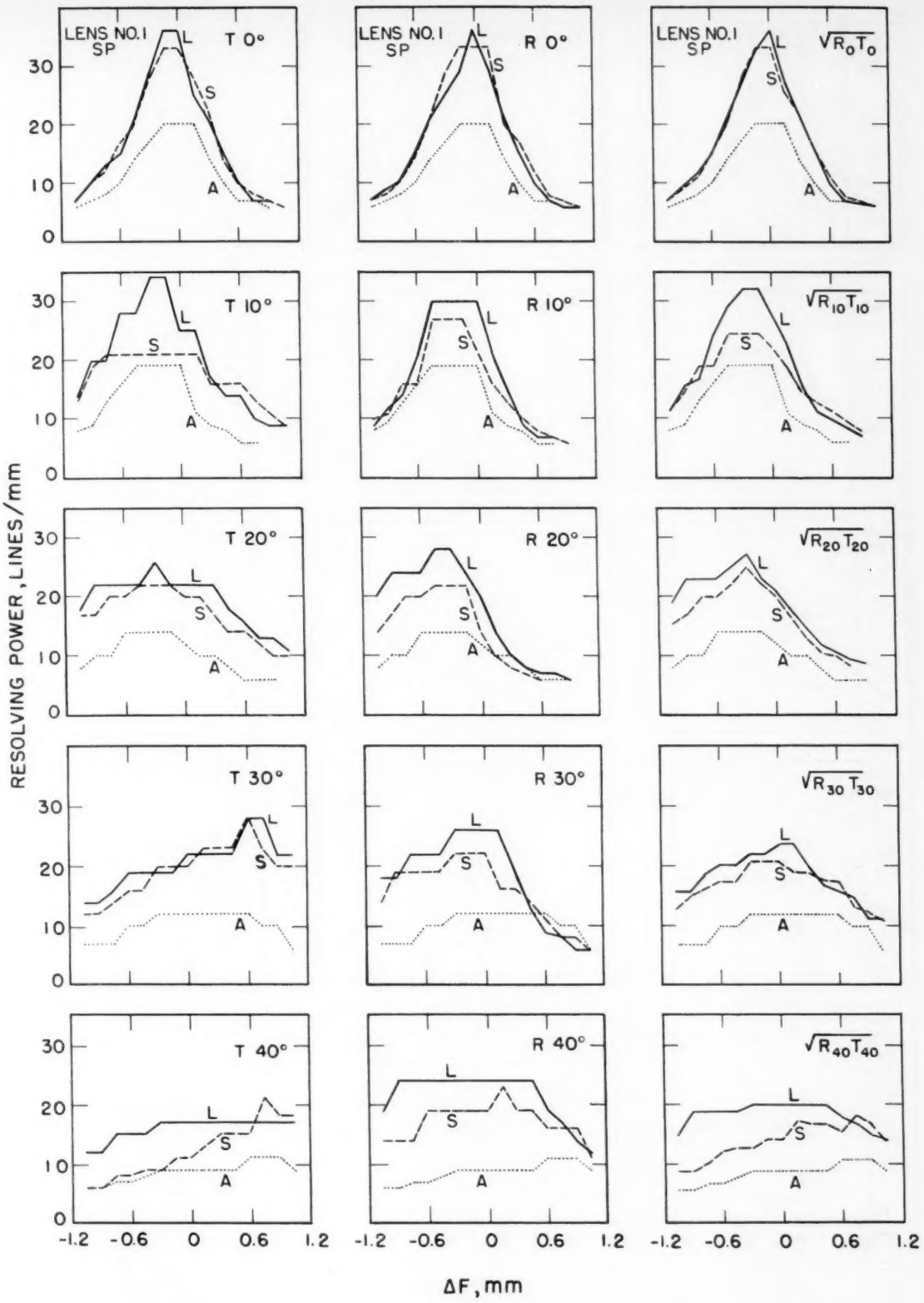

FIGURE 4. *Resolving power versus position of the image plane for lens No. 1 with SP emulsion.*

The resolving power throughout the region of usable imagery is shown for tangential (T) and radial (R) lines and for the average $\sqrt{R_\beta T_\beta}$ at 10° intervals from 0° to 40°. Values are given for long-line (L) and short-line (S) test patterns. Values for the annular (A) pattern are shown with the corresponding T, R, and $\sqrt{R_\beta T_\beta}$ values for ready comparison. The zero of abscissas (Δf) marks the position of best visual axial focus, and positive values of abscissas indicate positions farther from the lens.

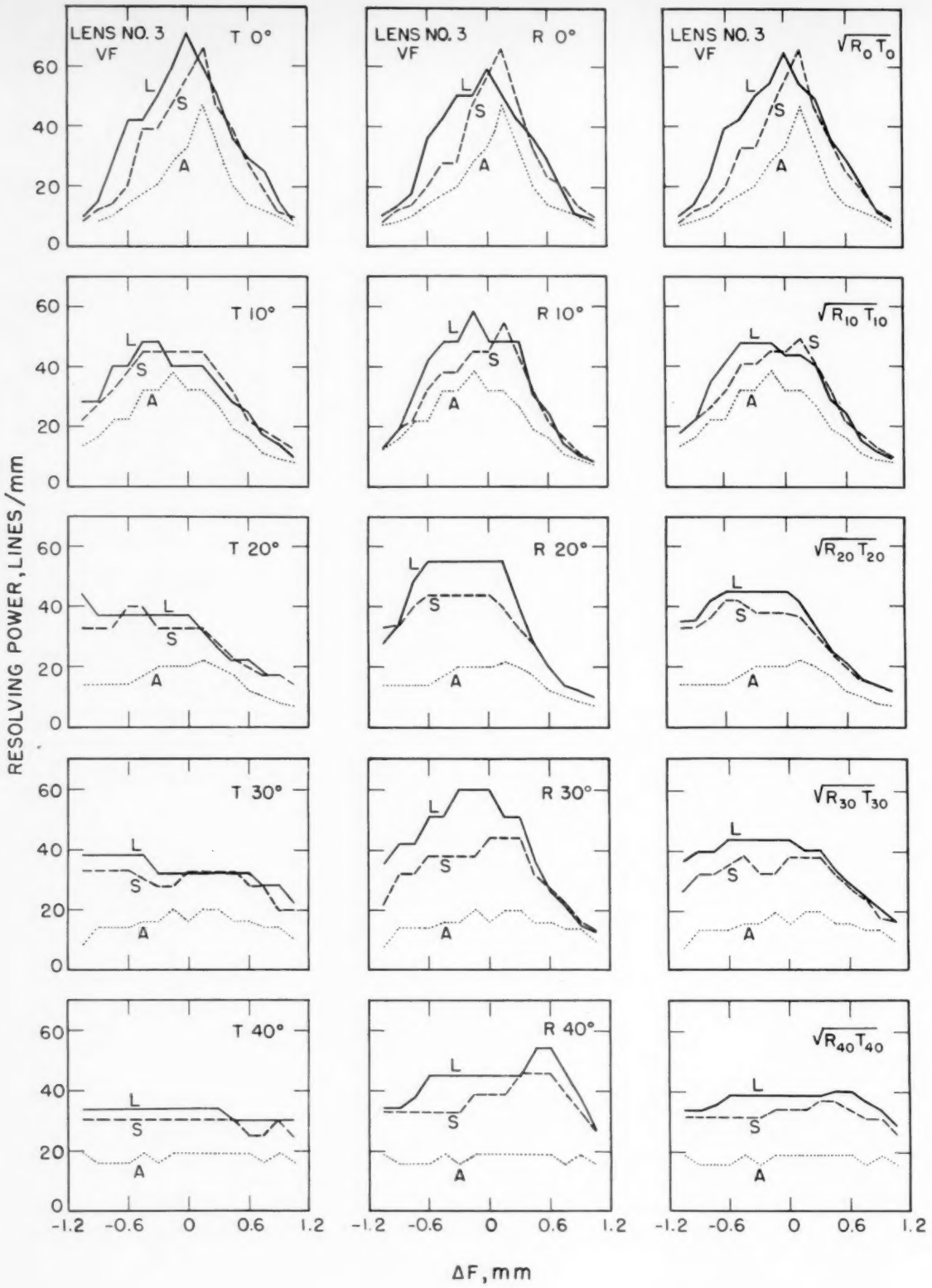

FIGURE 5. *Resolving power versus position of the image plane for lens No. 3 with VF emulsion.*

This set of curves gives information on lens No. 3 of the same type that is given in figure 3 for lens No. 1.

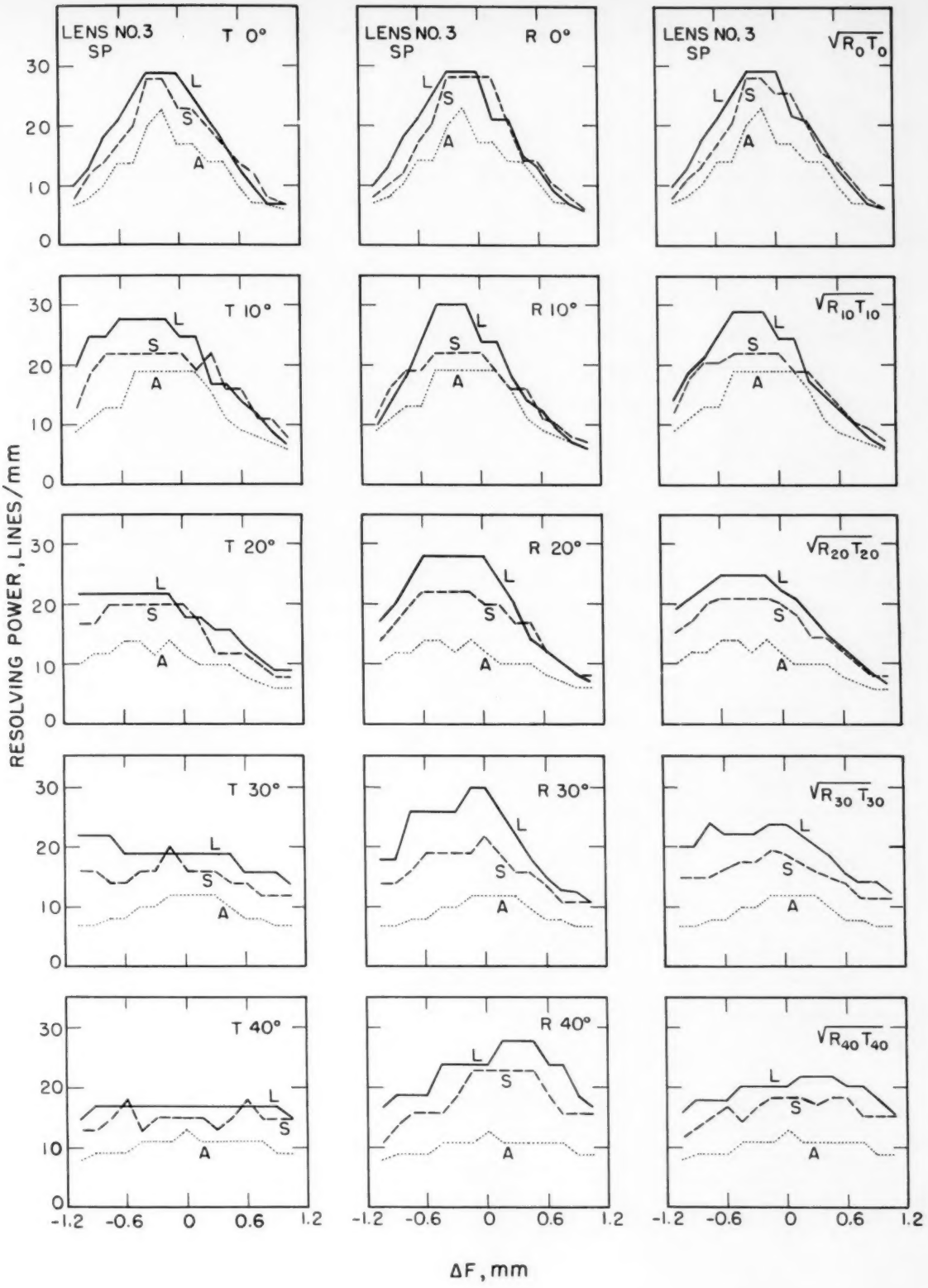

FIGURE 6. *Resolving power versus position of the image plane for lens No. 3 with SP emulsion.*

This set of curves gives information on lens No. 3 of the same type that is given in figure 4 for lens No. 1.

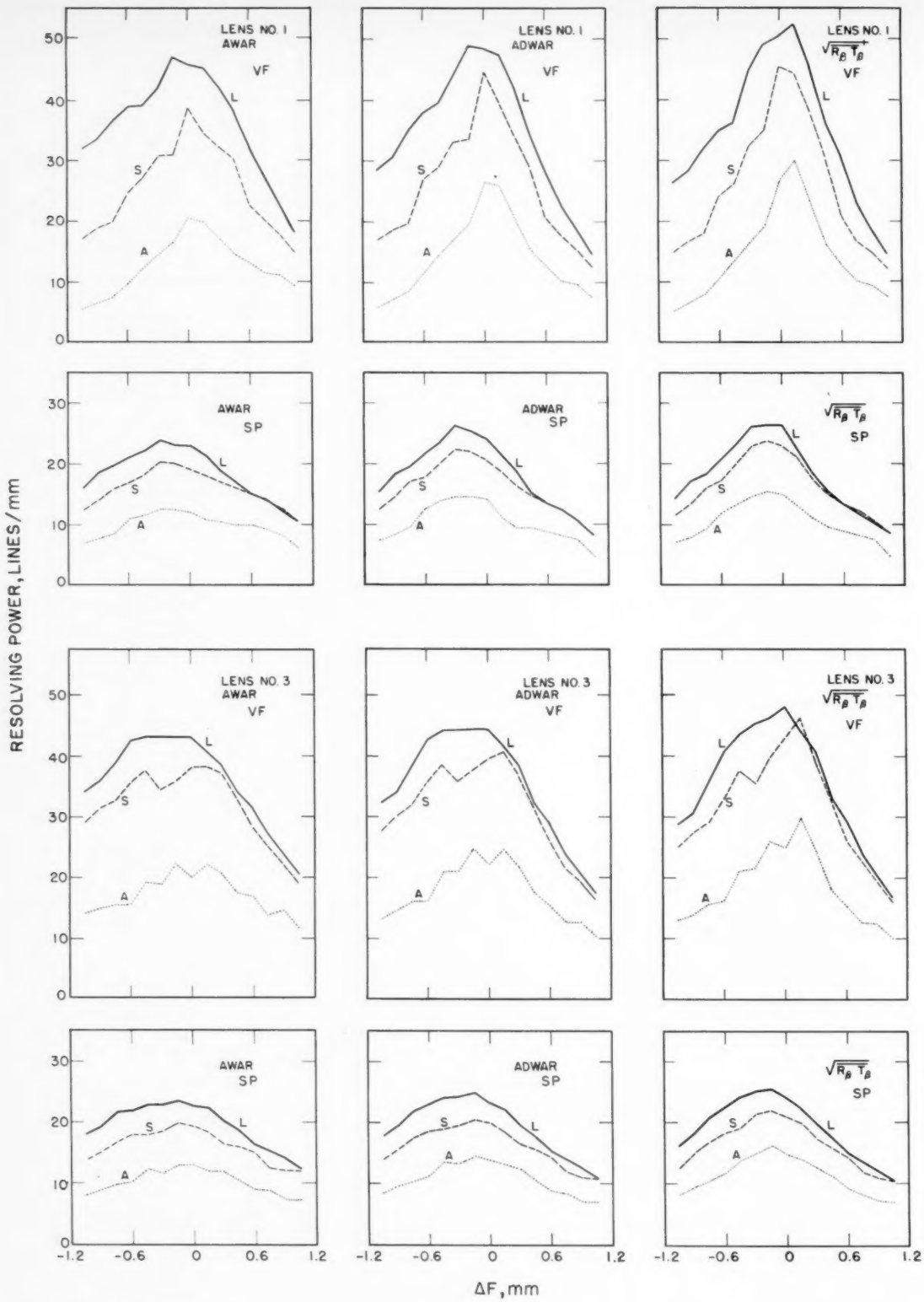

FIGURE 7. *Variation of AWAR, ADWAR, and $\sqrt{R_\beta T_\beta}$ with position of the image plane for lenses Nos. 1 and 3 for VF and SP emulsions.*

Values of these indices are given in lines per millimeter for long-line (*L*), short-line (*S*), and annular (*A*) patterns. The zero of abscissas (Δf) marks the position of best visual axial focus, and positive value of abscissas indicate positions farther from the lens.

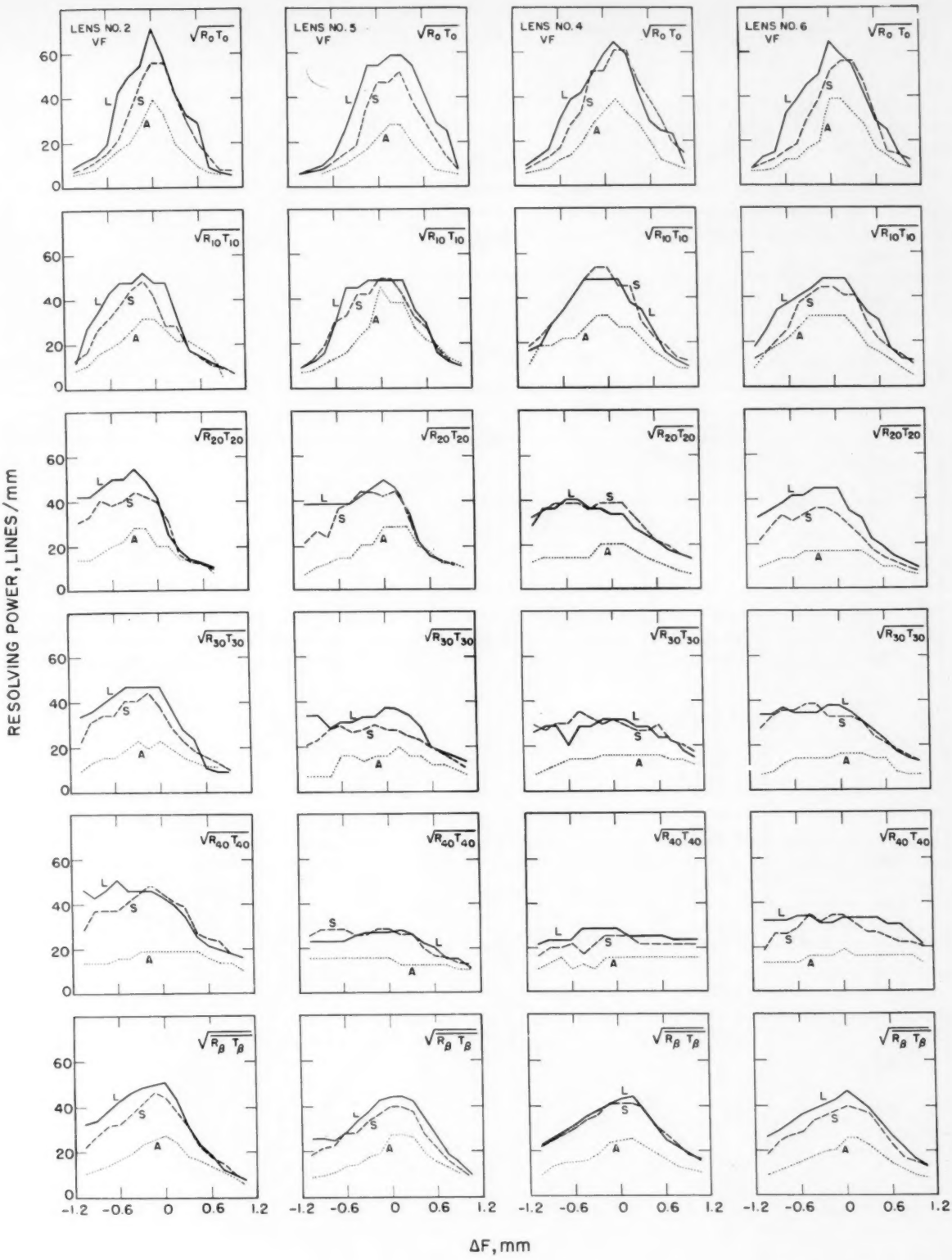

FIGURE 8. *Average resolving powers versus position of the image plane for four lenses with VF emulsions.*

Values of the average resolving power $\sqrt{R_\beta T_\beta}$ are shown at 10° intervals from 0° to 40°. The lowest box in each column shows values of the root mean square mean $\sqrt{\overline{R_\beta T_\beta}}$. Values are given for long-line (L), short-line (S), and annular (A) patterns. The zero of abscissas (Δf) marks the position of best visual axial focus, and positive value indicate positions farther from the lens.

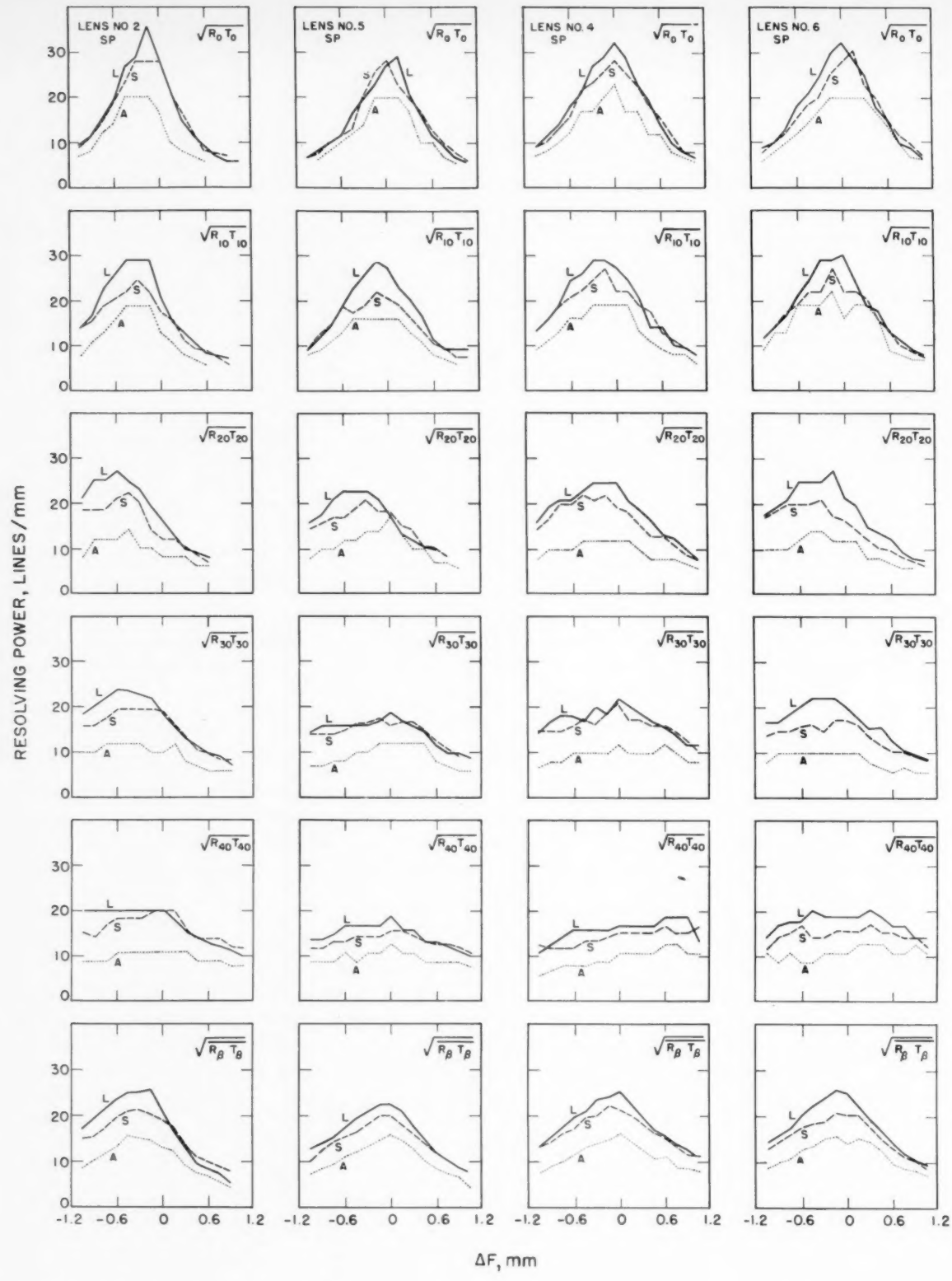

FIGURE 9. *Average resolving powers versus position of the image plane for four lenses with SP emulsions.*

Values of the average resolving power $\sqrt{R_\beta T_\beta}$ are shown at 10° intervals from 0° to 40°. The lowest box in each column shows values of $\sqrt{\overline{R_\beta T_\beta}}$. Values are given for long-line (*L*), short-line (*S*), and annular (*A*) patterns. The zero of abscissas marks the position of best visual axial focus, and positive value indicate positions farther from the lens.

b. Maximum Value of Indices

The plane of best average definition for each lens for each set of conditions was also located with the aid of each of the three indices, $\sqrt{\overline{R_\beta T_\beta}}$, AWAR, and ADWAR. In each instance, the optimum image plane was located with respect to the focal plane of best average definition for long-line patterns selected by graphical analysis. The results are shown in table 3. It is clear from this table that the variation is, in general, within the limits of experimental error.

TABLE 3. *Separations, Δf, of the focal plane of best average definition for long lines selected by graphical analysis from the focal planes indicated by the maximum value of the indices* $\sqrt{\overline{R_\beta T_\beta}}$, *AWAR, and ADWAR*

Results are shown for six lenses and two emulsions.

Lens No.	VF emulsion			SP emulsion		
	Long line	Short line	Annulus	Long line	Short line	Annulus
(a) Separations, Δf, of plane selected by graphical analysis from planes selected by maximum value of $\sqrt{\overline{R_\beta T_\beta}}$ for						
	mm	*mm*	*mm*	*mm*	*mm*	*mm*
1	0.15	0.00	0.15	0.00	0.00	0.00
2	.15	.00	.15	.15	.00	−.15
3	.15	.30	.30	.00	.00	.00
4	.15	.00	.15	.00	−.15	.00
5	.15	.15	.00	.00	.00	.00
6	.00	.00	.00	.00	.00	.00
(b) Separations, Δf, of plane selected by graphical analysis from planes selected by maximum value of AWAR for						
1	−0.15	0.00	0.00	−0.15	−0.15	0.00
2	−.15	.00	−.15	−.30	−.15	−.15
3	−.30	.30	.00	.00	.00	.15
4	.00	.00	−.15	.00	.00	.00
5	.00	.00	.00	.00	−.15	.00
6	.00	−.30	.00	.00	.00	.00
(c) Separations, Δf, of plane selected by graphical analysis from planes selected by maximum value of ADWAR for						
1	−0.15	0.00	0.00	−0.15	−0.15	0.00
2	.00	.00	.00	−.15	.00	−.15
3	−.15	.30	.00	.00	.00	.00
4	.00	−.15	−.15	.00	−.15	.00
5	.00	.00	.00	.00	−.15	.00
6	.00	−.15	.00	.00	.00	.00

4. Comparison of Results Obtained With the Three Charts

In the foregoing sections, it was shown that the focal plane of best average definition could be readily located using any one of the three types of test charts under consideration. Moreover, such minor differences in location that were noted could be regarded as negligible in comparison with experimental error.

In the present section, some attention is given to the actual magnitudes of the values of resolving power obtained with the various charts. Some attention is also given to the use of the indices as rating factors.

4.1. Values of Resolving Power in Focal Plane of Best Average Definition

Values of $\sqrt{R_\beta T_\beta}$, $\sqrt{\overline{R_\beta T_\beta}}$, AWAR, and ADWAR are shown in tables 4 and 5 for various patterns and emulsions. These values are all for the plane of best average definition for long-line patterns. In some instances, the value of a given index was higher for an adjacent plane. This is indicated in table 6 which shows the departure in percent of the maximum of a given index from the value reported in tables 4 and 5. It is noteworthy that the departures are for the most part negligible. It is clear from tables 4 and 5 that it would be difficult to determine the value of resolving power that might be obtained for a given type of pattern at a given angle β when

TABLE 4. *Comparison of values of average resolving power obtained with three types of test chart using VF emulsion in the plane of best average definition for long lines selected by graphical analysis.*

Values of $\sqrt{R_\beta T_\beta}$, $\sqrt{\overline{R_\beta T_\beta}}$, AWAR, and ADWAR are shown for six lenses for long line, short line, and annulus charts. All values of resolving power are given in lines per millimeter.

Lens No.	Target	$\sqrt{R_\beta T_\beta}$					Indices		
		0°	10°	20°	30°	40°	$\sqrt{\overline{R_\beta T_\beta}}$	AWAR	ADWAR
1	Long line	59	58	46	44	43	50	46	49
	Short line	56	49	56	35	19	45	38	45
	Annulus	33	38	28	16	8	27	20	26
2	Long line	54	52	49	47	46	50	48	49
	Short line	47	49	42	45	49	46	46	46
	Annulus	28	32	28	20	19	26	23	26
3	Long line	54	48	45	44	39	46	43	46
	Short line	66	49	36	38	34	46	38	41
	Annulus	33	32	20	16	19	25	20	22
4	Long line	59	48	39	32	29	43	35	38
	Short line	51	54	34	33	26	41	34	38
	Annulus	33	32	20	16	13	24	18	21
5	Long line	54	48	49	38	28	44	39	41
	Short line	47	49	42	28	29	40	34	38
	Annulus	23	45	28	16	16	28	23	28
6	Long line	65	48	45	38	33	47	39	42
	Short line	51	45	34	33	34	40	35	37
	Annulus	39	32	17	16	19	26	20	22

TABLE 5. *Comparison of values of average resolving power obtained with three types of test chart using SP emulsion in the plane of best average definition for long lines as selected by graphical analysis*

Values of $\sqrt{R_\beta T_\beta}$, $\sqrt{\overline{R_\beta T_\beta}}$, AWAR, and ADWAR are shown for six lenses for long line, short line, and annulus charts. All values of resolving power are given in lines per millimeter.

Lens No.	Target	$\sqrt{R_\beta T_\beta}$					Indices		
		0°	10°	20°	30°	40°	$\sqrt{\overline{R_\beta T_\beta}}$	AWAR	ADWAR
1	Long line	32	32	23	22	20	23	25	26
	Short line	33	24	22	21	14	24	20	22
	Annulus	20	19	14	13	9	15	12	15
2	Long line	29	29	23	23	20	25	23	25
	Short line	25	24	20	20	18	22	20	21
	Annulus	20	19	10	12	11	15	12	14
3	Long line	29	29	25	24	20	26	24	25
	Short line	28	22	21	20	19	22	20	21
	Annulus	23	19	14	12	11	16	13	14
4	Long line	32	27	25	22	17	25	22	24
	Short line	25	27	22	19	14	22	19	21
	Annulus	23	19	12	12	11	16	13	14
5	Long line	27	27	21	19	19	23	20	22
	Short line	28	20	18	16	16	20	17	18
	Annulus	20	16	17	12	13	16	14	15
6	Long line	30	29	27	22	19	23	25	26
	Short line	25	27	18	18	16	21	18	20
	Annulus	20	22	12	10	11	16	12	14

TABLE 6. *Departure in percent of the maximum value of a given index from that occurring in the plane of best average definition for long lines selected by graphical analysis*

Results are shown for $\sqrt{R_\beta T_\beta}$, AWAR, and ADWAR for six lenses with each type of target for VF and SP emulsions.

Lens No.	VF			SP		
	$\sqrt{R_\beta T_\beta}$	AWAR	ADWAR	$\sqrt{R_\beta T_\beta}$	AWAR	ADWAR
	Long-line			Long-line		
1	4.0	2.6	0.6	3.4	3.0	0.0
2	2.5	1.0	.0	2.7	1.7	1.6
3	3.3	0.0	3.3	0.0	0.0	0.0
4	3.0	.0	0.0	.0	.0	.0
5	0.9	.0	.0	.0	.0	.0
6	.0	.0	.0	.0	.0	.0
	Short-line			Short-line		
1	0.0	0.0	0.0	0.0	1.5	1.8
2	.0	.0	.0	.0	1.0	0.0
3	.0	.0	.0	.0	0.0	.0
4	.0	.0	.2	.0	.5	.0
5	.5	.0	.0	.0	1.2	1.6
6	.0	3.6	.5	.0	0.0	0.0
	Annulus			Annulus		
1	0.0	3.9	1.9	0.0	0.0	0.0
2	6.5	0.0	0.0	3.8	6.1	6.7
3	13.0	.0	.0	0.0	0.8	0.0
4	3.6	.5	.5	.0	.0	.0
5	0.0	.0	.0	.0	.0	.0
6	.0	.0	.0	.0	.0	.0

the value of resolving power for a different type pattern is known. The relative magnitudes of $\sqrt{R_\beta T_\beta}$ at a given value of β for the various type patterns are significantly different for the different lenses. Certain generalizations can, however, be drawn. The values of $\sqrt{R_\beta T_\beta}$ in general are highest for the long-line and lowest for the annular patterns with the values for the short-line patterns being usually slightly lower than those for the long-line patterns.

4.2. Use of Indices as Rating Factor

In table 7, the relative ratings of lenses 1 through 6 are shown for each of the various conditions of test. It is, at once, apparent that the order of merit is not the same for the various patterns. This variation in the order of merit emphasizes the fact that indices such as these ought not to be used to differentiate between lenses unless the differences are of the order of 10 percent or more. Thus, in considering the relative merits of these lenses, 1, 2, and 3 are usually more favorably rated than 4, 5, and 6. However, it would be difficult to arrange 1, 2, and 3 in order of decreasing performance. Likewise, it would be difficult to arrange 4, 5, and 6 in proper order. Most of this difficulty arises from the relatively small differences in the particular index.

4.3. Relative Magnitudes of Values of Resolving Power

a. For Three Types of Test Pattern

It was evident at a fairly early stage in the investigation that there is no clear-cut ratio existing between

TABLE 7. *Rating of six lenses in order of merit for VF and SP emulsions*

The ratings are made for each of three targets on the basis of the relative magnitude of the three indices $\sqrt{R_\beta T_\beta}$, AWAR, and ADWAR.

Lens No.	VF emulsion			SP emulsion		
	Rating based on			Rating based on		
	$\sqrt{R_\beta T_\beta}$	AWAR	ADWAR	$\sqrt{R_\beta T_\beta}$	AWAR	ADWAR
	(a) Long-line			(a) Long-line		
1	1	2	1	4	1	1
2	1	1	1	2	4	3
3	4	3	3	1	3	3
4	6	6	6	2	5	5
5	5	4	5	4	6	6
6	3	4	4	4	1	1
	(b) Short-line			(b) Short-line		
1	3	2	2	1	1	1
2	1	1	1	2	1	2
3	1	2	3	2	1	2
4	4	5	4	2	4	2
5	5	5	4	6	6	6
6	5	4	6	5	5	5
	(c) Annulus			(c) Annulus		
1	2	3	2	5	4	1
2	3	1	2	5	4	3
3	5	3	4	1	2	3
4	6	6	6	1	2	3
5	1	1	1	1	1	1
6	3	3	4	1	4	3

values of resolving power obtained for one type of pattern and those obtained for another type of pattern. This is at once apparent from consideration of the various curves in figures 3 through 9. Even on axis, there are variations which might be in part a consequence of the large interval between successive patterns but are more likely a consequence of the inherent uncertainty in locating the limit of resolution. However, some idea of the approximate magnitude of the values of resolving power for the various patterns relative to one another can be gained from consideration of the relative magnitudes of the various indices. Ratios have been computed for long-line versus short-line, short-line versus annulus, and long-line versus annulus for the various indices for VF and SP emulsions. These ratios are shown in table 8. From these values, one may infer that the values of resolving power obtained with long-line patterns using SP emulsion are likely to be 18 percent higher than values obtained with short-line patterns. In a similar manner, values for short-line patterns may be expected to be 45 percent higher than for annular patterns. Long-line patterns may be expected to yield values approximately 70 percent higher than annular patterns.

b. For Two Types of Emulsion

Of the two emulsions for which values are reported in this study, the VF emulsion has been used at the Bureau over a long period of years in making the negatives used in evaluating equivalent focal length, distortion, and resolving power of lenses. It has been eminently satisfactory for this purpose, and

TABLE 8. *Ratio of values of given indices as a function of pattern type*

Values are given (a) for the average ratio (L/S) of the values of a given index for long lines and the same index for short lines. Values are also given (b) of the average ratio (S/A) of the values of a given index for short lines and the same index for annulus type patterns. Values are also shown of the average ratio (L/A) of the values of a given index for long lines and the same index for annulus type patterns. Values are shown for both VF and SP emulsions together with the probable error of a single observation (PE_s) for each ratio.

Index	(a) Values of L/S and PE_s for emulsion			
	VF		SP	
	L/S	PE_s	L/S	PE_s
$\overline{R_\beta T_\beta}$	1.09	±0.04	1.11	±0.05
AWAR	1.11	.05	1.22	.06
ADWAR	1.08	.03	1.20	.03
	(b) Values of S/A and PE_s for emulsion			
	S/A	PE_s	S/A	PE_s
$\sqrt{R_\beta T_\beta}$	1.66	±0.11	1.40	±0.09
AWAR	1.82	.12	1.51	.11
ADWAR	1.70	.11	1.43	.07
	(c) Values of L/A and PE_s for emulsion			
	L/A	PE_s	L/A	PE_s
$\overline{R_\beta T_\beta}$	1.80	±0.07	1.55	±0.07
WAR	2.02	.14	1.84	.18
DWAR	1.84	.12	1.72	.08

numerous specifications involving resolving power of lenses are based upon determinations made therewith. In recent years, there has been a tendency on the part of many engaged in evaluating lens performance to use emulsions similar to the SP emulsion used in this study. This practice is justified on the grounds that with this emulsion, the test conditions more nearly approximate the conditions of use.

Because the two types of emulsion are used for much the same purpose, it is of interest to compare the values of resolving power under like conditions for the two emulsions. It is clear from the curves shown in figures 3 through 9, that there is no clear-cut ratio that is valid for all conditions of focus and for all angular separations from the axis. Accordingly, the ratios existing between the values of the various indices for the two emulsions were determined and are shown in table 9. From this table, one may infer that the values of resolving power obtained with VF emulsion are likely to be 84 percent higher for long-line patterns, 98 percent higher for short-line patterns, and 66 percent higher for annular patterns than are obtained for SP emulsion.

TABLE 9. *Ratio* q *of the value of a given index in plane of best average definition for VF emulsion to the value of the same index in the plane of best average definition for SP emulsion for three types of test patterns*

Values of the ratio are shown $\sqrt{R_\beta T_\beta}$, AWAR, and ADWAR obtained with long-line, short-line, and annular patterns. These are average values for six lenses, and the probable error of a single determination of each ratio is also shown.

Index	Ratio for patterns comprised of					
	Long lines		Short lines		Annuli	
	q	PE_s	q	PE_s	q	PE_s
$\sqrt{R_\beta T_\beta}$	1.94	±0.12	1.97	±0.09	1.66	±0.09
AWAR	1.80	.14	1.97	.11	1.64	.11
ADWAR	1.79	.11	1.99	.11	1.68	.13

5. Conclusion

In this study, the values of the resolving power of six lenses were measured using three types of target pattern and two emulsions. Analysis of the results of measurements leads to the following conclusions.

(1) For either of the two emulsions used, the same plane of best average definition is usually selected by graphical analysis for long-line, short-line, and annulus target patterns.

(2) The plane of best average definition located with the VF emulsion is generally identical with that located with SP emulsion.

(3) While small variations in the location of the focal plane occur with type of index used, these variations are generally sufficiently small that the plane selected by anyone of the three indices is likely to prove satisfactory.

The authors express their appreciation to other members of the staff of the National Bureau of Standards for assistance during this work and in particular to E. C. Watts who prepared the illustrations.

6. References

[1] Rept. of Comm. I, Intern. Soc. Photogrammetry, Specification of methods of calibrating photogrammetric cameras and measuring their resolution, image illumination, and veiling glare, Photogrammetria **X**, 85 (1953–1954).

[2] Military Standard MIL–STD–150–A; Photographic lenses.

[3] British Standard 1613 : 1949, Resolving power of lenses for cameras and enlargers.

[4] L. E. Howlett, Photographic resolving power, Can. J. Research **24** [A], 15–40 (1946).

[5] F. H. Perrin and J. H. Altman, Studies in the resolving power of photographic emulsions, VI. The effect of the type of test pattern and luminance ratio in the test object, J. Opt. Soc. Am. **43,** 780 (1953).

[6] P. Hariharan, Resolving power of photographic emulsions **46,** 315 (1956).

[7] F. E. Washer and I. C. Gardner, Method for determining the resolving power of photographic lenses, NBS Circ. 533 (1953).

[8] I. C. Gardner and F. A. Case, Precision camera for testing lenses, J. Research NBS **18,** 449 (1937) RP984.

[9] F. E. Washer and F. A. Case, Calibration of precision airplane mapping cameras, J. Research NBS **45,** 1 (1950) RP2108; Photogrammetric Eng. **XVI,** 502 (1950).

[10] F. E. Washer and W. P. Tayman, Location of the plane of best average definition for airplane camera lenses, Photogrammetric Eng. (June 1960).

[11] E. W. H. Selwyn and J. L. Tearle, The performance of aircraft camera lenses, Proc. Phys. Soc. **LVIII** (493) 1946.

(Paper 64C3–39)

JOURNAL OF RESEARCH of the National Bureau of Standards—Engineering and Instrumentation
Vol. 64C, No. 3, July–September 1960

A Multiple Isolated-Input Network With Common Output*

C. M. Allred and C. C. Cook

(March 31, 1960)

A circuit is described having n inputs which are isolated from each other but fed into a common output. Theoretically, the circuit presents matched impedances at each of the inputs and the output and has minimum transmission loss. Design equations are presented for the general case and performance data is given for a two-input and a three-input unit.

1. Introduction

In certain highly accurate and precise attenuation measurements a network having multiple inputs and a common output was needed. The following characteristics were to be met:

(a) The network should be symmetrical; that is, each input should have identical electrical characteristics with respect to the output and to every other input.

(b) The inputs should be isolated from each other; that is, an excitation applied to any input should produce negligible response at any other input.

(c) The network should have maximum sensitivity; that is, a change in the excitation at any given input should produce as large a power change in the output as possible.

(d) The input impedance is specified.

(e) Stability considerations require the use of passive, linear, bilateral elements: resistors, capacitors, and inductors.

(f) The system should be unbalanced so the inputs and output have a common ground.

(g) The network need have these characteristics at a single frequency only.

The design equations for such a network are given for a circuit with "n" input terminals. Experimental results for $n=2$ and $n=3$ are presented.

2. Theory

2.1. General

A network possessing the above characteristics will, of course, have properties not explicitly stated above. It is shown below that even less restrictive networks (those meeting only requirements (b), (e), and part of (a), where only the ratio of output power to input power for single input excitation need be equal for all inputs) must contain losses. This is true even when ideal lossless capacitors and inductances are available. These losses affect the sensitivity requirement (c), and therefore should be minimized. However, there is a limit to which the losses can be reduced.

Let α, called the sensitivity, be defined as:

$$\alpha=\frac{P_{ok}}{P_k}$$

where P_{ok} is the output power when only the kth input is excited. The power into the kth input is P_k.

It is shown in the following that the maximum attainable α is:

$$\alpha_{\max}=\frac{1}{n}.$$

Thus a specific network may well have an α which is less than $1/n$, but no network, no matter how nearly ideal, if it fulfills even the lesser requirements, can have an α greater than $1/n$.

To obtain the maximum value of α, consider a network with n inputs where the input impedances and phase shifts between output and input may be arbitrarily different for each input. However, it is assumed that the actual ratio, α, of the output power, P_{ok}, to the input power, P_k, where only the kth input is excited, is the same for each input and there is complete isolation between all inputs. Thus

$$\alpha=\frac{P_{ok}}{P_k}=\frac{E_{ok}^2}{E_k^2}\frac{G_L}{G_k}$$

for $k=1, 2, \ldots, n$. Here E_{ok} is the magnitude (rms) of the voltage across the load when only the kth input is excited with a voltage of magnitude E_k.

If all inputs are excited from coherent sources with magnitudes and phases such that the input powers are equal and the output voltages are all in phase, the following relationships hold.

$$P_{in}=nP_k$$

$$P_o=(nE_{ok})^2G_L=n^2P_{ok},$$

where P_{in} and P_o are the total input and output powers, respectively.

The conservation of energy requires that

$$P_{in}=P_o+P_c$$

or

$$nP_k=n^2P_{ok}+P_c,$$

where P_c is the power lost in the circuitry.

Rearranging terms and using the definition of α, one obtains

$$\alpha=\frac{1}{n}-\frac{P_c}{n^2P_k}.$$

*Contributions from Radio Standards Laboratory, National Bureau of Standards, Boulder, Colo.

The maximum value of α occurs when $P_c=0$ (passive networks only are considered). Thus

$$\alpha_{max}=\frac{1}{n}.$$

The following aspects of the discussion may well be emphasized:

(a) The maximum possible value of α, α_{max}, is a property of the network arising from the requirement of equal sensitivities for all inputs and total isolation between the inputs.

(b) The quantities, α and α_{max}, are defined only for single input excitation.

(c) The ratio of the total output power to total input power when more than one input is excited is not specified and may vary between the limits of zero and unity depending on the levels and phase relations between the excitations.

(d) The above proof does not imply that a network with maximum α contains no dissipative elements but merely that when all inputs are excited so as to have outputs that are equal in magnitude and phase, then no power must be dissipated within the network. This is a case where the ratio of the total power out to total power in is unity.

2.2. The Actual Circuit

While there are other networks possessing the desired characteristics, the one used here is a modification of the familiar bridged–T infinite rejection network.[1]

The familiar bridged–T network is shown in figure 1. This may be redrawn in the form of figure 2. The inductance L', which does not alter the infinite rejection characteristics, is added to make the input admittance purely conductive. Here, R is considered the load, R_L, which would be applied to the output terminals and is not included in the drawing. The circuit extended to four inputs is shown in figure 3.

The extension to n inputs is apparent. This consists of coupling each input with the output through a capacitor, C, and each input with every other input through a resistance-inductance series circuit (r and L). Again, a shunt inductance, L', is placed across each input in order to make the input admittance purely conductive. The nodal equations [2] may be readily written for the n input case. They are:

[1] G. E. Valley and H. Wallman, Vacuum tube amplifiers, ch. 10, Radiation Lab. Ser. (McGraw Hill Book Co., Inc., New York, N.Y., 1948).

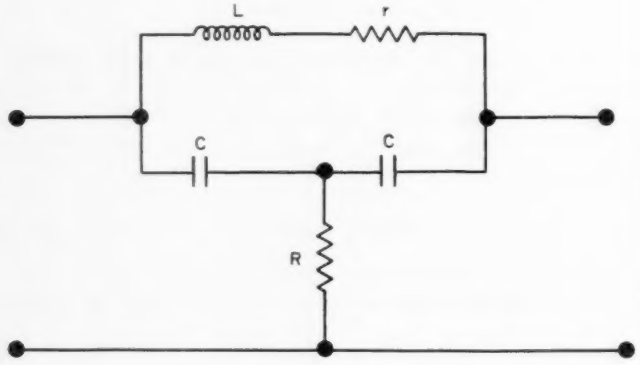

FIGURE 1. *Bridged-T infinite rejection network.*

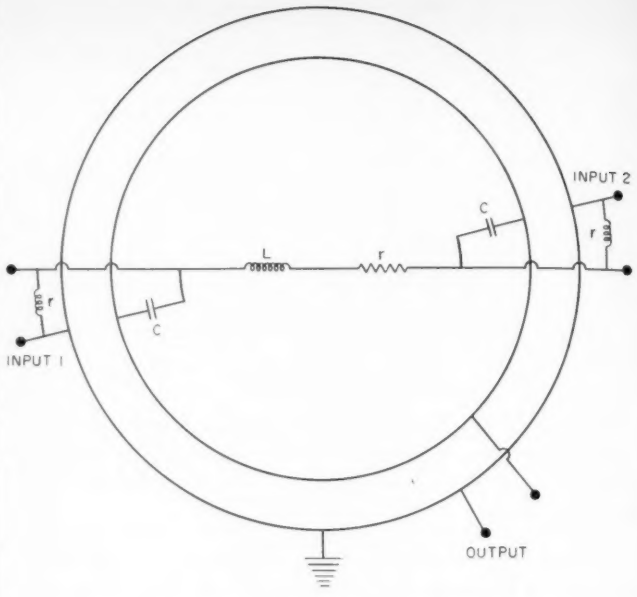

FIGURE 2. *Bridged-T network in different form.*

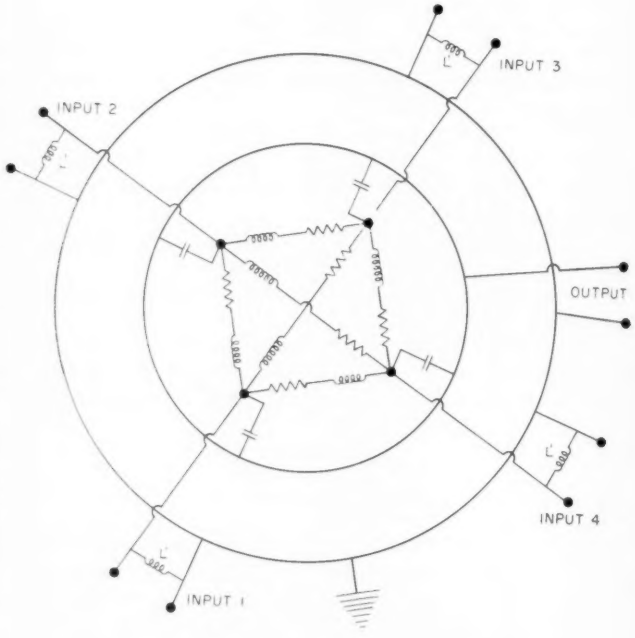

FIGURE 3. *Four-input infinite rejection network.*

[2] H. W. Bode, Network analysis and feedback amplifier design, ch. 1 (D. Van Nostrand Co., Inc., 250 Fourth Avenue, New York, N.Y., 1945); M. E. Van Valkenburg, Network analysis, ch. 3 (Prentice Hall, Inc., New York, N.Y., 1955).

$$e_1\left(j\omega c+\frac{n-1}{r+j\omega L}+\frac{1}{j\omega L'}\right)$$
$$-(e_2+e_3+\ldots+e_n)\frac{1}{r+j\omega L}-e_0 j\omega c=i_1 \quad (1)$$

$$e_2\left(j\omega c+\frac{n-1}{r+j\omega L}+\frac{1}{j\omega L'}\right)$$
$$-(e_1+e_3+\ldots+e_n)\frac{1}{r+j\omega L}-e_0 j\omega c=i_2 \quad (2)$$

.....

$$e_n\left(j\omega c+\frac{n-1}{r+j\omega L}+\frac{1}{j\omega L'}\right)$$
$$-(e_1+e_2+\ldots+e_{n-1})\frac{1}{r+j\omega L}-e_0 j\omega c=i_n \quad (3)$$

$$-(e_1+e_2+\ldots+e_n)j\omega c+e_0\left(nj\omega c+\frac{1}{R_L}\right)=0. \quad (4)$$

If all applied currents are zero except one, say i_1, and all input voltages are required to be zero except e_1, the equations reduce to:

$$e_1\left(j\omega c+\frac{n-1}{r+j\omega L}+\frac{1}{j\omega L'}\right)-e_0 j\omega c=i_1 \quad (5)$$

$$-e_1\frac{1}{r+j\omega L}-e_0 j\omega c=0 \quad (6)$$

$$-e_1 j\omega c+e_0\left(nj\omega c+\frac{1}{R_L}\right)=0. \quad (7)$$

Equations (6) and (7) require relationships between the components which are:

$$\omega^2 c^2 r R_L=1 \quad (8)$$

$$\omega L\omega c=n. \quad (9)$$

Subtracting eq (6) from eq (5) and obtaining the ratio, e_1/i_1, the input impedance is found. If this is required to be R_0 (purely resistive), the following relationship holds:

$$\frac{1}{R_0}=j\omega c+\frac{n}{r+j\omega L}+\frac{1}{j\omega L'}. \quad (10)$$

On equating real and imaginary components:

$$R_0=\frac{r^2+\omega^2 L^2}{rn} \quad (11)$$

$$\omega c-\frac{1}{\omega L'}-\frac{n\omega L}{r^2+\omega^2 L^2}=0. \quad (12)$$

From these equations, the various relationships between the circuit elements necessary to obtain the desired network characteristics may be obtained.

3. The Design Equations

The relationships between the various components that produce the desired response described above are given below. These are presented in terms of the parameters Q ($Q=\omega L/r$), the specified input resistance, R_0, the number of inputs, n, and the angular frequency, ω.

$$\frac{P_{ok}}{P_k}=\frac{1}{n}\text{ (for excitation at one input only)} \quad (13)$$

$$\frac{E_{ok}}{E_k}=\frac{Q}{n\sqrt{1+Q^2}}\,e^{j\theta} \quad (14)$$

$$\tan\theta=\frac{1}{Q}\equiv\frac{r}{\omega L} \quad (15)$$

$$R_L=\frac{R_0}{n}\,\frac{Q^2}{1+Q^2} \quad (16)$$

$$r=\frac{nR_0}{1+Q^2} \quad (17)$$

$$c=\frac{1}{R_0\omega}\,\frac{1+Q^2}{Q} \quad (18)$$

$$L=\frac{nR_0}{\omega}\,\frac{Q}{1+Q^2} \quad (19)$$

$$Z_{in}=R_0+j0 \quad (20)$$

$$Z_{out}=\frac{R_0}{n}\,\frac{Q^2}{1+Q^2}=R_L \quad (21)$$

$$L'=\frac{R_0 Q}{\omega} \quad (22)$$

where E_{ok} is the output voltage across R_L when E_k is applied across the kth input (the only input excited); and Z_{out} is the output impedance of the network, i.e., the impedance seen by R_L looking back into the network.

4. Experimental Results

Two units to operate at a frequency of 30 Mc were constructed. One unit (fig. 4) had two inputs and the other (fig. 5) three inputs.

Stray capacitance, lead inductance, and intercoupling between elements make it necessary to change the component values somewhat from the calculated values. Also, by letting the load impedance be complex, another parameter is available in the design. Since in the application intended for the units, the load impedance was arbitrary, this property was used. Thus the load is not purely resistive.

Two-Input Unit

Isolation between inputs	110 db
Input impedance:	
Input 1	$50.4+j0$ ohms
Input 2	$50.9+j0$ ohms

Sensitivity, α:	
Input 1 to output	4 db
Input 2 to output	4 db
Load impedance	$24.8+j7.5$ ohms

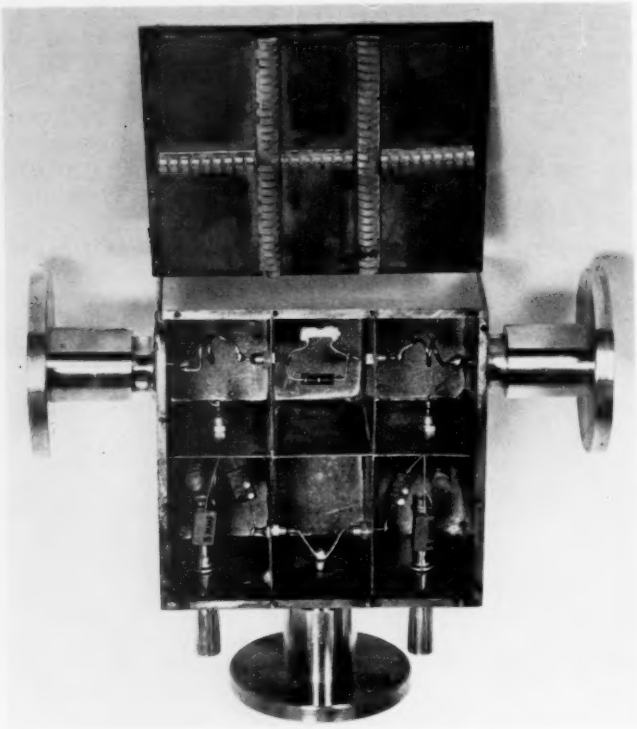

FIGURE 4. *Two-input unit.*

Three-Input Unit

Isolation between inputs:	
Input 1 and input 2	77.5 db
Input 1 and input 3	77.5 db
Input 2 and input 3	76.0 db
Input impedance:	
Input 1	$48.3+j0$ ohms
Input 2	$50.0+j0$ ohms
Input 3	$50.1+j0$ ohms
Sensitivity, α:	
Input 1 to output	6 db
Input 2 to output	6 db
Input 3 to output	6 db
Load impedance	$16.2+j1.5$ ohms

5. Conclusions

A useful network for unique applications in the field of precision measurements was obtained. It may be of interest to note that the properties of the network depend strongly on the load impedance except when a sufficient number of inputs is excited in a manner to produce a null at the load. For this case there can be no dependence on the load impedance as the load currents and voltages are zero. Also for this case, the total input power is dissipated entirely within the network.

The authors express their appreciation to Willard H. Long for the mechanical construction and William W. Kingston for his help in wiring, adjusting, and testing the units.

(Paper 64C3–40)

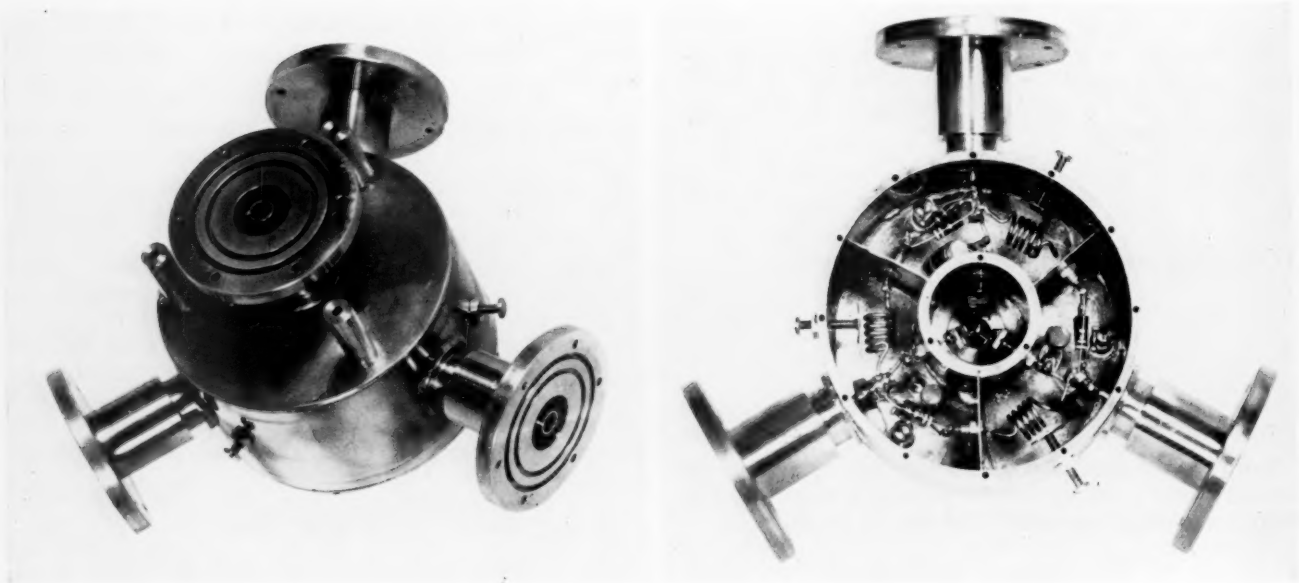

FIGURE 5. *Three-input unit.*

JOURNAL OF RESEARCH of the National Bureau of Standards—C. Engineering and Instrumentation
Vol. 64C, No. 3, July–September 1960

Phase Angle Master Standard for 400 Cycles per Second

J. H. Park and H. N. Cones

(January 25, 1960)

A continuously variable, 0- to 180-degree, phase shift standard for 400 cycles per second is described in detail. It consists of a π-section line made up of twelve 14.6 degree and three 4.3 degree sections to provide for two sizes of coarse steps and an RC circuit at the input to the line to provide for fine steps and a continuous fine control. A method for accurately adjusting the characteristic impedance of all π-sections to the same value, which is used as the termination, was devised. Under these conditions it is shown that the phase shift introduced by each π-section can be accurately computed from a measured value of inductance. The phase shift of each π-section was also determined by an experimental procedure dependent upon a 180-degree phase shift introduced by a toroidal transformer. The values obtained by these two independent methods agree to within 0.01 degree.

1. Introduction

Phase angle in this paper is defined as the quantity used to measure the time phase relation between two sinusoidal voltages of the same frequency. Highly accurate measurements of small angles, i.e., less than 3°, have long been made in connection with instrument transformer calibration testing and phase angle defect measurements of capacitors. Impedance and power factor measurements involving somewhat larger phase shifts but usually with less accuracy have also been performed for some time. However, until quite recently the accurate measurement of phase angle as such over a wide range and at frequencies higher than 60 cps has not received much attention.

Interest in precise phase angle measurements has been aroused as a result of computer and guidance problems. Various methods and devices for measuring phase shift have been developed in solving these problems. In order to obtain accurate comparisons and coordination of the test data obtained in various standardizing laboratories, reference standards must be available which will maintain their calibration when shipped from one laboratory to another. Also, at least one laboratory (probably the National Bureau of Standards) must be capable of checking the absolute calibration of such reference standards.

The calibration of reference standards is most conveniently carried out if a master standard is available which has been thoroughly investigated and accurately calibrated. The purpose of this paper is to describe such a master standard which has been designed and constructed for use at 400 cps at the National Bureau of Standards and to explain the methods used in arriving at its calibration.

2. Requirements of a Master Standard

Conferences with various persons concerned with accurate phase angle measurements indicated that the greatest current need was for measurements from 0° to 180° at 400 cps with an accuracy of 0.01°, if possible. There are numerous methods of obtaining phase shift in this range, and measurement accuracies to within a degree or even a few tenths of a degree can be attained without great difficulty. However, to cover the range from 0° to 180° with a 0.01° accuracy at any point, a master standard must contain several different magnitudes of phase-shift steps which can be switched in or out by selector switches and a continuously variable fine control. To obtain a usable calibration, the phase shift put in by each step on any selector switch or by any given change in the fine dial must be independent of the settings on all other switches and dials. In the case of a resistance decade box a similar requirement is nearly always automatically fulfilled, but for most phase shifting devices this is not true. For a master standard phase shifter it should also be possible to compute phase shift for each step from the measured values of resistance, capacitance, and inductances.

3. Description of Design Used

Resistance-capacitance circuits are commonly used to obtain phase shifts, and the phase shifts inserted by such circuits can, under certain conditions, be accurately computed from measured values of resistance and capacitance. However for such circuits phase shift is proportional to change in capacitance or resistance only up to a few degrees, and above that a fixed change in resistance or capacitance gives a different phase shift depending upon the total values of resistance and capacitance. Thus, decades of resistance or capacitance cannot be used to make up a calibrated phase shifter for large angles but fortunately they can be used for fine control up to about 5°.

To obtain coarse steps of 5° and larger, L–C lumped delay lines (multisection ladder networks) were tried and found to be suitable. The main advantage of such a delay line is that the phase shift added by any individual section is always the same no matter how many sections are already in use, provided the characteristic or surge impedance of all sections is accurately adjusted to the same value and the line is terminated with this same impedance.

Under these conditions the phase shift of each section can be computed from a measured value of inductance. Also the input impedance is independent of the number of sections so that the input can be part of an R–C circuit used to get fine control of phase angle.

The final design consisted of twelve 14.6° π-sections and three 4.3° π-sections with switching arrangements so that any desired combination of sections could be connected as a delay line. The input to this line was used as part of an R–C network which incorporated 10 capacitor steps giving 0.44° phase shift each and a variable air capacitor for continuous fine control.

Several circuit connections and switching arrangements for the complete phase shifter were considered and tried. The one finally selected is shown schematically in figure 1. The "input" or voltage to be shifted is connected to a 4,000-ohm noninductive resistor, shunted by a capacitance-remove type variable air capacitor (1,100 to 100 pf), in series with the input to the delay line. A decade set of mica capacitors (0.004 to 0.044 μf) and a zero adjusting capacitance are connected in parallel with the delay line input. A set of 13 single-pole, two-position, mercury-contact switches are arranged to connect any number from 0 to 12 of the 14.6° π-sections into this delay line. Also a set of 4 switches is arranged to connect any number from 0 to 3 of the 4.3° π-sections into the delay line. The end of the delay line is connected to a resistor of 1,000 ohms shunted by a capacitor of 0.0021 μf which was chosen to be equal to the characteristic impedance of the line. The terminated end of the line is connected to the "output" binding posts of the phase shifter through the "test-check" switch when it is in the "test" position.

4. Theory and Method of Measurements on π-Sections

The circuit diagram in figure 2 shows a generalized π-section delay line which can be used as a phase shifter. To eliminate reflections so that the shift introduced by any one section is constant irrespective of other sections in the line, the terminating impedance, Z_0, must be made equal to the input impedance, Z_{in}. Considering one section only and solving for Z_0 when $Z_0=Z_{in}$ gives

$$Z_0^2=\frac{Z_1Z_2}{1+\frac{Z_1}{4Z_2}}. \tag{1}$$

Also,

$$e_0=\frac{e}{1+\frac{Z_1}{2Z_2}+\frac{Z_1}{Z_0}}. \tag{2}$$

Equation (2) shows that for each section the output voltage lags the input voltage by the angle represented by the vector, $1+(Z_1/2Z_2)+(Z_1/Z_0)$.

For a properly terminated line made up of pure inductors and capacitors the phase shift per section

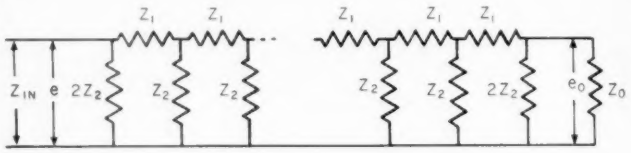

FIGURE 2. *Generalized π-section line.*

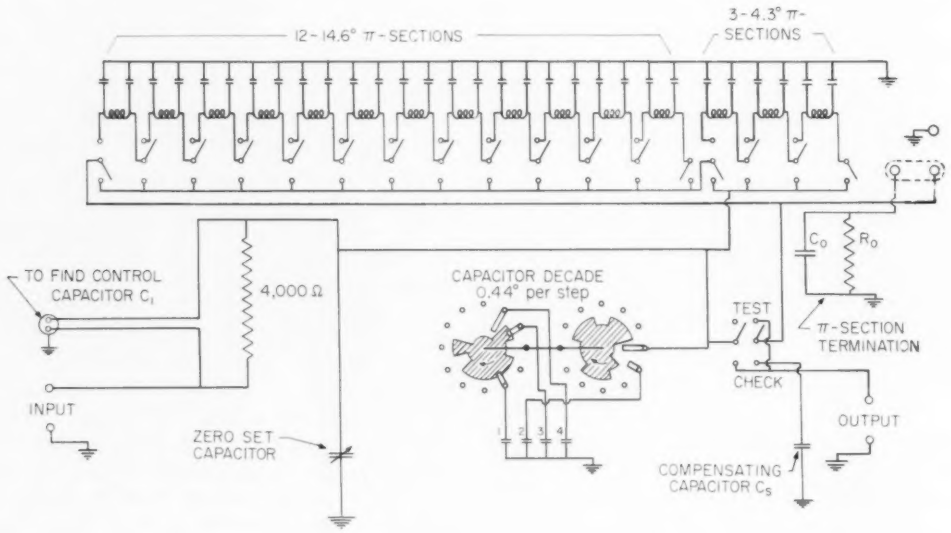

FIGURE 1. *Schematic wiring diagram for 0 to 180 degree reference standard phase shifter 400 cps.*

could be readily computed from the known values of inductance and capacitance. However, there are several practical considerations which tend to reduce the accuracy of the computed value. For $Z_1=j\omega L$ and $Z_2=1/j\omega C$, the terminating impedance as determined from eq (1) must be

$$Z_0^2=\frac{L}{C}\frac{1}{1-\frac{\omega^2 LC}{4}}. \tag{3}$$

Thus Z_0 is real (made up of resistance only), but its value depends to some extent upon frequency. If sections with different values of inductance are to have the same Z_0, then C must be determined from the above equation and becomes

$$C=\frac{L}{Z_0^2}\left(1+\frac{\omega^2 L^2}{4Z_0^2}+\frac{\omega^4 L^4}{8Z_0^4}\cdots\right). \tag{4}$$

Another practical consideration is the resistance of the inductors. To get a suitable value of terminating resistance (say 1,000 ohms) the inductance for a 15° section must be 100 mh. An air-core inductor of this magnitude would either have too much resistance if wound on a toroidal shaped core or would be too susceptible to nearby magnetic fields if made in the form of a circular coil for optimum [1] time constant. The best practical solution is a toroidal winding on a high permeability core. However, since both the inductance and effective resistance of such a high-Q coil would be dependent to some extent on the current through it, the current must be held to a nearly constant value—chosen to be considerably below that giving saturation of the core. Measurements of resistance to about 1 percent and inductance to a much higher accuracy must also be made at the same current, and these values should be stable.

4.1. Method Used To Measure Inductors

An accurate measurement of both the inductance and the resistance of the toroidal high-Q inductors was obtained by using a Maxwell-Wien bridge with a Wagner ground as shown in figure 3. Here R_2 and R_4 are precision woven wire resistance standards (300 ohms each) for which the time constant is less than 10^{-8} sec. C_1 consists of a 0- to 1.11-μf three-decade mica capacitor in parallel with a 50- to 1,100-pf variable air capacitor, both of which are completely shielded and accurately calibrated. R_1 is a four-decade resistance box (0 to 100,000 ohms) of low time constant woven wire resistors. The bridge balance is obtained by adjusting C_1 and R_1. When both the Wagner arm and the bridge are balanced the following relations hold for L_3 and R_3 (neglecting the second-order term):

$$L_3=C_1R_2R_4 \qquad \text{and} \qquad R_3=\frac{R_2R_4}{R_1}.$$

[1] H. B. Brooks, Design of standards of inductance and the proposed use of models in the design of air-core and iron-core reactors, BS J. Research (1931) RP342.

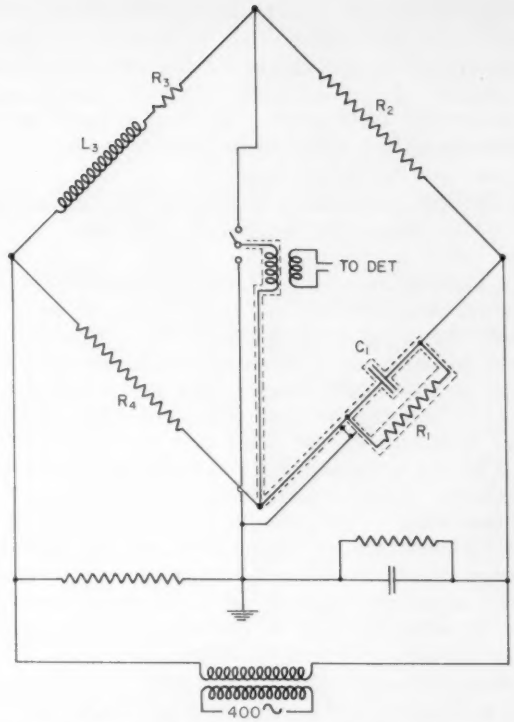

FIGURE 3. *Maxwell-Wien bridge with Wagner ground used to measure inductance and resistance of inductors.*

For the bridge components used, the second order corrections are negligible for an accuracy of 0.01 percent in L_3 and 1 percent in R_3. The values used for R_2 and R_4 should include any lead resistance up to the bridge corners.

An oscillator having an output waveform with total distortion less than 0.1 percent was used to supply this bridge. The frequency was accurately set to 400 cps by forming a Lissajous pattern with a 100-cps standard frequency signal. The voltage appled to the inductor was set by using a voltmeter connected from ground to the L_3 R_4 bridge corner. The actual values of L and r for the inductors used in the π-sections are listed in table 1. These are the values used in computing phase shift for each section.

TABLE 1. *Measured and computed data for inductors*

400 cps measurements using Maxwell-Wien Bridge				Phase shift computed from measured L in degrees	Phase shift from experimental calibration in degrees
Inductor no.	Volts across inductor	mh	ohms		
1	0.25	100.29$_8$	2.79	14.600	14.600
2		100.34$_0$	2.82	14.606	14.609
3		100.19$_9$	2.78	14.587	14.589
4		100.15$_4$	2.80	14.581	14.581
5		100.51$_3$	2.80	14.631	14.636
6		100.15$_2$	2.85	14.580	14.581
7		100.08$_8$	2.79	14.571	14.571
8		99.89$_9$	2.87	14.546	14.542
9		100.15$_4$	2.95	14.580	14.582
10		99.70$_6$	2.87	14.518	14.515
11		100.40$_7$	3.02	14.616	14.620
12		100.66$_9$	3.10	14.651	14.658
1	.075	29.876	1.025	4.307	4.308
2		29.852	1.020	4.304	4.304
3		29.891	0.986	4.309	4.310

Because of the procedure used in matching characteristic impedance for each π-section, as described in the following paragraphs, this computation does not require that the exact value of capacitance for the π-section be known. It does require an exact knowledge of the terminating impedance.

4.2. Procedure Used in Matching the Characteristic Impedance of Each π-Section

By arranging a potentiometer-bridge circuit with the π-section termination (C_0 and R_0 in parallel) as one of the arms and using a sensitive detector to obtain a balance, any small variation in this terminating impedance can readily be detected. If all circuit elements are kept the same after getting an initial balance, except that one π-section is added ahead of the termination, the detector would remain in balance if the characteristic impedance of the π-section were exactly equal to C_0 and R_0 in parallel. If the characteristic impedance is off slightly the detector can be rebalanced by a fine adjustment on the two capacitor legs of the π-section—thus experimentally making the impedance of the π-section exactly equal to C_0 and R_0 in parallel.

The circuit arrangement actually used in making these adjustments is shown schematically in figure 4. Most of the circuit elements shown in this diagram either represent or correspond directly to those used to make up the π-section phase standard (as shown in detail in fig. 1). R_1 is the 4,000-Ωresistor. C_1 is the fine control capacitor. C_2 represents the capacitor decade and the zero set capacitor. The single π-section is used to represent the entire delay line. C_0 and R_0 are the π-section termination. The only additional circuit elements required are the ratio transformer and detector (the detector transformer only being shown). The procedure used was to first balance the detector with the π-section disconnected (switch A up and B open) by adjusting the ratio transformer and capacitor C_2. Then with a π-section connected ahead of C_0 and R_0 (switch A down and B closed) the detector was balanced by adjusting $C'/2$ and $C''/2$, using fine trimmers in parallel with the main capacitance. This last balance is somewhat "tricky" to obtain because the two unbalanced voltages put in by $C'/2$ and $C''/2$ respectively are not 90° apart in phase—but after a little practice it can be obtained quite rapidly. By using a highly selective tuned amplifier as detector this method gives a very sensitive way to adjust the characteristic impedance of the π-section to be exactly equal to R_0 and C_0 in parallel.

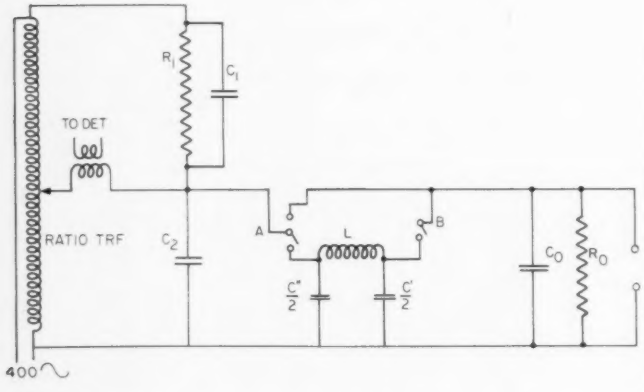

FIGURE 4. *Schematic diagram of phase standard with ratio transformer and detector as connected for adjustment of capacitor trimmers on each π-section.*

The derivation of the relations between the π-section circuit constants and the terminating impedance, for which the input and terminating impedance are equal, is given in appendix 1. The procedure used was to derive an expression for the input impedance of the π-section (terminated by C_0 and R_0 in parallel) and equate this to C_0 and R_0 in parallel, giving a complex equation in circuit parameters. The two separate equations obtained from the complex equation can then be used to determine any two of the circuit parameters in terms of the others. First, it is assumed that the capacitors in the two legs of the π-section are equal, i.e., $=C'/2=C''/2=C/2$. The expressions derived for C_0 and $C/2$ are given by eqs (9) and (10), respectively, in appendix 1. These values of C_0 and $C/2$ can now be put in the two original equations by letting $C''/2=C/2\ (1+\lambda'')$ and $C'/2=C/2\ (1+\lambda')$. Equations (11) and (12) obtained in this manner can be solved for actual values of λ' and λ'' which are measures of the adjustments required in the capacitance legs to maintain the same characteristic impedance for slight changes in other π-section parameters. To help clarify the above procedure an example using actual values for the 14.6° π-section is worked out in appendix 1.

The values of $C'/2$, i.e., $C/2\ (1+\lambda')$, obtained in this manner, together with the known or assigned values of the other circuit parameters can be used to compute phase shift as explained in the following section.

4.3. Computation of Phase Shift for a π-Section

The phase shift of a π-section, i.e., phase difference between voltage in and out, does not depend upon the input capacitance leg because it is in parallel with the input voltage. It does depend on all other circuit constants including the terminating impedance. A derivation for phase shift is given in appendix 2, and eq (19) gives an expression for tan θ as a function of these circuit constants. Actually for any π-section whose values of $C''/2$ and $C'/2$ have been adjusted experimentally (as described above) so that its characteristic impedance is equal to the termination (R_0 and C_0 in parallel) the phase shift can be computed from the measured value of inductance L only provided some limits are set for values of r, R', and R''. This can best be illustrated by using a specific example.

Take first the average 14.6° π-section values as given in appendix 1, i.e., $L=100$ mh, $r=2.8\Omega$,

$R'=10^7\Omega$. For $R_0=1{,}000\ \Omega$ and $C'/2=C''/2=C/2$, $C_0=0.002099\times10^{-6}$ and $C/2=0.0508191\times10^{-6}$ (as computed in appendix 1). Putting these values in eq (19), the phase shift angle θ, as shown in appendix 2, can be expressed as $\tan\theta=0.25968$. For the maximum changes in r, R' and R'' encountered in the twelve 14.6° π-sections as determined from actual measurements, the changes in tan θ, as computed in appendix 2, are given in the following table.

r	R'	R''	Tan θ
2.80	10^7	10^7	0.25968
3.10	10^7	10^7	.25968
2.80	10^8	10^7	.25967
2.80	10^7	10^8	.25969
2.80	10^8	10^8	.25968

Since tan θ is very nearly the same for all of these changes in r, R', and R'', an expression for tan θ in terms of L only, which holds for each of the 14.6° π-sections can be derived. As shown in appendix 2 this expression is

$$\tan\Theta=\frac{L}{R_0}2596.7_8.$$

Using the same procedure, as described for the 14.6° π-section, an expression for tan θ which holds for each of the 4.3° π-sections was also derived. This expression is

$$\tan\Theta=\frac{L}{R_0}2520.5.$$

5. Theory and Calibration of R–C Network

By using the special measuring techniques and theoretical relations described in the previous section, a computed value of phase shift for each of the π-sections can be derived, and such values are listed in table 1. The phase shift inserted by the R–C network, connected ahead of the π-sections as shown in figures 1 and 4, may also be computed using known values of R and C. Appendix 3 shows how this can be done, and actual phase shifts for various values of C_1 and C_2 are given in table 2.

One requirement for a standard phase shifter is that the phase shift introduced by any given change in the continuous fine control be independent of the setting of other phase shift dials. From the fourth column in table 2 it can be seen that the phase shift put in by a 500-pf change in the fine control capacitor is the same to within 0.0005° for all settings on C_2 (the 0.46° steps) up to 43,000 pf. Thus, if the π-sections are all matched so that the impedance looking into the line is the same no matter how many sections are connected, the phase shift put in by a given change in the setting of the fine control capacitor will be essentially the same irrespective of phase shift put in by the "capacitor decade" and the π-section line. As shown in table 2 the average value of this phase shift is 0.2305° for a change in C_1 of 500 pf. (0.0046° for 10 pf or 0.01° corresponds to 21.7 pf).

TABLE 2. *Phase shift for various settings of the capacitors in the R–C network*

(See figure 8)

R_1=4,000 ohms; R_0=1,000 ohms

C_1	C_2	Phase shift, θ	$\Delta\theta$ for 500 pf change in C_1	$\Delta\theta$ for 3,900 pf change in C_2
pf	pf	deg	deg	deg
1,200	4,000	$+0.0921_5$		
700		$-.1382_3$	0.2303_8	
200		$-.3686_2$	$.2303_9$	
1,200	7,900	$-.3570_3$		0.4491_8
700		$-.5874_2$	$.2303_9$	$.4491_9$
200		$-.8178_4$	$.2304_2$	$.4492_2$
1,200	11,800	$-.8060_9$		$.4490_6$
700		-1.0365_0	$.2304_1$	$.4490_8$
200		-1.2669_3	$.2304_3$	$.4490_9$
1,200	15,700	-1.2549_6		$.4488_7$
700		-1.4853_9	$.2304_3$	$.4488_9$
200		-1.7158_5	$.2304_6$	$.4489_2$
1,200	19,600	-1.7035_9		$.4486_3$
700		-1.9340_6	$.2304_7$	$.4486_7$
200		-2.1645_3	$.2304_9$	$.4487_0$
1,200	23,500	-2.1519_3		$.4483_4$
700		-2.3824_4	$.2305_1$	$.4483_8$
200		-2.6129_5	$.2305_4$	$.4484_3$
1,200	27,400	-2.5999_2		$.4479_9$
700		-2.8304_9	$.2305_7$	$.4480_5$
200		-3.0610_5	$.2305_6$	$.4480_7$
1,200	31,300	-3.0475_0		$.4475_8$
700		-3.2781_3	$.2306_3$	$.4476_4$
200		-3.5087_6	$.2306_2$	$.4477_1$
1,200	35,200	-3.4946_4		$.4471_4$
700		-3.7253_3	$.2306_9$	$.4472_0$
200		-3.9560_0	$.2306_7$	$.4472_4$
1,200	39,100	-3.9412_8		$.4466_2$
700		-4.1720_1	$.2307_5$	$.4466_8$
200		-4.4027_6	$.2307_5$	$.4467_6$
1,200	43,000	-4.3873_3		$.4460_7$
700		-4.6181_4	$.2308_1$	$.4461_3$
200		-4.8489_8	$.2308_4$	$.4462_2$

The last column in table 2 indicates that the phase shift put in by a 3,900-pf change in C_2, i.e., by one step on the decade capacitor dial, depends to a slight extent upon the total values for C_1 and C_2. For any given setting of C_2 the change in this phase shift for settings of C_1 from 1,200 to 200 pf is less than 0.00015°. Thus, the effect of the fine control capacitor setting on the decade capacitor steps is negligible. As C_2 is increased the phase shift for a 3,900-pf change in C_2 decreases somewhat, the maximum change being about 0.003°. The calibration for each step on the capacitor decade can take this change into account, but this does indicate that another capacitor decade could not be added. The phase shift for each step on the decade capacitor could be computed if the value of capacitance added for each step were known to a high accuracy (to about 1 pf for 0.0001°), but it was decided that the experimental method as explained in the following section would be easier to apply.

6. Experimental Calibrations

An experimental calibration can be devised for any phase shifter which fulfills the requirements given in section 2. In brief, the procedure is first to obtain the phase shift of each step of each dial in terms of settings on the other dials (including the fine control). These relative values can then be converted to absolute values either by using a known reference phase shift such as 180° or by assuming that the calibration of the fine dial is correct. In the procedure actually followed the computed values for the fine control dial were used to get a calibration on each of the decade capacitor steps. Using these, a preliminary calibration of first the small and then the large π-sections was obtained. Then the 180° point was checked using a special toroidal core transformer. Details of the method used will now be described.

A potentiometer-bridge circuit arrangement plus an auxiliary phase shifter (see fig. 5) were used to compare the phase shift settings on the various dials of the π-section standard. The auxiliary phase shifter, consisting of an R–C circuit supplied through a ratio transformer, need not be accurately calibrated, but it must be stable and continuously variable from 0° up to at least 15°. A sensitive amplifier with shielded input transformer was used to indicate when the phase shifts put in by standard and auxiliary phase shifters were equal. The ratio transformer was used to give a magnitude balance.

The phase shift put in by the fine control capacitor as computed in section 5 was assumed to be exactly correct, and then each step on the capacitor decade switch was measured in terms of the fine control capacitor, as follows. All π-sections were disconnected. With the fine control capacitor set on 0, i.e., maximum capacitance and the capacitor decade switch on step one, the auxiliary phase shifter was adjusted (together with the ratio transformer) until the detector showed a balance. Then, with the auxiliary phase shifter setting held constant and the decade capacitor switch set back to zero the detector was balanced by adjusting the fine control capacitor and ratio transformer. Since the auxiliary phase shifter remains unchanged for these two balances the phase shift put in by the first step on the decade capacitor must equal that read on the fine control dial after the second balance. The change in phase shift when the decade capacitor switch is changed from 2 to 3, 3 to 4, etc., can be measured in the same manner. The actual values as measured are given in table 3.

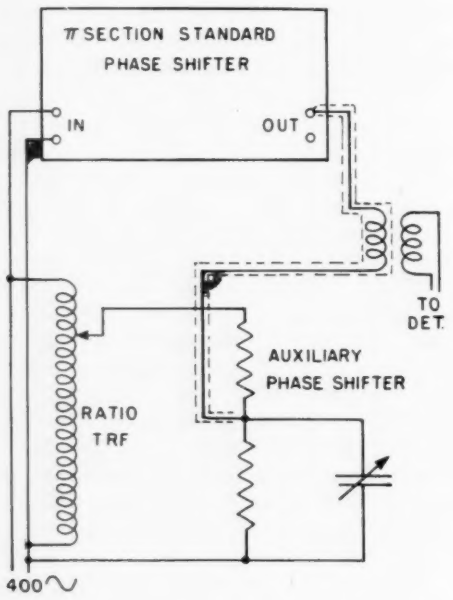

FIGURE 5. *Setup used in experimental calibration.*

TABLE 3. *Phase shift for each step of capacitor decade switch—as determined by comparison with fine control dial*

Decade capacitor step	Phase shift of each step	Σ	Phase shift corrected for 180° check	Σ
	deg			
1	0.4468		0.4470	
2	.4429	0.8897	.4431	0.8901
3	.4454	1.3351	.4456	1.3357
4	.4340	1.7691	.4342	1.7699
5	.4436	2.2127	.4438	2.2137
6	.4440	2.6567	.4442	2.6579
7	.4344	3.0911	.4346	3.0925
8	.4447	3.5358	.4449	3.5374
9	.4406	3.9764	.4408	3.9782
10	.4428	4.4192	.4430	4.4212

To measure the phase shift of each small π-section, the switching arrangement was modified slightly from that shown in figure 1, so that any one of the three sections could be connected or disconnected individually. Then by using the method just described for the capacitor decade steps, the phase shift of each small π-section was measured in terms of the decade capacitor switch and the fine control dial. Another modification of the switching arrangement made it possible to connect any individual large π-section in by itself, and the phase shift of each of these sections was measured in terms of the three small sections plus the setting on the capacitor decade and the fine control dial. Before measuring each π-section its impedance was checked and adjusted to be equal to R_0 and C_0 in parallel by the method described in section 4.2.

The experimental calibration values obtained by the method just described and those computed for the fine control dial (given in table 2) were actually carried out to 0.0001°. The estimated error for each step of the capacitor decade is 0.0005°. If this error is not completely random it would be accumulative and might add up to an appreciable value for the large π-sections. Consequently the values assigned to the 14.6° π-sections based entirely on the computed phase shift for the fine control capacitor were found to differ from computed values based on measured values of inductance of each section by as much as 0.02°. Variations in these differences upon repeated calibrations were usually found to be less

than 0.005°. In order to correct for these fairly large errors in the 14.6° π-sections introduced by very small errors in the calibration of the capacitor decade, an independent check of the 180° point was required.

This was done by connecting the primary of a uniformly wound toroidal transformer in parallel with the input to the standard phase shifter. The secondary of the toroidal transformer was used to get an exact 180° phase shift by (1) reversing polarity or (2) using its two coils as a center tap winding with the center grounded. The phase shifter zero was set with the secondary polarity giving zero phase shift, and then with the opposite polarity the 180° point was measured on the phase shifter. The magnitude was balanced by connecting a ratio transformer either at the primary or at the secondary of the toroidal transformer. The 180° point was measured using five different arrangements for the windings of the toroidal transformer and with the two locations of ratio transformer for each of the five arrangements. Since the results obtained on all measurements were the same to within 0.01° it was concluded that the phase shift being measured was exactly 180°. Using the preliminary experimental calibration, based on computed values of phase shift for the fine control capacitor, the measured value came out to be 179.92°. Thus a correction factor of 180/179.92 or (1+0.000417) was applied to the preliminary calibration values to get the correct values as listed in table 1 for the 14.6 and 4.3 degree π-sections and in columns 4 and 5 of table 3 for the capacitor decade steps. As indicated in table 1 these measured values agree quite well with the values computed from measured values of inductance for each π-section. Although the change in the capacitor decade calibration introduced by the 180° check is quite small, as seen from table 3, it should be included for accurate measurements.

7. Requirements for Use of Phase Standards

The master phase angle π-section standard described in this paper is a continuously variable phase shifter whose absolute calibration has been accurately determined. It is primarily intended to be used to establish corrections for other continuously variable phase shifters and phasemeters used as standards. Herein, a phasemeter is defined as an instrument capable of measuring the phase shift between two alternating voltages of the same frequency. Throughout this kind of calibration testing the two factors most likely to affect accuracy are (1) the impedance of the instrument under test and (2) waveform distortion in supply voltage. These two points are of sufficient importance to be considered separately

7.1 Compensation for Impedance of Instrument Under Test

The connections used for calibrating a phasemeter are shown in the block diagram in figure 6. The

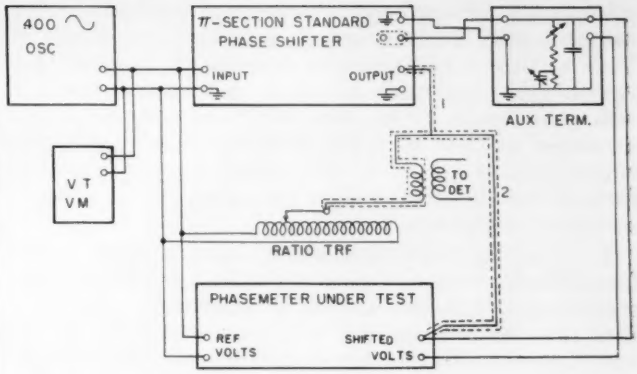

FIGURE 6. *Setup used for calibrating a phasemeter.*

"input" to the π-section phase standard is supplied by a 2-w low distortion oscillator with a regulated output of 5 v. This value of voltage was chosen because it puts 0.25 v across each 14.6° π-section, at which value the change of inductance with voltage is minimum for the iron core inductors. It was found that a 5-percent change in voltage at this level was required to produce a detectable change in inductance. Actually the voltage is maintained constant to within 2 percent. The reference or unshifted voltage input terminals of the meter under test are connected in parallel with the standard "input." At this point the value of impedance of the instrument under test is not critical because it merely acts as an additional load on the oscillator, and its only possible effect would be a slight change in waveform of the supply voltage. This effect would be entirely negligible for most instruments used as reference standards. If a value of voltage other than that required for the π-section standard (5 v) is required by the meter under test, a transformer would normally be used. In such a case the phase shift introduced by the transformer must be known so that a correction for it can be applied.

If the impedance looking into the phasemeter through the shifted voltage binding posts were infinitely high, the output of the π-section standard could be connected directly to these "shifted voltage" binding posts without affecting the terminating impedance of the π-section line. Under this condition the "auxiliary termination" would not be needed. However, since the performance of the π-section line is sensitive to small changes in its termination, Z_0, some compensation will normally be required for the impedance at the "shifted voltage" binding posts. This compensation is provided for by two insulated binding posts at the output end of the π-section phase standard, (see figs. 6 and 1), one being connected to the output end of the π-section line and the other to R_0 and C_0 (in parallel) which form the normal line termination. When these two binding posts are connected by a copper link the π-section line is terminated inside the π-section standard case and the normal output terminals can be used. By removing the link the internal line ter-

mination is disconnected and the "auxiliary termination" may be connected as shown in figure 6. This auxiliary termination consists of a stable adjustable R–C network which is connected in parallel with the leads from the π-section standard and arranged so that with the "shifted volts" leads also connected in parallel, the total impedance thus formed can be adjusted to be equal to Z_0 (the π-section impedance).

In order to make this adjustment a ratio transformer and a sensitive detector with a shielded input transformer are connected as shown in figure 6. First the leads from the π-section standard to the auxiliary termination are disconnected, the link replaced on the π-section standard and the switch put in "check" position (see fig. 1). Under these conditions the π-section line termination is the same as it was when the capacitor legs were adjusted, i.e., it consists of C_0, R_0, and the compensating capacitor C_s in parallel. With the detector transformer lead in position "1" and all π-section standard dials set on "zero," the detector is balanced by adjusting the ratio transformer and the "zero set capacitor." Next the line termination C_0, R_0, C_s is replaced by the "auxiliary termination." This is done by removing the link from the π-section standard binding posts, putting the switch in the "test" position, and connecting the auxiliary termination to the π-section standard and the phasemeter under test as shown in figure 6. The detector is then balanced by adjusting the impedance of the auxiliary termination. To correct for any phase shift introduced by the "auxiliary termination" and its leads, the detector lead position is changed from "1" to "2" and the zero set capacitor is adjusted to balance the detector. Any correction for the phase shift in the ratio transformer can be made during this balance by actually setting this phase shift on the π-section standard fine control dial before making the final balance. The phasemeter under test can now be calibrated for any phase shift angle by first disconnecting all leads from the phase shifters to the detector transformer, then setting the required angle on the π-section phase standard and reading the corresponding value on the phasemeter.

If a voltage higher than the 1 v available from the π-section standard output must be applied to the phasemeter under test, an amplifier can be used between the auxiliary termination and the "shifted volts" binding posts. The only requirements are (1) the amplifier must have low distortion and (2) the three balances as described in the previous paragraph must be made with the amplifier and its leads in position and the amplifier gain set to the same voltage as to be used during the calibration. The phase shift introduced by the amplifier may be fairly large, thus requiring considerable change in the zero set capacitor during the final detector balance before starting actual calibration.

For calibrating another continously variable phase shifter the procedure would be essentially the same as that just described for a phasemeter except that an external detector must be used to indicate when the phase shift put in by the phase shifter being tested is equal to that of the standard. For a given setting of the phase shifter being tested the detector would be balanced by adjusting the phase shift put in by the π-section standard and the magnitude of the output voltage from the phase shifter being tested by using a ratio transformer.

7.2. Effect of Waveform Distortion

At the very beginning of this paper phase angle was defined to be the quantity used as a measure of the time phase relation between two voltages having pure sine waveform. So far the effects of distortion have not been mentioned. However, since it is impossible to obtain pure sine waves in practice, such effects must be considered. For a distorted waveform, phase angle is herein defined as the time phase relation between the fundamental sine-wave components of the two voltages. Thus, there is no change in definition but a definite basis is established for a discussion of the effects of unwanted harmonics. If all the circuit elements were linear (i.e., no iron cores or lossy dielectrics were used) and if measuring and detecting instruments were only sensitive to the fundamental, then the use of a distorted waveform for making the measurements would make no difference. Unfortunately, these postulations cannot be met in practice even though very selective amplifier detectors are available.

Since the π-section standard as described in this paper is made up of iron core inductors the voltage drop across each inductor is always kept low enough so that flux density in the core is well below saturation. Yet it is possible that distortion could be introduced by the inductors even though the supply voltage has a pure sine wave form. To investigate this possibility, first an oscillator of very low distortion was used to supply the phase shifter "input," and distortion was measured at the "output" posts for various phase angle settings, i.e., for different numbers of π-sections in the "line." The waveform with phase shifter set on "0" i.e., no iron core inductors connected contained 0.02 percent 2d harmonic, 0.01 percent 3d harmonic, and 0.01 percent of higher harmonics. As inductors were connected all harmonics remained at about the same value except the 3d which gradually increased to about 0.04 percent with all twelve 14.6° π-sections in circuit. Thus for a nearly pure sine-wave input the inductors in the π-sections slightly increase the 3d harmonic distortion.

Similar tests were made using an oscillator with somewhat greater distortion, i.e., about 0.03 percent 2d, 0.5 percent 3d, and 0.16 percent 4th. For this input voltage the effect of adding π-section inductors on the distortion was too small to be significant (less than about 0.02 percent). In order to check for possible effects of this distortion on measurements involving only the fundamental component, the 180° point was checked as described in section 6 using each of the oscillators whose distortions have just been given. The results using the oscillator with 0.5 percent 3d harmonic agreed with those using the

nearly pure sine wave oscillator to within about 0.005°. Thus it was concluded that for accuracies within 0.01° the total wave form distortion should be less than 0.5 percent. It should be borne in mind that in making these tests a highly selective, feed-back tuned, amplifier was used in the detector circuit.

Waveform may also have an effect on or may be affected by the phase shifter or phasemeter being calibrated. For testing another phase shifter of the same design as the π-section standard the restrictions on distortion should be the same as those given above. For other types of phase shifters or phasemeters the effects of wave-form distortion should be determined by repeat tests using two oscillators of significantly different waveform. From a limited number of such tests it is believed that in general for all oscillators with less than 0.5 percent total distortion the phase-angle test results would be the same to within about 0.01°.

8. Summary and Conclusions

A continuously variable, 0° to 180° phase shifter for 400 cps has been described in detail. By using a special procedure for matching the characteristic impedance of the L–C π-sections used in this phase shifter, a method for experimentally measuring the phase shift of each section has been devised. This phase shift has also been computed from measured values of inductance for each π-section. The results obtained by these two methods agree to within 0.01°. These results indicate that this phase shifter can be used as a master standard in calibrating other phase shift devices.

Similar phase angle standards for higher audio-frequencies could be designed, but on the basis of the experience gained it is thought that the upper limit in frequency would be about 20 kc. At higher frequencies, stray capacitance introduced by connecting and switching leads might prove troublesome. It might be feasible to use the same master standard over a frequency range of about 2 to 1 by some readjustments on the π-sections and termination for each frequency.

Appendix 1. Computation of Characteristic Impedance of π-Section—Losses Considered

A single terminated π-section with losses in both inductor and capacitor considered, is shown schematically in figure 7. To keep the derivation general, the two capacitor legs are not assumed to be equal. R'' represents the total losses in $C''/2$ expressed as a parallel resistance and likewise R' for $C'/2$. The total losses in the inductor are represented by r, as a series resistance. Five circuit equations may be written by inspection of figure 7:

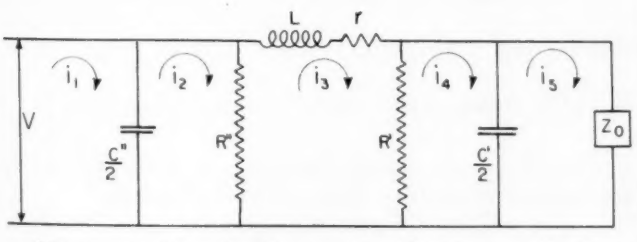

FIGURE 7. *A terminated π-section with losses considered.*

$$
\begin{aligned}
i_1a - i_2a &= V,\\
-i_1a + i_2b - i_3R'' &= 0,\\
-i_2R'' + i_3d - i_4R' &= 0,\\
-i_3R' + i_4f - i_5g &= 0,\\
-i_4g + i_5(Z_0+g) &= 0,
\end{aligned}
$$

where

$$
a=\frac{1}{j\omega\frac{C''}{2}}, \qquad b=R''+\frac{1}{j\omega\frac{C''}{2}}, \qquad d=R''+r+R'+j\omega L,
$$

$$
f=R'+\frac{1}{j\omega\frac{C'}{2}}, \qquad \text{and} \qquad g=\frac{1}{j\omega\frac{C'}{2}}.
$$

Using these equations and putting $1/Z_0=(1/R_0)+j\omega C_0$, the following expression for input admittance Y_{in} is obtained:

$$
Y_{in}=j\omega\frac{C''}{2}+\frac{\left[1+j\omega R_0\left(C_0+\frac{C'}{2}\right)\right]\left[1+\frac{r}{R''}+j\omega\frac{L}{R''}\right]}{\left[1+j\omega R_0\left(C_0+\frac{C'}{2}\right)\right](r+j\omega L)} + \frac{+R_0\left[\frac{1}{R'}+\frac{r}{R'R''}+\frac{1}{R''}+\frac{j\omega L}{R'R''}\right]}{+R_0\left[1+\frac{r}{R'}+\frac{j\omega L}{R'}\right]}. \tag{5}
$$

To obtain a relation which requires the characteristic impedance of the π-section to be $R_0/(1+j\omega C_0R_0)$ equate the above value of Y_{in} to $(1/R_0)+j\omega C_0$. This gives a complex equation from which two equations involving circuit parameters only can be formed. By equating the real parts of the complex equation the following is obtained:

$$
\omega^2R_0rC_0^2-\left[\omega^2R_0r\left(\frac{C''}{2}-\frac{C'}{2}\right)-2\omega^2L\right]C_0+\omega^2L\left(\frac{C'}{2}-\frac{C''}{2}\right)-\omega^2R_0r\frac{C'C''}{4}-\frac{r}{R_0}+m=0, \tag{6}
$$

where

$$
m=\frac{R_0}{R'}\left[1+\frac{R'}{R''}-\frac{r}{R_0}+\frac{rR'}{R_0R''}+\frac{r}{R''}-\frac{\omega^2LR'}{R''}\left(C_0+\frac{C'}{2}\right)+\omega^2L\left(C_0-\frac{C''}{2}\right)\right].
$$

By equating the imaginary parts of the complex equation the following is obtained:

$$\omega r\left(2C_0+\frac{C'}{2}-\frac{C''}{2}\right)+\frac{\omega L}{R_0}\left[1-\omega^2R_0^2\left(C_0^2+\frac{C_0C'}{2}-\frac{C_0C''}{2}-\frac{C'C''}{4}\right)\right]+\omega R_0\left(-\frac{C''}{2}-\frac{C'}{2}\right)+\frac{n}{R_0}=0, \quad (7)$$

where

$$n/R_0=\omega L\left(\frac{1}{R'}-\frac{1}{R''}-\frac{R_0}{R'R''}\right)+\omega rR_0\left[\frac{C_0-\frac{C''}{2}}{R'}-\frac{C_0+\frac{C'}{2}}{R''}\right].$$

For $C'/2=C''/2=C/2$ these two equations can be used to solve for $C/2$ and C_0 when L, R_0, r R', R'' are known. Equation (6) is used to solve for C_0. Putting $C/2=(L/2R_0^2)\ (1+\delta)$ where $\delta<1$, this equation becomes:

$$\omega^2R_0rC_0^2+2\omega^2LC_0-\frac{r\omega^2L^2}{4R_0^3}\ (1+\delta)^2-\frac{r}{R_0}+m=0. \quad (8)$$

Solving it for C_0 gives

$$C_0=\frac{r}{2\omega^2LR_0}\ (1+\alpha), \quad (9)$$

where

$$1+\alpha=\left[1+\frac{\omega^2L^2}{4R_0^2}(1+\delta)^2-\frac{R_0}{r}m\right]\left(1-\frac{\Delta}{4}+\frac{\Delta^2}{8}-\frac{5\Delta^3}{64}+\cdots\right),$$

$$\Delta=\frac{r^2}{\omega^2L^2}\left[1+\frac{\omega^2L^2}{4R_0^2}\ (1+\delta)^2-\frac{R_0}{r}\ m\right].$$

An estimated value is used first for δ. The exact value is determined later from eq (10) and a recomputation made if necessary. Using this value for C_0 and $C'/2=C''/2=C/2$, eq (7) becomes

$$\omega^2L\left(\frac{C}{2}\right)^2-2\frac{C}{2}+\frac{L}{R_0^2}\left[1+\frac{3r^2}{4\omega^2L^2}\left(1+\frac{2\alpha}{3}-\frac{\alpha^2}{3}\right)+\frac{n}{\omega L}\right]=0.$$

Solving for $C/2$ gives

$$\frac{C}{2}=\frac{L}{2R_0^2}\left[1+\gamma+\frac{\omega^2L^2}{4R_0^2}(1+\gamma)^2+\frac{\omega^4L^4}{8R_0^4}(1+\gamma)^3+\cdots\right] \quad (10)$$

where

$$\gamma=\frac{3r^2}{4\omega^2L^2}\left(1+\frac{2\alpha}{3}-\frac{\alpha^2}{3}\right)+\frac{n}{\omega L}.$$

Now going back to eq (6) and putting $C'/2=C/2\ (1+\lambda')$ and $C''/2=C/2\ (1=\lambda'')$, where $C/2$ is the value from eq (10), it follows that

$$\lambda'-\lambda''+\frac{C_0R_0r}{L}\ (\lambda'-\lambda'')-\frac{rR_0C}{2L}\ (\lambda'+\lambda''+\lambda'\lambda'')=\frac{rR_0}{L}\frac{C}{2}-\frac{rR_0C_0^2}{LC}-\frac{2C_02}{C}+\frac{r2}{\omega^2LR_0C}-\frac{m2}{\omega^2LC} \quad (11)$$

Likewise eq (7) gives

$$\lambda'+\lambda''-\frac{r}{R_0}(\lambda'-\lambda'')+\omega^2LC_0\ (\lambda'-\lambda'')-\omega^2L\frac{C}{2}\ (\lambda'+\lambda''+\lambda'\lambda'')=\frac{2rC_02}{R_0C}+\frac{L2}{R_0^2C}-\frac{\omega^2LC_0^22}{C}+\frac{\omega^2LC}{2}-2+\frac{2n}{\omega R_0^2C}. \quad (12)$$

Equations (11) and (12) can be used to compute actual changes in $C'/2$ and $C''/2$ that are made experimentally when adjusting the characteristic impedance of a given π-section to exactly match the terminating impedance (R_0 and C_0 in parallel). First the values for $C/2$ and C_0 are computed using eqs (10) and (9) by assuming average values for L, r, R' and R''. A value for R_0 must also be chosen. Then if these values of R_0 and C_0 are kept the same the effect of small changes in r, R', and/or R'' on values of $C''/2$ and $C'/2$ can be computed using eqs (11) and (12). The actual value of $C'/2$ can then be used to accurately compute the phase shift for each individual π-section as indicated in appendix 2.

The above procedure may be best illustrated by taking actual values for the 14.6° π-section:

$L=100$ mh, $r=2.8\ \Omega$, $R'=R''=1\times10^7\Omega$,

$R_0=1{,}000\ \Omega$, $\omega=2513.27$, $\omega^2=6.31653\times10^6$.

Putting these values in eqs (9) and (10) gives

$$C_0=0.002099\times10^{-6},$$

$$C/2=0.050819_1\times10^{-6}.$$

When these values are put in eqs (11) and (12) they give $\lambda'=\lambda''=0$ for the values of r, R', and R'' given above. For small changes in r, R', and R'' these equations give the corresponding values for λ' and λ'' required to keep the characteristic impedance the same.

First keep all values the same as above except change r to 3.1 ohms. Putting values in eq (11) gives

$$0.99849\ \lambda'-1.00164\ \lambda''=0.00952. \quad (13)$$

Putting values in eq (12) gives

$$0.96613\ \lambda'+0.96967\ \lambda''=0.000065. \quad (14)$$

Solving eqs (13) and (14) for λ' and λ'' gives

$$\lambda'=0.00480 \quad \text{and} \quad \lambda''=-0.00472.$$

Next keep all values the same as assumed above except put $R'=10^8$. Then eq (11) becomes:

$$0.99864\ \lambda'-1.00148\ \lambda''=0.00275. \quad (15)$$

Equation (12) becomes

$$0.96643\ \lambda'+0.96937\ \lambda''=-0.000137 \quad (16)$$

Solvings eqs (15) and (16) for λ' and λ'' gives:

$$\lambda'=0.00131 \quad \text{and} \quad \lambda''=-0.00144$$

If the same computation is made for R'' changed to 10^8 the values of λ' and λ'' will be very nearly the same because m is the same and the effect of the change in n is quite small.

Now keep all values as originally assumed except $R'=R''=10^8$. Then eq (11) becomes

$$0.99864\ \lambda'-1.00148\ \lambda''=0.00544. \quad (17)$$

Equation (12) becomes

$$0.96643\ \lambda'+0.96937\ \lambda''=0.000040. \quad (18)$$

Solving (17) and (18) for λ' and λ'' gives

$$\lambda'=0.00274 \quad \text{and} \quad \lambda''=-0.00270.$$

These values of λ' and λ'' were worked out so that they could be used to compute phase shift under these particular assumed conditions, as will be done in appendix 2.

Appendix 2. Computation of Phase Shift of a π-Section From Value of Inductance

For computing phase shift the first capacitor leg of the π-section need not be considered because it is in parallel with the supply voltage or "V_{in}." Thus the circuit diagram is as shown in figure 8.

The purpose of this derivation is to obtain an expression for the phase shift between V_{in} and V_{out} when the complete π-section (see fig. 7) has been adjusted experimentally so that its impedance as seen from the input end is equal to Z_0.

Three circuit equations may be written by inspection of figure 8:

$$i_1(R'+r+j\omega L)-i_2R'=V_{in},$$

$$-i_1R'+i_2\left(R'+\frac{1}{j\omega\frac{C'}{2}}\right)-i_3\frac{1}{j\omega\frac{C'}{2}}=0,$$

$$-i_2\frac{1}{j\omega\frac{C'}{2}}+i_3\left(\frac{1}{j\omega\frac{C'}{2}}+Z_0\right)=0.$$

For $Z_0=R_0/1+j\omega C_0R_0$, these equations give the relation

$$\frac{V_{out}}{V_{in}}=\frac{1}{1+\frac{r}{R_0}+\frac{r}{R'}-\frac{\omega LA}{R_0}+\frac{jrA}{R_0}+\frac{j\omega L}{R'}+j\frac{\omega L}{R_0}},$$

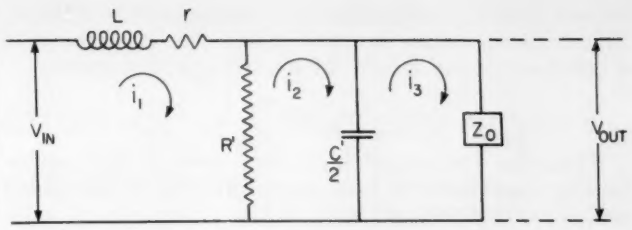

FIGURE 8. *A terminated π-section without first capacitor leg.*

where

$$A=\omega R_0\left(C_0+\frac{C'}{2}\right).$$

The phase shift, θ, is then the angle of the vector in the denominator, thus,

$$\tan\theta=\frac{\omega L/R_0+\omega L/R'+r\omega\left(C_0+\frac{C'}{2}\right)}{1+r/R_0+r/R'-\omega^2L\left(C_0+\frac{C'}{2}\right)}. \quad (19)$$

This equation can be used to compute tan θ for various values of L, r, $C'/2$, R', C_0, and R_0. First using average values ($L=100$ mh, $r=2.8\Omega$, $R'=R''=10^7\Omega$, and $R_0=1{,}000\Omega$) from eqs. (9) and (10), $C/2=C'/2=0.0508191$ μf and $C_0=0.002099$ μf. These values give

$$\tan\theta=0.25968.$$

For the next set of values assumed in appendix 1, i.e., $L=100$ mh, $R'=R''=10^7\Omega$, $r=3.1$ Ω, $R_0=1{,}000$ Ω, $C_0=0.002099$ μf, $C'/2=0.051063$ μf (from $\lambda'=0.00480$).

$$\tan\theta=0.25968.$$

For $L=100$ mh, $r=2.8$ Ω, $R_0=1{,}000$ Ω, $C_0=0.002099$ μf, $R''=10^7\Omega$, $R'=10^8\Omega$, $C'/2=0.05089$ μf (from $\lambda'=0.00131$),

$$\tan\theta=0.25967.$$

For the same values as above, except $R''=10^8\Omega$ and $R'=10^7\Omega$, $C'/2$ still equals 0.05089 μf and

$$\tan\theta=0.25969.$$

Now for all values the same, except $R'=R''=10^8\Omega$, giving $C'/2=0.05095$ μf (from $\lambda'=0.00274$) and $C_0+C'/2=0.05305$ μf

$$\tan\theta=0.25968.$$

The changes in r, $R'+R''$ as assumed above are the maximum to be encountered among the twelve 14.6° sections, as found from actual measurements. Since tan θ is very nearly the same for all of these assumed values, the average values based on the actual measurements may be used, i.e., $r=2.8$ ohm, $R'=R''=10^7$ ohm. For $R_0=1{,}000$ ohms these

values give $C/2=0.0508191$ μf and $C_0=0.002099$ μf. When these values are put in eq (19) it reduces to a constant times L and for $f=400$ cps this gives

$$\tan\theta=2.59678\ L.$$

Thus for the actual inductors used, if the terminating impedance is held constant ($R_0=1{,}000$ ohms and $C_0=0.002099$ μf) and if the trimmers on each capacitance leg are adjusted so that the impedance looking into the line equals the terminating impedance (by the method explained in section 4.2), the phase shift introduced by each section is equal to a constant times its inductance.

Appendix 3. Computation of Phase Shift of the R–C Network

Figure 9 is a simplified circuit diagram of the R–C network. R_1 is a precision resistor accurately adjusted to 4,000 ohms. C_1 is a precision air capacitor with a capacitance remove dial variable from 1,050 to 50 pf. The change in C_1 can be read from the dial setting to within 1 pf so that it can be used as a fine control of phase shift. R_0 is the resistance component of the π-line input impedance (1,000 ohms). C_2 includes the capacitance component C_0 of the π-line together with the decade capacitor (ten steps of 0.44° each), the zero setting capacitor and any lead capacitance. The purpose of the following derivation is to get an expression for phase shift between voltages E and e in terms of the circuit constants.

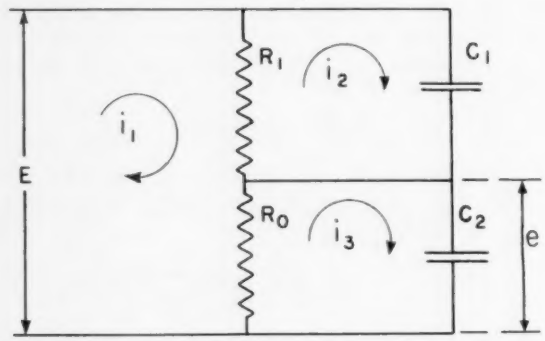

FIGURE 9. *Schematic diagram of the RC circuit in the phase standard.*

The following circuit equation may be written by inspection of figure 9:

$$i_1(R_1+R_0)-i_2R_1-i_3R_0=E,$$

$$-i_1R_1+i_2\left(R_1+\frac{1}{j\omega C_1}\right)=0,$$

$$-i_1R_0+i_3\left(R_0+\frac{1}{j\omega C_2}\right)=0.$$

These equations yield the following relation:

$$\frac{e}{E}=\frac{R_0}{R_1+R_0}\,\frac{1+j\omega C_1R_1}{1+\dfrac{j\omega R_1R_0}{R_1+R_0}(C_1+C_2)}. \tag{20}$$

By clearing the j term from denominator the following expression for tan θ is obtained where θ is the angle by which e leads E:

$$\tan\theta=\frac{\omega R_1\left(C_1\dfrac{R_1}{R_1+R_0}-C_2\dfrac{R_0}{R_1+R_0}\right)}{1+\dfrac{\omega^2R_1^2R_0}{R_1+R_0}C_1(C_1+C_2)}. \tag{21}$$

For

$R_1=4{,}000$ ohms, R_0 $=1{,}000$ ohms, and $\begin{cases}\omega=2513.27\\ \omega^2=6.3165_3\times10^6,\end{cases}$

the expression becomes

$$\tan\theta=\frac{2.01062\times10^6(4C_1-C_2)}{1+20.213\times10^{12}C_1(C_1+C_2)}.$$

Using this expression, phase shifts, θ, were computed for three values of C_1 (200, 600, and 1,200 pf) and for values of C_2 from 0.004 μf to 0.043 μf in steps of 0.0039 μf. The results which were carried out to 0.0001° in order to show small changes are presented in table 2.

(Paper 64C3–41)

JOURNAL OF RESEARCH of the National Bureau of Standards—C. Engineering and Instrumentation
Vol. 64C, No. 3, July–September 1960

Disturbances Due to the Motion of a Cylinder in a Two-Layer Liquid System[1]

Lloyd H. Carpenter and Garbis H. Keulegan

(April 7, 1960)

The disturbance created at the interface of a two-layer liquid system by the horizontal motion of a cylinder in the upper layer is studied for various sizes and shapes of cylinders, depths of the liquids, cylinder velocities, and density ratios. The disturbances fall into three categories. First, when the layers are of equal thickness, in most cases a train of progressive oscillatory waves is produced at the interface. Second, when the depth of the denser layer is much less than the depth of the fresh-water layer, the profile of the interface usually resembles that corresponding to positive internal solitary waves. Third, when the depth of the denser layer is much greater than the depth of the fresh-water layer, in most cases an internal hydraulic jump is produced. The characteristics of the disturbances in each category are related to the size of the cylinder, the depths of the liquids, the cylinder velocity, the density ratio, and the total distance of travel of the cylinder. A theoretical analysis is given for disturbances of the first category.

1. Introduction

Almost a century ago Stokes gave the theory of internal waves of infinitesimal height in a two-layer system, the lighter liquid resting on the heavier one [1],[2] and about a quarter century later the problems of multilayer systems were considered by Webb [2], Grenhill [3], and Burnside [4]. Following these, the wave motions of hetrogeneous liquids with continuously varying density gradients in the vertical were taken up by Love [5], Rayleigh [6], and Lamb [7]. These studies relate to an endless succession of waves, standing or progressive, without reference to the generation of the disturbance such as would result from the motion of objects through a stratified medium or from the uniform flow of fluids over a ridge fixed on the bottom.

The first studies of the latter category go back to Ekman, who considered disturbances of the interface of a two-layer system initiated when a body is towed over the surface [8]. The occasion of the study was the classical account by Nansen of dead water experienced by the Fram during the North Polor Expedition near the coast of Siberia. Ekman approached the problen with much encouragement from Bjerknes both from an experimental and theoretical point of view. In addition to constituting the first serious attempt at model procedures in stratified fluids, the investigation is significant in two respects. First, working with a model of the Fram, Ekman showed that the internal waves brought into play an added resistance having a magnitude dependent on the ratio of draft to fresh water depth, the ratio of layer depths, and the proportionate density differences. The maximum values of the added resistances were obtained when the ratio of the velocity of the model to the velocity of long internal waves of the bilayer system attained the value 0.73, and the added resistance gradually decreased for larger velocities of the model. Second, the question of the added resistance was considered using a method of approach originally adopted by Kelvin in a similar problem applied to a homogeneous fluid. In the evaluation the complete representation of the rufflement of the interface was avoided, and attention was focused only on the parts contributing to the resistance. In this theory the incidence of the maximum is correctly predicted.

The converse problem, that is the problem of a two-layer system moving over a ridge, was considered by Zeilon [9]. The investigation had its inspiration in the views of Pettersson to the effect that the internal boundary waves resulting from the interaction of the Atlantic tides on the irregular bottom configurations had a dominating influence upon the circulation of the Baltic. The problem investigated, thus, was the perturbed state of the interface owing to a ridge at the bottom of a two-layer system in simple harmonic horizontal motion. Experiments were carried out which were intended to verify in a qualitative sense the results of the lengthy mathematical analysis.

Among the recent studies the contributions of Robert Long have much to offer. A novel aspect is the first integration of the hydrodynamic equation for the two-dimensional case of nonviscous flow confined to the space between two rigid horizontal boundaries, the initial velocities (always horizontal) and the densities of the undisturbed regions being prescribed. Rigorous solutions were obtained for the cases where the liquid flows initially with uniform velocity and with linearly varying densities over a flat rectangular ridge [10]. The analysis was repeated for a smooth object, and experiments were made which showed a wave motion giving qualitative confirmation of the theoretical results [11]. The interpretations of the theory and ex-

[1] Sponsored by the Office of Naval Research.
[2] Figures in brackets indicate the literature references at the end of this paper.

periments have numerous aspects, but it should suffice to state here that in general the criterion of the densimetric Froude number (to be defined later) equaling $1/\pi$ divides the types of internal flow. Of particular interest is the examination, experimental and theoretical, of the flow of two superimposed layers over a ridge. Internal waves were generated when the ridge was of small projection, whereas with the much enlarged and elevated ridges the most significant event was the formation of leeward hydraulic jumps [12].

The question of critical flows and the manifestation of hydraulic jumps in a bilayer or a multilayer system is an important one. The significance of the occurrence to meteorology was first emphasized by Tepper [13]. The matter has been approached from various points of view by Rossby [14], Craya [15], Benton [16], Yih [17], and others.

The matter of finite amplitude waves for a two-layer system has been considered by Keulegan and Long [18, 19]. Theory predicts the existence of positive internal solitary waves for the condition that the upper layer has the greater depth. The experiments by Keulegan tend to confirm the results of theory relating to shape and dependence of velocity of propagation on wave height [20].

In common with the disturbances produced in a nonhomogeneous system by liquid moving over ridges on the bottom or of objects being towed on the surface, other related phenomena would be associated with bodies moving through the interior of the medium. The simplest situation arises with the two-dimensional flow of a two-layer system, and this is the subject of the present study. We are here concerned with disturbances of the interface produced by a cylinder moving with constant horizontal velocity in the upper layer as illustrated in figure 1. The liquids are initially at rest, and the density difference is small. Experiments are made with various depths of the layers, sizes and shapes of cylinders, and cylinder velocities. Further experiments with continuous density gradients will be described in a later report.

2. Apparatus and Procedures

The experimental channel is 26.25 m long, 23.3 cm wide, 57 cm deep, and is made up of 21 glass-paneled sections, each 125 cm long. The salt water was mixed and dyed with acid chrome blue and then admitted to the channel to a depth of 2 or 3 cm above the desired level of the interface. The salt water was circulated in the channel by a circulating pump to assure uniform density of the salt layer. After the mixing was complete and the circulation had subsided, fresh water for the upper layer was introduced at the center of the channel through the device shown in figure 2. The device was lowered until the lips touched the water surface. The fresh water was introduced very slowly at first so as to produce as little mixing as possible. A siphon was placed at each end of the channel to remove the mixed liquid at the interface. The process was continued until the interface had been reduced to the desired depth, h, and the total depth had increased to the desired value, $h+h'$ (see fig. 5).

After the channel was filled and all internal motion of the liquid subsided, the density distribution was determined by traversing vertically with a salinity electrode. Various shunts were used in the circuit for greater accuracy in determining salinities within various ranges. The electrode was calibrated with each shunt so the milliampere current readings could be used to determine the density of salt solutions. An example of the vertical distri-

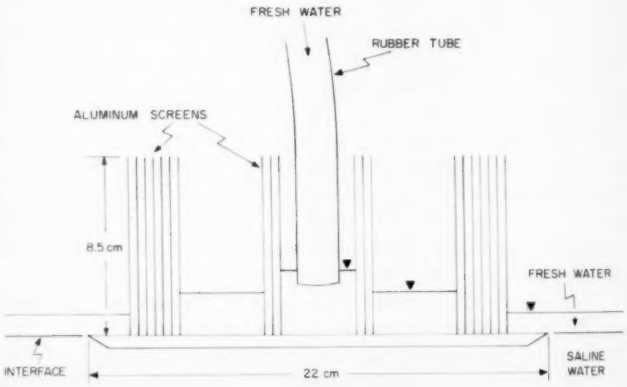

FIGURE 2. *Longitudinal section of device for introducing fresh water on top of saline water.*

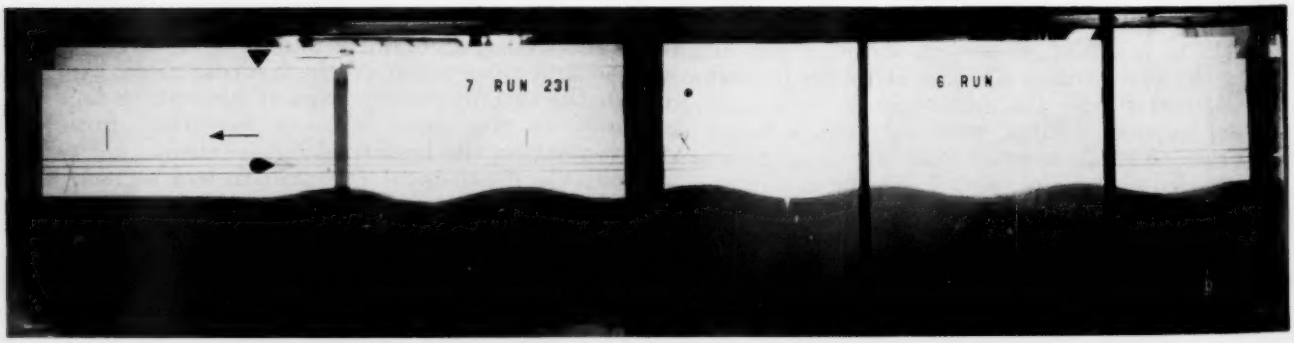

FIGURE 1. *Disturbance at the interface between two liquids produced by a cylinder moving with constant velocity in the upper layer.*

The symbol ▼ indicates the water surface.

bution of density is given in figure 3. The thickness of the layer of mixed liquid was 1 to 1.5 cm in all cases which was small compared to the depths of the fresh and salt layers.

Cylinders of three different diameters, 2.54, 5.08, and 10.16 cm, and three different shapes, circular, lenticular, and tear drop, were used. The lenticular and tear drop shapes are shown in figure 4. In all cases the center of the cylinder was placed 30.0 cm from the bottom.

The cylinders were towed by an electric motor through a variable speed transmission, a system of pulleys, and two 0.81-mm phosphor bronze towing wires. Four 1.22-mm piano wires under tension were used as guide wires to prevent vertical oscillations of the cylinder. Through the variable speed transmission any velocity from 0 to over 1 m/sec could be selected. The cylinder velocity was determined by timing the travel over a distance of 5 m, the first reference mark being 2 m from the starting position.

The profile of the interface during the run was recorded with three fixed cameras which could be triggered simultaneously or individually. For the majority of the runs, the pictures were taken after the cylinder had traveled about 8 m.

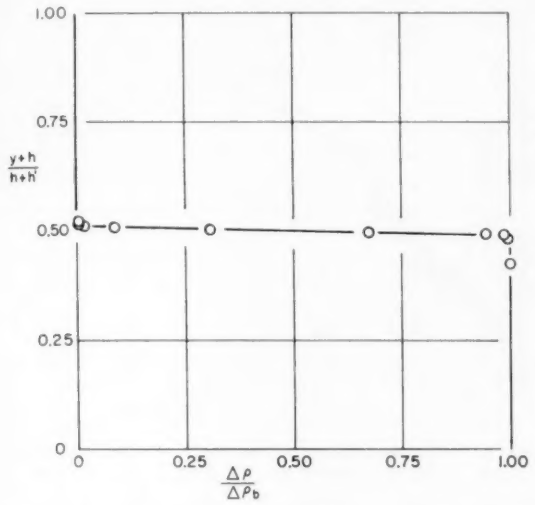

FIGURE 3. *Example of vertical distribution of density.*

y is the vertical coordinate with origin at the interface. $\Delta\rho_b$ is the difference between the densities at the bottom and at the free surface.

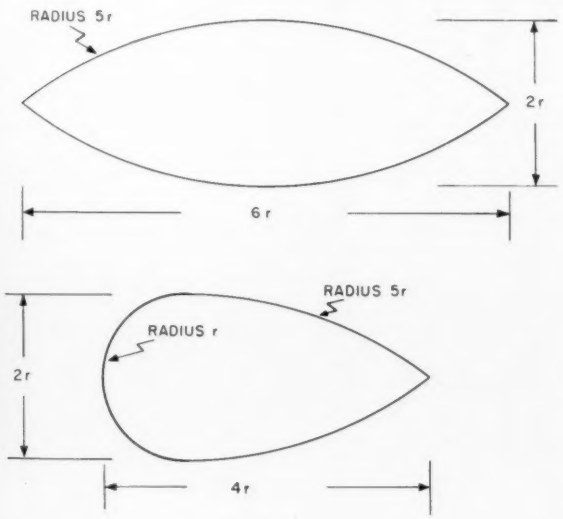

FIGURE 4. *Cross sections of lenticular and tear drop cylinders.*

3. Scope of the Experiments

In an experimental study relating to the effects of a cylinder when moving in one of the layers of a two-layer system, the items to consider first are the state of rufflement of the interface, the deformation of the free surface, and the particle velocities in the parts far removed from the cylinder. The examination and the measurement of the last two quantities may be omitted in a first study, as these may be inferred from the interface deformation on the basis that the flows are irrotational and the liquids incompressible. A second item would be the additional resistance due to the effect of the internal waves. The observation of this quantity may be omitted, likewise, as it is amenable to a close evaluation from a description of the interface, using for example, the method of Ekman [8].

Accordingly, in the present study only the interface deformation is considered (see fig. 5). The two

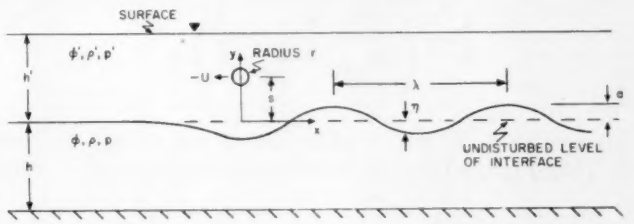

FIGURE 5. *Notation diagram for interfacial disturbance produced by a cylinder moving with constant horizontal velocity in the upper layer.*

fundamental quantities to be established were the wave height and wave length in relation to the cylinder speed, cylinder position, the thickness of layers, and the proportionate density difference. It was very surprising to find that the tests in their entirety failed to show a unique type of disturbance. In effect, three modes of deformation could be distinguished. If the layers were nearly of the same thickness, then the interface in most cases yielded a picture of numerous progressive oscillatory waves. If the lower layer was of a smaller thickness than that of the upper, the cylinder was usually followed by an internal solitary wave. On the other hand, if the upper layer was much thinner than the lower, the interface ordinarily deformed into a hydraulic jump.

4. Internal Oscillatory Progressive Waves

For those runs of the study for which the salt water and fresh water layers were of equal depth, $h'=h$, progressive waves were produced at the

interface as illustrated in figure 1. The wavelength, λ, and the semiwave height, a, of the internal waves depend on the following variables:

U, velocity of cylinder;
r, radius of cylinder;
h, depth of saline layer;
h', depth of fresh layer;
ρ, density of saline layer;
ρ', density of fresh layer;
g, acceleration of gravity;
s, vertical distance of center of cylinder above the undisburbed level of the interface;
β, shape parameter of cylinder;
L, distance traveled by cylinder at time of observation.

Viscous effects are not considered. For the densities used, $\rho'=1$ and $1.02\leq\rho\leq1.08$, we may write

$$2\frac{\rho-\rho'}{\rho+\rho'}=\frac{\Delta\rho}{\bar{\rho}}\approx\frac{\Delta\rho}{\rho}.$$

The values of the variables for the various runs of this class, $h=h'$, are given in table 1. Now

$$\lambda=\lambda\left(U, r, h, \frac{\Delta\rho}{\rho}g, s, \beta, L\right)$$

or

$$\frac{\lambda}{h}=f\left(\frac{U^2}{\frac{\Delta\rho}{\rho}gh}, \frac{r}{h}, \frac{s}{h}, \beta, \frac{L}{h}\right).$$

In figures 6, 7, and 8 plots are given of λ/h against $U^2/(\Delta\rho/\rho)gh$, a form of densimetric or internal Froude number. The wavelengths for the experiments were taken as the mean value for three or four waves immediately following the cylinder. The line representing the theoretical wavelength is taken from Lamb, Art. 231 eq (17) [21], which represents wave motion of two superposed fluids with the upper surface free. For the case

$$\frac{\Delta\rho}{\rho}\ll1$$

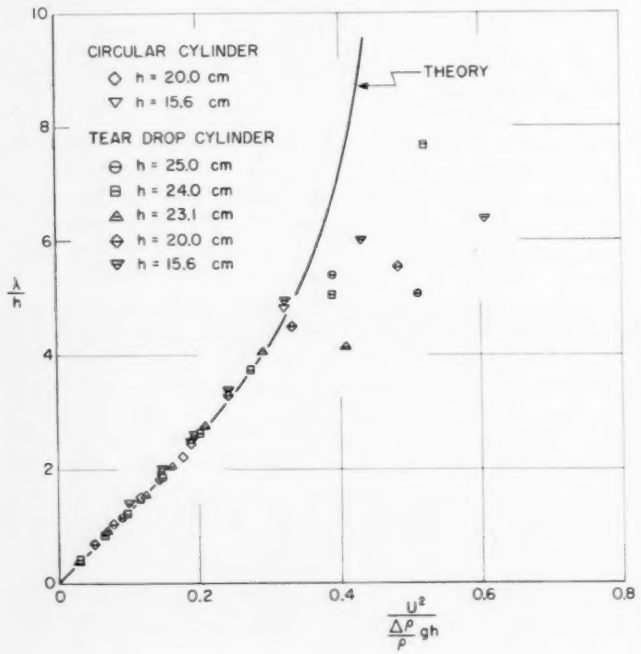

FIGURE 6. *Variation of the wavelength of internal progressive waves,* r=*1.27 cm.*

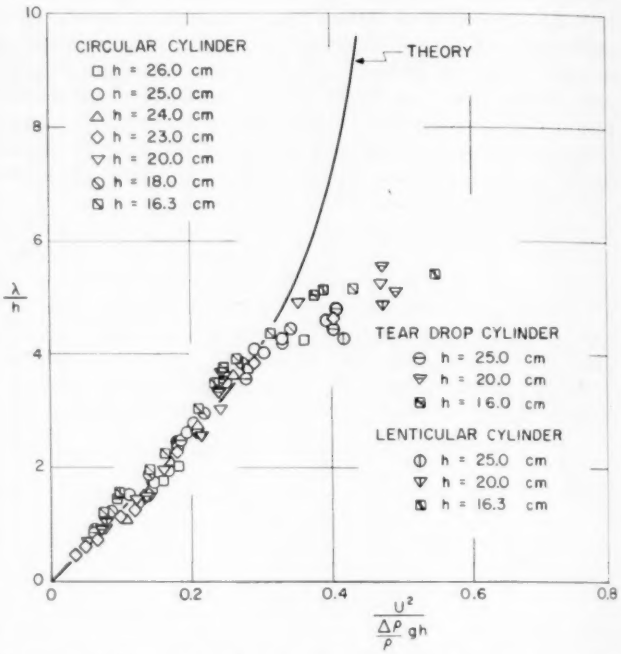

FIGURE 7. *Variation of the wavelength of internal progressive waves,* r=*2.54 cm.*

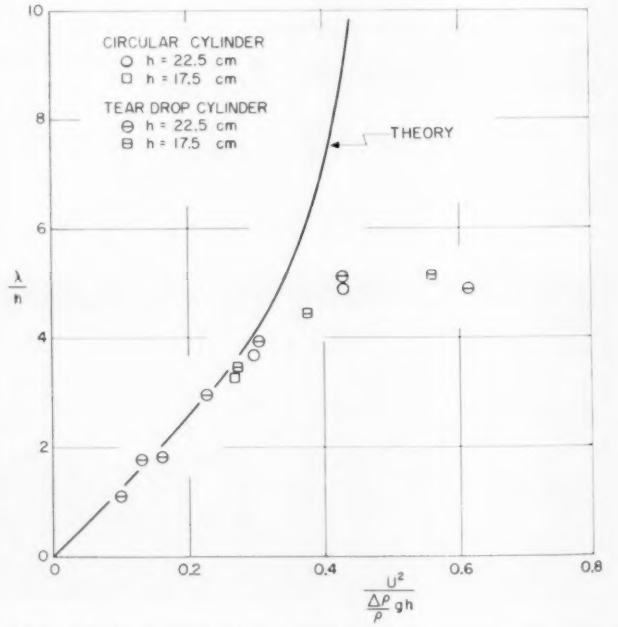

FIGURE 8. *Variation of the wavelength of internal progressive waves,* r=*5.08 cm.*

TABLE 1. *Variables for* h′=h

Run	Cylinder [a]	$h'=h$	s	$\frac{\Delta\rho}{\rho}$	U	a	λ
		cm	*cm*		*cm/sec*	*cm*	*cm*
1	2.54A	25	5	0.02	8.4	3.9	40.0
2	2.54	25	5	.02	12.1	5.3	101.0
4	2.54	25	5	.02	15.0	2.5	----------
5	2.54	25	5	.02	4.0	1.2	10.5
10	2.54	25	5	.02	9.1	3.6	48.5
11	2.54	25	5	.02	10.0	4.0	70.0
12	2.54	25	5	.02	13.9	2.3	115.0
15	2.54	25	5	.04	12.0	3.5	43.5
16	2.54	25	5	.04	13.8	4.3	65.5
17	2.54	25	5	.04	15.7	4.7	87.5
18	2.54	25	5	.04	18.0	5.2	107.0
19	2.54	25	5	.04	21.3	2.2	----------
21	2.54	25	5	.08	16.9	4.3	44.3
22	2.54	25	5	.08	18.9	3.5	59.5
23	2.54	25	5	.08	23.9	5.1	102.5
24	2.54	25	5	.08	22.2	5.0	90.5
25	2.54	25	5	.08	27.6	2.2	----------
71	2.54	26	4	.04	13.7	4.4	52.7
72	2.54	26	4	.04	19.2	3.3	111.0
75	2.54	26	4	.04	12.8	4.2	46.3
76	2.54	26	4	.04	17.0	4.5	97.5
77	2.54	26	4	.04	22.7	1.3	----------
78	2.54	24	6	.04	12.8	3.9	59.6
79	2.54	24	6	.04	10.2	3.3	26.2
80	2.54	24	6	.04	11.3	3.5	36.3
81	2.54A	24	6	.04	14.1	4.1	66.1
82	2.54	24	6	.04	15.7	5.0	87.5
83	2.54	24	6	.04	19.5	2.5	107.0
85	2.54	23	7	.04	10.4	2.8	29.3
86	2.54	23	7	.04	11.3	3.3	36.0
87	2.54	23	7	.04	12.8	3.8	53.0
88	2.54	23	7	.04	13.8	3.8	61.3
89	2.54	23	7	.04	16.2	4.8	89.0
90	2.54	23	7	.04	19.1	2.8	107.0
91	2.54	23	7	.04	21.6	1.4	----------
92	2.54	23	7	.04	9.5	1.8	26.4
93	2.54	23	7	.04	5.7	0.4	11.1
94	2.54	23	7	.04	6.7	1.2	14.8
95	2.54	23	7	.04	7.8	1.7	16.7
96	2.54	20	10	.04	6.4	0.6	14.4
97	2.54	20	10	.04	7.7	1.1	19.8
98	2.54	20	10	.04	9.8	2.1	28.8
99	2.54	20	10	.04	11.3	2.7	39.3
100	2.54	20	10	.04	13.0	3.4	52.0
101	2.54	20	10	.04	13.8	3.8	61.0
102	2.54	20	10	.04	16.7	4.0	98.7
103	2.54	20	10	.04	19.2	2.2	105.0
104	2.54	18	12	.04	6.7	0.5	16.6
105	2.54	18	12	.04	7.8	1.0	22.2
106	2.54	18	12	.04	10.0	1.8	33.8
107	2.54	18	12	.04	11.4	2.7	44.6
108	2.54A	18	12	.04	12.4	3.2	53.5
109	2.54	18	12	.04	14.1	3.4	68.3
110	2.54	18	12	.04	15.6	3.8	80.5
112	2.54	16.25	13.75	.04	7.0	0.7	19.8
113	2.54	16.25	13.75	.04	9.5	2.8	32.2
114	2.54	16.25	13.75	.04	10.3	3.2	37.0
115	2.54	16.25	13.75	.04	11.6	5.2	49.4
116	2.54	16.25	13.75	.04	13.0	6.4	63.7
117	2.54	16.25	13.75	.04	14.2	6.3	71.3
118	2.54	16.25	13.75	.04	16.6	4.1	84.0
142	2.54B	25	5	.04	11.1	3.4	35.5
143	2.54	25	5	.04	16.6	5.7	89.3
144	2.54	25	5	.04	20.0	3.2	120.0
145	2.54	20	10	.04	7.7	1.0	19.2
146	2.54	20	10	.04	13.7	4.5	66.7
147	2.54	20	10	.04	19.7	1.7	102.0
148	2.54	16.25	13.75	.04	7.8	1.0	24.0
149	2.54	16.25	13.75	.04	12.6	4.6	61.5
150	2.54	16.25	13.75	.04	15.5	4.7	82.2
153	2.54C	25	5	.04	11.1	3.5	34.8
154	2.54	25	5	.04	16.4	4.2	96.0
155	2.54	25	5	.04	20.2	2.7	107.0
156	2.54	20	10	.04	7.9	0.8	21.1
157	2.54	20	10	.04	13.9	3.8	73.7
158	2.54	20	10	.04	19.3	2.1	97.5
160	2.54C	16.25	13.75	.04	8.0	0.9	25.6
161	2.54	16.25	13.75	.04	12.3	5.8	57.0
162	2.54	16.25	13.75	.04	15.8	4.2	83.5
163	2.54	16.25	13.75	.04	18.7	1.8	88.0
170	5.08A	17.54	12.46	.04	14.0	7.3	----------
171	5.08	17.54	12.75	.04	16.0	6.0	----------
172	5.08	17.54	12.75	.04	19.5	4.5	----------
173	5.08	17.54	12.75	.04	22.8	5.2	----------
174	5.08	22.46	7.54	.04	16.2	9.0	83.0
175	5.08	22.46	7.54	.04	19.5	3.5	110.0
176	5.08	22.46	7.54	.04	22.4	3.5	----------
178	5.08	17.54	12.46	.04	13.6	----------	57.5
183	5.08B	22.46	7.54	.04	11.9	4.9	41.0
184	5.08	22.46	7.54	.04	10.8	----------	40.0
185	5.08	22.46	7.54	.04	9.4	3.3	25.0
186	5.08	22.46	7.54	.04	14.2	6.3	67.0
187	5.08	22.46	7.54	.04	16.4	8.3	89.0
188	5.08	22.46	7.54	.04	19.5	4.5	115.0
189	5.08	22.46	7.54	.04	23.3	2.2	110.0
196	5.08	17.54	12.46	.04	13.7	----------	61.0
197	5.08	17.54	12.46	.04	16.1	----------	78.0
198	5.08	17.54	12.46	.04	19.6	----------	90.0
210	1.27B	25	5	.04	8.0	1.2	21.6
211	1.27	25	5	.04	5.3	0.5	11.3
212	1.27	25	5	.04	9.5	1.5	29.2
213	1.27	25	5	.04	10.7	1.6	38.2
214	1.27	25	5	.04	12.0	1.6	48.8
215	1.27B	25	5	.04	13.8	1.8	64.5
216	1.27	25	5	.04	16.3	2.0	----------
217	1.27	25	5	.04	19.6	1.7	135.0
218	1.27	25	5	.04	22.4	0.9	127.0
219	1.27	23.12	6.88	.04	5.2	0.1	10.0
220	1.27	23.12	6.98	.04	8.0	0.8	21.3
221	1.27	23.12	6.88	.04	9.5	1.2	29.5
222	1.27	23.12	6.88	.04	10.6	1.3	36.0
223	1.27	23.12	6.88	.04	12.1	1.5	47.3
224	1.27	23.12	6.88	.04	13.8	1.6	64.0
225	1.27	23.12	6.88	.04	16.3	2.3	94.0
226	1.27	23.12	6.88	.04	19.3	1.5	146.5
227	1.27	23.12	6.88	.04	21.5	0.9	----------
228	1.27	24	6	.04	5.3	0.2	10.4
229	1.27	24	6	.04	7.8	0.9	19.8
230	1.27	24	6	.04	9.6	1.3	29.3
231	1.27	24	6	.04	10.5	1.5	35.1
232	1.27	24	6	.04	11.8	1.5	45.0
233	1.27	24	6	.04	13.8	1.8	63.0
234	1.27	24	6	.04	16.1	2.0	90.5
235	1.27	24	6	.04	19.2	1.9	146.0
236	1.27	24	6	.04	22.2	0.8	162.5
237	1.27	20	10	.04	6.3	0.2	14.0
238	1.27	20	10	.04	7.9	0.4	20.9
239	1.27	20	10	.04	9.5	0.8	30.5
240	1.27	20	10	.04	10.7	1.0	37.7
241	1.27	20	10	.04	12.2	1.2	49.2
242	1.27B	20	10	.04	13.8	1.5	66.0
243	1.27	20	10	.04	16.2	2.3	90.2
244	1.27	20	10	.04	19.5	1.0	160.5
245	1.27	15.635	14.365	.04	6.2	0.1	----------
246	1.27	15.635	14.365	.04	7.9	0.2	22.0
247	1.27	15.635	14.365	.04	9.6	0.8	31.6
248	1.27	15.635	14.365	.04	10.9	1.3	41.0
249	1.27	15.635	14.365	.04	12.2	1.9	53.0
250	1.27	15.635	14.365	.04	14.1	3.3	77.5
251	1.27	15.635	14.365	.04	16.3	2.0	126.0
252	1.27	15.635	14.365	.04	19.3	1.0	138.4
275	1.27A	20	10	.04	11.8	1.0	45.0
276	1.27	15.635	14.365	.04	10.8	1.2	39.0
277	1.27	15.635	14.365	.04	14.1	3.7	75.5

[a] Cylinders are tabulated by radius (in centimeters) and by shape; A circular B tear drop, C lenticular.

in which we are interested the equation may be written

$$\sigma^4\rho N_1-\sigma^2\rho gkN_2+\Delta\rho g^2k^2=0$$

where

$$N_1=\coth kh \coth kh'+1$$
$$N_2=\coth kh+\coth kh'$$
$$k=2\pi/\lambda$$
$$\sigma=kU.$$

The equation reduces to

$$\frac{U^2}{\frac{\Delta\rho}{\rho}gh}=\frac{N_2}{2N_1\epsilon kh}\left[1\pm\sqrt{1-\frac{4N_1\epsilon}{N_2^2}}\right]$$

where $\epsilon=\Delta\rho/\rho$. There are two solutions of this equation corresponding to the plus and minus signs for the last term. The minus sign represents the case of interest here where waves are produced primarily at the interface. Since the quantity $N_1\epsilon/N_2^2$ is small, we may expand the square root obtaining.

$$\frac{U^2}{\frac{\Delta\rho}{\rho}gh}=\frac{1}{N_2kh}\left[1+\frac{N_1\epsilon}{N_2^2}+\cdots\right].$$

For the present experiments $N_1\epsilon/N_2^2<0.03$, so only the first term is taken

$$\frac{U^2}{\frac{\Delta\rho}{\rho}gh}=\frac{1}{2\pi}\frac{\lambda}{h}\frac{1}{\coth\frac{2\pi h}{\lambda}+\coth\frac{2\pi h'}{\lambda}}.$$

This relation is the general expression for wave velocity of a two-layer system. Taking the limit as $\lambda/h\to\infty$ we obtain

$$\frac{U_c^2}{\frac{\Delta\rho}{\rho}gh}=\frac{h'}{h+h'} \qquad (a)$$

for the velocity of long waves. For the condition of the experiments, $h'=h$, we have

$$\frac{U^2}{\frac{\Delta\rho}{\rho}gh}=\frac{1}{4\pi}\frac{\lambda}{h}\tanh\frac{2\pi h}{\lambda}$$

which is the basis of the theoretical curves in figures 6, 7, and 8. The agreement is good when $U^2/(\Delta\rho/\rho)gh$ does not exceed 0.3. For larger values of $U^2/(\Delta\rho/\rho)gh$ the wavelength tends to be constant. At the present time no explanation can be given for this result.

For the wave heights, neglecting viscous effects, we have

$$a=a\left(U,\ r,\ h,\ s,\ \beta,\ \frac{\Delta\rho}{\rho}\ g,\ L\right)$$

or

$$\frac{a}{r}=f\left(\frac{U^2}{\frac{\Delta\rho}{\rho}gh},\ \frac{U^2}{\frac{\Delta\rho}{\rho}gs},\ \frac{r}{h},\ \beta,\ \frac{L}{h}\right).$$

A plot of a/r against $U^2/(\Delta\rho/\rho)gs$ is given in figure 9. Those points corresponding to cases where the cylinder touches the free surface, $(s+r)/h'=1$, would not correlate well with the other points and are plotted separately in figure 10. An explanation for this will appear in the theoretical development where

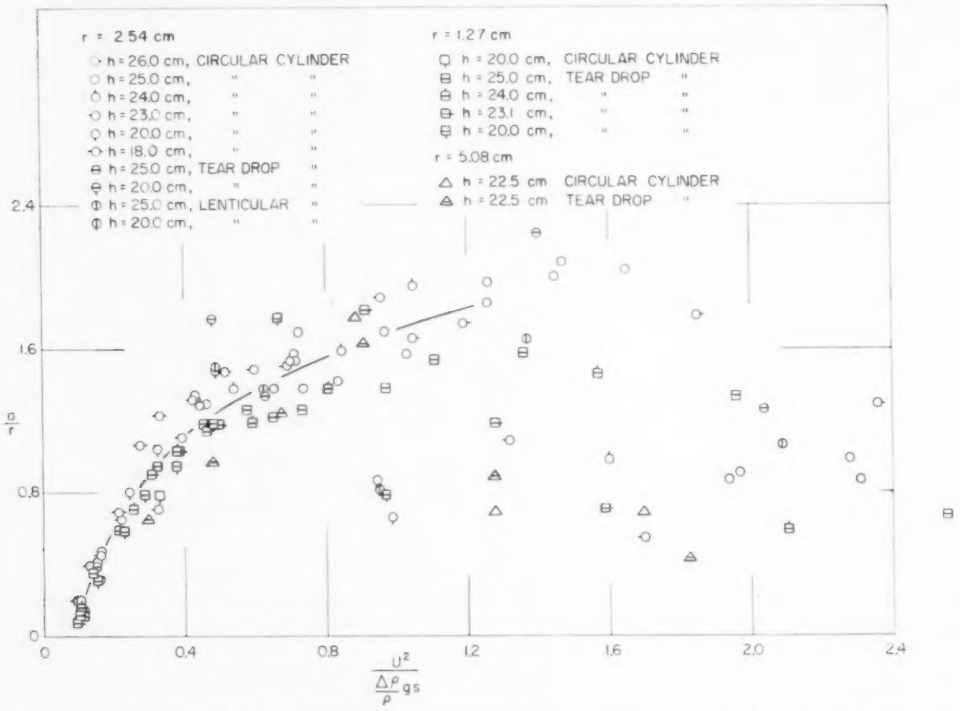
r = 2.54 cm
h = 26.0 cm, CIRCULAR CYLINDER
h = 25.0 cm, " "
h = 24.0 cm, " "
h = 23.0 cm, " "
h = 20.0 cm, " "
h = 18.0 cm, " "
h = 25.0 cm, TEAR DROP "
h = 20.0 cm, " "
h = 25.0 cm, LENTICULAR "
h = 20.0 cm, " "
r = 1.27 cm
h = 20.0 cm, CIRCULAR CYLINDER
h = 25.0 cm, TEAR DROP "
h = 24.0 cm, " "
h = 23.1 cm, " "
h = 20.0 cm, " "
r = 5.08 cm
h = 22.5 cm CIRCULAR CYLINDER
h = 22.5 cm TEAR DROP "
2.4
1.6
0.8
0
0.4
0.8
1.2
1.6
2.0
2.4
a/r
U²/(Δρ/ρ)gs

FIGURE 9. *Variation of the wave height of internal progressive waves for those cases where the cylinder does not touch the surface.*

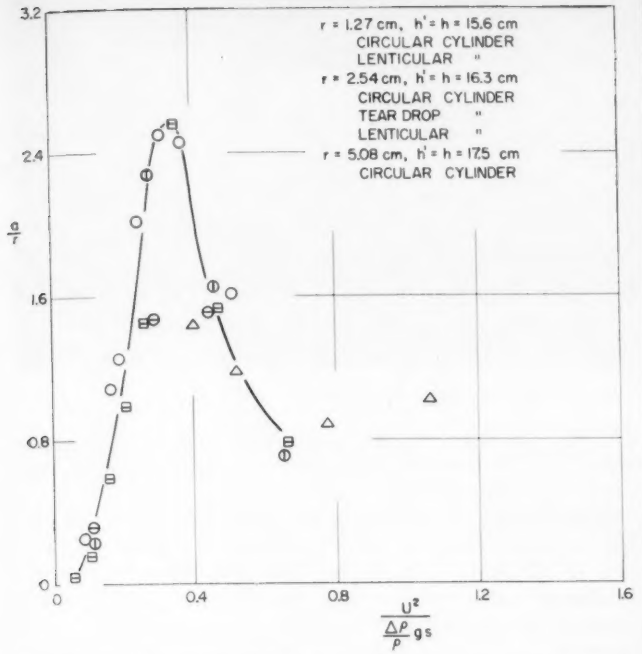
r = 1.27 cm, h' = h = 15.6 cm
CIRCULAR CYLINDER
LENTICULAR "
r = 2.54 cm, h' = h = 16.3 cm
CIRCULAR CYLINDER
TEAR DROP "
LENTICULAR "
r = 5.08 cm, h' = h = 17.5 cm
CIRCULAR CYLINDER
a/r
U²/(Δρ/ρ)gs

FIGURE 10. *Variation of the wave height of internal progressive waves for those cases where the cylinder touches the surface.*

successive images of the cylinder in the surface are taken. A plot of a/r against $U^2/(\Delta\rho/\rho)gh$ is given in figure 11. The maximum value of a/r occurs at about $U^2/(\Delta\rho/\rho)gh=0.3$. Comparing this with the expression for wave velocity U_c of long waves it is seen that $U_m/U_c=0.77$, where U_m is the velocity corresponding to maximum wave height. In this respect there appears to be a close agreement with Ekman's results of maximum added resistance, as large wave height reflects the largeness of the added resistance. The data of a/r from runs where the cylinder was not in contact with the surface are plotted against

$$\frac{U^2}{\frac{\Delta\rho}{\rho}gs} \text{ for } \frac{U^2}{\frac{\Delta\rho}{\rho}gh}<0.3$$

in figure 12.

From the data on wavelengths and wave heights it would be difficult to distinguish any significant

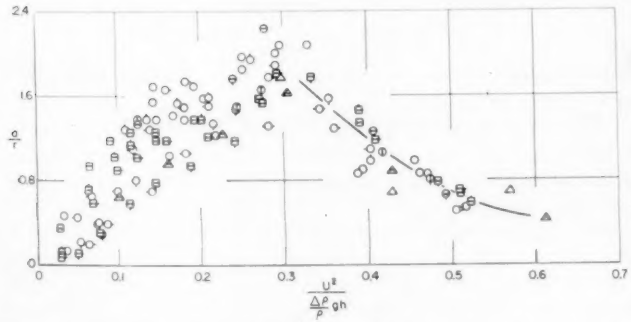

FIGURE 11. *Variation of the wave height of internal progressive waves where the cylinder does not touch the surface.*

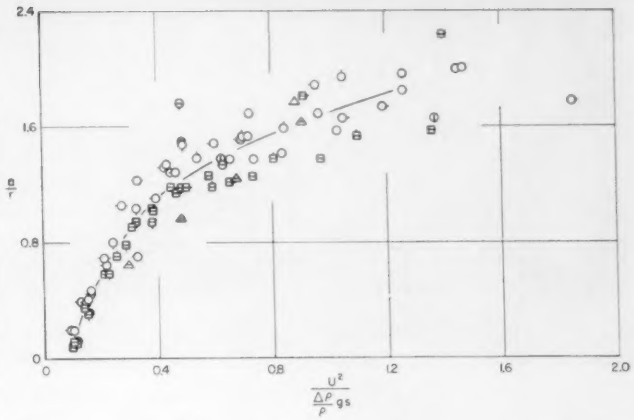

FIGURE 12. *Variation of the wave height of internal progressive waves where the cylinder does not touch the surface for* $U^2/(\Delta\rho/\rho)gh<0.3$.

difference between the waves produced by the cylinders of various shapes. This may be due to the wake being independent of the cylinder shape, although no observations were made of the wake.

For sufficiently large values of r/s there exists a minimum velocity below which progressive waves are not produced. Instead, there is a vortex formation below the cylinder followed by a smooth undisturbed boundary. It can be seen from figure 12 that the wave height increases as r/s is increased.

For large values of r/h the disturbance assumes the form of an internal hydraulic jump which will be discussed in section 6.

The effect of the parameter L/h cannot be evaluated at this time since L was nearly constant for all the runs.

5. Translation Waves of the Bottom Layer

For those runs for which $h<<h'$, translation waves of the form illustrated in figure 13 were formed at the interface. In all the runs of this class the cylinder touches the free surface. If the cylinder were completely below the surface, waves of the same form would be produced. The characteristics of the intumescence are similar to those of internal solitary waves. Letting a be the height of the wave crest above the undisturbed level of the interface, we have, neglecting viscous effects

$$a=a\left(U, r, h, h', s, \beta, \frac{\Delta\rho}{\rho}g, L\right)$$

or

$$\frac{a}{r}=f\left(\frac{U^2}{\frac{\Delta\rho}{\rho}gh}, \frac{h'}{h}, \frac{s}{h}, \frac{L}{h}, \beta, \frac{r}{h}\right).$$

The values of the variables for the runs of this class are given in table 2.

In figure 14 a plot is given of a/r against $U^2/(\Delta\rho/\rho)gh$. Examining the figure, the maximum value of a/r occurs for $U^2/(\Delta\rho/\rho)gh=0.52$. Comparing this with the velocity for long waves, eq (a), the ratio

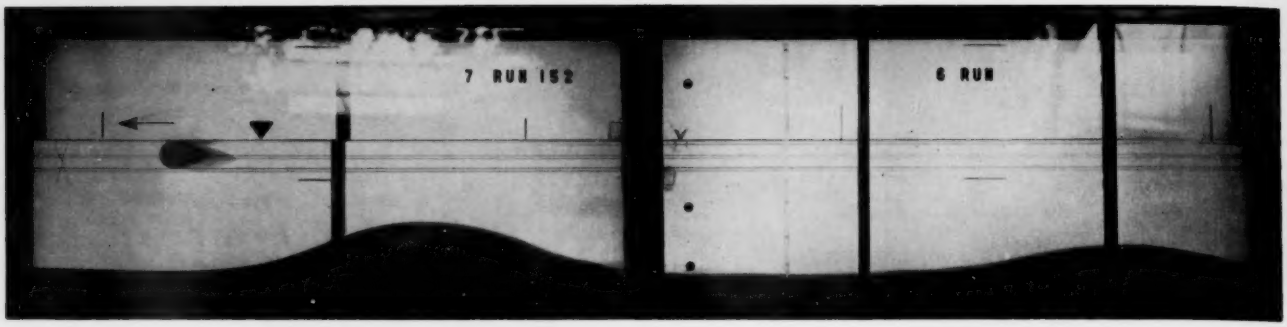

FIGURE 13. *Example of translation waves of the bottom layer produced when* h<<h′.

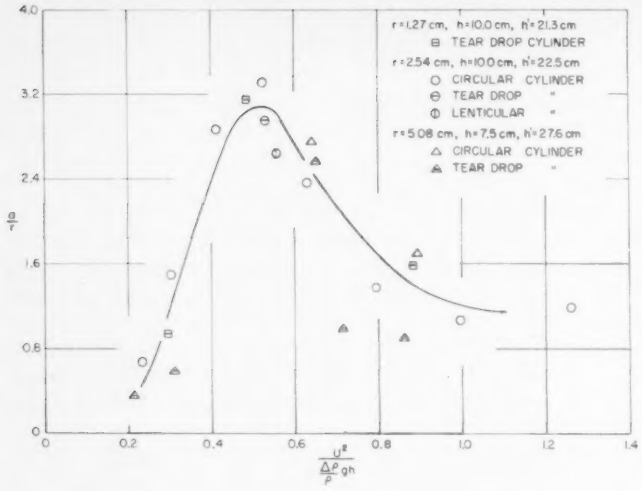

FIGURE 14. *Variation of the wave height of translation waves of the bottom layer.*

TABLE 2. *Variables for* h<<h′

$\frac{\Delta\rho}{\rho}$=0.04 for all runs

Run	Cylinder[a]	h'	h	s	U	a
		cm	*cm*	*cm*	*cm/sec*	*cm*
131	2.54A	22.5	10	20	9.6	1.7
132	2.54	22.5	10	20	11.0	3.8
133	2.54	22.5	10	20	12.7	7.3
134	2.54	22.5	10	20	14.3	8.4
135	2.54	22.5	10	20	15.7	6.0
139	2.54	22.5	10	20	19.8	2.7
140	2.54	22.5	10	20	22.2	3.0
141	2.54	22.5	10	20	17.7	3.5
152	2.54B	22.5	10	20	14.4	7.5
164	2.54C	22.5	10	20	14.8	6.7
180	5.08A	27.62	7.46	22.54	13.7	14.0
181	5.08	27.62	7.46	22.54	16.2	8.6
199	5.08B	27.62	7.46	22.54	7.9	1.8
200	5.08	27.62	7.46	22.54	9.5	3.0
201	5.08	27.62	7.46	22.54	10.7	5.0
207	5.08	27.62	7.46	22.54	13.8	13.0
208	5.08	27.62	7.46	22.54	15.9	4.6
278	1.27B	21.27	10	20	10.8	1.2
279	1.27	21.27	10	20	13.8	4.0
281	1.27	21.27	10	20	18.6	2.0

[a]Cylinders are tabulated by radius (in centimeters) and by shape; A circular B tear drop, C lenticular.

U_m/U_c has the values 0.87, 0.87, and 0.81 corresponding to the cylinders r=1.27 cm, 2.54 cm, and 5.08 cm, respectively.

For the runs of this class, $h<<h'$, the cylinder touches the surface so the value of r/s is small in nearly all cases. Thus for low velocities, waves are produced and these are of small wave height. For these cases progressive waves are produced as in section 4. The apparent criterion for transition from progressive waves to translation type waves is the following: For low velocities progressive waves of small amplitude are produced. For larger velocities the amplitudes increase until they become significantly large in comparison to the depth h of the lower layer for the translation type waves to be produced. No effort was made to determine precisely these transition velocities.

6. Hydraulic Jump of the Upper Layer

For those runs for which $h'<<h$, translation waves of the form illustrated in figure 15 were formed at the interface. Here again the cylinder touches the free surface in all cases. At the start of a run progressive waves are formed. As the cylinder moves on, the waves grow in amplitude and the first crest flattens out because of the proximity of the fresh water surface. Letting Λ be the horizontal distance between the center of the cylinder and the first trough, Λ increases with the distance of travel L. In general, neglecting viscous effects,

$$\Lambda=\Lambda\left(U, r, h', h, \frac{\Delta\rho}{\rho} g, s, \beta, L\right).$$

The values of the variables for the runs of this class are given in table 3.

We wish Λ/L as a function of dimensionless combinations of the variables. The best correlation that was obtained is given in figure 16 where Λ/L is plotted against

$$\frac{U^2}{\frac{\Delta\rho}{\rho} gh'}\sqrt{r/L}.$$

Here again, as in section 5, there are cases, for low

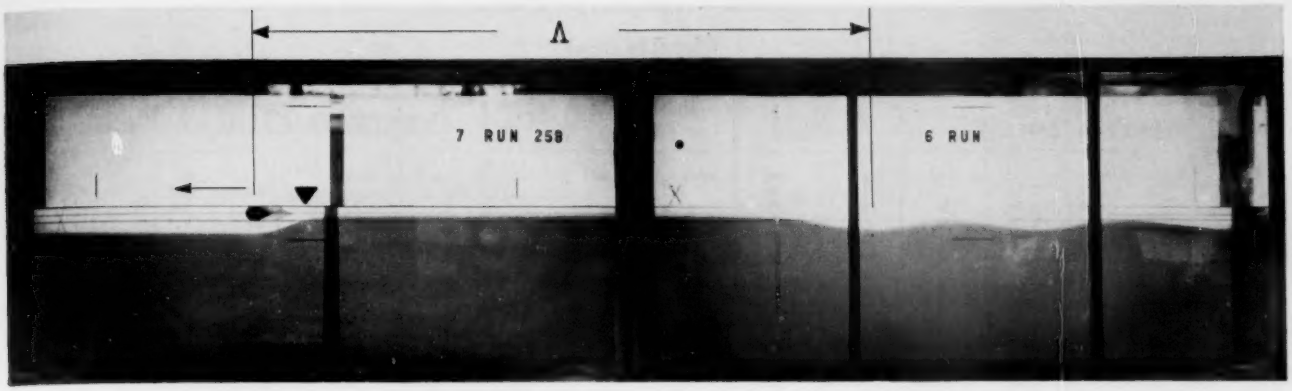

FIGURE 15. *Example of internal hydraulic jump of the upper layer produced when* h′<<h.

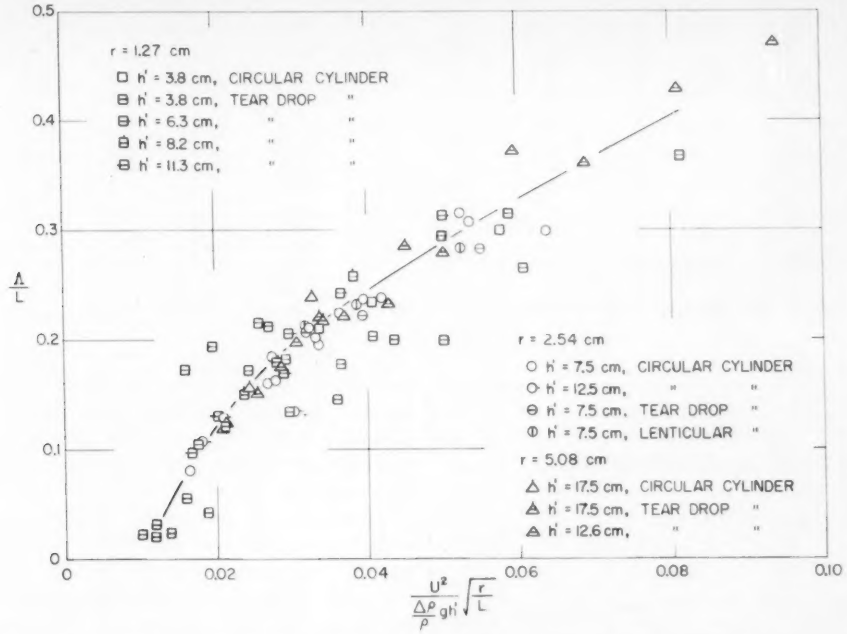
r = 1.27 cm
□ h′ = 3.8 cm, CIRCULAR CYLINDER
⊟ h′ = 3.8 cm, TEAR DROP "
⊟ h′ = 6.3 cm, " "
⊟ h′ = 8.2 cm, " "
⊟ h′ = 11.3 cm, " "
r = 2.54 cm
○ h′ = 7.5 cm, CIRCULAR CYLINDER
○ h′ = 12.5 cm, " "
⊖ h′ = 7.5 cm, TEAR DROP "
⏀ h′ = 7.5 cm, LENTICULAR "
r = 5.08 cm
△ h′ = 17.5 cm, CIRCULAR CYLINDER
△ h′ = 17.5 cm, TEAR DROP "
△ h′ = 12.6 cm, " "
A/L
0.5
0.4
0.3
0.2
0.1
0
0.02
0.04
0.06
0.08
0.10
U²/(Δρ/ρ) gh′ √(r/L)

FIGURE 16. *Variation of the length of the "plateau" of translation waves of the upper layer.*

velocities where progressive waves are produced at the interface. There are also intermediate cases where the first crest is flattened, but in other respects the profile has the characteristics of a progressive wave train. There are still further cases when r/h is large where the hydraulic jump is produced when the two liquids are of equal depth (runs 178, 196, and 197 listed in table 3).

7. Theoretical Development

In order to see to what degree the observed wave heights are in conformity with the laws of hydrodynamics, the case of a cylinder moving with uniform horizontal velocity in the upper layer is considered. This analysis refers to the oscillatory waves of the interface. Corresponding analyses of the translation waves of the bottom and upper layers are being considered.

It will be assumed that r is small compared with the distance s (see fig. 5). Since the speed of motion U is many times smaller than the quantity $\sqrt{g(h+h')}$ the surface disturbance due to motion of the cylinder as it would be in a homogeneous liquid would be unappreciable, and also owing to small $\Delta\rho/\rho$ ratio the surface displacement associated with internal waves would be negligible. In this case, when the cylinder is near the free surface, it will be necessary to take the successive images of the cylinder in the surface as if it were a plane boundary in order to reduce the normal velocity at the surface to zero. For the present purpose, since r/s is assumed small, all of the image doublets within the cylinder may be placed at the center which effectively increases the radius of the cylinder by a factor γ. The values of γ as a function of $(h'-s)/r$ are determined by the methods of reference [22] and plotted in figure 17. The sharp rise in γ for $(h'-s)/r=L$ accounts for the

TABLE 3. *Variables for* h′≪h

$\frac{\Delta\rho}{\rho}$=0.04 for all runs

Run	Cylinder [a]	h'	h	s	U	A_1	L_1	A_2	L_2	A_3	L_3
		cm	cm	cm	cm/sec	cm	cm	cm	cm	cm	cm
119	2.54A	7.5	25	5	9.4					73.0	867.5
124	2.54	12.5	20	10	12.6					94.0	839.0
125	2.54	12.5	20	10	13.7					114.0	842.0
126	2.54	12.5	20	10	16.3					115.5	819.0
128	2.54	7.5	25	5	10.8	91.0	517.0	96.0	557.5		
129	2.54	7.5	25	5	12.1	96.0	363.0	121.5	572.0	164.0	851.0
130	2.54	7.5	25	5	13.2	107.0	309.0	151.8	622.0	187.0	848.0
136	2.54	7.5	25	5	15.5	136.0	415.0	206.0	613.0		
151	2.54B	7.5	25	5	13.1	91.5	284.5	131.5	553.0	183.0	846.0
159	2.54C	7.5	25	5	13.1	99.0	310.0	142.0	571.0	186.0	839.0
178	5.08A	17.54	17.54	12.46	13.6	90.0	344.0	102.0	615.0	106.0	834.5
196	5.08B	17.54	17.54	12.46	13.7	82.0	331.0	94.0	582.0	111.0	840.0
197	5.08	17.54	17.54	12.46	16.1	112.0	352.0	142.0	614.5	159.0	867.5
203	5.08B	12.62	22.46	7.54	14.0	100.0	317.5	138.0	583.0	176.0	848.0
204	5.08	12.62	22.46	7.54	16.6	131.0	332.5			208.0	854.0
205	5.08	12.62	22.46	7.54	19.5	177.0	336.0			328.0	840.0
206	5.08	12.62	22.46	7.54	22.6					370.0	824.0
253	1.27B	3.77	27.5	2.5	6.2	20.5	331.5	20.0	591.0	20.5	847.5
255	1.27	3.77	27.5	2.5	6.7	15.5	324.0	15.5	609.5	17.5	828.5
256	1.27	3.77	27.5	2.5	7.8	78.0	322.0	115.0	551.0	152.0	841.0
257	1.27	3.77	27.5	2.5	9.6	68.0	294.5	112.0	573.5	152.0	837.0
258	1.27	3.77	27.5	2.5	10.6	66.0	292.0	88.0	565.0	118.0	840.0
259	1.27	3.77	27.5	2.5	11.8	91.0	305.0	126.0	590.0	156.0	839.0
260	1.27	3.77	27.5	2.5	13.8	131.0	317.5	204.0	609.0	259.0	840.0
263	1.27	6.27	25	5	10.5	58.0	303.5	73.5	568.5	90.0	817.5
264	1.27	6.27	25	5	13.8	107.0	302.5	148.0	571.0	186.0	865.0
269	1.27	8.15	23.12	6.88	13.9	92.0	317.0	113.0	590.0	131.0	826.0
272	1.27	11.27	20	10	13.8	77.5	324.5	80.5	575.0	84.0	829.5
274	1.27A	3.77	27.5	2.5	11.4	100.2	294.3	147.5	590.2	188.5	857.5

[a] Cylinders are tabulated by radius (in centimeters) and by shape; A circular, B tear drop, C lenticular.

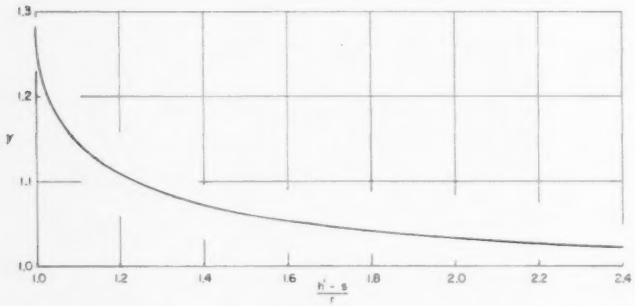

FIGURE 17. *Variation of radius factor with distance below the surface.*

increased wave heights when the cylinder touches the free surface found in section 4.

Letting ϕ' be the velocity potential of the upper layer and ϕ that of the lower we write, after superposing a velocity U on the system,

$$\phi'=-Ux\left[1+\frac{(\gamma r)^2}{x^2+(s-y)^2}+\frac{(\gamma r)^2}{x^2+(2h'-s-y)^2}\right]+\chi'+\chi_1' \tag{1}$$

and

$$\phi=-Ux\left[1+\frac{(\gamma r)^2}{x^2+(s-y)^2}+\frac{(\gamma r)^2}{x^2+(2h'-s-y)^2}\right]+\chi+\chi_1 \tag{2}$$

Thus the normal velocity at the cylinder is zero provided $\chi'+\chi_1'$ is negligible there. The origin is taken at the undisturbed level of the interface directly below the center of the cylinder. The y—coordinate is positive upwards and x is positive to the right in figure 5.

If $r/(s+h)$ is small the normal component of velocity at the bottom from the terms in the bracket would vanish. Again $\chi+\chi_1$ and $\chi'+\chi_1'$ are so selected that the normal components of velocity due to these terms vanish at the surface and at the bottom. Thus assume

$$\chi'=\int_0^\infty \alpha'(k)\cosh k(y-h')\sin kx\,dk \tag{3}$$

$$\chi_1'=\int_0^\infty \alpha_1'(k)\cosh k(y-h')\cos kx\,dk$$

and

$$\chi=\int_0^\infty \alpha(k)\cosh k(y+h)\sin kx\,dk \tag{4}$$

$$\chi_1=\int_0^\infty \alpha_1(k)\cosh k(g+h)\cos kx\,dk$$

where $\alpha'(k)$ and $\alpha(k)$ are to be determined. For the equation of the interface, assumed to be steady, we put

$$\eta=\int_0^\infty \beta(k)\cos kx\,dx, \tag{5}$$

and

$$\eta_1=\int_0^\infty \beta_1(k)\sin kx\,dk.$$

The kinematic boundary conditions at the interface require that

$$U\frac{d}{dx}(\eta+\eta_1)=-\left[\frac{\partial\phi'}{\partial y}\right]_{y=0}=-\left[\frac{\partial\phi}{\partial y}\right]_{y=0}. \quad (6)$$

Equations (1) and (2) may be written in the form

$$\phi'=-Ux-U(\gamma r)^2\int_0^\infty [e^{-k(s-y)}+e^{-k(2h'-s-y)}]\sin kx\,dk+\chi'+\chi_1' \quad (7)$$

and

$$\phi=-Ux-U(\gamma r)^2\int_0^\infty [e^{-k(s-y)}+e^{-k(2h'-s-y)}]\sin kx\,dk+\chi+\chi_1 \quad (8)$$

for $s-y>0$. Differentiating eq (5) with respect to x and eq (3), (4), (7), and (8) with respect to y, eq (6) yields

$$\alpha'(k)\sinh kh'=-\alpha(k)\sinh kh \quad (9)$$

so that

$$\alpha'(k)=-\frac{U}{\sinh kh'}\{\beta(k)+(\gamma r)^2[e^{-ks}+e^{-k(2h'-s)}]\} \quad (10)$$

and

$$\alpha(k)=\frac{U}{\sinh kh}\{\beta(k)+(\gamma r)^2[e^{-ks}+e^{-k(2h'-s)}]\}. \quad (11)$$

Also

$$\alpha_1'(k)\sinh kh'=\alpha_1(k)\sinh kh=\beta_1(k)$$

So the terms χ_1', χ_1, and η_1 correspond to a system of free waves and will be dropped from the equations.

If the pressure at the free surface is taken as zero

$$\frac{p'}{\rho'}=-gy-\frac{1}{2}\left(\frac{\partial\phi'}{\partial x}\right)^2+gh'+\frac{1}{2}U^2 \quad (12)$$

and

$$\frac{p}{\rho}=-gy-\frac{1}{2}\left(\frac{\partial\phi}{\partial x}\right)^2+\frac{\rho'}{\rho}\left(gh'+\frac{U^2}{2}\right). \quad (13)$$

provided that ρ'/ρ is nearly unity. Letting $p'=p$ for $y=\eta$ and omitting higher order terms in the disturbance

$$\rho'\int_0^\infty \{g\beta(k)+U^2(\gamma r)^2k[e^{-ks}+e^{-k(2h'-s)}]-Uk\alpha'(k)\cosh kh'\}\cos kx\,dk$$
$$=\rho\int_0^\infty \{g\beta(k)+U^2(\gamma r)^2k[e^{-ks}+e^{-k(2h'-s)}]-Uk\alpha(k)\cosh kh\}\cos kx\,dk \quad (14)$$

or

$$\int_0^\infty \{U^2(\gamma r)^2k[e^{-ks}+e^{-k(2h'-s)}](\rho'-\rho)+g\beta(k)(\rho'-\rho)-\rho'Uk\alpha'(k)\cosh kh'+\rho Uk\alpha(k)\cosh kh\}\cos kx\,dk=0. \quad (15)$$

Introducing $\alpha'(k)$ and $\alpha(k)$ from eqs (10) and (11)

$$U^2(\gamma r)^2k[e^{-ks}+e^{-k(2h'-s)}][(\rho'-\rho)+\rho'\coth kh'+\rho\coth kh]+\beta(k)[g(\rho'-\rho)+U^2k\rho'\coth kh'+U^2k\rho\coth kh]=0 \quad (16)$$

or

$$\beta(k)=-(\gamma r)^2\left\{1-\frac{(\rho'-\rho)\left(\frac{g}{U^2}-k\right)}{\rho'\left[\frac{g}{U^2}+k\coth kh'\right]-\rho\left[\frac{g}{U^2}-k\coth kh\right]}\right\}[e^{-ks}+e^{-k(2h'-s)}]. \quad (17)$$

Now eq (5) becomes

$$\eta=-(\gamma r)^2\int_0^\infty \left\{1-\frac{(\rho'-\rho)\left(\frac{g}{U^2}-k\right)}{\rho'\left[\frac{g}{U^2}+k\coth kh'\right]-\rho\left[\frac{g}{U^2}-k\coth kh\right]}\right\}\cdot[e^{-ks}+e^{-k(2h'-s)}]\cos kx\,dk \quad (18)$$

or

$$\eta=-(\gamma r)^2\left[\frac{s}{x^2+s^2}+\frac{2h'-s}{x^2+(2h'-s)^2}\right]+(\gamma r)^2\int_0^\infty \frac{(\rho'-\rho)\left(\frac{g}{U^2}-k\right)[e^{-ks}+e^{-k(2h'-s)}]}{\rho'\left[\frac{g}{U^2}+k\coth kh'\right]-\rho\left[\frac{g}{U^2}-k\coth kh\right]}\times\cos kx\,dk. \quad (19)$$

The integral in eq (19) is improper, the denominator becoming zero at the value of k for which

$$k[\rho\coth kh+\rho'\coth kh']=\frac{g}{U^2}(\rho-\rho'). \quad (20)$$

This value, $k_0=2\pi/\lambda$, corresponds to the wavelength of free interfacial waves at the velocity U, as derived in section 4. As U increases the wavelength λ also increases. Taking the limit of eq (20) as $k\to 0$ we have

$$\frac{\rho}{h}+\frac{\rho'}{h'}=\frac{g}{U_c^2}(\rho-\rho')$$

or

$$U_c=\sqrt{\frac{g(\rho-\rho')hh'}{\rho h'+\rho' h}} \tag{21}$$

which is the velocity of propagation of long waves. For larger values of U there is no real singularity of the integrand in eq (19). Taking the principal value of the integral in eq (19) for x positive,

$$\eta=-(\gamma r)^2\left\{\left[\frac{s}{x^2+s^2}+\frac{2h'-s}{x^2+(2h'-s)^2}\right]+\frac{\pi(\rho'-\rho)\left(\frac{g}{U^2}-k_0\right)[e^{-k_0 s}+e^{-k_0(2h'-s)}]\sin k_0 x}{\rho'\,[\coth k_0h'-k_0h'\,\operatorname{csch}^2 k_0h']+\rho\,[\coth k_0h-k_0h\,\operatorname{csch}^2 k_0h]}\right.$$

$$\left.-\int_0^\infty\frac{(\rho'-\rho)\frac{g}{U^2}[\sin ms+\sin(2mh'-ms)]e^{-mx}}{\rho'\left[\frac{g}{U^2}+m\cot mh'\right]-\rho\left[\frac{g}{U^2}-m\cot mh\right]}dm-\int_0^\infty\frac{(\rho'-\rho)m[\cos ms+\cos(2mh'-ms)]e^{-mx}}{\rho'\left[\frac{g}{U^2}+m\cot mh'\right]-\rho\left[\frac{g}{U^2}-m\cot mh\right]}dm\right\}. \tag{22}$$

For large values of x only the second term is significant. Since η is an even function of x, eq (5), the corresponding expression with x replaced by $-x$ holds for negative x. Adding a system of free waves to cancel the disturbance far upstream, the result is

$$\eta=-(\gamma r)^2\left\{\left[\frac{s}{x^2+s^2}+\frac{2h'-s}{x^2+(2h'-s)^2}\right]+\frac{2\pi(\rho'-\rho)\left(\frac{g}{U^2}-k_0\right)[e^{-k_0 s}+e^{-k_0(2h'-s)}]\sin k_0 x}{\rho'\,[\coth k_0h'-k_0h'\,\operatorname{csch}^2 k_0h']+\rho\,[\coth k_0h-k_0h\,\operatorname{csch}^2 k_0h]}\right\}$$

$$+\text{ etc for } x>0 \tag{23}$$

and

$$\eta=-(\gamma r)^2\left[\frac{s}{x^2+s^2}+\frac{2h'-s}{x^2+(2h'-s)^2}\right]+\text{ etc for } x<0.$$

Thus there is a local disturbance followed by progressive waves of length λ, where

$$\lambda=\frac{2\pi}{k_0}$$

is determined by eq (20).

8. Comparison With Observation

Recalling the conditions of the theory, it is clear that it does not apply to the translation waves of either section 5 or 6. For a comparison with the observed progressive waves, when $h=h'$, eq (20) gives

$$4\pi\frac{h}{\lambda}\coth\frac{2\pi h}{\lambda}=\frac{\Delta\rho}{\rho}\frac{gh}{U^2} \tag{24}$$

which can be solved numerically to give λ/h as a function of $U^2/(\Delta\rho/\rho)gh$.
The values are given by the curves in figures 6, 7, and 8. The agreement with experiment is good for

$$\frac{U^2}{\frac{\Delta\rho}{\rho}gh}<0.3.$$

Regarding the wave height a, we have from eq (23)

$$\frac{a}{r}=\gamma^2\frac{r}{h}\frac{\pi\frac{\Delta\rho}{\rho}\left(\frac{gh}{U^2}-k_0h\right)\left[e^{-k_0h}\frac{s}{h}+e^{-k_0h}\left(2-\frac{s}{h}\right)\right]}{\coth k_0h-k_0h\operatorname{csch}^2 k_0h} \tag{25}$$

approximately. Thus a/r is a function of $U^2/(\Delta\rho/\rho)gh$ for given values of s/h and r/h. In figure 18 one of the theoretical curves is given along with the corresponding experimental points. For small wave heights the observed values are considerably greater than the theoretical values. This disparity may be due to the wake produced by the cylinder or the limitation of the theory to small waves. For the smallest waves which could be measured accurately, figure 18, the observed values are approximately twice as large as predicted by theory. It appears that the disparity between observed and theoretical wave heights is largely due to the wake produced by the cylinder.

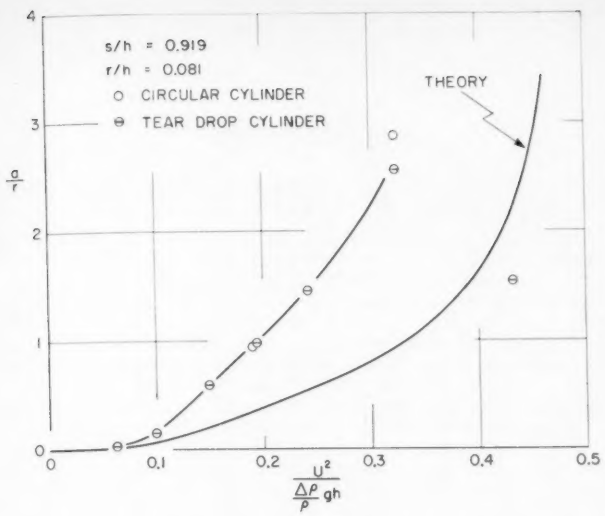

FIGURE 18. *Variation of wave height of internal oscillatory waves; comparison with theory.*

9. Summary

The disturbances created at the interface of a two-layer liquid system by the horizontal motion of a cylinder in the upper layer fall into three categories. First, when the layers are of equal thickness, in most cases a train of progressive oscillatory waves is produced at the interface. Second, when the depth of the lower layer is much less than the depth of the fresh-water layer, the profile of the interface usually resembles that corresponding to a succession of positive internal solitary waves. Third, when the depth of the lower layer is much greater than the depth of the fresh-water layer, in most cases an internal hydraulic jump is produced. The exceptional cases correspond to low cylinder velocities. The theory for disturbances of small amplitude predicts waves of the type observed in the first category, but the observed amplitudes are greater by a factor of two in those cases where the conditions of the theory are most nearly satisfied. This discrepancy is ascribed to the effect of the wake behind the cylinder.

For the progressive oscillatory waves there is a distinct change in the manner of variation of the wave heights corresponding to $U^2/(\Delta\rho/\rho)gh=0.3$ where the wave height reaches a maximum. For $U^2/(\Delta\rho/\rho)gh<0.3$ the wave height a/r depends primarily on the quantity $U^2/(\Delta\rho/\rho)gs$ while for $U^2/(\Delta\rho/\rho)gh>0.3$ the wave height depends on $U^2/(\Delta\rho/\rho)gh$. Figure 12 shows that the wave height increases as r/s is increased.

The experiments with different shapes of cylinders did not yield a significant difference in the disturbances produced. This may be due to the manner in which the wake depends on the cylinder shape.

References

[1] G. G. Stokes. On the theory of oscillatory waves, Trans. Camb. Phil. Soc. **8,** 441 (1847) (Papers I).
[2] R. R. Webb. Math. Tripos Papers (1884).
[3] A. G. Greenhill. Wave motion in hydrodynamics, J. Math. IX, 62, (1887).
[4] W. Burnside. On the small wave motion of a hetrogeneous fluid under gravity, Proc. London Math. Soc. (1), 392 (1889).
[5] A. E. H. Love. Wave motion in a hetrogeneous heavy liquid, Proc. London Math. Soc. **22,** 307 (1891).
[6] Lord Rayleigh, Investigation of the character of the equilibrium of an incompressible heavy liquid of variable density, Proc. London Math. Soc. (1) **14,** 170 (1891) (Papers II, 200).
[7] Sir Horace Lamb. On atmospheric oscillations, Proc. Roy Soc. **84,** 566, 571 (1910).
[8] V. W. Ekman. On dead water, Scientific results of the Norwegian North Polar expedition, pt XV, Christiania, 1904.
[9] N. Zeilon. On tidal boundary waves and related hydrodynamical problems, Kungl. Svenska Vetenskapsaksademiens Handlingar Band **47,** No. 4 (1912).
[10] R. R. Long. Some aspects of flow of stratified fluids I. A theoretical investigation, Tellus **5,** 42–58 (1953).
[11] R. R. Long. Some aspects of flow of stratified fluids III. Continuous density gradients, Tellus **7,** 341 (1955).
[12] R. R. Long. Some aspects of flow of stratified fluids II. Experiments with a two fluid system, Tellus **6,** 97 (1954).
[13] M. Tepper. A proposed mechanism of squall lines—the pressure jump line, J. Meteor. **7,** 21 (1950).
[14] C. G. Rossby. On the vertical and horizontal concentration of momentum in air and ocean currents, Tellus **3,** 15 (1951).
[15] A. Craya. Critical regimes of flows with density stratification, Tellus **3,** 28 (1951).
[16] G. S. Benton. The occurrence of critical flow and hydraulic jumps in a multi-layer system, Tech. Rept. No. 1 (The Johns Hopkins University, Dept. of Civ. Eng., 1953).
[17] C. S. Yih and C. R. Guha. Hydraulic jump in a fluid system of two layers, Tellus **7,** 358 (1955).
[18] G. H. Keulegan. Characteristics of internal solitary waves, J. Research NBS **51** (1953) RP2442.
[19] R. R. Long. The solitary wave in one and two fluid systems, Tellus **8,** 460 (1956).
[20] G. H. Keulegan. An experimental study of internal solitary waves, NBS Report to Chief of Engineers, U.S. Army, Tenth progress report on model laws for density currents (Nov. 28, 1955).
[21] H. Lamb. Hydrodynamics, Sixth Ed. (Cambridge Univ. Press).
[22] L. H. Carpenter. On the motion of two cylinders in an ideal fluid, J. Research NBS **61,** 2 (1958) RP2889.

(Paper 64C3–42)

Publications of the National Bureau of Standards*

Selected Abstracts

Phase shift effects in Fabry-Perot interferometry, C. J. Koester, *J. Research NBS* **64A,** *No. 3, May–June 1960.*

A method is demonstrated for utilizing in Fabry-Perot interferometry the data on reflection phase shift dispersion obtained from fringes of equal chromatic order. Unknown wavelengths can be calculated from the Fabry-Perot patterns obtained with a large etalon spacing, even without prior knowledge of the phase shift of the reflecting surfaces. When the theoretical phase shift as a function of wavelength is known approximately, then the correct orders of interference can be determined for both the Fabry-Perot fringes and fringes of equal chromatic order. From the wavelengths of the latter the phase shift dispersion can be measured to an accuracy of about 10A. The method is especially useful for reflectors with large dispersion of phase shift, such as multilayers. Results in the visible spectrum are reported for aluminum films and a pair of dielectric 15 layer broad-band reflectors.

Separation and determination of small quantities of aluminum in steel, B. B. Bendigo and R. K. Bell, *J. Research NBS* **64A,** *No. 3, May–June 1960.*

A method is described for determining small amounts of aluminum (0.01 to 0.3 percent) in carbon and stainless steels. A perchloric-sulfuric acid solution of the steel is electrolyzed in a mercury cathode cell to remove most of the iron, and a chloroform extraction removes elements such as aluminum, residual iron, and titanium as cupferrates from a solution buffered at *p*H 3.5. These elements are converted from cupferrates to perchlorates; all except aluminum are then extracted as cupferrates with chloroform from 4*N* hydrochloric acid. Aluminum in the acid solution is determined photometrically, using aluminon (ammonium aurintricarboxylate) and a wavelength of approximately 540 mμ. Accuracy to within ± 0.005 percent aluminum is indicated.

A symmetric continuous poker model, A. J. Goldman and J. J. Stone, *J. Research NBS* **64B,** *No. 1, January–March 1960.*

Beginning with Von Neumann, mathematicians concerned with the rational analysis of conflict situations have realized that investigation of accurate or simplified versions of common card games leads to techniques and insights applicable to situations of military or economic interest. In the present paper, a symmetric poker model one stage more complicated than the original Von Neumann game is solved. There are two bet levels a, b and an ante of 1 unit ($a>b>1$); no raises are permitted. The game has a unique optimal strategy, which forbids bluffing on a low hand. The limiting case $b=1$ is shown to yield the Von Neumann model.

Characteristics of 488 megacycles per second radio signal reflected from the moon, B. C. Blevis and J. H. Chapman, *J. Research NBS* **64D,** *No. 4, July–August 1960.*

Radio signals at 488 Mc, received after reflection from the moon, have been studied using a continuous wave bistatic radar system located near Ottawa, Canada. These experiments were carried out during 1957 and consisted of monitoring the signals received on two orthogonal dipoles mounted at the focus of a 28-foot parabolic tracking antenna. The total mean received signal yielded an effective radar cross section of the moon at this frequency of 0.05 of the projected area. The libration fading as observed in the two orthogonal receiver channels was in sychronism, with a cross-correlation coefficient of 0.89. It was established that the signal is not depolarized significantly on reflection at the surface of the moon, or in passing through the ionosphere. Rotation of the plane of polarization of the radio wave in the double passage through the ionosphere was observed to change by nearly 180 degrees over a 6-hour period during quiet ionospheric conditions.

The use of polarization fading of satellite signals to study the electron content and irregularities in the ionosphere, C. G. Little and R. S. Lawrence, *J. Research NBS* **64D,** *No. 4, July–August 1960.*

A procedure is described for using the Faraday-rotation fading of a satellite radio signal to measure the ionospheric electron content per unit column up to the height of the satellite. Full account is taken of ionospheric refraction by using the collision-free form of the Appleton-Hartree equation. Results based on observations of 1958 Delta 2 are presented. The sub-satellite electron contents derived throughout the satellite passes for heights below the *F*-peak compare well with values deduced from simultaneous ionograms. Ionospheric irregularities, having lateral dimensions of a few hundred kilometers, and fractional deviations in sub-satellite electron content of about 0.02 have been detected. Our observations suggest that satellite polarization studies offer important advantages over other methods of investigating these irregularities.

Determination of piezoelectric properties as a function of pressure and temperature, J. E. McKinney and C. S. Bowyer, *J. Acoust. Soc. Am.* **32,** *No. 1, 56 (1960).*

Piezoelectric data on a mixed titanate system (82% $BaTiO_3$, 9.1% $CaTiO_3$, 3.6% $PbTiO_3$, and 4.4% TiO_2) was obtained from an apparatus intended to measure the dynamic compressibility of materials. The calibration constant of the apparatus involves the piezoelectric and dielectric constants of the ceramics used as transducers. The method is discussed and an operating equation for the apparatus derived. Piezoelectric and dielectric constants have been measured over a fairly extensive temperature and pressure range and an apparent phase transition observed near 5° C. This transition corresponds to that found in pure barium titanate, and might be due to imperfect mixing of the titanates that leaves a small amount of pure barium titanate present. The method described appears more sensitive for the detection of changes in crystal symmetry in such materials than either X-ray or dielectric measurements.

Determination of the recording performance of a tape from its magnetic properties, E. D. Daniel and I. Levine, *J. Acoust. Soc. Am.* **32,** *No. 2, 258 (1960).*

This is the second of two papers. The first (I) dealt with the general magnetic properties of recording tape. The present paper gives an analysis of hf biased recording based upon the anhysteretic properties of the tape as specified in I. Calculations of performance are compared with the results of absolute measurements carried out on a conventional recording machine, and on large scale models. Satisfactory agreement is obtained when the theory is corrected to take into account a loss attributed largely to a dynamic form of demagnetization which takes place during recording. The corrected theory can be used to compare tape performance under a variety of operating conditions without reference to a particular test recorder. Attention is confined to recorded wavelengths which are large compared with coating thickness.

Gages for measuring the thickness of chromium on the internal surface of small-bore tubes, V. A. Lamb and P. A. Krasley, *Plating* **47,** *No. 2, 176 (1960).*

Two gages of the eddy-current type for measuring the thickness of chromium coatings on the internal surface of caliber .30 and caliber .50 gun barrels have been developed. Measurements are nondestructive and are localized to a small area, less than ⅛ inch diameter. The gages may readily be modified to be generally applicable to the measurement of the thickness of various coatings on the internal surfaces of metallic tubes of the same or larger diameters.

Experimental and theoretical investigation of the magnetic properties of iron oxide recording tape, E. D. Daniel and I. Levine, *J. Acoust. Soc. Am.* **32,** *No. 1, 1 (1960).*

Part A gives the results of remanent magnetization tests made under ordinary and anhysteretic conditions, and shows that the major anhysteretic properties of a recording tape can be expressed in terms of three easily measured constants. The design of the test equipment is discussed and test results are listed for thirteen representative types of tape. Part B reviews some of the theories of fine particle magnets that can be applied to recording tape, and gives an extensive treatment of remanent magnetization based upon the Preisach diagram. Some aspects of the Preisach diagram treatment may be of interest to workers outside the magnetic recording field. The anhysteretic properties are important in hf biased recording and a second paper describes how these properties can be used to predict certain recording performance characteristics.

Efficient harmonic generation, G. F. Montgomery, *Proc. IRE* **48,** *No. 2, 251 (1960).*

An harmonic generator using a rectifier multiplier followed by an amplifier is more efficient than its equivalent class-C multiplier. A proposed rectifier-transistor harmonic generator is capable of high efficiency that is nearly independent of harmonic number.

Precise measurement of heat of combustion with a bomb calorimeter, R. S. Jessup, *NBS Monograph 7 (1960).*

This Monograph gives detailed descriptions of apparatus and methods which are used at the National Bureau of Standards for precise determinations of heats of combustion of liquid hydrocarbon fuels. Numerical examples are given of methods of calculating results of measurements from observed data. The technique of making and filling glass bulbs to contain samples of volatile liquid fuels is described.

The accuracy of the methods described is about 0.1 percent. This is intermediate between the accuracy of 0.01 or 0.02 percent attained in certain measurements on pure compounds, and the accuracy of several tenths of one percent obtainable with published standard procedures for measurements on fuels.

Conductive flooring for hospital operating rooms, T. H. Boone, F. L. Hermach, E. H. MacArthur, and R. C. McAuliff, *NBS Monograph 11 (1960).*

Characteristics and performance of available types of conductive flooring materials were investigated in the laboratory. The study showed that the electrodes and instruments used to measure the floor greatly affected the measured resistance, but that the method specified by the National Fire Protection Association for measuring the electrical resistance reasonably simulated the conditions under which a floor functions in reducing electrostatic hazards. The physical, chemical, and serviceability characteristics of conductive floorings investigated showed results comparable with those of nonconductive flooring of the same type. Consequently, with some limitations, an architect may base his choice of a conductive flooring material on his knowledge of the behavior of similar nonconductive materials.

Tabulation of data on receiving tubes, C. P. Marsden, W. J. Keery, and J. K. Moffitt, *NBS Handb. 68 (1959).*

A tabulation of Receiving Type Electron Tubes with some characteristics of each type has been prepared in the form of two major listings, a Numerical Listing in which the tubes are arranged by type number, and a Characteristic Listing in which the tubes are arranged by tube type and further ordered on the basis of one or two important parameters. The tabulation is accompanied by a listing of similar tube types and basing diagrams for the listed tubes.

Are life testing procedures robust? M. Zelen and M. C. Dannemiller, *Proc. 6th Natl. Symp. Reliability and Quality Control in Electronics, Jan. 11–13, 1960, Inst. Radio Engrs. Inc., p. 185 (1960).*

Almost all the statistical procedures in current use for evaluating the reliability of components or equipments rest on the assumption that the failure times follow the exponential distribution. In practical situations one rarely has enough data to determine whether failure times are actually exponential. This paper studies the behavior of several statistical life testing procedures based on the exponential failure law if the true failure law is the Weibull distribution. It is found that these statistical techniques, which are widely used, are very sensitive to departures from initial assumptions. Applying these techniques to life test data when the exponential failure law is not satisfied may result in substantially increasing the probability of accepting components or equipments having poor reliability.

Improved NBS abrasive jet method for measuring abrasion resistance of coatings, A. G. Roberts, *ASTM Bull. No. 244, 48 (TP52) (1960).*

A description is given of the changes made in the NBS Abrasive Jet Method since publication of the original article describing this rapid, reproducible, and versatile means for measuring the abrasion resistance of organic and other coatings. Improvements include use of a free-flowing abrasive, a redesigned abrasive sifting chamber to minimize turbulence and interference effects, better control of abrasive flow, addition of an electronic contact device for setting nozzle-to-coating distance, and automatic timing. Precision of measurement has been significantly increased by use of a reference panel.

Flame-spread measurements by the radiant panel flame-spread method, D. Gross, *Forest Products J. X, No. 1, 33 (1960).*

The results of a limited number of tests for evaluation of the flame spread properties of untreated and of fire-retardant coated wood-base materials are presented. It is shown by use of the radiant panel flame spread test method that variations in moisture content and mean density can have a significant effect upon the flame spread index of untreated wood. For the same mean density and moisture content, it was observed that variations in the surface grain structure of untreated wood had an appreciable effect upon the flame spread index. The flame spread indices of the fire-retardant coated assemblies were considerably lower than those obtained with uncoated or conventionally coated materials although significant differences between coated assemblies were observed. A test method such as this can be used to advantage for the development and evaluation of effective and practical fire-retardant coatings for wood-base materials.

Report of the 44th National Conference on Weights and Measures 1959, *NBS Misc. Publ. 228 (1959).*

This is a report of the proceedings (edited) of the Forty-fourth National Conference on Weights and Measures, sponsored by NBS, held in Washington, D.C., June 8–12, 1959, and attended by State, county, and city weights and measures officials, and representatives of the Federal Government, business, industry, railroads, and associations.

What price accurate test methods? A. T. McPherson, *ASTM Bull. (ACR Notes Column) No. 244, 7 (1960).*

Inaccurate test methods used in specifications frequently lead to difficulty, misunderstandings, and unnecessary rejections because much of the tolerance that is allowed in dimensions, composition, or other characteristics of a product may be taken up by the uncertainty in testing. Accurate methods can pay dividends by lowering the rejection rate, avoiding referee tests and other sources of delay, and affording greater assurance that products which are found by test to comply with the specification will actually serve the intended purpose. A further saving may be effected with many products by widening the tolerances and thereby reducing the cost of production. The development of accurate test methods, however, may require long and expensive research. Before undertaking to develop any specific new test method, a critical survey should be made to determine whether the anticipated savings and other benefits will exceed the probable cost. Such a survey will involve both economic and technical factors and may well make use of methods and techniques which are employed in market research.

Many changes reflected in new dry cell standard, W. J. Hamer, *Mag. of Standards* **31**, *No. 3, 81 (1960).*

The seventh edition of the American Standard Specification for Dry Cells and Batteries was published in December 1959 as Handbook 71 of the National Bureau of Standards. It supersedes the previous specification which was published in 1954 as Circular 559 of the National Bureau of Standards. The new specification includes many changes. Cell dimensions are given in both the English and metric systems: the metric system was added in line with the trend toward its increased use in commerce and industry. Cell and battery designations recommended by TC–35 Committee on Primary Cells and Batteries of the International Electrotechnical Commission was incorporated in keeping with attempts to secure international cooperation in the standardization of primary batteries. The most notable change in the new specification is the inclusion, for the first time, of cells and batteries for use with transistorized circuits. Other minor changes include a new test for lantern batteries used in alarm circuits, some new terminal designs, and the dropping of specifications for batteries to be used with "carbon-type" hearing aids since these types of instruments are rapidly becoming obsolete.

Water penetration testing machine for sole leather, T. J. Carter, *J. Am. Leather Chem. Assoc.* **LV**, *No. 3, 139 (1960).*

A test to measure the water resistance of sole leather has been developed. A leather specimen is flexed at a frequency of 30 cycles per minute with one side exposed to water until penetration occurs. The specimen is clamped so that the angle of bend is approximately 90°. The results show that flexing increases the rate of water absorption as well as the rate of water penetration compared to the rates under static conditions. Studies were made on the influence of thickness of specimen, location on the sole leather bend, and compression of the specimen on dynamic water penetration and water absorption. The logarithm of the number of flexes required for penetration is a direct function of the thickness of the leather. The rates of water penetration and water absorption depend on the location of the specimen on the sole leather bend. Compression of the impregnated leather decreases the rate of water penetration and the rate of water absorption.

Bending and stretching of corrugated diaphragms, R. F. Dressler, *Trans. ASME* **81D**, *No. 4, 651 (1959).*

Solutions of the exact linear elastic shell equations for all stresses and displacements in a typical corrugated diaphragm are presented for three cases over a 9 to 1 range of thicknesses. Results were obtained by numerical integration in an electronic digital computer. The effect of thickness variation is discussed with respect to both stresses and resultants, and peak values needed for design purposes are presented. Circumferential and meridional stresses are found to be equally important throughout the thickness range analyzed. Bending and membrane stresses are likewise equally important throughout the range. Peak values in some cases occur near the outer rim.

Triaxial tension at the head of a rapidly running crack in a plate, J. M. Frankland, *Trans. ASME, Ser. E* **26**, *No. 4, 570 (1959).*

Two-dimensional solutions have been found for the state of stress in a plate loaded in tension at right angles to a crack. One of these concerns the stationary crack and the other an advancing crack. No three-dimensional solutions are available. It is shown, however, that it is highly probable that cracks propagating at high speeds develop an appreciable triaxial tension near the head of the crack. This is believed to be significant with regard to the observed brittle behavior of plates under such circumstances.

Transistor P-A amplifier, G. F. Montgomery and F. R. Bretemps, *Electronic Ind.* **19**, *No. 1, 196 (1960).*

A portable public-address amplifier using transistors and powered by flashlight cells develops an electrical power of about 0.75 watt and is useful for moderately large audiences. The complete unit consists of the amplifier, two loudspeakers, batteries, and a dynamic microphone and is contained in an attache case. Battery life is about 20 hours.

Other NBS Publications

Journal of Research, Section A. Physics and Chemistry, Volume 64A, No. 3, May–June 1960. 70 cents.

Phase shift effects in Fabry-Perot interferometry. C. J. Koester. (See above abstracts.)

Infrared absorption spectrum of methane from 2470 to 3200 cm^{-1}. E. K. Plyler, E. D. Tidwell, and L. R. Blaine.

Elastic constants of synthetic single crystal corundum at room temperature. J. B. Wachtman, Jr., W. E. Tefft, D. G. Lam, Jr., and R. P. Stinchfield.

Radial distribution study of vitreous barium borate. A. Bienenstock, A. S. Posner, and S. Block.

Separation and determination of small quantities of aluminum in steel. B. B. Bendigo and R. K. Bell. (See above abstracts.)

Conformations of the pyranoid sugars. II. Infrared absorption spectra of some aldopyranosides. R. S. Tipson and H. S. Isbell.

Journal of Research, Section B. Mathematics and Mathematical Physics, Volume 64B, No. 2, April–June 1960. 75 cents.

Non-self-adjoint boundary value problems in ordinary differential equations. W. Greub and W. C. Rheinboldt.

Criteria for the existence and equioscillation of best Tchebycheff approximations. J. R. Rice.

Note on the solution of Riccati's differential equation. H. H. Howe.

On a generalization of the index notation for absolute tensors of arbitrary order. E. H. Brown.

Upper and lower bounds for the center of flexure. L. E. Payne.

Half-round inductive obstacles in rectangular wave guide. D. M. Kerns.

Journal of Research, Section D. Radio Propagation, Volume 64D, No. 4, July–August 1960. 70 cents.

Relation of turbulence theory to ionospheric scatter propagation experiments. A. D. Wheelon.

Propagation at oblique incidence over cylindrical obstacles. M. P. Bachynski.

Diffraction by smooth conical obstacles. H. E. J. Neugebauer and M. P. Bachysnki.

Characteristics of 488 megacycles per second radio signal reflected from the moon. B. C. Blevis and J. H. Chapman. (See above abstracts.)

The use of polarization fading of satellite signals to study the electron content and irregularities in the ionosphere. C. G. Little and R. S. Lawrence. (See above abstracts.)

Note on a test of the equivalence theorem for sporadic *E* propagation. J. W. Wright and T. N. Gautier.

Daytime attenuation rates in the very low frequency band using atmospherics. W. L. Taylor.

Measured electrical properties of snow and glacial ice. A. D. Watt and E. L. Maxwell.

Some extremely low frequency phenomena. E. T. Pierce.

Mode theory and the propagation of extremely low frequency radio waves. J. R. Wait.

Studies of natural electric and magnetic fields. G. D. Garland and T. F. Webster.

Natural electromagnetic energy below the ELF range. W. H. Campbell.

Possible application of the system loss concept at extremely low frequencies. K. A. Norton.

Measurements of the spectrum of radio noise from 50 to 100 cycles per second. M. Balser and C. A. Wagner.

Half-wave cylindrical antenna in a dissipative medium: current and impedance. R. King and C. W. Harrison.

Standard X-ray diffraction powder patterns, H. E. Swanson, M. I. Cook, T. Isaacs, and E. H. Evans, NBS Circ. 539, Vol. 9, (1960) 40 cents.

Properties of high-temperature ceramics and cermets—Elasticity and density at room temperature, S. M. Lang, NBS Monograph 6 (1960) 20 cents.

Specification for dry cells and batteries, (supersedes NBS Circ. 559). NBS Handb. 71 (1959) 25 cents.

Research Highlights of the National Bureau of Standards Annual Report, Fiscal Year 1959. NBS Misc. Publ. 229 (1959) 55 cents.

Basic theorems in matrix theory, M. Marcus. NBS Applied Math. Series 57 (1960) 15 cents.

Survey of Central Radio Propagation Laboratory research in tropospheric propagation 1948–1956, J. W. Herbstreit and P. L. Rice, NBS Tech. Note 26 (PB151385) (1959) $4.00.

An atlas of oblique-incidence ionograms, V. Agy, K. Davies, and R. Salaman, NBS Tech. Note 31 (PB151390) (1959) $2.25.

Distribution of incoming lettermail at the Baltimore, Maryland City Post Office, B. M. Levin and A. E. Newman, NBS Tech. Note 33 (PB151392) (1959) $2.50.

A multiplet table of astrophysical interest, C. E. Moore, NBS Tech. Note 36 (PB151395) (1959) $4.00.

Application of RF micropotentiometers for calibration of signal generators to 1000 Mc, L. F. Behrent, NBS Tech. Note 37 (PB151396) (1960) 50 cents.

Design and construction of a liquid hydrogen temperature refrigeration system, D. B. Chelton, J. W. Dean, and B. W. Birmingham, NBS Tech. Note 38 (PB151397) (1960) 75 cents.

Helium refrigeration and liquefaction using a liquid hydrogen refrigerator for precooling, D. B. Chelton, J. W. Dean, and T. R. Strobridge, NBS Tech. Note 39 (PB151398) (1960) 50 cents.

Mean electron density variations of the quiet ionosphere I—March 1959, J. W. Wright and L. A. Fine, NBS Tech. Note 40–1 (PB151399–1) (1960) $1.25.

Mean electron density variations of the quiet ionosphere 2—April 1959, J. W. Wright and L. A. Fine, NBS Tech. Note 40–2 (PB151399–2) (1960) $1.25.

Expendable modules as bases for disposal-at-failure maintenance, R. O. Stone, P. Meissner, and K. M. Schwarz, NBS Tech. Note 41 (PB151400) (1960) $2.25.

Analog-digital conversion equipment for electrocardiographic data, L. Taback, NBS Tech. Note 42 (PB151401) (1960) $1.25.

A summary of VHF and UHF tropospheric transmission loss data and their long-term variability, D. A. Williamson, V. L. Fuller, A. G. Longley, and P. L. Rice, NBS Tech. Note 43 (PB151402) (1960) $2.25.

Tables for the statistical prediction of radio ray bending and elevation angle error using surface values of the refractive index, B. R. Bean, B. A. Cahoon, and G. D. Thayer, NBS Tech. Note 44 (PB151403) (1960) 50 cents.

Operating instructions for ARN–2 auxiliary log-linear noise recorder, R. T. Disney and C. A. Samson, NBS Tech. Note 45 (PB151404) (1960) 50 cents.

Direction findings on whistlers, J. M. Watts, J. Geophys. Research **64,** No. 11, 2029 (1959).

The construction of Hadamard matrices, E. C. Dade and K. Goldberg, Michigan Math. J. **6,** 247 (1959).

Geomagnetic and ionospheric phenomena associated with nuclear explosions, S. Matsushita, Nature **184,** BA33 (1959).

Stress corrosion cracking in low carbon steel, H. L. Logan, Proc. Phys. Met. Stress Corrosion Fracture Conf., Pittsburgh, Pa., Apr. 2–3, 1959, reprinted from Met. Soc. Conf., p. 295 (Interscience Publishers, New York, N.Y., 1959).

Higher oxides of silver, H. E. Swanson, J. Electrochem. Soc. **106,** No. 12, 1073 (1959).

Oscillatory behavior of magnetic susceptibility and electronic conductivity, A. H. Kahn and H. P. R. Frederikse, ch. in Vol. IX, Adv. Solid State Phys., p. 257 (Academic Press Inc., New York, N.Y., 1959).

Geomagnetic activity following large solar flares, C. S. Warwick and R. T. Hansen, J. Atmospheric and Terrest. Phys. **14,** 287 (1959).

Simplification of systems of units currently evolving in the electrical field, F. B. Silsbee, Systems of Units, Am. Assoc. Advance. Sci., p. 7 (1959).

Atoms and free radicals by γ-irradiation at 4.2° K, L. A. Wall, D. W. Brown, and R. E. Florin, J. Phys. Chem. **63,** 1762 (1959).

Rotation transfer in the fluorescence spectrum of OH($^2\Sigma^+$), T. Carrington, J. Chem. Phys. **31,** No. 5, 1418 (1959).

Poly(tetrafluorethylene)—a radiation-resistant polymer, L. A. Wall and R. E. Florin, Letter to Ed., J. Appl. Polymer Sci. III, No. 5, 251 (1959).

On the approximate daytime constancy of the absorption of radio waves in the lower ionosphere, S. Chapman and K. Davies, J. Atmospheric and Terrest. Phys. **13,** No. 1–2, 86 (1958).

An X-ray crystallographic study of Schroeckingerite and its dehydration product, D. K. Smith, Am. Mineralogist **44,** 1020 (1959).

Modular forms whose coefficients possess multiplicative properties, M. Newman, Ann. Math. **70,** 478 (1959).

A note on the scattering of electrons from atomic hydrogen, A. Temkin, Phys. Rev. **116,** No. 2, 358 (1959).

The analysis of latin squares with a certain type of row-column interaction, J. Mandel, Technometrics **1,** No. 4, 379 (1959).

Design of free-air ionization chambers for the soft X-ray region (20–100 kv), V. H. Ritz, Radiology **73,** No. 6, 911 (1959).

Thermal conductivity of indium antimonide at low temperatures, E. V. Mielczarek and H. P. R. Frederikse, Phys. Rev. **115,** 888 (1959).

Model for vibrational relaxation of diatomic gases behind shock waves, R. Herman and R. J. Rubin, Phys. of Fluids **2,** No. 5, 547 (1959).

A note on algebras, A. J. Goldman, Am. Math. Mo. **66,** 795 (1959).

Linear differential equations of the second order with a large parameter, F. W. J. Olver, J. Soc. Indust. Appl. Math. **7,** 306 (1959).

Sorting devices in postal tests. 1: Proposal for an electromagnetic sorter, S. Henig, Automatic Control **11,** No. 6, 6 (1959).

The dissociation constant of $CaOH^+$ from 0° to 40°C, R. G. Bates, V. E. Bower, R. G. Canham, and J. E. Prue, Trans. Faraday Soc. **55,** No. 444, 2062 (1959).

Evaluation of chemical analyses on two rocks, W. J. Youden, Technometrics **1,** No. 4, 409 (1959).

Nuclear electronics, L. Costrell, Nucleonics Mag. **18,** No. 1, 124 (1960).

Microscopical studies of failure in polymers, S. B. Newman, ASTM Spec. Tech. Pub. **257,** 132 (1959).

Flare-associated bursts at 18 Mc/s, C. Warwick and J. W. Warwick, Paris Symp. on Radio Astron. (IAU Symp. No. 9 and URSI Symp. No. 1), p. 203 (1959).

Quantum-mechanical calculation of the probability of an exchange reaction for constrained linear encounters, J. Mazur and R. J. Rubin, J. Chem. Phys. **31,** No. 5, 1395 (1959).

Monte Carlo calculations of gamma ray backscattering, M. J. Berger and D. J. Raso, Radiation Research **12,** No. 1, 20 (1960).

On the diffraction of electromagnetic pulses by curved conducting surfaces, J. R. Wait and A. M. Conda, Can. J. Phys. **37,** 1384 (1959).

Identification of textile coatings by infrared spectroscopy, F. H. Forziati, R. T. Hite, and M. K. Wharton, Am. Dyestuff Reptr. **49,** No. 4, 29 (1960).

New wavelengths for some helium (He I) lines, W. C. Martin, J. Opt. Soc. Am. **50,** No. 2, 174 (1960).

Geomagnetic effects of high-altitude nuclear explosions, A. G. McNish, J. Geophys. Research **64,** No. 12, 2253 (1959).

Propagation and production of electromagnetic waves in a plasma, R. Gallet, Nuovo Cimento Suppl. **13,** No. 1, 234 (1959).

Fading rate recorder for propagation research, J. W. Koch, W. B. Harding, and R. J. Jansen, Electronics **32,** No. 51, 78 (1959).

Matrix algebra for calculating multicomponent mixtures, F. Ordway, Portland Cement Assoc. J. Research and Devel. Labs. **2,** No. 1, 28 (1960).

Line shape and f value in the $OH^2\Sigma^+$-$^2\pi$ transition, T. Carrington, J. Chem. Phys. **31,** No. 5, 1243 (1959).

Leonard Euler's integral: A historical profile of the gamma function, P. J. Davis, Am. Math. Mo. **66,** 849 (1959).

Departures from the Saha equation under varying conditions of Lyman continuous opacity, S. R. Pottasch and R. N. Thomas, Astrophys. J. **130,** No. 3, 941 (1959).

Vibration-rotation bands of ammonia. IV. The stretching fundamentals and associated bands near 3μ, W. S. Benedict, E. K. Plyler, and E. D. Tidwell, J. Chem. Phys. **32,** No. 1, 32 (1960).

Electron impact studies of aromatic hydrocarbons. I. Benzene, napthalene, anthracene, and phenanthrene, M. E. Wacks and V. H. Dibeler, J. Chem. Phys. **31,** No. 6, 1557 (1959).

Value of the Rydberg constant, W. C. Martin, Phys. Rev. **116,** No. 3, 654 (1959).

Characteristics of deposits, W. H. Metzger, Jr., Symp. Electroless Nickel Plating, ASTM Spec. Tech. Publ. **265,** p. 13 (1959).

Turbulent motion, G. B. Schubauer and C. M. Tchen, Sec. B, Vol. V, Princeton Ser., High Speed Aerodynamics and Jet Propulsion, Turbulent Flows and Heat Transfer, p. 75 (Princeton University Press, Princeton, N.J., 1959).

Confidence intervals for the expectation of a Poisson variable, E. L. Crow and R. S. Gardner, Biometrika **46,** 441 (1959).

Electron characteristic energy losses in some intermetallic compounds, B. Gauthe, Phys. Rev. **114,** No. 5, 1265 (1959).

Adsorption, diffusion, and evaporation of carbon monoxide or tungsten, R. Klein, J. Chem. Phys. **31,** No. 5, 1306 (1959).

The ninth plenary assembly of the CCIR, J. W. Herbstreit, IRE Proc. **48,** 45 (1960).

Effect of fluorides on infrared transmittance of certain silicate glasses, G. W. Cleek and T. S. Scuderi, J. Am. Ceram. Soc. **42,** No. 12, 599 (1959).

Studies of borate minerals. VI: Veatchite, J. R. Clark, M. E. Mrose, A. Perloff, and G. Burley, Am. Mineralogist **44,** No. 11–12, 1141 (1959).

Conditions at the ionization and shock fronts in collisions of gas clouds—Bright rims in diffuse nebulae, Pt. VI, S. R. Pottasch, Rev. Mod. Phys. **30,** No. 3, 1053 (1958).

The adhesion of electrodeposited nickel to chromium at elevated temperatures, W. E. Reid, Jr., and F. Ogburn, J. Electrochem. Soc. **107,** No. 2, 91 (1960).

Chloride content of the diffusion layer at a silver anode, P. A. Krasley, J. Electrochem. Soc. **107,** No. 2, 139 (1960).

Spectral emittance of ceramic-coated and uncoated specimens of Inconel and stainless steel, J. C. Richmond and J. E. Stewart, J. Am. Ceram. Soc. **42,** No. 12, 633 (1959).

Chemical structure and stability relationships in polymers, B. G. Achhammer, M. Tryon, and G. M. Kline, Kunststoffe Combined with German Plastics Digest **49,** No. 11, 600 (1959); Mod. Plastics **37,** No. 4, 131 (1959).

A study of 17–7 *p*H stainless steel, N. L. Carwile and S. J. Rosenberg, WADC Tech. Rep. 58–653 (1959) (Available from the Office of Technical Services, Department of Commerce, Washington 25, D.C.).

High-altitude observation techniques, D. M. Gates, Letter Science **131,** 266 (1960).

The relation between confidence intervals and tests of significance—a teaching aid, M. G. Natrella, Am. Stat. **14,** No. 1, 20 (1960).

Electrophoretic deposition of metals, metalloids, and refractory oxides, V. A. Lamb and W. R. Reid, Plating **47,** No. 3, 291 (1960).

The effect of the earth's magnetic field on m.u.f. calculations, K. Davies, J. Atmospheric and Terrest. Phys. **16,** 187 (1959).

Fusion of polymer networks formed from linear polyethylene: Effect of intermolecular order, L. Mandelkern, D. E. Roberts, J. C. Halpin, and F. P. Price, J. Am. Chem. Soc. **32,** 46 (1960).

Sauter theory of the photoelectric effect, U. Fano, K. W. McVoy and J. R. Albers, Phys. Rev. **116,** No. 5, 1147 (1959).

Bremsstrahlung and the photoelectric effect as inverse processes, K. W. McVoy and U. Fano, Phys. Rev. **116,** No. 5, 1168 (1959).

Surface area and exchange capacity relation in a Florida kaolinite, W. C. Ormsby and J. M. Shartsis, J. Am. Ceram. Soc. **43,** No. 1, 44 (1960).

Balmer decrements: the diffuse nebulae, S. R. Pottasch, Astrophys. J. **131,** No. 1, 202 (1960).

Standard frequency transmission and time signals, W. D. George, Proc. 2d all-IRIG Symp., prepared by Secretariat, Inter-Range Instrumentation Group, Oct. 1958, p. 141, IRIG Document No. 107–58.

Atomistic approach to the rheology of sand-water and clay-water mixtures, W. A. Weyl and W. C. Ormsby, ch. 7, Vol. III, Rheology—Theory and applications, Edited by F. R. Eirich, p. 249 (Academic Press, New York, N.Y., 1960).

Diffusion of particles in trubulent flow, C. M. Tchen, Adv. Geophys. 6: Atmospheric diffusion and air pollution, p. 165, Proc. Symp. Oxford, England, Aug. 1958 (Academic Press Inc., New York, N.Y., 1959).

Atmospheric tides and ionospheric electrodynamics, M. L. White, Jr., Geophys. Research **65,** 153 (1960).

Some evidence for structural anomalies in pure cristobalite, R. F. Walker, S. J. Schneider, and R. S. Roth, J. Am. Ceram. Soc. **42,** No. 12, 642 (1959).

La Recherche sur les radicaux libres au National Bureau of Standards, H. P. Broida, J. chim. phys. **56,** No. 2392, 813 (1959).

Isotope exchange processes in solid nitrogen under electron bombardment, R. Klein and E. M. Horl, J. Chem. Phys. **32,** No. 1, 307 (1960).

Relative measurement of the photodetachment cross section for H^-, S. J. Smith and D. S. Burch, Phys. Rev. **116,** No. 5, 1125 (1959).

Interference of orbital and spin currents on bremsstrahlung and photoeclectric effect, U. Fano, K. W. McVoy and J. R. Albers, Phys. Rev. **116,** No. 5, 1159 (1959).

Use of the equation of hydrostatic equilibrium in determining the temperature distribution in the outer solar atmosphere, S. R. Pottasch, Astrophys. J. **131,** No. 1, 68 (1960).

Reception of space diversity transmitters, J. W. Koch, Wireless World (England) **65,** No. 10, 512 (1959).

Réactions en chaine de radicaux gelés, J. L. Jackson, J. chim. phys. **56,** No. 2392, 771 (1959).

Etude spectroscopique des produits de la decharge electrique dan L'Azote condenses a l'etat solide a tres basse temperature, prevues en faveur de l'existence d'Azote triatomique dan le solide, M. Peyron, E. M. Horl, H. W. Brown, and H. P. Broida, J. chim. phys. **56,** No. 2392, 736 (1959).

Apparent temperatures measured at melting points of some metal oxides in a solar furnace, J. J. Diamond and S. J Schneider, J. Am. Ceram. Soc. **43,** No. 1, 1 (1960).

Perovskite-type compounds in binary rare earth oxide systems, S. J. Schneider and R. S. Roth, J. Am. Ceram. Soc. **43,** No. 2, 115 (1960).

Use of disodium *m*-benzenedisulfonate as a hardening agent in Watts nickel bath, W. H. Metzger, P. A. Krasley, and F. Ogburn, Plating **47,** No. 3, 285 (1960).

On the convergence of the Rayleigh quotient iteration for the computation of characteristic roots and vectors, VI. (Usual Rayleigh quotient for nonlinear elementary divisors), A. M. Ostrowski, Arch. Rat. Mech. Anal. **4,** No. 2, 153 (1959).

An analysis of time variations in tropospheric refractive index and apparent radio path length, M. C. Thompson, H. B. Janes, and A. W. Kirkpatrick, J. Geophys. Research **65,** 193 (1960).

Neutron detection by reactions induced in scintillators, C. O. Muehlhause, Pt. I, Fast neutron physics, Sec. III, Pt. III. B, p. 387 (Interscience Publ., New York, N.Y., 1960).

A relationship between the lower ionosphere and the [OI] 5577 nightglow emission, J. W. McCaulley and W. S. Hough, J. Geophys. Research **64,** No. 12, 2307 (1959).

Etude aux infrarouges de certains solides condenses a partir de decharges en phase gazeuse, K. B. Harvey and H. W. Brown, J. chim. phys. **56,** No. 2392, 745 (1959).

Theory of flame propagation in solid nitrogen at low temperatures, S. G. Reed and C. M. Herzfeld, J. Chem. Phys. **32,** No. 1, 1 (1960).

A note regarding the mechanism of UHF propagation beyond the horizon, A. D. Watt, E. F. Forman, and R. W. Plush, Letter Proc. IRE **48,** 252 (1960).

High-frequency limit of bremsstrahlung in the Sauter approximation, U. Fano, Phys. Rev. **116,** No. 5, 1156 (1959).

The weighted compounding of two independent significance tests, M. Zelen and L. S. Joel, Ann. Math. Stat. **30**, No. 4, 885 (1959).

A model of the F region above h_{max} $F2$, J. W. Wright, J. Geophys. Research **65,** 185 (1960).

Interference of antioxidant in the determination of low polymer in SBR synthetic rubber, L. T. Milliken and F. J. Linnig, J. Polymer Sci. **XLI,** No. 138, 544 (1959).

**Publications for which a price is indicated (except for NBS Technical Notes) are available only from the Superintendent of Documents, U.S. Government Printing Office, Washington 25, D.C. (foreign postage, one-fourth additional). Technical Notes are available only from the Office of Technical Services, U.S. Department of Commerce, Washington 25, D.C. (Order by PB number.) Reprints from outside journals and the NBS Journal of Research may often be obtained directly from the authors.*

UNITED STATES
GOVERNMENT PRINTING OFFICE
DIVISION OF PUBLIC DOCUMENTS
WASHINGTON 25, D.C.

OFFICIAL BUSINESS

PENALTY FOR PRIVATE USE TO AVOID
PAYMENT OF POSTAGE, $300
(GPO)

JOURNAL OF RESEARCH of the National Bureau of Standards Vol. 64C, No. 3 July–September 1960
C. Engineering and Instrumentation

Contents

Page

A new method of measuring gage blocks. James B. Saunders. 173

Gage blocks of superior stability: initial developments in materials and measurement. M. R. Meyerson, T. R. Young, and W. R. Ney. 175

Variation of resolving power and type of test pattern. Francis E. Washer and William P. Tayman. 209

A multiple isolated-input network with common output. C. M. Allred and C. C. Cook. 225

Phase angle master standard for 400 cycles per second. J. H. Park and H. N. Cones. 229

Disturbances due to the motion of a cylinder in a two-layer liquid system. Lloyd H. Carpenter and Garbis H. Keulegan. 241

Publications of the National Bureau of Standards. 255

For sale by the Superintendent of Documents, U.S. Government Printing Office, Washington 25, D.C. Price 75 cents (single copy)
Subscription price: $2.25 a year; 50 cents additional for foreign mailing.

UNITED STATES GOVERNMENT PRINTING OFFICE, WASHINGTON : 1960